1995

Analysis and design of air-jet pumps for pneumatic transportation of bulk solids in pipelines

Demao Wang
University of Wollongong

ANALYSIS AND DESIGN OF AIR-JET PUMPS FOR PNEUMATIC TRANSPORTATION OF BULK SOLIDS IN PIPELINES

A thesis submitted in fulfilment of the requirements
for the award of the degree of

Doctor of Philosophy

UNIVERSITY OF WOLLONGONG

by

DEMAO WANG

B.Sc. (WUHEE), M.Sc. (WUHEE)

Department of Mechanical Engineering

1995

DECLARATION

This is to certify that the work presented in this thesis was carried out by the author in the Department of Mechanical Engineering at the University of Wollongong and has not been submitted for a degree to any other university or institution.

Dèmao Wang

ACKNOWLEDGMENT

I would like to express my sincerest appreciation to Dr. P.W. Wypych, Associate Professor in the Department of Mechanical Engineering at the University of Wollongong, for his supervision, continued efforts in finding financial assistance, encouragement and valuable advice during the course of this research program.

I gratefully acknowledge the University of Wollongong for providing me with the University Postgraduate Research Award, and the Bulk Materials Handling and Physical Processing Research Program for some financial assistance. I am also particularly grateful to J.S. Melbourne Controls Pty Ltd for providing the financial support to supplement the University Postgraduate Research Award.

I also appreciate the support of Nu-Con Australia for providing a Fox eductor for the initial experimental research.

The practical assistance of the technical staff was extremely valuable. In particular, the author would like to thank Mr. D. Cook, Mr. I. Frew, Mrs. W. Halford, Mr. I. McColm and Mr. S. Dunster for their enthusiastic support. Acknowledgment also is made of the assistance given by Dr. R. Pan and Dr. Bo Mi during experimental investigations.

Finally, special acknowledgment is made to my parents, my wife Dongyan Liu and son for their understanding, unfailing help and spiritual support, without which this work would never have been completed.

SUMMARY

Air-jet pumps are being used increasingly in industry to feed and transport a wide range of bulk solids because of their simplicity in structure, lack of moving parts, convenience of installation and operation and with little damage to the product. However, to date, the design of this type of equipment and associated conveying system still is a "black art" due to the shortage of theoretical analysis and experimental data reported in the literature regarding the design and application of these pumps. For this reason, this thesis aims at formulating a mathematical model to predict jet pump performance under air-solids flow conditions and developing a general design procedure by investigating into the effect of air-jet pump geometry and operating conditions on the performance of these pumps, so that options to improve efficiency can be determined.

To obtain detailed information on the interaction between the operating conditions and the jet pump geometry, a systematic experimental investigation is undertaken into the characteristic performance of central air-jet pumps with five different nozzle geometry and annular air-jet pumps with multi-hole ring nozzles operating under both air-only and air-solid flow conditions. These experiments were conducted by varying motive pressure, back pressure respectively for each particular jet pump design to observe the effect of operating conditions and geometric parameters on pump performance. The factors affecting performance also are analysed.

Generally, the efficiency of annular air-jet pumps with multi-hole ring nozzles is less than that of central air-jet pumps. Based on the experimental results, options to improve efficiency by modifying the geometrical design are suggested.

To assess the energy-effectiveness of an air-jet pump operating under different conditions, dimensional and non-dimensional parameters are defined and employed to

represent jet pump characteristic performance and efficiency. A mathematical model to predict air-jet pump performance is formulated on the basis of fluid mechanics and a numerical solution is obtained. This model is used to predict the non-dimensional relationship between the motive, suction and discharge flow through an air-jet pump with a given geometry. The predicted performance agrees well with experimental results for numerous jet pump geometries, operating conditions and different materials.

Based on the performance prediction model and experimental results, optimum parameters for maximum efficiency are analysed and correlated with experimental data. A design procedure for an air-jet pump conveying system is developed to maximise efficiency and reliability. This design procedure also is applied to the proper sizing of an air-jet pump for a given application requirement. A mathematical optimisation model for the optimal design of an air-jet pump system is formulated and the numerical solution to this model is obtained. The optimisation results agree well with the optimum parameters obtained from experiments.

It is concluded on the basis of the analyses and experimental investigations that it is possible to improve the efficiency of air-solids jet pumps by modelling its performance and optimising its geometry for a given operating condition or adjusting the operating condition for a jet pump with a given configuration.

KEY WORDS: jet pumps, air-solids flow, piping systems, performance, optimisation

TABLE OF CONTENTS

LIST OF FIGURES

LIST OF TABLES

NOMENCLATURE

A_0	cross-sectional area of section 0 - 0, as shown in Fig. 3.1	[m^2]
A_n	cross-sectional area of nozzle outlet	[m^2]
A_2, A_3	cross-sectional area of throat tube, as shown in Fig. 3.1	[m^2]
A_1, A_4	cross-sectional area of sections 1-1 and 4-4 , as shown in Fig. 3.1	[m^2]
A_5	cross-sectional area of section 5 - 5, as shown in Fig. 3.1	[m^2]
a	distance as shown in Fig. 2.33	[m]
a_n	ratio of external to internal diameter at the nozzle outlet	[-]
b_1^*, b_2^*	acceleration parameters appeared in Fig. 2.34	[-]
C	suction area ratio	[-]
C_w	drag force coefficient for single sphere, Eq. (2.11)	[-]
c	discharge coefficient of nozzle	[-]
c_{vk}	volumetric concentration of combined flow at section k-k (k = 1, 2, 3, 5)	[-]
c_{vs}	volumetric concentration of secondary flow at suction port	[-]
D	internal pipeline diameter	[m]
d_4	diameter at section 4-4 as shown in Fig. 3.1	[m]
d_5	diameter at section 5-5 as shown in Fig. 3.1	[m]
d_w	external diameter of nozzle outlet	[m]
d_v, d_T	geometric diameter as shown in Fig. 2.33	[m]
d_M, d_R	geometric diameter as shown in Fig. 2.33	[m]
d_h	diameter of single hole in multi-hole nozzle	[m]
d_m, d_{Mm}	mean diameter, as shown in Fig. 2.33, [10-13]	[m]
d_n	diameter of nozzle outlet	[m]
d_p	particle diameter	[m]

d_t	diameter of throat tube	[m]
F, F_1	distance as shown in Fig. 4.5	[m]
F_A	cross-sectional area as shown in Fig. 2.33	[m^2]
F_m	average area determined by mean diameter [10-13]	[m^2]
F_r, F_r^*	Froude number appeared in Bohnet's model (Chapter 2)	[-]
$F_{r\infty}$	Froude number	[-]
$f(X)$	function relation	[-]
g	acceleration due to gravity, 9.803	[ms^{-2}]
$g_i(X)$	function of unequal constraints	
h	pressure ratio defined by Eq. (3.6)	[-]
h_{opt}	optimum pressure ratio	[-]
$h_k(X)$	function of equal constraints	
h_u	shut-off pressure ratio	[-]
k_{01}	coefficient due to friction and variation of flow passage between nozzle inlet and exit section	[-]
k	iteration count number	[-]
k_{12}	coefficient due to flow friction between sections 1 and 2 shown in Fig. 3.1	[-]
k_{23}	coefficient due to flow friction between sections 2 and 3, shown in Fig. 3.1	[-]
k_{35}	coefficient due to flow friction between sections 3 and 5, shown in Fig. 3.1	[-]
k_{41}	coefficient between suction port and section 1, shown in Fig. 3.1	[-]
L^*	parameter of length appeared in Bohnet's model	
L_c	nozzle-throat gap, as shown in Fig. 3.1	[m]
L_d	length of diffuser	[m]

L_t	throat tube length	[m]
l	length used by Bohnet [10-13]	[m]
l_M, l_D	length as shown in Fig. 2.33	[m]
$\dot{M}_A, \dot{M}_T$	mass flow rate of air	[kg s^{-1}]
$\dot{M}$	mass flow rate of air ($\dot{M} = \dot{M}_A + \dot{M}_T$)	[kg s^{-1}]
M_p	mass flow rate of solids, used by Bohnet [13]	[kg s^{-1}]
$\dot{m}_p$	mass of particles, Eq. (4.1)	[kg]
m	area ratio of throat cross-section to nozzle outlet	[-]
m_d	ratio of diffuser outlet area to inlet area	[-]
m_n	ratio of nozzle inlet area to outlet area	[-]
m_u	optimum area ratio	[-]
M_{oai}	ideal motive air mass flow rate	[kg s^{-1}]
M_{oa}	motive air mass flow rate	[kg s^{-1}]
M_s	conveying solid mass flow rate	[kg s^{-1}]
M_{sa}	suction air mass flow rate	[kg s^{-1}]
M_{sd}	conveying solid mass flow rate required	[kg s^{-1}]
M_{sp}	suction solids mass flow rate	[kg s^{-1}]
N	number of holes in multi-hole ring nozzle	[-]
N_{cs}	theoretical power consumed by air-jet pump, Eq. (3.10)	[w]
n_p	number of particles, Eq. (4.1)	[-]
P	penalty function	[-]
p	static pressure	[Pa]
p_T	pressure at the feeding hopper	[Pa]
p_v	pressure at nozzle inlet, as shown in Fig. 2.33	[Pa]
p_R	pressure at R section as shown in Fig. 2.33	[Pa]
p_U	atmospheric pressure, Eq. (2.2)	[Pa]
p_V^*, p_T^*	dimensional parameter, defined in [10-13]	[-]

p_R^*	dimensional parameter, defined in [10-13]	[-]
p_0	motive static pressure	[Pa]
p_{0opt}	optimum of motive pressure to obtain best efficiency	[Pa]
p_1, p_2, p_3	static pressure at sections 1-1, 2-2, 3-3 shown in Fig. 3.1	[Pa]
p_4	static pressure at suction port	[Pa]
p_5	static pressure at jet pump exit	[Pa]
p_b	static pressure in the receiving bin	[Pa]
p_d	delivery pressure available at jet pump exit	[Pa]
p_{dr}	delivery pressure required by pipeline system	[Pa]
p_n	static pressure at nozzle outlet	[Pa]
p_k	static pressure at section k-k (k = 1, 2, 3, 4, 5)	[Pa]
p_{x1}	first pressure in Equation 4.2	[Psig]
p_{x2}	second pressure in Equation 4.2	[Psig]
$\overline{p_0}$	total pressure at nozzle inlet section	[Pa]
$\overline{p_4}$	total pressure at suction port	[Pa]
$\overline{p_5}$	total pressure at jet pump exit	[Pa]
Q_a	volumetric air flow rate,	[$m^3 s^{-1}$]
Q_{o1}	volumetric flow rate of motive air flow at section 1-1	[$m^3 s^{-1}$]
Q_{o2}	volumetric flow rate of motive air flow at section 2-2	[$m^3 s^{-1}$]
Q_3	volumetric flow rate of air-solids mixture at section 3-3	[$m^3 s^{-1}$]
Q_p	volumetric solids flow rate	[$m^3 s^{-1}$]
Q_{s1}	volumetric flow rate of secondary flow at section 1-1	[$m^3 s^{-1}$]
Q_{s2}	volumetric flow rate of secondary flow at section 2-2	[$m^3 s^{-1}$]
Q_{sa}	volumetric flow rate of air in secondary flow at section 4-4 as shown in Fig. 3.1	[$m^3 s^{-1}$]
Q_{sp}	volumetric flow rate of solids in secondary flow	[$m^3 s^{-1}$]
q_a	volumetric flow rate ratio of suction air to motive air	[-]

q_p	volumetric flow rate ratio of solids to motive air	[-]
R	gas constant	[N m kg^{-1}K^{-1}]
Re_p	particle Reynolds number [10-13]	[-]
R^*	friction parameter [10-13]	[-]
r	controlling parameter	[-]
r^*	friction parameter [10-13]	[-]
S	velocity ratio of gas to particle at suction port	[-]
S^*	gravitational parameter [10-13]	[-]
T_0	temperature at nozzle inlet section	[K]
V_a	air volume	[m^3]
V_p	solids volume	[m^3]
V_a	added cell volume of a stereo pycnometer in Eq. (4.2)	[cm^3]
V_c	sealed sample cell volume of a stereo pycnometer	[cm^3]
V_{px}	powder sample volume in Eq. (4.2)	[cm^3]
V_{sa}	volume of suction air	[m^3]
V_{sb}	volume of secondary bulk solids	[m^3]
V_{sp}	volume of suction particles	[m^3]
v_0	velocity at nozzle inlet	[m s^{-1}]
v_{o1}	motive air velocity at section 1-1	[m s^{-1}]
v_{o2}	motive air velocity at section 2-2	[m s^{-1}]
v_{a2}	superficial air velocity at section 2-2	[m s^{-1}]
v_{a3}	superficial air velocity at section 3-3	[m s^{-1}]
v_3	average velocity of air-solids mixture at section 3-3	[m s^{-1}]
v_4	average velocity at suction port	[m s^{-1}]
v_{4a}	velocity of secondary air flow at section 4-4	[m s^{-1}]
v_{4p}	solid velocity at section 4-4	[m s^{-1}]
v_5	average velocity at jet pump exit	[m s^{-1}]

v_a	superficial air velocity	[m s^{-1}]
v_d	average velocity of air-solids mixture in conveying pipe	[m s^{-1}]
v_{mp}	acceptable superficial air velocity in conveying pipeline	[m s^{-1}]
v_{s1}	average velocity of secondary flow at section 1-1	[m s^{-1}]
v_{s2}	average velocity of secondary flow at section 2-2	[m s^{-1}]
v_∞	terminal velocity	[m s^{-1}]
w_m	mean velocity determined by Eq. (2.3), [10-13]	[m s^{-1}]
w_{Mm}	mean velocity determined by Eq. (2.7), [10-13]	[m s^{-1}]
w, w_T, w_M	air velocity [10-13]	[m s^{-1}]
w_R	air velocity at diffuser exit [10-13]	[m s^{-1}]
w_p	particle velocity [10-13]	[m s^{-1}]
w_s	terminal velocity [10-13]	[m s^{-1}]
w_p^*	velocity ratio [10-13]	[-]
X	a set of design variables	
X^*	solution of optimisation problem	
x	mass flow rate ratio of secondary flow to motive flow	[-]
x_{opt}	optimum mass flow rate ratio	[-]
Y	expansion factor	[-]
y	pressure ratio in Equation (7.2)	[-]
z	dynamic pressure of motive jet flow	[Pa]
ρ	density of air appeared in Bohnet's model	[kg m^{-3}]
ρ_1, ρ_2, ρ_3	density of air flow at sections 1, 2 and 3, as shown in Fig. 2.33	[kg m^{-3}]
ρ_3	density of air-solids mixture at section 3-3 as shown in Fig. 3.1	[kg m^{-3}]
ρ_R, ρ_T	density of air flow at sections R and T, as shown in Fig. 2.33	[kg m^{-3}

ρ_{a0}	density of motive air at nozzle inlet section	[kg m^{-3}]
ρ_m,ρ_{Mm}	average density used in Bohent 's model [10-13]	kg m^{-3}]
ρ_{o1}	density of motive air at section 1-1	[kg m^{-3}]
ρ_{o2}	density of motive air at section 2-2	[kg m^{-3}]
ρ_{a3}	density of air at section 3-3	[kg m^{-3}]
ρ_{a4}	density of air at suction port	[kg m^{-3}]
ρ_{a5}	density of air at jet pump exit	[kg m^{-3}]
ρ_{ak}	density of air at section k-k (k=1, 2, 3, 5)	[kg m^{-3}]
ρ_b	bulk density of particles	[kg m^{-3}]
ρ_p	particle density of particles	[kg m^{-3}]
ρ_m	average density of air appeared in [10-13]	[kg m^{-3}]
ρ_{m3}	density of air-solids mixture at section 3-3	[kg m^{-3}]
ρ_{m5}	density of air-solids mixture at jet pump exit	[kg m^{-3}]
ρ_{mk}	density of air-solids mixture at section k-k (k=1, 2, 3, 5)	[kg m^{-3}]
ρ_{s1}	density of secondary flow at section 1-1	[kg m^{-3}]
ρ_{s2}	density of secondary flow at section 2-2	[kg m^{-3}]
ρ_{s4}	density of secondary flow at section 4-4	[kg m^{-3}]
κ	ratio of specific heat at constant pressure to that at constant volume	[-]
α	throat entry function Eq. (3.60)	[-]
Δp_T	total pressure drop	[Pa]
Δp_a	pressure drop due to air flow	[Pa]
Δp_s	pressure drop due to solids flow	[Pa]
δ	acceptable error	[-]
ε	void fraction, Eq. (4.3)	[-]
ε_k	void fraction of combined flow at section k-k (k=1, 2, 3, 5)	[-]

ε_s	void fraction of secondary flow at suction port	[-]
ϕ, Φ	function relation	
ψ	mass flow ratio of particle to air, also stands for function relation in section 7.2	[-]
λ_a, λ_G	friction factor due to air-only flow	[-]
λ_s	friction factor due to solids	[-]
λ_s^*	coefficient due to particle wall friction [10-13]	[-]
η_α	efficiency defined by Eq. (3.9)	[%]
η	efficiency defined by Eq. (3.11)	[%]
η_μ	efficiency defined by Eq. (3.12)	[%]
η_T, η_M	coefficient related to friction [10-13]	[-]
η_D, η_S	coefficient related to friction [10-13]	[-]
β	half conical angle of throat entry as shown in Fig. 3.1,	[°]
	also coefficient due to gravitational influence [10-13]	[-]
θ	half conical angle of diffuser as shown in Fig. 3.1	[°]
ω	semi-contracting angle of convergent nozzle	[°]
μ	solid loading, $\mu = \dot{M}_p / \dot{M}$ [10-13]	[-]
μ_3	momentum correction coefficient due to non-uniform velocity distribution;	[-]
ζ_{o2}	momentum modification coefficient due to the variation of motive air-jet profile	[-]
ζ_{s2}	momentum modification coefficient due to non-uniform velocity distribution in secondary flow at section 2-2	[-]
ξ_d	coefficient related to friction in diffuser	[-]

CHAPTER 1

INTRODUCTION

Fluid transportation is being used increasingly in industry to convey a wide range of bulk solids. Experience has demonstrated that any successful positive-pressure fluid conveying system lies in the proper design/selection of the feeding device to feed the material into a pipeline which is above atmospheric pressure. Therefore, numerical efforts have been made to investigate desirable feeding devices to cope with an increasing number of applications (especially over the last two decades). As a result, different types of feeding device are being developed continually. Among them, the most common ones are *blow tank*, *rotary valve*, *screw feeder* and *venturi* [66].

In recent years, the *jet pump* shown in Fig. 1.1 (also known as *eductor*, *suction nozzle* and/or *injector*) has been increasing in popularity as another feeding device for pneumatic transportation systems [19, 30, 33, 36, 38, 58, 70, 72, 73]. For example, hundreds of jet pump systems have been installed in industry all over the world since the early 70's [37, 38]. The reason is that the jet pump feeder possesses the following advantages.

1 Simplicity and reliability: no moving parts in the pump make the conveying system installation simpler in structure and more reliable in operation; furthermore, jet pumps have the ability to self-regulate and prevent blockage if overloaded;

2 No air leakage: all rotary airlocks connected to positive-pressure conveying systems lose air due to clearance and carry-over (caused by empty pockets); if the product conveyed is fine or abrasive, air leakage can cause extreme wear problems; even with freely flowing products, air leakage may cause bridging, housekeeping problems and explosion hazards;

3 Low capital cost and little or no requirement of maintenance: no moving parts in jet pump structure allow for lower capital cost and less maintenance, compared with other types of feeding device;

4 Minimum attrition of material to be conveyed: jet pump feeders do not suffer from the shearing, smearing or degradation problems that can occur in mechanical feeders;

5 High temperature applications: due to lack of moving parts, seals and clearance, jet pumps can be designed to handle much higher operating temperature.

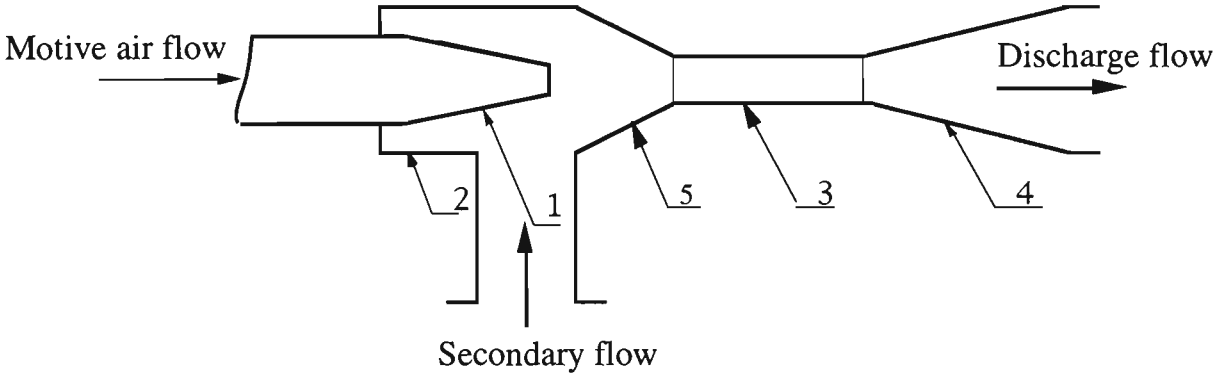

1. Nozzle; 2. Suction Chamber; 3. Throat Tube; 4. Diffuser; 5. Throat Entry.

Fig. 1.1 General Configuration of Jet Pump

It should be noted that some confusion exists in the literature between the terms *jet pump* and *venturi feeder* . For example, sometimes, a *jet pump* is referred to as a *venturi feeder* [26, 28]. However, a *jet pump* is quite different to a *venturi feeder* in terms of structure and operation. Further discussion and clarification of terminology occurs in Chapter 2.

1.1 Description of Jet Pump and Associated System

Jet pumps, in general, utilise a motive fluid flow under controlled conditions to entrain a secondary flow containing the solid particles to be pumped. As shown in Fig. 1.1, it consists of: a nozzle to generate a high velocity jet (motive flow) with the motive port

connected to motive fluid supply; a suction chamber with the suction port connected to the feeding hopper; a throat entry, a throat tube (also referred to as the mixing tube); and in majority of cases a diffuser on the downstream side with the delivery port connecting to the piping system (Fig. 1.2).

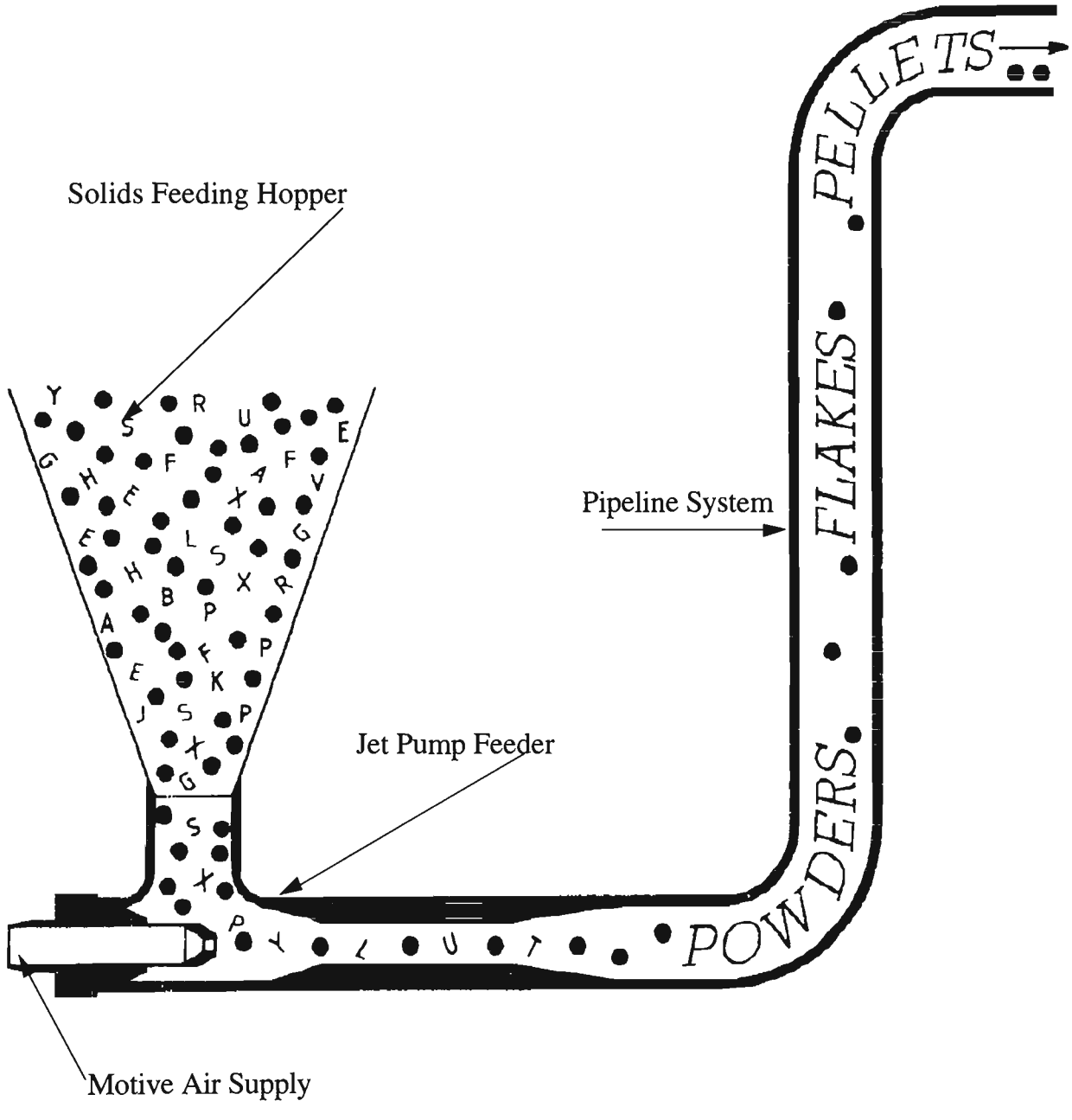

Fig. 1.2 Typical Jet Pump Conveying System [38]

The basic principles of operation are based on fluid dynamics, and are quite different to that used by other types of pump (*e.g.* centrifugal pump, reciprocating pump, *etc.*). For

example, the motive fluid flowing through the nozzle creates a jet flowing at high velocity and a low pressure region in the suction chamber; air and material from the feeding hopper are drawn through the suction port into the suction chamber where entrainment takes place; the two fluid streams with different velocity and density mix in the mixing section of the air-jet pump; the momentum transfer from the motive fluid to the secondary stream accelerates the suction stream in the direction of motive jet flow and produces a uniformly mixed stream travelling at a velocity intermediate to the motive and suction velocity at the throat exit; the combined flow then is discharged to the conveying pipeline with a given delivery pressure and velocity through the diffuser, which serves as a pressure recovery device. It is shaped to reduce the velocity gradually and convert the kinetic energy to pressure energy on the discharge with as little loss as possible. Hence, the suction flow is pumped by means of the momentum of the motive fluid. Unlike rotary feeders, it is possible to feed granular or pulverised solids into pipelines under pressure using an air-jet pump, without any additional valves. A pulse free product flow can be obtained.

Jet pumps, particularly those with all the wearing surfaces made of alloy cast iron, ceramics, or other wear-resistant alloys for abrasive applications, also are commonly used in place of rotary valves to feed bulk solids, i.e. powders, pellets, and particulate matter into positive-pressure dilute-phase conveying systems. For example, air leakage with an abrasive, fine product (e.g. fly ash, alumina) can destroy an air-lock in a short period of time. Since jet pumps completely eliminate air leakage, this problem is avoided. As yet, no ceramic-lined jet pump has shown signs of wear [36-38]. Fig. 1.3 illustrates the use of a jet pump instead of a rotary airlock to provide maintenance-free conveying.

Note in most cases, the feed material is "dropped" into the jet pump under the action of gravity. However, jet pumps also can be used to lift bulk materials out of product containers (e.g. barrels, tote bins, *etc.*) as shown in Fig. 1.4.

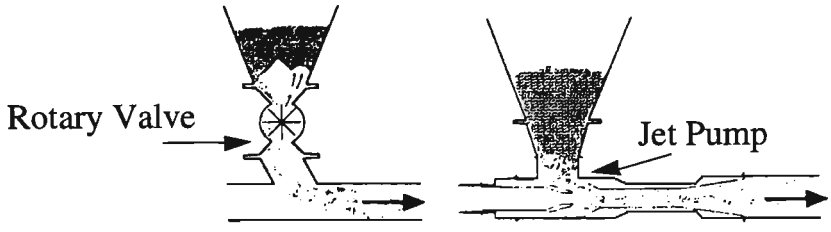

Fig. 1.3 Use of Jet Pump instead of Rotary Airlock [37]

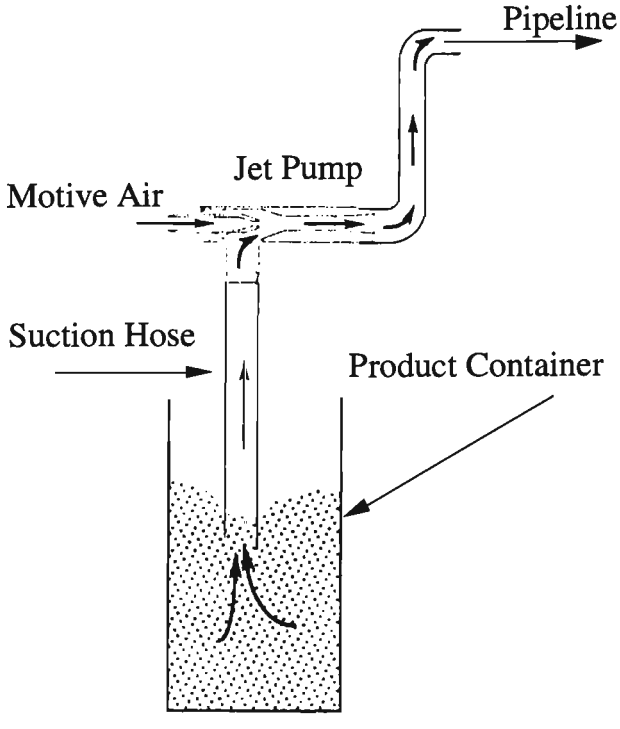

Fig. 1.4 Use of Jet Pump to Lift Materials out of Container [38]

Jet pumps also can be used to assist in the venting of rotary valves, as shown in Fig. 1.5. This produces a suction effect on the rotary valve vent port, and conveys the product-laden air either directly into the conveying line, or back into the feeding hopper, silo or bin.

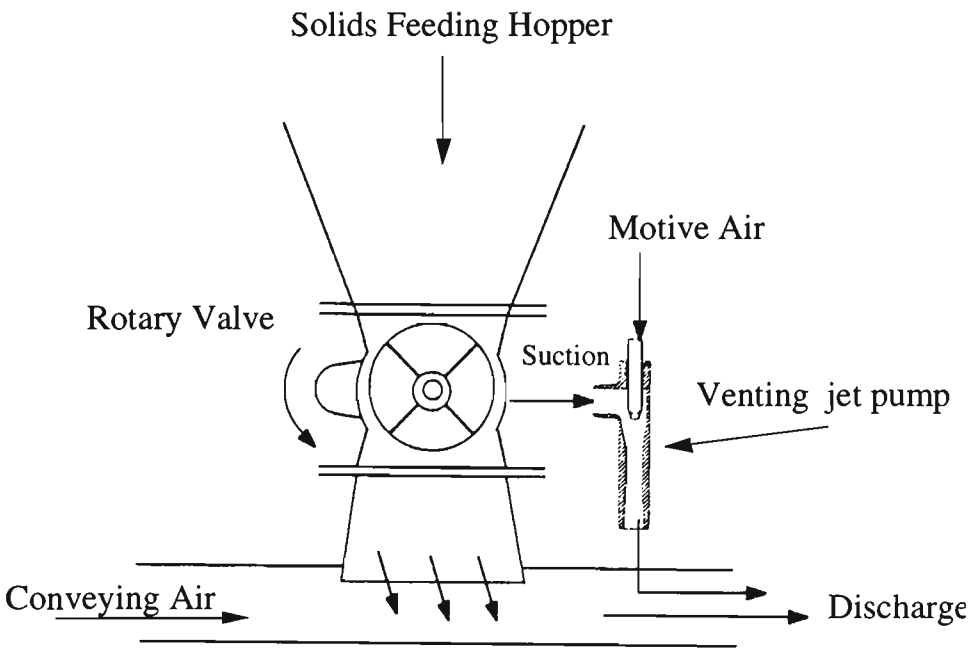

Fig. 1.5 Use of Jet Pump for Rotary Valve Venting [38]

1.2 Description of Present Research

To obtain a reliable design of a jet pump and associated conveying system, it is essential to understand the relationship between the motive flow condition (pressure and air mass flow rate) and the ability of the jet pump to induce a solids flow from the feeding hopper for a given delivery pressure and the parameters that affect this relationship. To data, due to its considerable importance for industry, the jet pump has been investigated both experimentally and theoretically [1, 3, 5, 8, 9, 10-16, 18-24, 26, 28, 29, 33, 36, 37]. As a result, some commercial air-jet pump conveying systems have been developed and applied successfully in industry. In spite of this effort, the reliable and energy-effective design of this equipment and associated system is still a "black art" and relies heavily on experience and trial-and-error. The reasons are that the performance of an air-jet pump subjected to air-solids (two-phase) flow still can not be predicted with sufficient accuracy and that there is a shortage of systematic experimental data relating the geometrical parameters to the operating performance conditions. Hence, it is imperative to investigate the effect of air-jet pump geometry and operating conditions on pump performance and

also develop the necessary mathematical models to formulate an optimum design methodology and provide a reliable design strategy for designing air-jet pump transportation system. It should be pointed out that while both central and annular air-jet pumps have been tested extensively and systematically to obtain optimum parameters and an energy-effective configuration, the performance prediction model and optimum design techniques are confined to central-jet pumps. The reason is that this type of feeder appears to be the most energy-effective and widely accepted in industry (e.g. food industry, chemical plants).

1.2.1 Objectives and Structure of the Thesis

The main aim of this thesis is the formulation of a theory to predict pump performance and an optimum design strategy for the air-jet pump and pneumatic pipeline transport system. To achieve this overall aim, particular objectives of the work are listed below:

1. Reviewing published literature to assess the current state of the knowledge of jet pumps (Chapter 2);

2. Introducing parameters to represent pump characteristics and to evaluate the energy-effectiveness of the jet pump (Chapter 3);

3. Analysing the flow characteristics in a jet pump based on the principle of fluid dynamics and developing a performance prediction model (Chapter 3);

4. Undertaking experiments to investigate the influence of geometrical parameters and operating conditions on pump performance (Chapter 4);

5. Analysing and discussing the experimental results to examine the factors affecting jet pump performance (Chapters 5 and 6);

6. Formulating a strategy for the optimal design of a jet pump conveying system based on the performance prediction model developed (Chapter 7);

Finally, concluding remarks based on the investigations and suggestions for further study are presented in Chapter 8.

1.2.2 Significance

To date, the most significant work concerned with the modelling of air-jet pump performance subjected to air-solids flow has been undertaken by Bohnet [10-13]. The principal distinctions between the work of Bohnet [10-13] and the present study are:

1. Considering the influence of throat entry configuration (converging angle) and nozzle-throat gap L_c on performance by introducing a throat entry function (Eqn. 3.60);

2. Treating the motive air flow through the nozzle as subsonic or sonic (depending on motive pressure), while only subsonic flow was considered by Bohnet [10-13];

3. Determining the air sucked in through the feeding hopper while solids are being conveyed, based on the ratio of particle to suction air velocity and the variation of volumetric concentration (e.g. more air may be sucked in for coarse particles than for final particles) - not only based on the area of suction port and the pressure difference between the feeding hopper and the suction port;

4. Considering the air flow as isothermal, so the density of air-solids mixture in jet pump is related to the variation of pressure-not determined only by the arithmetic mean of particle density and air density;

5. Different consideration of particle velocity and pressure drop in the jet pump.

In addition to the distinctions described above, the present work has the following special features:

1. Dimensional and non-dimensional parameters are introduced to represent pump characteristics; conversion between dimensional and non-dimensional characteristics are formulated;

2. The performance prediction model is employed to formulate a design strategy for the design of jet pump conveying system;

3. The design strategy is based on the determination of optimum parameters; the design of the jet pump also is considered in conjunction with the piping system so that the jet pump characteristic can match the characteristic of the pipeline;

4. The optimum design of air-solids jet pumps is formulated by means of mathematical optimisation techniques; the numerical solution to the optimisation model is obtained and compared with experimental data;

5. Systematic experiments are conducted with a wide range of motive pressures and area ratios (e.g. area ratios up to 25 and motive pressures up to 500 kPag) to confirm the optimum parameters experimentally;

6. The influence of nozzle-throat gap also is investigated in detail for different combinations of geometrical configuration and operating condition so as to determine the optimal value;

7. Jet pump characteristics under air-solids flow are compared with that under air-only conditions;

8. Efficiency is introduced and defined to evaluate jet pump performance; options to maximise efficiency also are determined by optimising the geometrical configuration and operating condition;

9. Optimum parameters are correlated with experimental data and compared with the mathematical optimisation results;

10. A method to size jet pump is formulated to enable computerisation of the design process .

Based on all the improvements described above, the air-jet pump feeding system now can be designed to operate as close to its best efficiency point as possible for a given transportation requirement.

CHAPTER 2

LITERATURE REVIEW

2.1 Introduction

The jet pump dates back to the first application made by James Thomson in 1852 [93] and to the first theoretical development on the mixing of two streams by Rankine in 1870 [76] and Lorenz in 1910 [64]. To date, numerous research and development efforts have been devoted to the improvement of the design of jet pumps and associated systems, and to the better understanding of the interaction between motive and secondary flow in jet pumps. More than 400 papers are available in the literature with respect to the theory and application of jet pumps, as shown by previous reviews of jet pumps and ducted jets [9, 14-16]. Despite this considerable effort, there still exists confusion/misconception amongst those that have general knowledge on this type of equipment, even though the jet pump has been in use for over several decades. The main reasons are:

- Terminology: numerous names are given to jet pumps, and this leads to air-jet pumps being confused with other types of equipment having the same or similar name;

- Application: many people still believe that operating air pressure need to be above 400 kPag for effective material transport and also that air-jet pumps only can be used to handle light products at low conveying rates and over very short distances;

- Sophistication in characteristics: the complexity of jet pump characteristics often is under-estimated. For example, many designs have been based on trial-and-error and/or experience and hence, pay little attention to the influential parameters that affect performance. The interaction between jet pump performance and piping system characteristics also has not received a great deal of attention.

To clarify these confusions and misconceptions, consistent terminology and an overall introduction to jet pump characteristics and applications are required initially. This chapter reviews the literature published to present the current state of knowledge on air-jet pump performance, application and design. As a large amount of literature has been published in the area of jet pumps, this review is confined only to those pumps subjected to air-only and air-solids flow conditions and encompasses the following aspects:

- Air-jet pump design and terminology.
- Experimental investigations.
- Performance prediction models.
- Design methodology.

2.2 Jet Pump Designs and Terminology

2.2.1 Classification of Jet Pumps

The significant advantages of jet pump make them very attractive to various engineering applications. As a result, different designs of jet pump have resulted from the intention of improving pump performance and applying jet pumps to specific areas. Generally, the great variety of jet pump designs have been named on the basis of the nozzle geometry and layout, the properties of the motive and the suction fluid, the applications they serve, and/or the materials from which they are constructed. A brief classification is given below:

Classification by Nozzle Location: in accordance with the location of the nozzle with respect to the jet pump axis, there are two main types of jet pump:

Central jet pump: Motive jet flows along the axis of the jet pump throat tube. This type of jet pump includes single-hole nozzle, multi-hole

nozzle, proportioning jet pump and flat jet pump. In this type of jet pump, the throat tube possesses a circular cross-section.

Annular jet pump: Motive jet flows along the internal wall of the jet pump throat tube. This type of jet pump covers annular slot jet pump and annular multi-hole nozzle jet pump.

Classification by Nozzle Structure: based on the geometry and structure of the nozzle, jet pumps may be classified as:

Single-nozzle jet pump: Generally, a single-nozzle jet pump is known simply as a jet pump.

Multi-nozzle jet pump: These pumps contain more than one hole at the nozzle exit.

Proportioning jet pump: This type of jet pump also is called adjustable jet pump. The significant feature of this type of pump is that the flow area at the nozzle exit can be adjusted within a certain range to suit the operating conditions.

Bi dimensional jet pump In this type of jet pump, either the nozzle or throat tube is not of circular shape or the circular nozzles are not positioned in a concentric circle.

Classification by Type of Motive and Suction Fluid: this is a specific classification indicating that the pump is designed to handle a particular type of fluid or product using a particular type of motive fluid, for instance, air-jet solid pump, air-jet air pump (air-only jet pump) and so on. Also, if the motive and suction fluids are the same, the jet pump is referred to as single-phase flow pump (for example, air-only jet pump), otherwise, it is a multi-phase flow or dissimilar fluid jet pump. This classification is imperative to the prediction and evaluation of jet pump performance.

Classification by Application and Operation: this classification basically describes the design duty of the jet pump, *e.g.* feeder, jet primer, sand/mud/slurry pump, hopper pump, and so on.

Classification by Material: this classification describes the materials from which the pump is constructed and thus indicating its suitability in handling say, abrasive or non-abrasive fluids, chemical active or corrosive fluids, and so on.

2.2.2 Miscellaneous Jet Pump Designs

2.2.2.1 Central Jet Pumps

A typical central jet pump, as shown in Fig. 2.1 comprises a central driving nozzle, an annular suction passage, a general cylindrical throat tube and a divergent diffuser with a small included angle (7° to 8°), even though it may be given different names and may be slightly different in structure to suit specific applications. In order to improve efficiency and compactness, miscellaneous designs have been investigated and employed in engineering practice, as shown in Figs. 2.2 to 2.11.

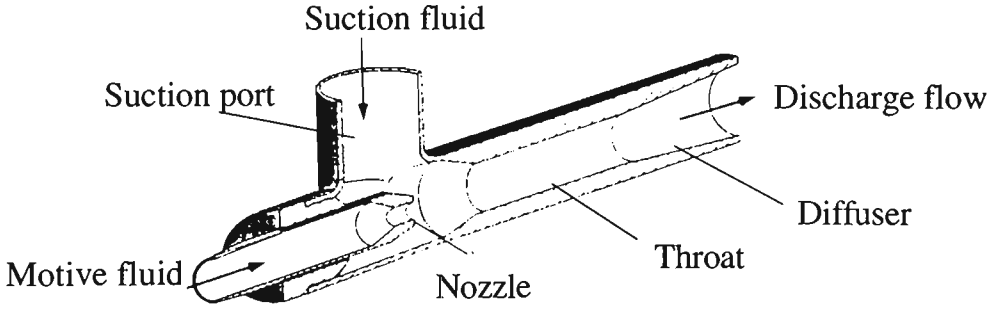

Fig. 2.1 Fox eductor [38]

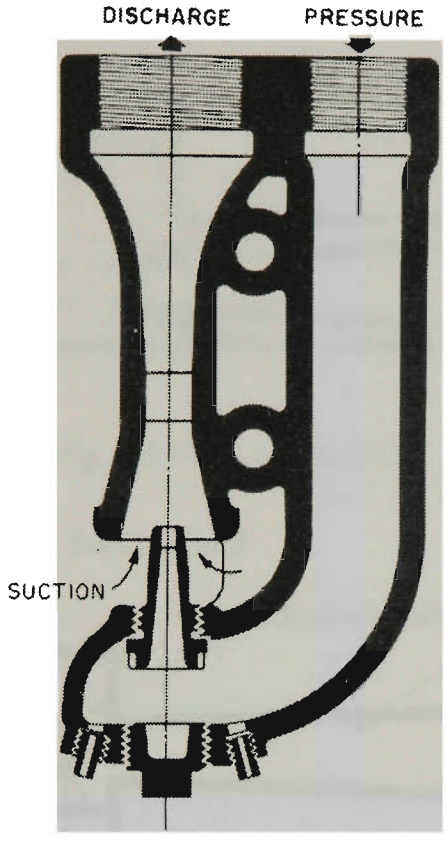

Fig. 2.2 Sand and mud eductor (Schutte and Koerting Co.) [49]

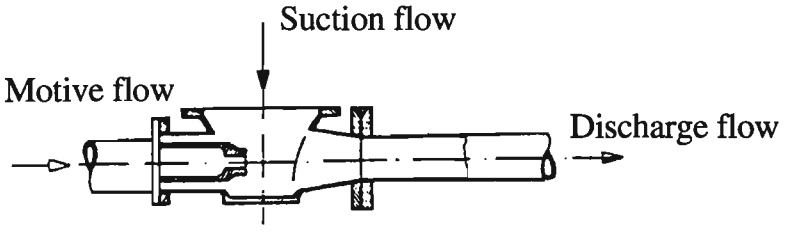

Fig. 2.3 Jet pump [121]

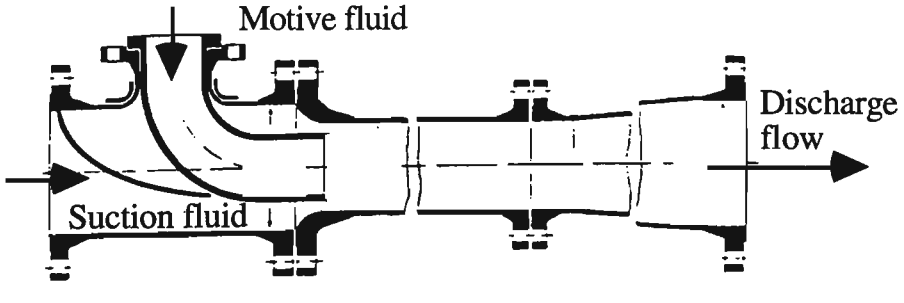

Fig. 2.4 Jet pump [121]

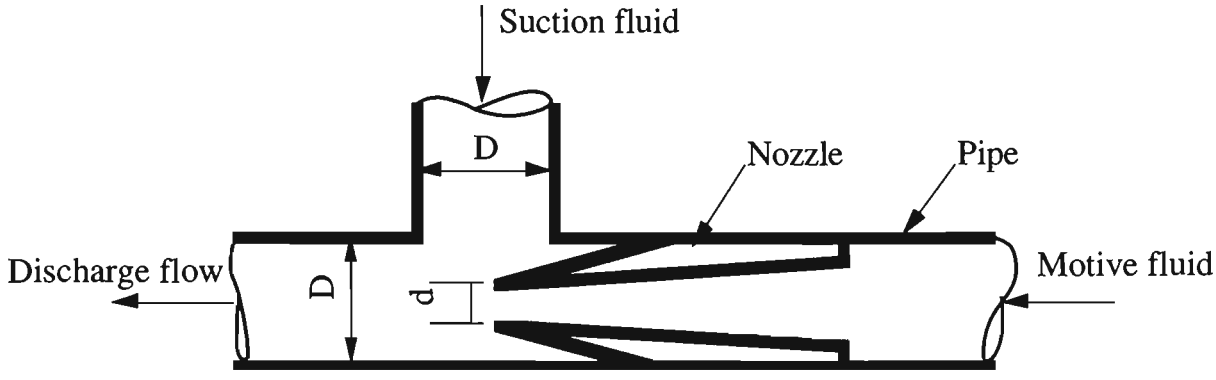

Fig. 2.5 Flow nozzle [72]

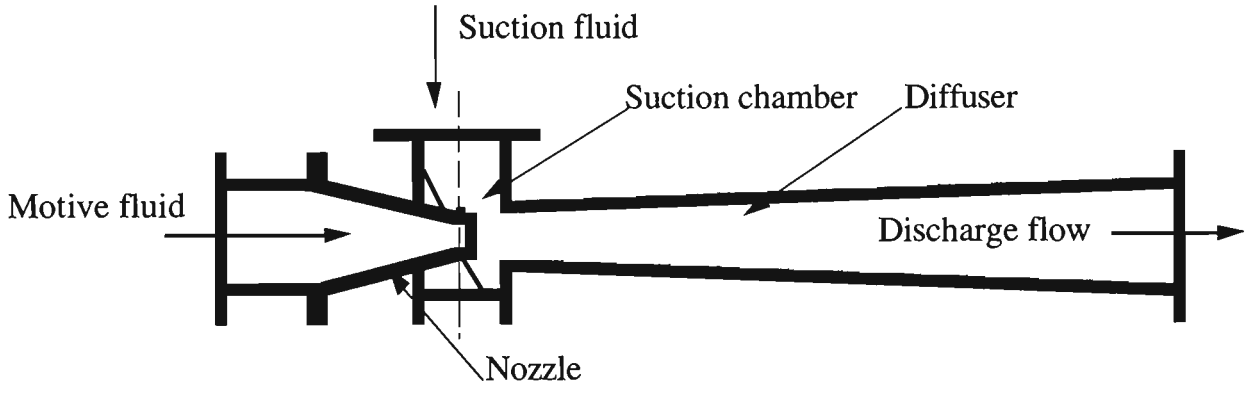

Fig. 2.6 The feed venturi [30]

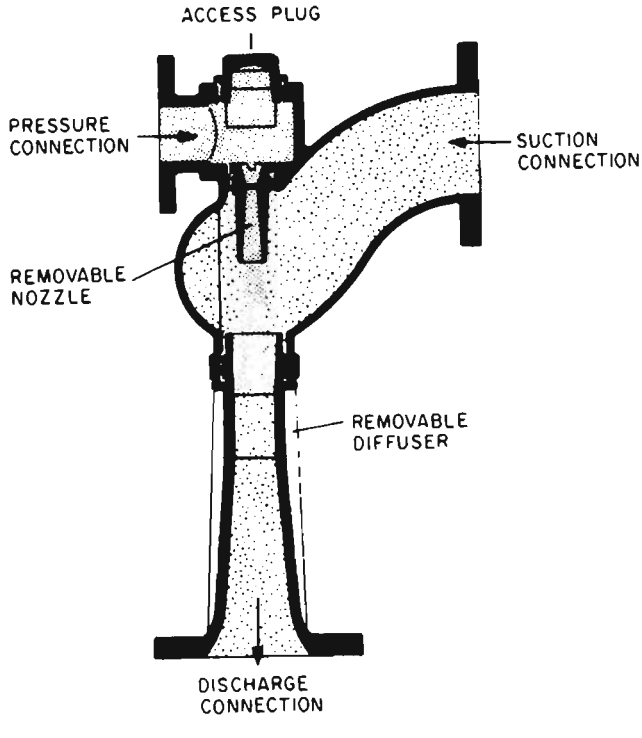

Fig. 2.7 Streamlined eductor (Schutte and Koerting Co.) [49]

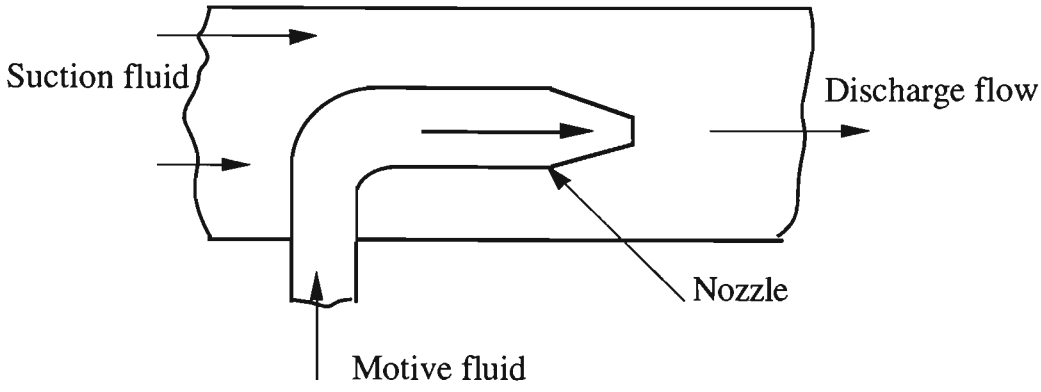

Fig. 2.8. Coaxial tube ejector [73]

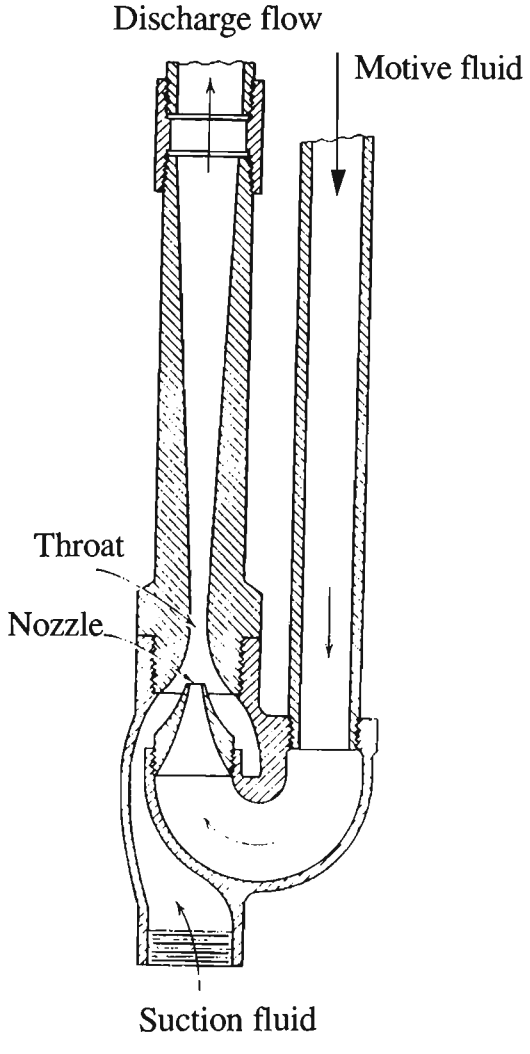

Fig. 2.9 Jet pump [90]

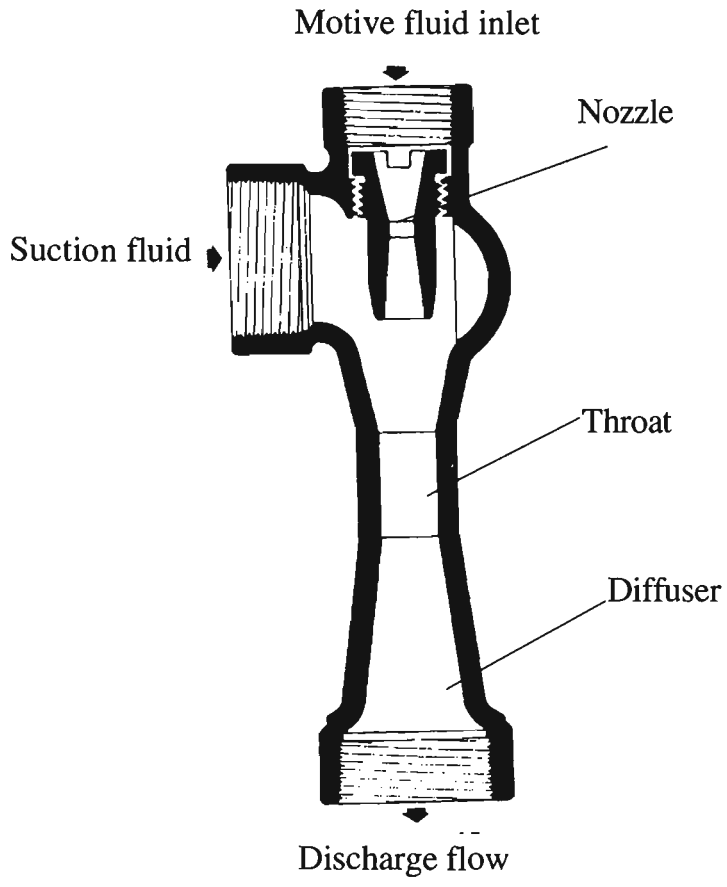

Fig. 2.10 Siphon eductor (Schutte and Koerting Co.) [49]

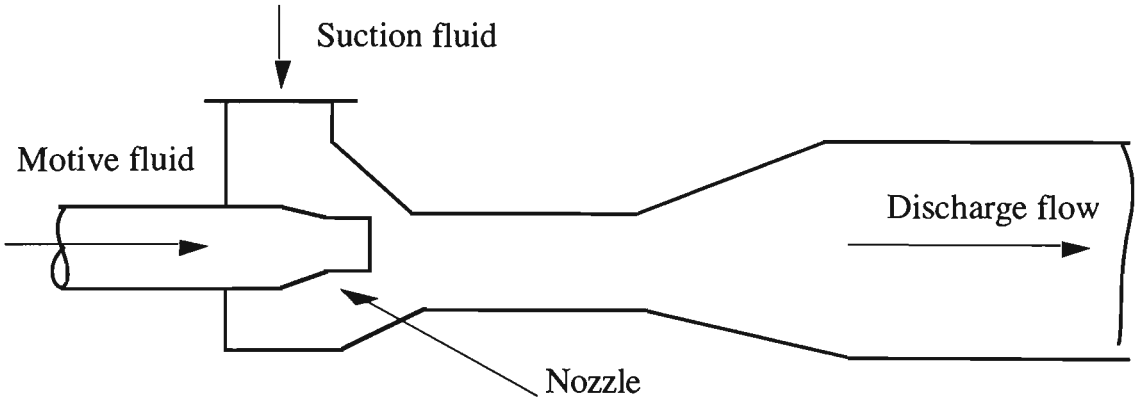

Fig. 2.11 Injector feeder [11-13]

2.2.2.2 Annular Jet Pump

Fig. 2.12 shows the general configuration of an annular jet pump, in which the motive fluid is introduced in the annular region and the suction fluid in the core. The basic principle of operation is: motive fluid flows through the annular chamber and then throttled through the annular nozzle (also called annular gap). The shape of the annular

nozzle creates a thin layer of air flowing at high-velocity. This fast-moving thin layer of fluid "follows" the outlet profile of the annular nozzle, as shown in Fig. 2.12, at a high enough velocity to create a low pressure region in the neighbourhood of the annular nozzle (Coanda effect). Suction fluid is drawn into this low-pressure zone and a larger flow rate is established instantly. The high-velocity fluid jet acts as a "jacket" to minimise the solids in the suction fluid striking the nozzle and throat wall. Therefore, this configuration shows promise in reducing erosion of the pump nozzle and throat regions (that presently limit the durability of conventional jet pumps in the application of fluid transportation of solids) by separating the erosive suction flow from the pump wall [107].

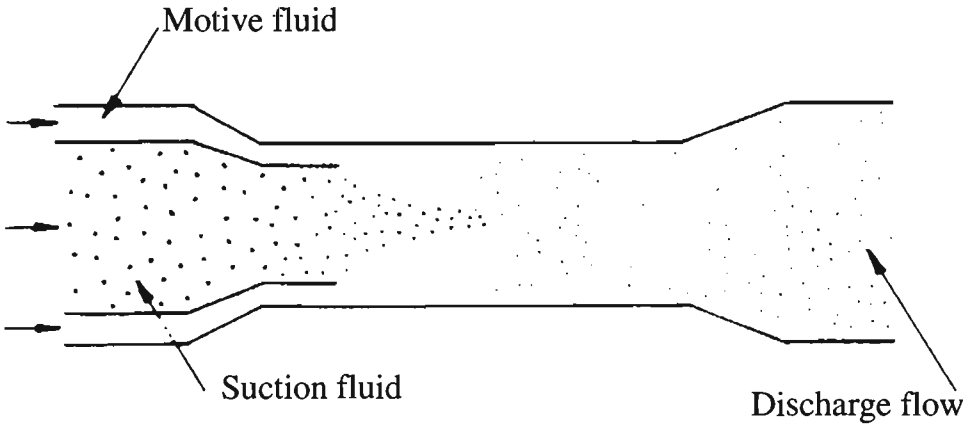

Fig. 2.12 General configuration of annular jet pump [107]

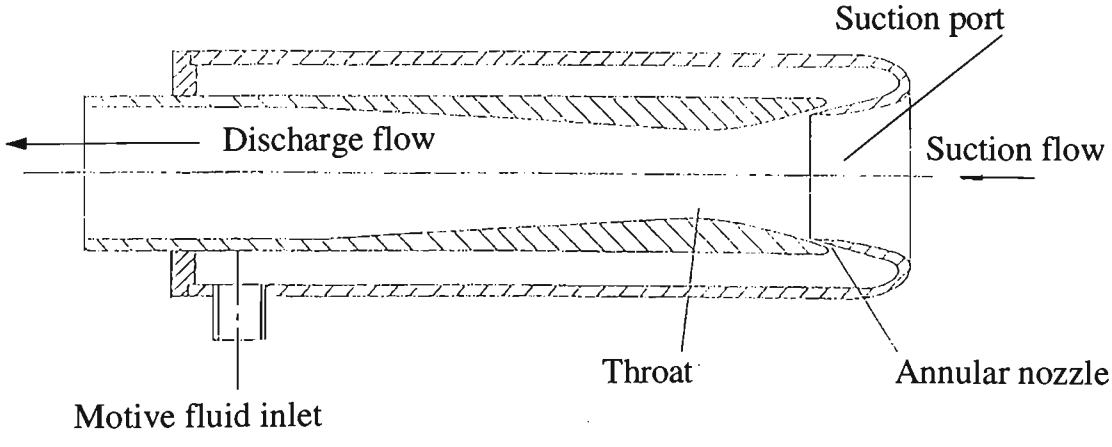

Fig. 2.13 Vacuum aerated feed nozzle [73]

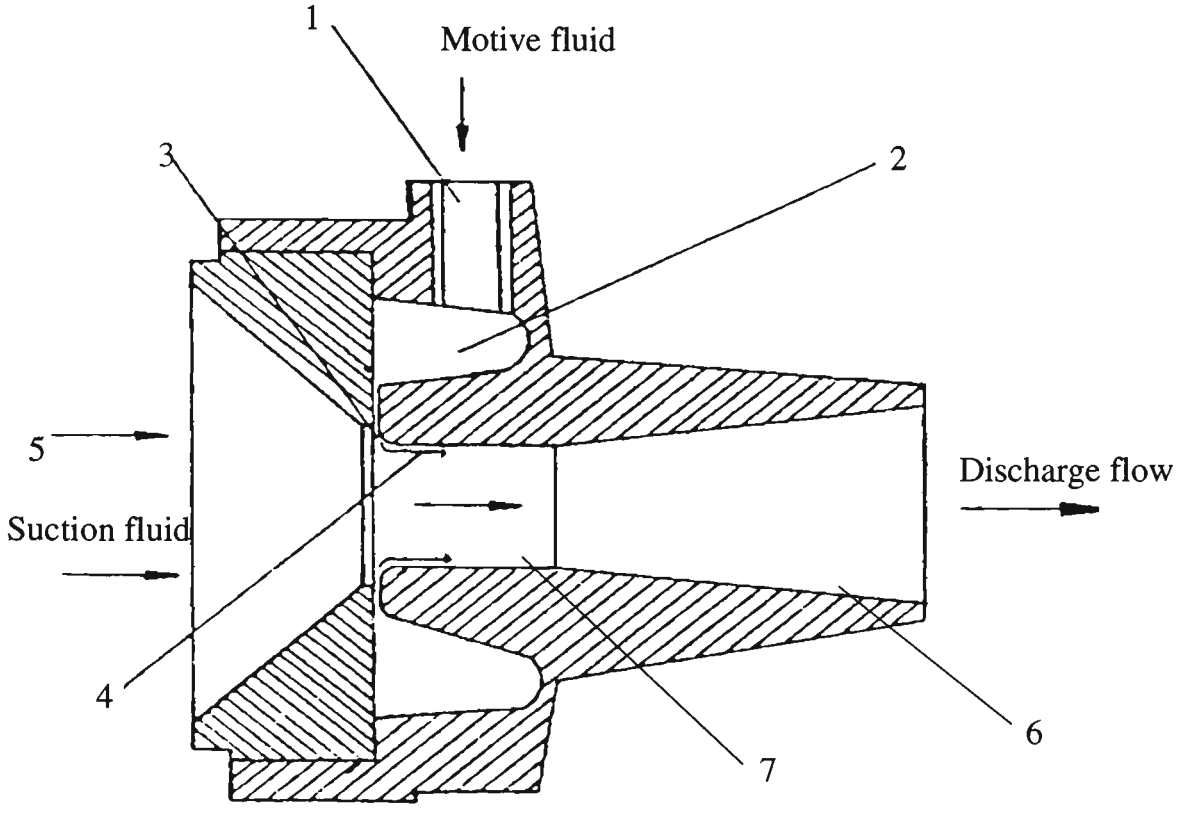

Fig. 2.14 Cross-sectional view of annular jet pump [80]
1. Motive fluid inlet; 2. Annular chamber; 3. Annular nozzle;
4. Outlet profile of annular nozzle; 5. Suction port, 6. Diffuser; 7. Throat.

This type of jet pump sometimes is called an advanced jet pump [60], parietal jet pump or annular slots jet pump [84].

Various types of annular jet pump are shown in Fig. 2.13 to 2.21. Annular jet pumps have the advantages of a shorter throat tube length and lower cost, but the characteristic is completely different from that of conventional jet pumps [94].

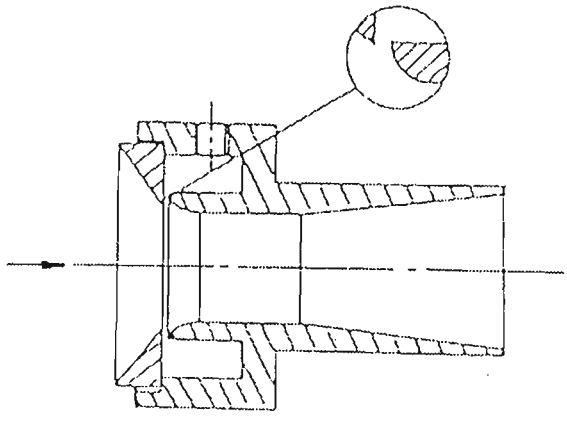

Fig. 2.15 Air mover ejector [73]

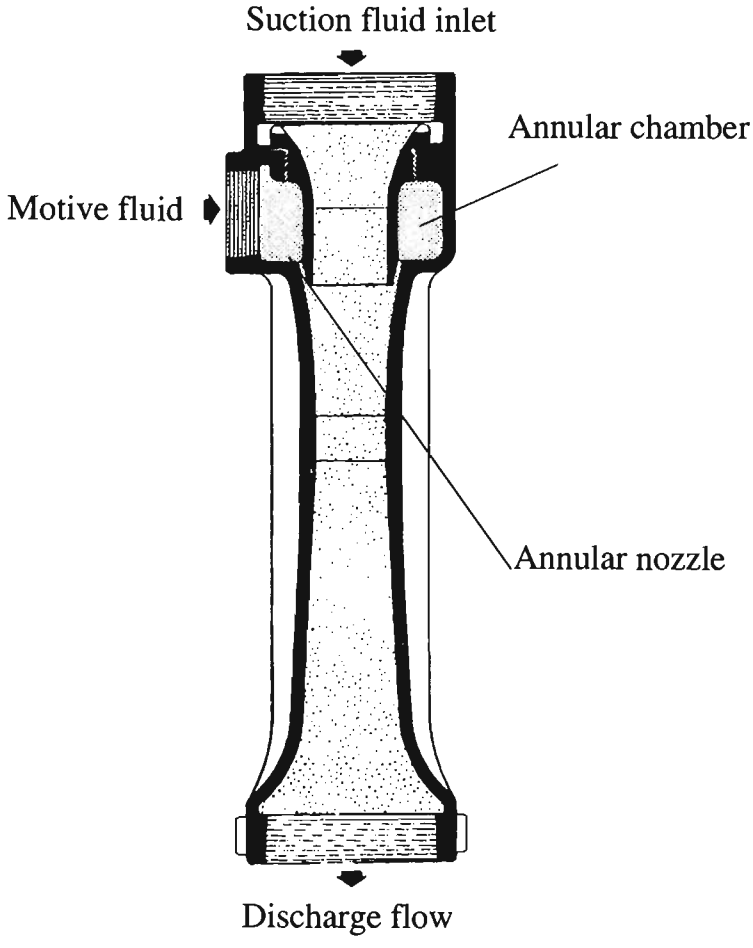

Fig. 2.16 Annular siphon (Schutte and Koerting Co.) [49]

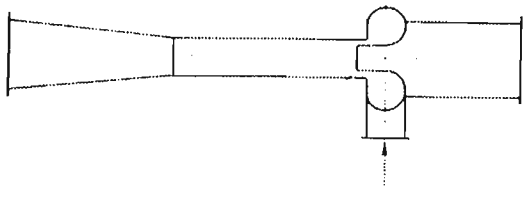

Fig. 2.17 Jet pump with ring-shape nozzle [29]

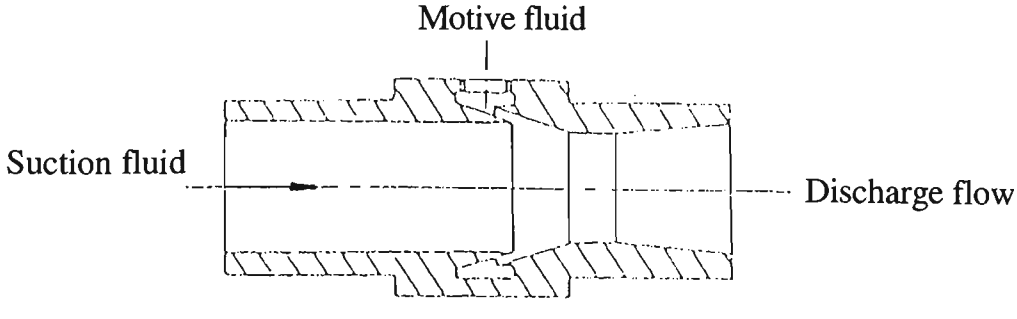

Fig. 2.18 Air mover ejector [73]

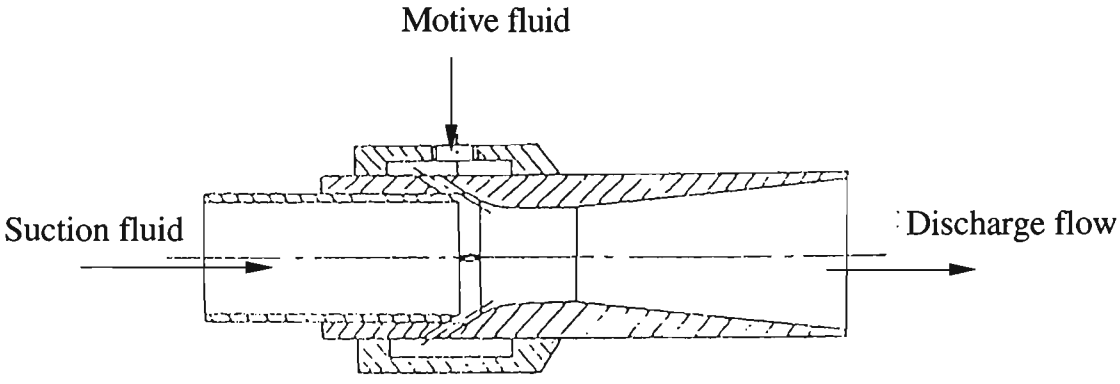

Fig. 2.19 PIAB ejector [73]

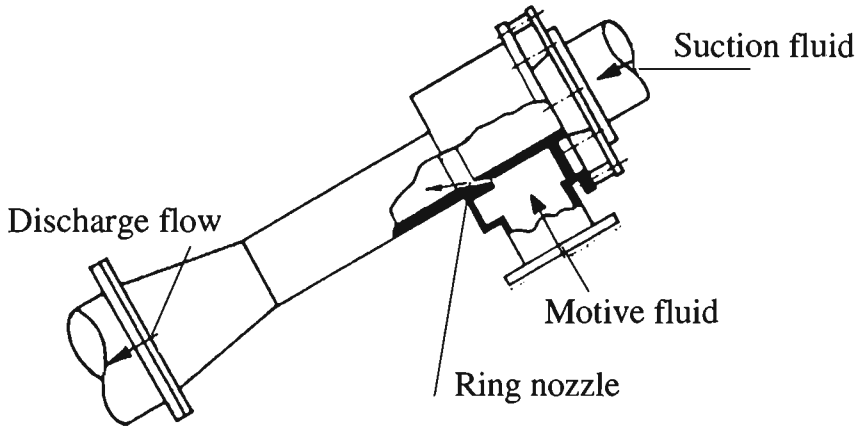

Fig. 2.20 Jet pump with ring nozzle [94]

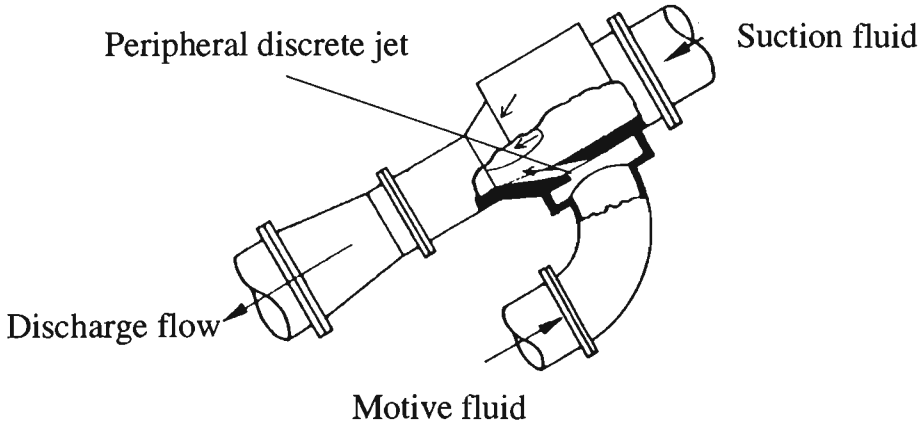

Fig. 2.21 Jet pump with peripheral discrete jet [94]

2.2.2.3 Multi-Nozzle Jet Pump

Fig. 2.22 shows a configuration of a typical central multi-nozzle jet pump. This type of jet pump can comprise from three to at least nine driving nozzles generally placed at the

corner of a grid of equilateral triangles. It has been reported that efficiency increases with the number of nozzles [84]. However, there are often practical limits to the number of nozzle for a given jet pump design.

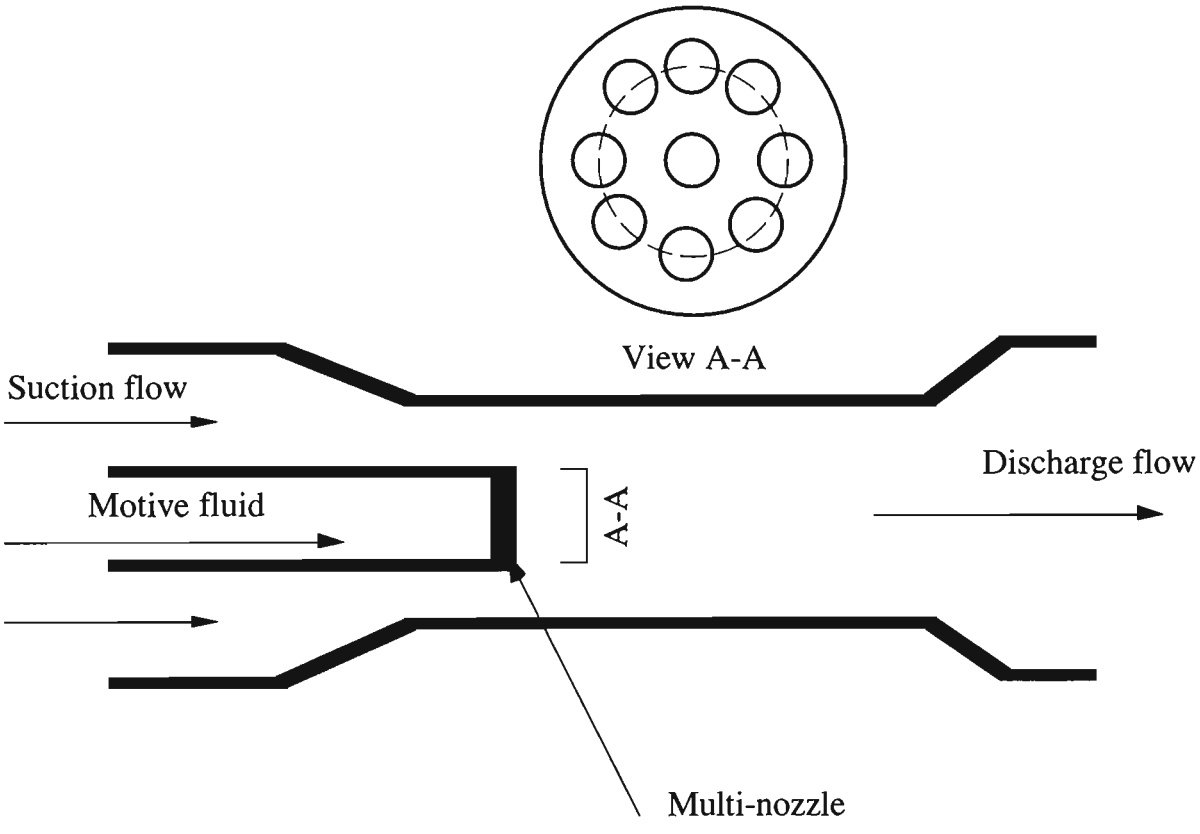

Fig. 2.22 General configuration of Multi-nozzle jet pump

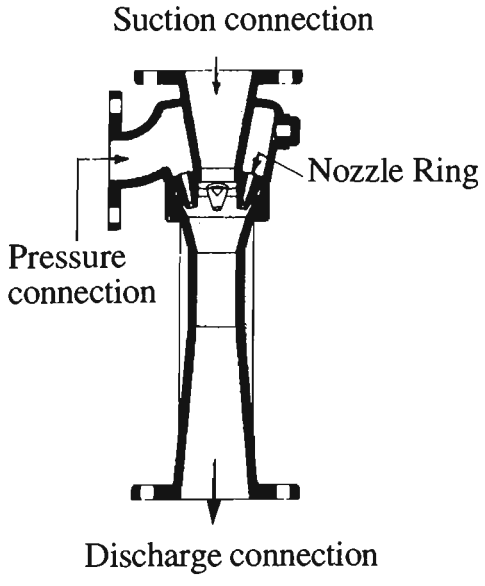

Fig. 2.23 Annular multi-nozzle eductor (Schutte and Koerting Co.) [49]

Figs. 2.23 and 2.24 illustrate some typical annular multi-nozzle jet pumps designed for special applications. In this type of jet pump, the motive fluid is introduced by holes distributed uniformly around a ring, and the suction fluid enters axially along the central passage. The manufacturers [49] refer to this type of pump as an annular multi-nozzle eductor.

A similar design simply referred to as an air pump, as shown in Fig. 2.24, has been produced by J. S. Melbourne and employed in pneumatic conveying installations throughout Australia. The main feature with this type of pump is that the nozzles are angled to provide a helical flow pattern in the discharge pipe.

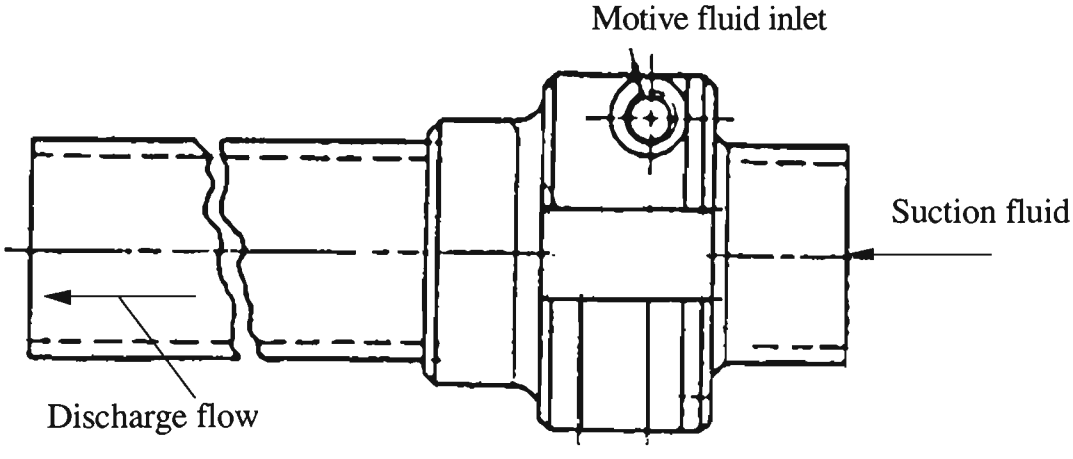

Fig. 2.24 General layout of air pump (J. S Melbourne Co.)

2.2.2.4 Proportioning Jet Pump

Figs. 2.25 and 2.26 illustrate typical spindle-type proportioning jet pumps. This type of jet pump also is called a spindle proportioning eductor [49]. The difference in structure between the spindle proportioning and conventional jet pumps is that the former consists of a spindle nozzle, the necessary sealing and adjusting device. The proportioning jet pump possesses the capability of adjusting performance characteristics by moving the spindle back and forth manually or automatically to suit the operating conditions [99]. In critical applications, the regulating spindle is sometimes fitted with a diaphragm actuator to achieve close control [90].

Fig. 2.27 shows an adjustable nozzle which contains a preset air mass flow regardless of downstream pressure fluctuations. It has been reported [30] that the main application of an adjustable nozzle is in pneumatic conveying to enable a number of conveying systems to be supplied from a single compressor. Another advantage claimed is that the breakage of fragile material is reduced or eliminated by the use of minimal air flow and velocity [30].

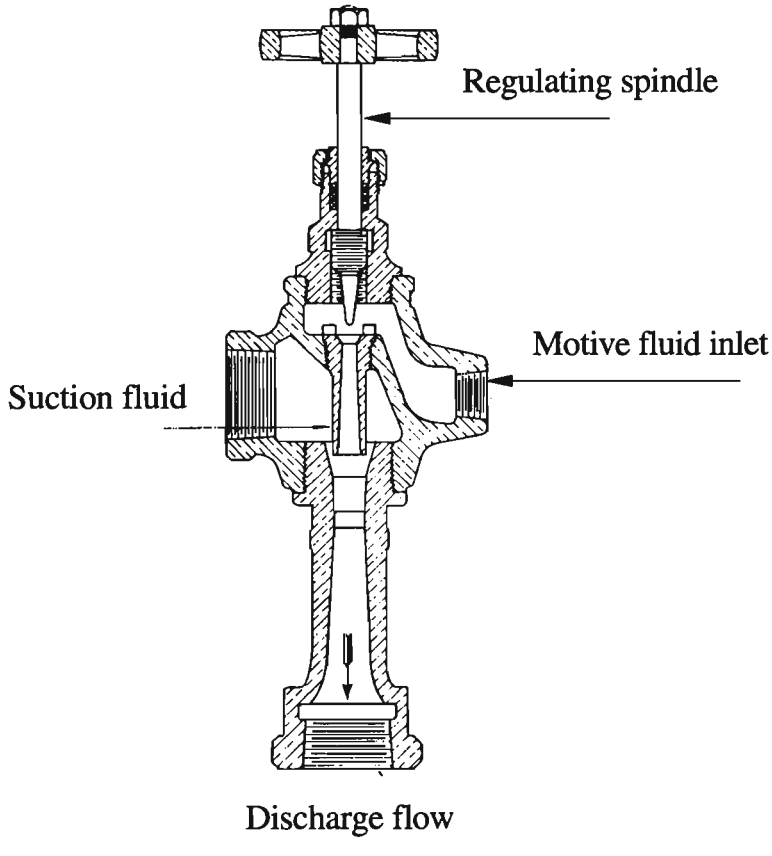

Fig. 2.25 Steam primer (Schutte & Koerting Co.) [52]

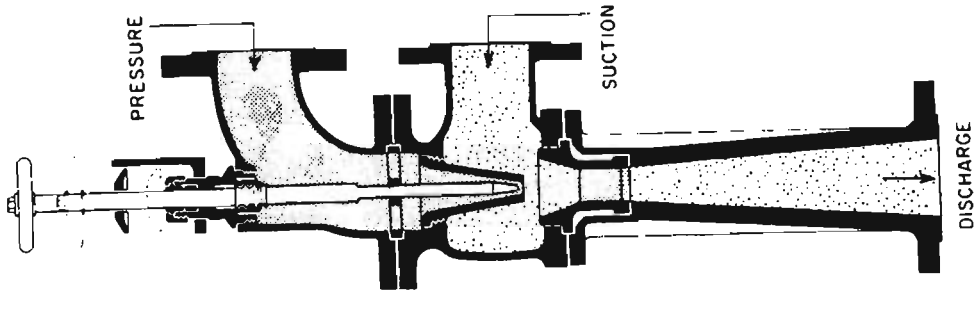

Fig. 2.26 Proportioning eductor (Schutte and Koerting Co.) [49]

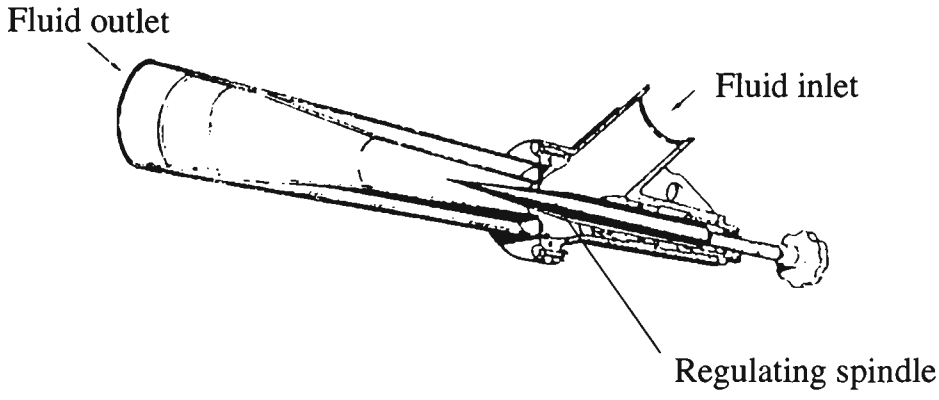

Fig. 2.27 Adjustable nozzle [30]

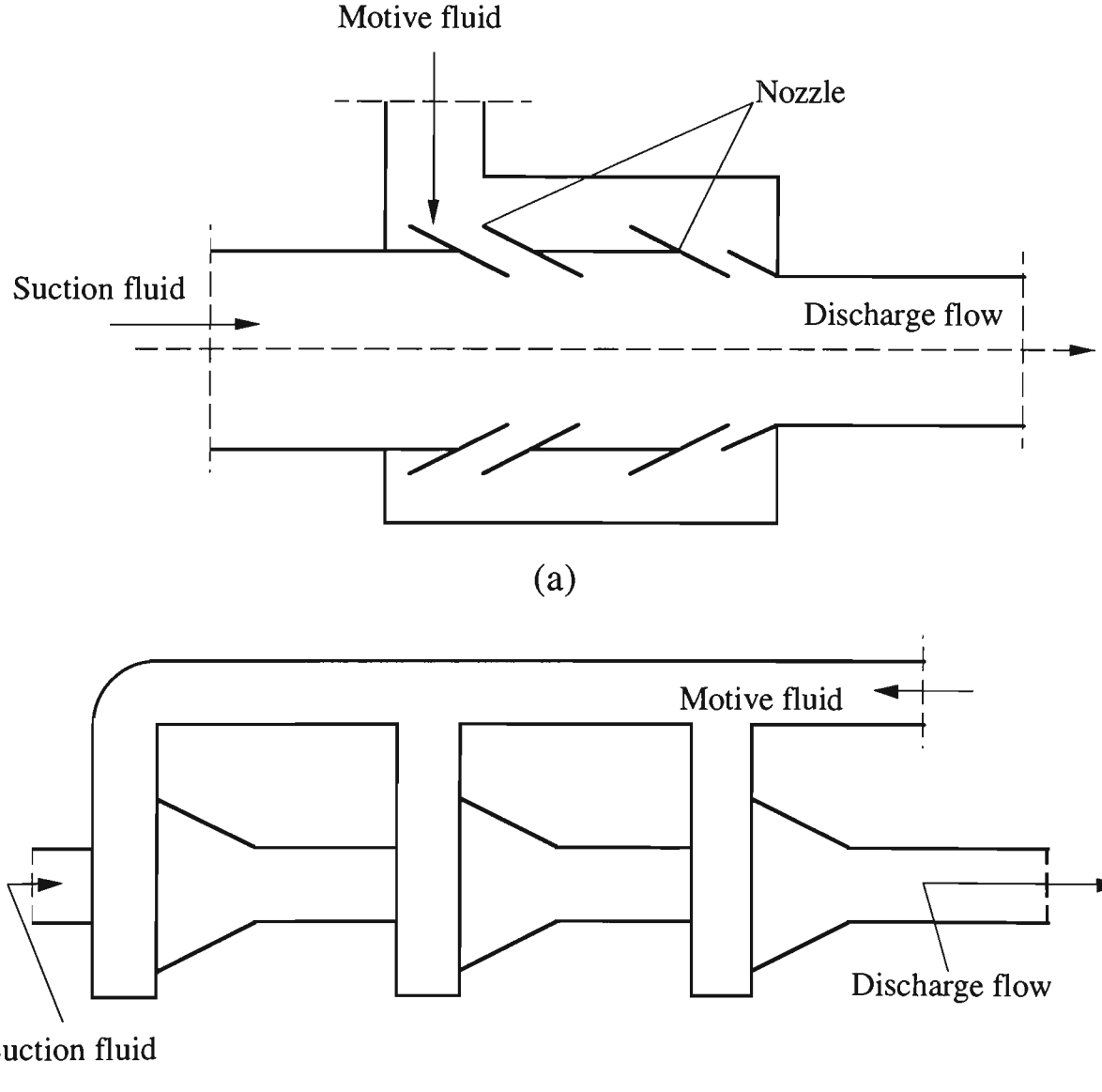

Fig. 2.28 Simplified sketches of two patented jet pumps

(a) from U. S. Patent 38576511 [17]; (b) from U. S. Patent 4028009 [42]

2.2.2.5 Multi-stage jet pump

Fig. 2.28 shows two examples of jet pumps which use multiple injection ports. This type of jet pump can't be included in the annular multi-nozzle category because it can be separated into different jet pumps with no diffuser.

2.2.2.6 Bi-Dimensional Jet Pump

Bi-dimensional jet pumps comprise motive slots or nozzles in line. It has been reported [84] that their performance can be similar to central multi-nozzle jet pumps with an equivalent space distribution of nozzles in the inlet of the throat tube [84]. Fig. 2.29 shows a jet pump containing flat jet, which is quite different from the shape of the conventional jet pump nozzle. A convergent nozzle has been used [59] to create a flat fluid jet providing a larger capture area for entrainment of suction fluid.

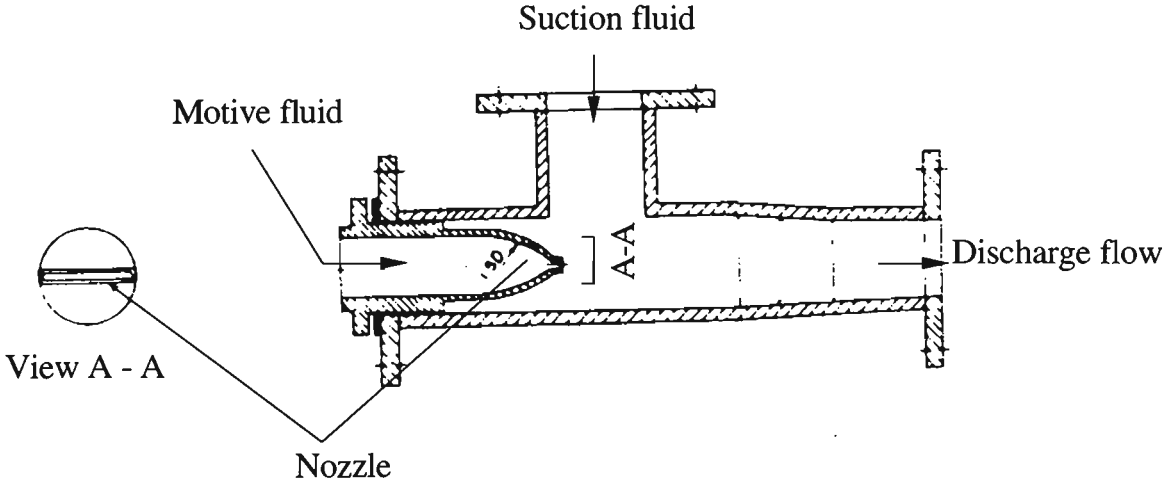

Fig. 2.29 Flat jet pump [59]

2.2.2.7 Differences between Jet Pumps and Venturi Feeders

The venturi feeder (also called venturi injector [72]) is one of the simplest feeding devices in the fluid transportation of solids. Fig. 2.30 shows a basic design of venturi feeder which consists of a contracting region so arranged that high-velocity fluid passing through the throat creates a region of low-pressure. It has been reported [89] that for the injection of large quantities of material, the desirable configuration is a two-dimensional

venturi, as shown in Figs. 2.31 and 2.32. Such a design eliminates flow separation and permits the introduction of solids at the throat followed by mixing and acceleration of the solids and diffusion in the diverging section which recovers some of the static pressure of the mixture. Strictly speaking, venturi feeders operate on the well-known Bernoulli principle, which is quite different from the operation principle of jet pump/ejector illustrated above. For this reason, venturi feeders are not considered in this study.

One of the main differences in structure between the jet pump and venturi injector is that the jet pump consists of a nozzle followed by convergent throat entry, cylindrical throat tube and a diffuser, whereas a convergent-divergent nozzle concept is used in a venturi feeder. Also, the throat tube in a jet pump usually is much longer than that in a venturi. In terms of operation, suction fluid/solid enters through the suction chamber in a jet pump, while a venturi feeder has no additional nozzle, and the suction flow/solid enters at the throat.

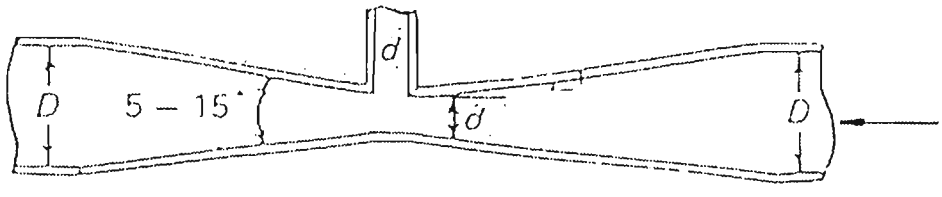

Fig. 2.30 General view of venturi feeder [72]

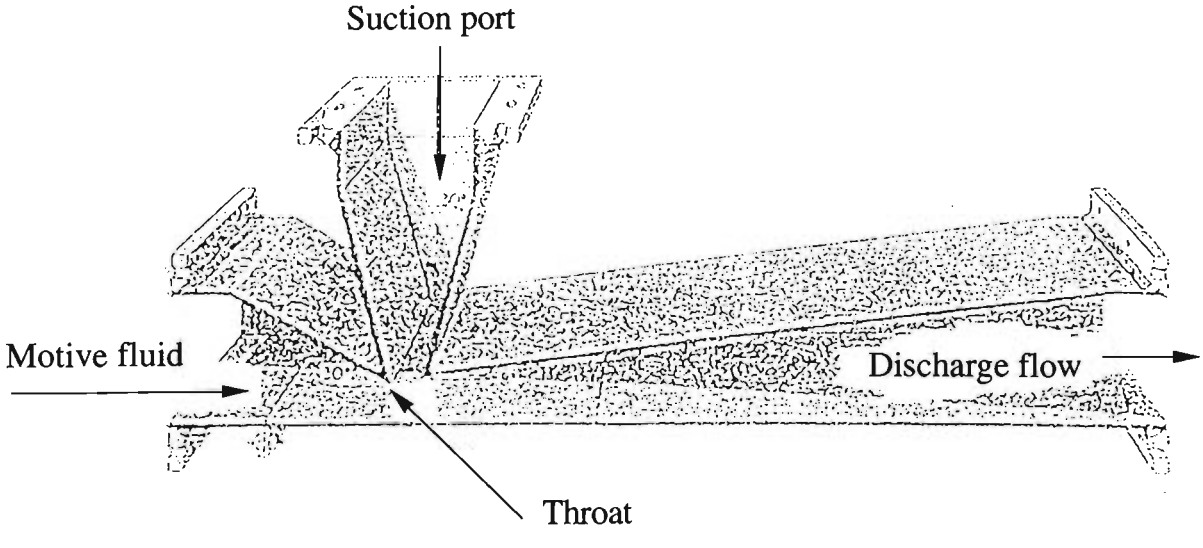

Fig. 2.31 Duct venturi feeder [40]

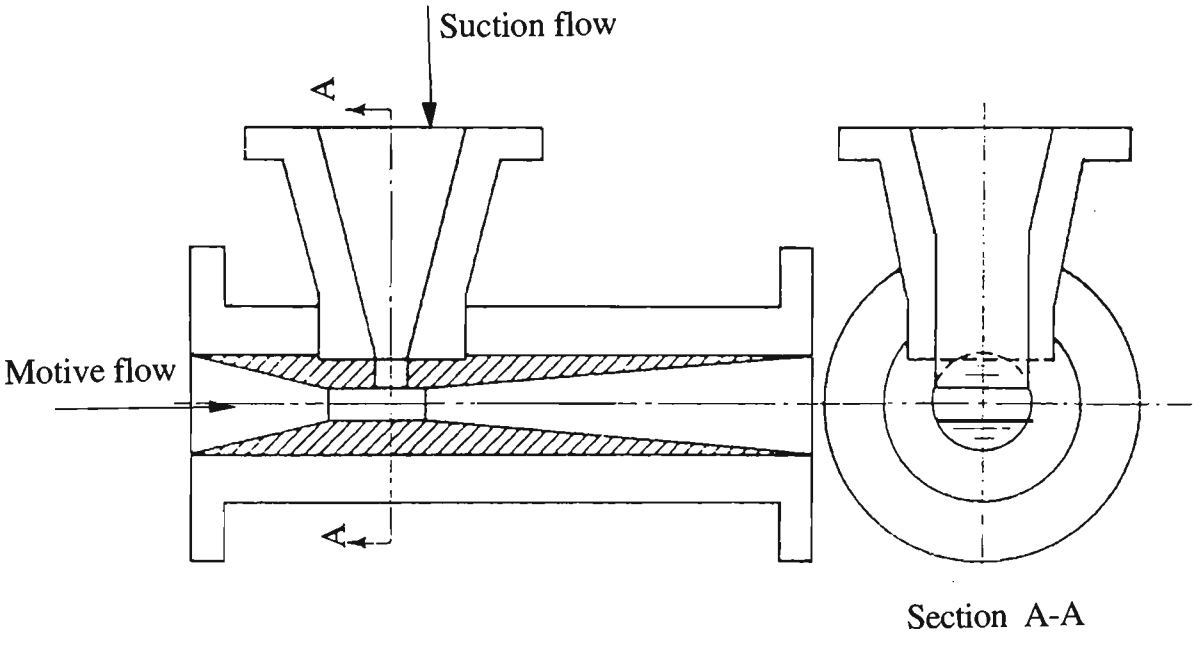

Fig. 2.32 Two-dimensional Venturi Injector [89]

2.2.3 Jet Pump Terminology

Due to the development and improvement of jet pump design over time, different names even for the same type of pump continue to appear in manufacturers' catalogues and engineering literature. This often causes confusion over the understanding and use of jet pumps in engineering practice. Hence, consistent terminology on jet pumps is imperative. Up to now, there are no industrial standards available that define the terms used to describe the various types of jet pump. A definition of terminology relating to jet pump was given as follows [49]:

Ejector General name used to describe all types of jet pump which discharge at a pressure intermediate to the motive and suction pressures.

Eductor A jet pump using liquid as the motive fluid.

Injector A particular type of jet pump which uses a condensable gas to entrain a liquid and discharge against a pressure higher than either the motive or suction pressure.

According to the above definition, the term jet pump or ejector could be used for pneumatic conveying applications. However, most of the names in the literature (such as eductor, venturi eductor, gas-solid injector and venturi injector) that are used to describe feeding devices in pneumatic conveying applications are contradictory to the definition given above. Due to the resulting confusion, it appears that a consistent terminology is required. For example, the term eductor should be used to describe jet pumps using water or another liquid (but not compressed air) to convey solids; air-jet pump or ejector instead of injector should be used in pneumatic conveying applications because injector is a specific term referring to the jet pump using condensable gas as motive fluid; Also, the term of venturi injector should be replaced by venturi feeder in order to avoid confusion over the specific meaning or purpose of injectors. Furthermore, venturi eductor is a confusing name. Jet pumps also should be distinct from venturi feeders, due to the differences in structure and operation discussed in Section 2.2.2.

From the jet pump classification given in Section 2.2.1, the name of jet pump comes mainly from the nozzle geometry and arrangement, and the state of motive fluid. Therefore, it is suggested that a standard name should refer to the geometry and arrangement of the nozzle, the states of motive and suction fluid, and the main application area. The state of suction fluid may be omitted where the motive fluid and suction fluid are the same kind (for example, both motive and suction fluid are air). In accordance with this suggestion, the standard names of various jet pumps used in pneumatic transportation are listed in Table 2.1. Even so, it is extremely difficult to formulate an international standard of jet pump terminology used in the field of fluid transportation of solids.

Table 2.1. Suggested names for miscellaneous designs of jet pump

Suggested Names	Frequently Used Names	Suction Fluid	Geometry of Nozzle	Examples
central air-jet air pump	air injector pneumatic ejector air-air jet pump	air	central single nozzle	Fig. 2.1 to Fig. 2.8 Fig. 2.11
central multi-air-jet air pump (ejector)	multi-nozzle jet pump	air	central multi-nozzle	Fig. 2.22
central air-jet solid pump	venturi injector feed venturi gas/solid injector injector feeder pneumatic ejector flow nozzle, jet pump Venturi eductor	bulk solids	central single nozzle	Fig. 2.1 to 2.11
central multi-air-jet solid pump	multiple nozzle ejector	bulk solids	central multi-nozzle	Fig. 2.22
annular air-jet air pump	annular jet pump	air	annular slot nozzle	Fig. 2.18
annular multi-air-jet pump	air pump	air	annular multi-nozzle or multi-hole in ring	Fig. 2.23, Fig. 2.24
annular air-jet solid pump	vacuum aerated feed nozzle air mover ejector	bulk solids	annular slot nozzle	Fig. 2.18 to 2.21
annular multi-air-jet solid pump	air pump snow pump	bulk solids	annular multi-nozzle or multi-hole in ring	Fig. 2.23
bi-dimensional air-jet solid pump	bi-dimensional ejector	bulk solids	bi dimensional slot nozzle	Fig. 2.29
adjustable air-jet air pump	proportioning ejector	air	adjustable nozzle	Fig. 2.25, Fig. 2.26
adjustable air-jet solid pump	adjustable ejector	bulk solids	adjustable	Fig. 2.25, Fig. 2.26

2.3 Experimental Investigations

A few experimental investigations into the air-jet pump have been carried out over the past 2 decades. These investigations mainly have concentrated on the applications in industry and the influence of geometrical configuration on jet pump performance.

2.3.1 Development of Air-Jet Pump Application in Industry

Jet pumps for generating vacuum and pumping liquids have been commercially available and widely marketed in a broad range of materials for about six decades. However, air-jet pumps have never been considered seriously as a component in pneumatic conveying

systems until the 60's and 70's [36,38]. Over the past two decades, air-jet pumps have received increased attention in investigation and development efforts. As a result, a wide range of different jet pump designs and associated systems have been developed. Air-jet pumps for pneumatic conveying of powders and bulk solids have been commercially available [38] and applied in an enormously broad range of industries with considerable success [19, 36, 37, 40, 73, 80, 94, 108]. Using air-jet pumps, a very broad spectrum of granular materials has been conveyed, and numerous pneumatic conveying problems have been solved [36, 37, 58, 70]. The application of air-jet pumps throughout industries as diverse as food, plastics, petrochemical, mining and power generation has increased dramatically in recent years. For example, an air-jet pump for the extraction of cement from hoppers and its transportation over distances up to 150m was developed and manufactured in the U.S.S.R. in 1973 [19]. The capacity was up to 52 tonnes/hr, with a lift of 17 to 30m. The air consumption was 25 to 30m^3 of free air per minute at a pressure of 3 to 4 atm. The transporting pipeline was 150 to 200 mm in diameter. Operating performance was given but no generalised design method was reported.

A system for the pneumatic transport of dust using a central-jet pump was developed [70]. In this system, dust travelled from a hopper to the jet pump; the jet pump discharged a dust-air mixture along the pipe into a cyclone heat exchanger. The motive air pressure for the jet pump was 290 to 310 kPag and the nozzle diameter was 14 mm. The design of the jet pump made it possible to pneumatically transport hot dust with a relatively high density (2800 kg/m^3) over a considerable vertical distance (more than 50 m). It was possible to achieve a dust conveying rate of 1490 kg/hr using this system.

The application of a central-jet pump to the pneumatic conveying of copper strip waste was investigated experimentally [58]. A jet pump operating at a motive pressure of 600 kPag was used to feed strips from a vibratory feeder via a wide mouth funnel. A conveying rate of 1200 kg/hr was achieved. The jet pump allowed free passage of the strips, while producing a delivery pressure at its outlet. It was reported [58] that the jet of

air from the nozzle could entrain up to 110% of the motive air supply, through the suction port. The entrained air resulted in a very high velocity in the throat, which accelerated the strips before loading them into the pipeline.

The collection of oily fly-ash from electrostatic precipitator hoppers often causes problems in electric utility stations. An air-jet pump system for handling this material was applied at Long Island Lighting Company's North port station in U.S.A. to solve this problem [78].

To reduce energy consumption, an annular air-jet pump, named Conjector, was developed and placed on the market [108]. This type of jet pump was specially designed to operate under Roots-type blower air conditions (i.e. motive air pressures not exceeding 80 kPag) for dilute phase conveying over short distances. Some claimed applications included:

- conveying vulnerable, abrasive, cohesive, corrosive or fibrous products;
- conveying products at low flow rates (up to approximately 4000 kg/hr) with limited system back pressure;
- discharging materials from bins, bag slitters and hoppers, where lack of space prevents positioning of conventional equipment (e.g. rotary feeder).

To control erosion, another innovative design of annular air-jet pump based on the vortex effect (see Fig. 2.24) has been produced by J.S. Melbourne Controls, and used successfully in several pneumatic conveying applications over recent years.

Jet pumps can be combined with a pre-dosing device, such as a rotary valve, screw or vibratory feeder, etc. Using air-jet pumps instead of rotary valves in pneumatic conveying systems to reduce wear has been developed and applied successfully in industry [36-38].

The advantages of using air-jet pumps in place of, or in conjunction with rotary valves are:

- By placing an air-jet pump directly beneath a rotary valve, a negative pressure is produced and pulled across the air-lock, completely eliminating the problem of air leakage (also called blow back). Instead of air attempting to leak out through the rotary valve, a strong suction effect drowns particulate, even the finest particulate, from the hopper into the conveying pipeline;

- For the system which does not require the volumetric metering of a rotary valve, the airlock can be eliminated entirely. In this situation, the high maintenance, high-cost and low-reliability air-lock (especially on abrasive products) can be replaced with an effective substitute that has no moving parts.

2.3.2 Influence of Geometrical Configuration on Performance

The performance of two-stream flows through jet pumps has been the subject of on-going research since the turn of this century. A basic understanding of the underlying phenomena is vital to the design and application of jet pumps and associated systems. In order to obtain the best designed air-jet pump system to meet a specific requirement, a command of the influence of geometrical configuration and operating conditions on pump characteristic is necessary. Hence, numerous experiments were conducted to ascertain the effect of geometrical factors on jet pump characteristics [2, 39, 41, 47, 48, 50, 54]. These geometrical factors include length and shape of throat tube, length and shape of diffuser, nozzle-throat gap, configuration of nozzle and the ratio of cross-sectional area of throat tube to motive nozzle. Most of these investigations were undertaken under air-only flow conditions. If the pressure and velocity were sufficiently low to avoid compressibility effects, the results from experiments on air jet pump could be compared with those obtained by using water as the test fluid [53]. The results from comparing the

influence of geometrical factors on air-only performance with that on water jet pump performance are summarised below:

- Throat Tube Shape

Most of the experimental research work on air-jet pumps and water jet pump appears to support the contention that using a constant-area throat tube followed by a conical diffuser achieves a higher efficiency than that obtained using a variable area throat tube [55, 57]. However, arguments also exist that using a variable area throat tube (for example, a convergent-divergent venturi tube or a conical throat tube) can improve efficiency [32, 45].

- Throat Length

Many experimental results show that a throat tube length of 6 to 8 diameters of throat tube is optimal for a central air-jet pump with constant-area throat tube [2, 53, 54], which agrees with the results from water jet pump tests [14-16, 18, 96]. However, some experiments illustrate particular cases where an increase from 7 to 14 diameters of throat tube was necessary to produce fully-developed pipe flow [21], and a reduction to 5.6 diameters gave a small increase in peak efficiency for water jet pumps [81, 82]. The influence of Reynolds number on throat length also was investigated and can be found in reference [8].

It was found that maximum efficiencies of annular jet pump were obtained at throat length of 3.5 to 4 diameters [47, 87].

Practical demonstrations that the mixing length can be reduced by using multiple nozzles have been performed by different researchers [32, 44, 51, 63, 85]. A theoretical analysis of multiple nozzles ejectors has been covered in reference [3], and the extent to which single jet research might be applied to multi-jet configurations has been examined in [32]. The optimum throat length for central nozzle, multiple nozzle, annular nozzle, annular

multi-hole and adjustable nozzle pumps also have been investigated experimentally [96]. It has been proved that using annular nozzle, annular multi-nozzle, and multiple nozzle can reduce the throat length of the jet pump. For adjustable jet pumps, the optimum throat length is of the same order as that of a central jet pump [97-99].

- Nozzle-Throat Spacing

Nozzle-throat spacing is defined as the distance between the outlet of nozzle and the inlet of the throat, represented by L_c as shown in Fig. 4.5. A larger nozzle-throat spacing enables the motive and suction streams to be parallel at the entrance of the throat. For a particular throat tube configuration, the mixing efficiency increases with nozzle-throat spacing and reaches an optimum value; with a further increase in nozzle-throat spacing, efficiency decreases [61]. Although this is not a particularly critical parameter (wide tolerances are possible without serious loss of efficiency [43, 54]), the optimum spacing of 1.57 throat diameters has been reported [48]. For the fluid transportation of solids, the nozzle-throat spacing should be greater than the throat diameter in order to avoid blockage in the throat entry [65].

Some tests on jet pumps with a bell-mouth entry to the mixing tube from a larger suction chamber tends to show an improvement in efficiency from the use of a relatively large nozzle-throat spacing [83]. Mueller also shows that the inlet shape of throat influences the optimal nozzle-throat spacing [69]. It has been shown that the optimal nozzle-throat spacing should be a function of the throat length. Shorter throat lengths require larger spacing of the nozzle exit from the throat entrance, and longer throat lengths require shorter nozzle-throat spacing to avoid extra mixing losses in the jet pump [83, 96].

- Nozzle Geometry

Nozzle geometry affects the optimal throat length. Multiple nozzle and annular nozzle will have shorter throat length, and permit the design of more compact units [32, 44, 47]. It

has been reported by considering the comparative change in the efficiency of various jet pump designs that central single nozzle jet pumps cover a vast domain of the ratio of suction flowrate to motive flowrate according to their manufacturers, but have the poorest performance; they are followed by annular jet pumps without diffusers, and then multi-nozzle, bi-dimensional nozzle and annular jet pumps with diffuser whose performances are rather similar [84]. Unfortunately this opinion has not been confirmed by other experimental results. Quite opposite results have been presented in [96]. The difference might result from whether the jet pump designs used in experiments are optimised or not. It has been shown that jet pumps with adjustable nozzles have better performance and higher efficiency compared with that of central single nozzle jet pumps [94, 97, 98]. Also, it has been shown that fitting helical vanes in the motive nozzle of an annular jet pump might improve the air-only efficiency over certain parts of the flow range [5].

Although different results and trends exist, it is clear that the design of the nozzle is one of the most important factors influencing the efficiency and the performance of the jet pump.

- Diffuser

The diffuser is a gradually diverging passage which converts the kinetic energy of a mixed stream to potential energy. For a given area ratio of diffuser outlet to inlet, the losses due to separation increase as the angle increases, but the length of diffuser also increases and the friction loss increases correspondingly as the angle decreases. Thus there is an optimum conical angle for a given area ratio. It has been shown that the optimum conical angle was in the range of 5° to 10°, and increased with motive pressure [54]. It also has been reported that the flow behaviour in the diffuser will not affect considerably the flow in the throat tube [48]. This is true only where separation of fluid from the wall of diffuser does not occur.

- Swirl Component of Motive Jet

Energy exchange between the motive jet and the suction flow, namely the mixing of two streams, is important for improving efficiency. In the case of the annular jet pump, the effect of the swirl component on performance has been tested [87]. It has been reported [87] that remarkable differences are not seen through the addition of the swirling component. For pumps with a reducing passage at the throat entrance, a weak swirl component in the motive jet does not affect efficiency, and only a small change occurs at medium swirl. In comparison, an intensive swirl reduces the efficiency and provokes flow instability. This phenomenon may be explained from the view point of an increase of the flow rate due to the reduction of the boundary layer thickness in the converging or straight part of the pump and the degree of energy loss with a weak or intensive swirl. Another experiment supporting this result can be found in [96].

Despite a wealth of excellent experimental work, the present knowledge of the fundamentals of air-jet pump characteristic is rather incomplete. For example, although it has been clearly shown by experimental investigation that jet pump geometrical factors have a great influence on air-only jet pump performance, there are some uncertainties of how the geometrical designs actually influence jet pump performance, especially for jet pumps with annular nozzle and multi-hole ring nozzles.

To date, only a few experimental investigations cover the influence of geometrical factors on air-solids performance. Chellappan and Ramaiyan [20] carried out an experimental investigation into the influence of jet pump geometry on the mass flow rate of solids for a given delivery pressure (discharged to atmospheric). They used wheat as the test material and varied nozzle-throat gap, throat tube length and the contracting angle of throat entry. Useful trends between the ratio of mass flow rate of solids to motive air and the distance between the nozzle outlet and the throat entry inlet F as shown in Fig. 4.5 were reported to illustrate the effect of geometrical parameters. It was found that a combination of the throat length of 7 to 9.5 diameters of throat tube, 15° of the semi-contracting angle of throat entry, 2° of the semi-diverging angle in diffuser and a proper nozzle location (as

shown in Fig. 4.5, F = 10 to 15 mm) is optimal in terms of maximising mass flow rate of solids for a given motive flow condition.

The effect of geometrical designs and operating parameters on air-solids performance of the jet pump also has been investigated experimentally by Dawson et al. [28]. The principal difference between these two experimental works is that the latter artificially induced a back pressure in their experiments. The experimental data were presented by means of plotting solid mass flow rate with respect to the delivery pressure (at jet pump exit). It can be seen from these plots that the solid mass flow rate decreases as the delivery pressure increases. An optimum value of throat length between 0 and 3 diameters of throat tube was obtained, which conflicts that reported in [20]. Argues also exists on the influence of the semi-diverging angle of diffuser. It was reported that not much difference was observed while varying the semi-conical angle from 3°, 5° to 7° [28].

A comparison between a central air-jet pump and annular air-jet pump of different geometrical designs was made experimentally by using 76 mm conveying pipeline [26]. It was observed that the central air-jet pump is more energy-efficient than the annular air-jet pump in terms of power consumption per unit solids mass flow rate at a specific delivery pressure.

Fox [36] reported data collected from the actual performance of proprietary design eductors in industrial installations with pulverised and coarse coal, plastic pellets and talc. Experimental data obtained from a jet pump with a 33.3 mm throat diameter on a few different products were reported by Wagenknecht and Bohnet [10]. Pittman and Mason [73] reported some graphical information on the flow rate of product against the volumetric flow rate of air supplied for different bulk materials and pipe lengths, and illustrated some of the many different air-jet pump configurations for solids conveying.

Westaway [101] reported comprehensive sets of experimental data encompassing a wide range of operating conditions with many different products tested.

Table 2.2 summaries the main jet pump dimensions and system configurations used in experimental investigations into air-jet pumps under air-solids flow conditions.

It can be seen from Table 2.2 that the experimental investigations into the effect of geometrical parameters and operating conditions on the performance of jet pumps subjected to air-solids flow still are very limited. The major limitations are stated briefly below:

- The influence of nozzle-throat gap on air-solids performance were only investigated under atmospheric discharge with both constant and variable solid mass flow rate.
- All of the experimental investigations were undertaken at constant motive mass flow rates for motive pressures less than 100 kPag, with only a few trials looking at the effect of varying motive pressure. No optimum value of the motive pressure for a given conveying system design has been obtained.
- There exists conflict between the optimum throat lengths obtained by different researchers. Also, the optimum throat lengths were obtained under limited variation in operating conditions.
- There seems to exist a void in examining the effect of area ratio on air-solids performance. Based on the results obtained from the investigation into the performance of jet pumps under single-phase flow conditions (e.g. water or air) [48, 81, 83, 96, 120], area ratio is seen to play a vital role on performance. In terms of the flow area ratio of throat to motive nozzle, most of the experiments were carried out within the ratio range 2 to 6, except for the trials using an area ratio of 10.9, 16 and 25.7 for a motive pressure of 68 kPag. Furthermore, no optimum area ratio for a given operating condition has been investigated for pneumatic conveying.

Table 2.2 Summary of experimental investigations into air-solids performance of air-jet pumps

Reference	Material(s)	β (deg)	d_n (mm)	d_0 (mm)	d_t (mm)	d_5 (mm)	L_t/d_t	D (mm)	L_p (m)	M_a (kg/s)	F (mm)	p_0 (kPag)	θ (deg)	m	Comments
[20]	wheat	15.7 14.2 11.9 10.0 7.9	10	50		28	4.7 6.3 7.9 9.5 11.0	28	35	0.0294	0 3 8 13 18 23		3.6 3.0 2.4		central jet pump; discharging to atmosphere;
[28]	casein beach sand polystyrene polypropylene	const.	21 15 19 23		34.5 41 54 76		0 3 6 9	76. 2		0.1 0.065	25	 68	3 5 7	2.7 3.8 6.6 13.1 10.9 16 25.7	central jet pump; varying delivery pressure; the value of m was calculated by the present author;
[10]	polyethylene cement etc.	20	20		33.3	52.5	1~4	50	7	0.03~0.08	0~80	< 20		1.2~4.9	constant mass flow rate of solids
[101]	PVC powder long grain rice coarse sand iron powder		20.1 26.7 31.8 37.6	2, 3 and 4 inch Fox type eductor designed and manufactured by Fox Valve Development Corp.				98. 4 73 47. 6	66 49 30. 6			20~90			central jet pump; discharging to atmosphere;
[26]	maize wheat Dune sand magnate casein		0.64 0.89 1.17 1.42 1.65		50					0.1 0.15		36 81.5 58 25.5 16.5	3		annular air-jet pump; varying delivery pressure; d_n means slot width of annular slot nozzle here.
[36]	plastics, coke etc	Not reported													atmospheric discharge

- Some experiments were undertaken by connecting the jet pump to different conveying pipeline systems under atmospheric discharge, so as to examine the influence of conveying pipeline configuration on the mass flow rate of solids from the jet pump and to formulate a scale-up procedure for jet pump conveying systems similar to that for conventional pneumatic conveying pipelines. This work involved a lot of unnecessary repetition to the work conducted in the research on pneumatic conveying pipeline systems. Also, the representation of pump performance in terms of solid mass flow rate with respect to motive pressure for a particular pipeline system results in significant difficulties in the scale-up of such experimental results to other systems. Actually, the air-solids flow at the jet pump exit has the same behaviour as pipe flow in conventional pneumatic conveying pipelines. Hence, to benefit from the numerous results obtained from the investigations into air-solids flow in pneumatic conveying pipelines, the best approach to investigate the air-jet pump performance for pneumatic conveying purpose is to concentrate on the relationship between solid mass flow rate and the delivery pressure at the jet pump exit, as that adopted by Dawson *et al.* [28].

- All the experimental investigations into factors affecting air-solids pump performance were concentrated on central air-jet pumps, and there is very little research into annular air-jet pumps. Also, it is believed that no experimental work exists on the air-solids performance of an annular air-jet pump with a multi-hole ring nozzle.

Therefore, to determine a strategy for improving pump performance and develop a reliable design theory for practical pneumatic conveying applications, it is necessary to undertake extensive experiments and research on the influence of geometrical designs and operating conditions, especially the influence of area ratio, nozzle-throat gap and motive pressure.

2.4 Performance Prediction Model

2.4.1 Air-Only Performance Prediction

Most of the air-only jet pump performance prediction models have been developed based on one-dimensional mass, energy and momentum balance and the ideal gas law [31, 34, 55, 91, 109] or based on dimensional analysis to relate the secondary mass flow rate with other variables [68]. The performance of multi-nozzle jet pump can be predicted by means of a model using an equivalent central air-jet pump [3]. Fairly close agreement has been shown between the air-only performance predicted by using the above approaches and the measured results. The above approaches have been used successfully in conjunction with experimental results for designing air-only jet pump and associated system.

A radical departure from the above approaches was based on turbulent flux equations of conservation of mass, momentum, turbulent energy and turbulence dissipation to predict two-dimensional axisymmetric jet-pump flows. For example, Croft and Lilley [22] employed this approach to model the performance of a central jet pump. The numerical techniques involved a staggered grid system for axial and radial velocity, a line relaxation procedure for efficient solution of the equations and a two-equation turbulence model (also known as κ-ε model). The analytical results obtained from this approach permit the explanation of the mechanism of mixing between motive and secondary fluid. A similar procedure was applied to analysing the detailed performance of a two-dimensional air-jet pump with a symmetrical variable area mixing section and co-axial converging motive nozzle [41], and the flow characteristic in an air-jet pump diffuser [71]. However, at the present time, the necessary computer solution by using finite difference, finite element or other mathematical method is more suitable for research than direct engineering design.

2.4.2 Air-Solid Performance Prediction

Because of the complexity of two-phase (air-solid) flow, a mathematical solution to the general fluid dynamics problem of air-solid flow in an air-jet pump has been a forbidden task for several decades. Preliminary attempts have been made to extend the model for air-jet pump performance based on integral momentum equations to study the momentum-exchange process in a jet pump throat tube under air-solids flow condition, such as [33], which involved a theoretical analysis supported by measurements of velocity and concentration distributions. Equations were developed to include the influence of solid material. The solids were assumed to be completely separate from the fluid with no interaction between them. An experimental rig for velocity and concentration measurements was built with provision to eject air into a pipe, which represented a jet pump throat tube. The secondary flow stream was air containing polystyrene beads of a mean diameter of 700 microns. It was shown that integral momentum equations are adequate for predicting the air-solids characteristic in air-jet pump throat tube if an appropriate allowance is made for the disparity between air and solids velocities.

Bohnet [10-13] derived a mathematical model using continuity and conservation of momentum to calculate the variation of static pressure along the jet pump with respect to the solids to air mass flow rate ratio and the particle velocity at constant solids flow rate. For a better understanding of this model and its difference with that presented in Chapter 3, the derivation of these equations is outlined below:

These equations correspond to three sections of the central air-jet pump, as shown in Fig. 2.33. The first section includes the suction chamber, throat entry and motive nozzle; the second section consists of the throat tube and the third section is the diffuser. In the first section, the motive air flow through the nozzle was considered by neglecting drag forces as

$$p_V = p_T + \frac{\rho}{2} w_T^2 [1 - (d_T / d_V)^4] \tag{2.1}$$

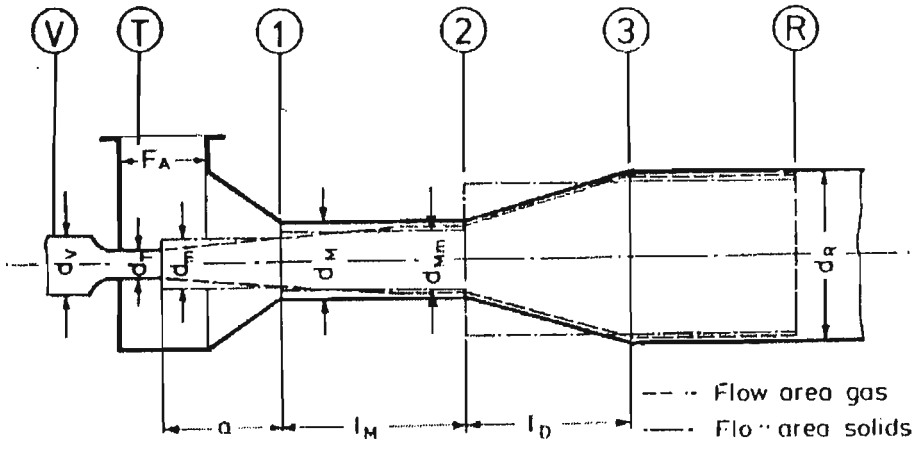

Fig. 2.33 Graphical depiction of analytical model presented by Bohnet [12]

The flow rate of air sucked in or blown out through the suction port was approximated by

$$\dot{M}_A = F_A \sqrt{2\rho(p_T - p_U)} \tag{2.2}$$

The velocity of air-solids mixture between the nozzle exit and throat inlet sections was assumed as an average value of motive air-jet velocity and air velocity in the throat tube, that is

$$w_m = (w_T + w_M)/2 \tag{2.3}$$

By assuming $\rho_m = (\rho_T + \rho_1)/2$ and $\dot{M}_m = (\dot{M}_T + \dot{M})/2$, where $\dot{M} = \dot{M}_T + \dot{M}_A$, the velocity w_m was expressed as

$$w_m = \dot{M}_m / (\rho_m F_m) \tag{2.4}$$

The average jet diameter d_m was calculated by means of

$$d_m = d_T d_M \sqrt{\frac{2\left(\dot{M}_T/\dot{M} - 1\right)}{\dot{M}_T/\dot{M}\left(1 + \rho_1/\rho_T\right)d_M^2 + \left(1 + \rho_T/\rho_1\right)d_T^2}} \tag{2.5}$$

The pressure difference between sections T and 1, as shown in Fig. 2.33 was considered as the result of the motive air-jet velocity decreasing from w_T to w_m by subtracting the

pressure losses required to accelerate the sucked air and the solids. A coefficient η_T was used to consider the energy losses occurring in the energy transformation of motive air flow. The expression was presented in the form of

$$p_1 - p_T = \frac{\rho_T}{2} w_T^2 \left\{ \eta_T \frac{(1+\rho_1/\rho_T)}{2} \left[1 - \left(\frac{\dot{M}/\dot{M}_T + 1}{1+\rho_1/\rho_T} \right)^2 \left(\frac{d_T}{d_M} \right)^4 \right] - \Delta p_1 \right\} \tag{2.6}$$

where $\Delta p_1 = \left[\left(\frac{\dot{M}}{\dot{M}_T} \right)^2 - 1 \right] \left(\frac{d_T}{d_M} \right)^4 - \mu \frac{w_{p1}}{w_T} \left(\frac{\dot{M}}{\dot{M}_T} + 1 \right) \left(\frac{d_T}{d_M} \right)^2$.

By using a similar method of analysis, the following equations were obtained.

$$w_{Mm} = (w_{m1} + w_M)/2 \tag{2.7}$$

where $w_{m1} = \dot{M}/(F_m \rho_1)$;

$$d_{Mm} = \frac{2 d_m d_{Mm}}{\sqrt{(1+\rho_2/\rho_1)(d_m^2 \rho_1/\rho_2 + d_M^2)}} \tag{2.8}$$

Introducing a coefficient η_M to allow for the energy loss due to the transformation of the kinetic energy of the motive air jet to pressure energy, and considering the pressure losses due to air-solid mixture flow in the throat tube as conventional air-solid two-phase pipe flow, an equation to calculate the pressure difference over the throat tube was obtained as

$$p_2 - p_1 = \eta_m \frac{\rho_{Mm}}{2} w_M^2 \left[\left(\frac{\rho_2}{\rho_1} \right)^2 \left(\frac{d_M}{d_m} \right)^4 - 1 \right] - \Delta p_2 \tag{2.9}$$

where $\Delta p_2 = \mu \rho_{Mm} w_{Mm} (w_{p2} - w_{p1}) - (\lambda_G + \mu \lambda_s) \frac{l_M}{d_M} \frac{\rho_{Mm} w_{Mm}^2}{2}$;

$$\rho_{Mm} = (\rho_1 + \rho_2)/2.$$

The pressure difference over the diffuser was calculated by

$$p_R - p_2 = \frac{\rho_R w_R^2}{2} \left\{ \eta_D \frac{(1+\rho_2/\rho_3)}{2} \left(\frac{\rho_R}{\rho_3} \right) \left[\left(\frac{\rho_3}{\rho_2} \right)^2 \left(\frac{d_R}{d_M} \right)^4 - 1 \right] + 2\eta_s \mu \frac{w_{pR} - w_{p2}}{w_R} \right\} \tag{2.10}$$

The solid particle velocity could be calculated by relating the drag force of solid particles to the mass of solid material and introducing the terminal velocity of the particles. The expression of the terminal velocity of the particle is

$$w_s = \sqrt{\frac{4}{3}\frac{g}{C_w}\frac{\rho_p - \rho}{\rho}d_p} \tag{2.11}$$

where the value of C_w can be obtained from [13].

The resulting equation to calculate the particle velocity was given by:

$$\mathrm{d}L^* = \frac{w_p^* \mathrm{d}w_p^*}{(1-w_p^*)^{2-n} - R^* w_p^{*2} - S^*} \tag{2.12}$$

where $w_p^* = w_p / w$; $Fr = w^2/(gd)$; $Fr^* = w_s^{2-n} w^n/(gd)$;

$L^* = lg/\left(w_s^{2-n} w^n\right)$; $R^* = Fr^* \lambda_s^* / 2$; $S^* = \beta Fr^* / Fr$;

n is an exponent: if $Re_p = \rho(w - w_p)d_p / \nu < 1$, n=1; if $10^3 < Re_p < 2\times10^5$, n=0.

For most calculations, it was believed that n=0.5 could be used with sufficient accuracy.

β is a coefficient due to gravitational influence. For horizontal conveying, an average value of 0.4 was suggested to be used for the flow conditions in an air-jet pump [10-13].

The accuracy of the above equations for calculating the pressure at a jet pump exit was claimed to be within 10% with the product tested. However, it is doubtful whether this accuracy can be achieved with a wider range of products and greater variation in jet pump geometry and particle size. For example, the following limitations can be seen from reviewing the theoretical analysis given by Bohnet:

- The fundamental assumption involved in the above approach is that the particles are 'accelerated' with an average superficial air velocity from the nozzle outlet to the

throat inlet (Eq. (2.3)); and from the throat inlet to the throat outlet of the tube section (Eq. (2.7)). In fact, the acceleration of solid particles in a jet pump is affected by the solid mass flow rate, physical properties of solid particles, the ratio of solid to air mass flow rate, jet pump geometry, etc., in addition to the influence of air velocity. Hence, this assumption may not be acceptable over all the range of operating conditions.

- The effect of air compressibility was ignored in Eq. (2.1). Hence, a limitation exists that this equation is only valid for incompressible flow or flows which may be regarded as incompressible such as air flowing at low velocity/pressure.

- The air mass flow rate being sucked through suction port was over-estimated in Eq. (2-2). Actually, the suction air can only flow through the void between the solid particles (an area obtained by subtracting the area occupied by solid particles from the total suction port flow area).

- The location of the motive nozzle (expressed by nozzle-throat gap) was not considered in this model, although it was noted that this factor had a significant influence on the performance of the jet pump.

- Also, this model has not been proven valid for the variation in solid mass flow rate and the jet pump geometry, for example, the variation in nozzle diameter with the combination of throat tube with different diameters.

- Four pressure transformation coefficients were included in this model. These coefficients were determined by experimental measurements obtained from a jet pump with a 15 to 30 mm nozzle diameter and 33.3 mm throat diameter for a few different products conveyed at a constant solid mass flow rate (M_p = 0.08 kg/s). Due to the limitation of experimental data used to determine these coefficients which contribute to the calculating results, the application of this model is very limited.

Another significant performance prediction model for an annular air-jet pump transporting tows was published by Pogorelov [75], who looked closely at the interaction force between tows and the motive air. However, this model has not been confirmed by experimental data.

2.5 Design Methodology

The extensive use of air-jet pumps in industry has brought into focus the need for an adequate design procedure. The design of air-only jet pumps is based normally on experimental results and a performance prediction model. The latter provides a relationship for pump characteristic in terms of the non-dimensional parameters, while experiments establish the numerical values of some of the coefficients that are required in the performance calculation process [67, 109].

The optimal design of an air-jet pump conveying system depends on the performance prediction models of the jet pump. Design diagrams as shown in Figs. 34 (a) to (d), were presented by means of some simplification of the model reviewed in detail in Section 2.4. This simplification was made for a special case, where no air was sucked in or blown out and furthermore, the pressure change along the air-jet pump was so small that the air density remained constant [12]. The design diagrams were calculated to show the main influences dependent on the ratio d_T/d_M by using the simplified equations for the special case with average values of the coefficients obtained from experimental measurements ($\eta_T = 0.45, \eta_M = 0.78, \eta_D = 1.0$).

In these graphs, the dimensionless parameters were defined as:

$$p_1^* - p_T^* = \frac{p_1 - p_T}{\rho w_T^2 / 2}, \qquad p_2^* - p_1^* = \frac{p_2 - p_1}{\rho w_T^2 / 2}, \qquad p_R^* - p_2^* = \frac{p_R - p_2}{\rho w_T^2 / 2};$$

$$b_1^* = \mu \frac{w_{p1}}{w_T}, \qquad b_2^* = \mu \frac{w_{p2} - w_{p1}}{w_T}, \qquad r^* = (\lambda_G + \mu \lambda_S) \frac{l_M}{d_M}.$$

where the coefficient λ_s was determined by

$$\lambda_s = \frac{w_p}{w}\lambda_s^* + 2\beta \Big/ \left(\frac{w_p}{w} + Fr\right) \tag{2.13}$$

In Eq. (2.13), λ_s^* is a loss coefficient due to particle wall friction. Average values of λ_s^* between 0.002 and 0.005 were suggested by Bohnet [13].

These design diagrams may only be useful for determining approximate value of delivery pressure at the jet pump exit for given jet pump dimensions and operating conditions.

Despite the mathematical model to describe the air-solid flow in central air-jet pump and the simplified design procedure that have been proposed, manufacturers still prefer to rely on their own previous experience and testing products in their own test facilities. For example, a tremendous amount of data collected from actual jet pump industrial installations with pulverised and coarse coal and plastics were condensed into two graphs that permit a reasonably simple prediction of motive pressure and mass flow rate requirements for a given conveying installation and solid conveying rate [36]. Among these graphs, one shows the relationship between solid conveying rate and motive air pressure in terms of nominal jet pump size, and the other presents the dependence of the required motive air mass flow rate on motive pressure for a series of required delivery pressures. It was claimed that these two graphs were proven to be an excellent guide for predicting the operating requirements of a central air-jet pump with materials with some slightly varying bulk densities such as petroleum coke, limestone, ash, sugar, whey, cement, silica, plastic chips, resins and powders. A step-by-step procedure in selecting an adequate air-solid jet pump using these graphs was presented. Because these graphs were produced with respect to a series of dimensions of a particular jet pump design, this kind of design procedure is suitable only to systems using this type of commercially available pump.

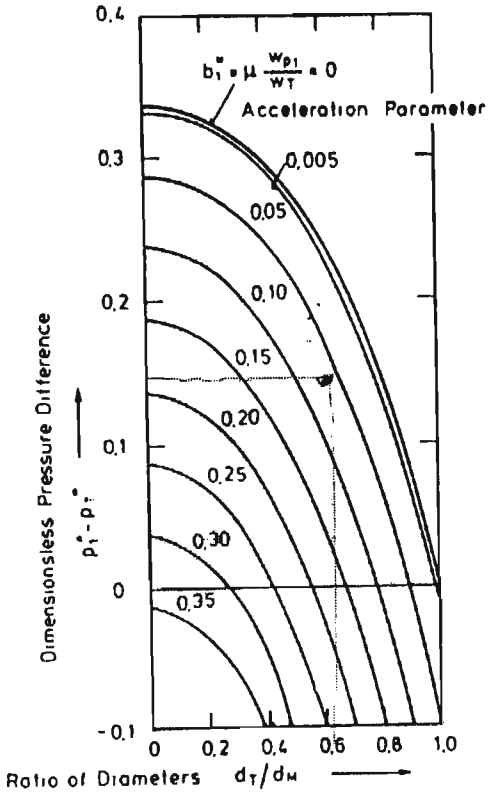
0,4
0,3
0,2
0,1
0
-0,1
$b_1^* = \mu \frac{w_{p1}}{w_T} = 0$
Acceleration Parameter
0,005
0,05
0,10
0,15
0,20
0,25
0,30
0,35
Dimensionsless Pressure Difference
$p_1^* - p_T^*$
0 0,2 0,4 0,6 0,8 1,0
Ratio of Diameters d_T/d_M

(a)

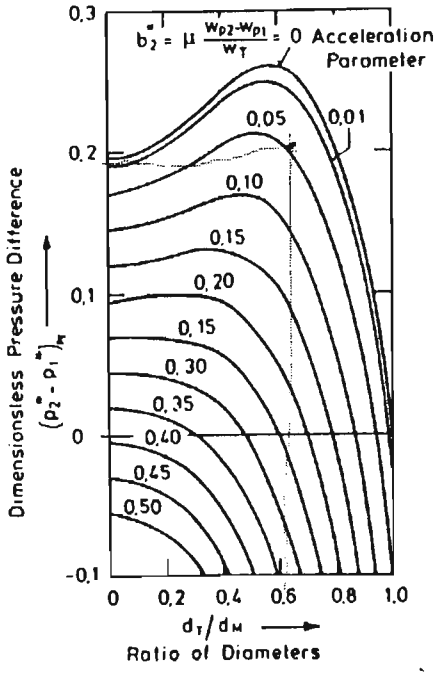
0,3
0,2
0,1
0
-0,1
$b_2^* = \mu \frac{w_{p2}-w_{p1}}{w_T} = 0$ Acceleration Parameter
0,05
0,01
0,10
0,15
0,20
0,15
0,30
0,35
0,40
0,45
0,50
Dimensionsless Pressure Difference
$(p_2^* - p_1^*)_M$
0 0,2 0,4 0,6 0,8 1,0
d_T/d_M
Ratio of Diameters

(b)

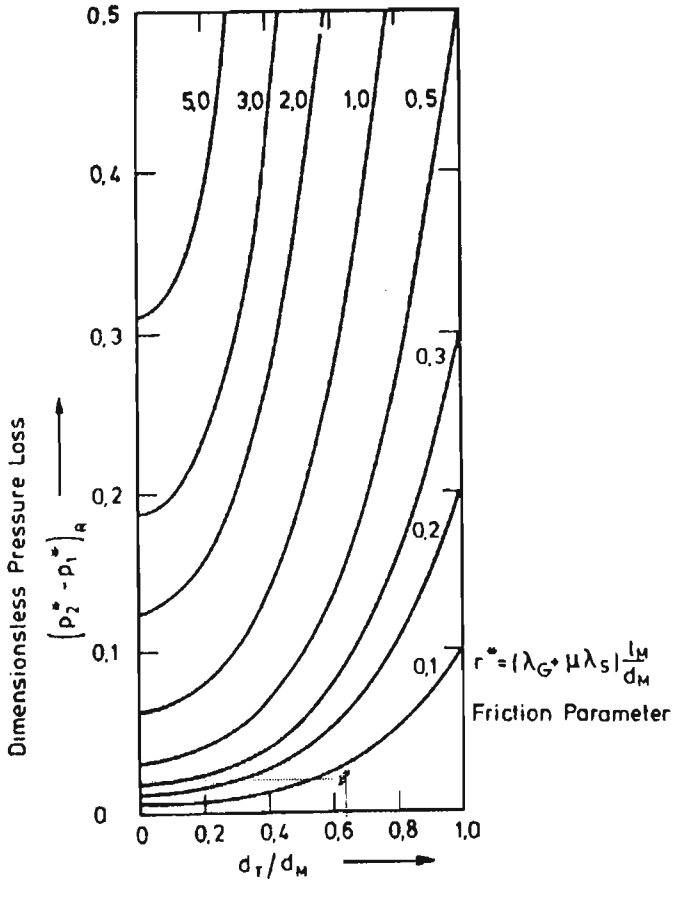
0,5
0,4
0,3
0,2
0,1
0
5,0
3,0
2,0
1,0
0,5
0,3
0,2
0,1
Dimensionsless Pressure Loss
$(p_2^* - p_1^*)_R$
0 0,2 0,4 0,6 0,8 1,0
d_T/d_M
$r^* = (\lambda_G + \mu\lambda_S)\frac{l_M}{d_M}$
Friction Parameter

(c)

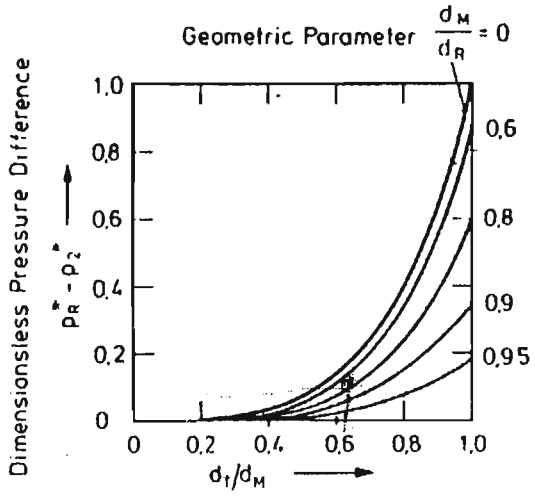

(d)

Fig. 2.34 Design diagrams presented by Bohnet [12]

With respect to the design of air-jet pumps and associated systems, up to now, no parameter to describe the energy-effectiveness of an air-jet pump to transport a given bulk solid in a pipeline has been developed or presented in the literature. Furthermore, no practical optimal design procedure has been reported. As a result, the design of this type of equipment is still a "black art" - trial and error and empiricism being used widely in engineering practice.

The conclusions that can be drawn from this review are that a significant contribution to the science of air-jet pump conveying system can be made by

- investigating systematically the influence of geometrical parameters and operating conditions on air-jet pump performance;
- developing a mathematical model to predict air-jet pump performance;
- formulating a reliable design strategy;
- investigating methods to optimise the air-jet pump conveying system by using mathematical optimisation techniques.

CHAPTER 3

THEORETICAL MODELLING OF AIR-JET PUMP PERFORMANCE

3.1 Introduction

Understanding the relationship between motive, suction and discharge flows in an air-jet pump is vital to designing and operating a reliable and energy-effective air-jet pump conveying system. For example, to determine the motive pressure and air mass flow rate for an air-jet pump to provide a particular solid mass flow rate in a given pipeline system, or to determine the conveying capacity of an air-jet pump operating at given motive, suction and delivery pressures, the relationships between suction solid mass flow rate, motive air mass flow rate, motive, suction and delivery pressures are mandatory. As reviewed in Section 2.4, this topic attracted considerable investigations both experimentally and theoretically over the past two decades. Despite these numerous investigations, the development of a reliable theoretical model has been hindered by the complexities of two-phase (gas-solid) flow. Trial and error and empiricism still are used to design these gas-solid jet pumps in engineering practice.

To describe air-solid two-phase flow through jet pump in such situations as shown in Fig. 3.1, either one or two dimensional modelling approaches may be employed. Both axial and radial velocity profiles for the air and solid phase can be obtained by using the two dimensional approach. However, as the variables in two dimensional flow have to be solved using a numerical method, no direct formula suitable to jet pump design can be obtained from this approach. Furthermore, even for single phase flow, this sort of approach still is being pursued, even though some flow simulation softwares are commercially available, such as PHOENICS and FLOW-3D. The design of single-phase

flow pumping systems still relies heavily on one-dimensional analysis and empirically derived formulae. Therefore, the two-dimensional modelling approach is more suitable to research other than to jet pump design practice. To formulate an air-jet pump design procedure, a one-dimensional modelling approach is adopted in the present research.

In this chapter, parameters to represent the characteristic performance and geometry of the air-jet pumps are defined. Each component of the pump is analysed based on the fundamental principles of fluid dynamics. These analyses finally lead to a mathematical model to predict the air-solids jet pump performance. Analytical and computational results obtained using the proposed model for five different central air-jet pump geometries under various operating conditions to convey a particular product are verified by using experimental data. Further investigations into formulating a reliable design procedure using the proposed analytical model is presented in Chapter 7.

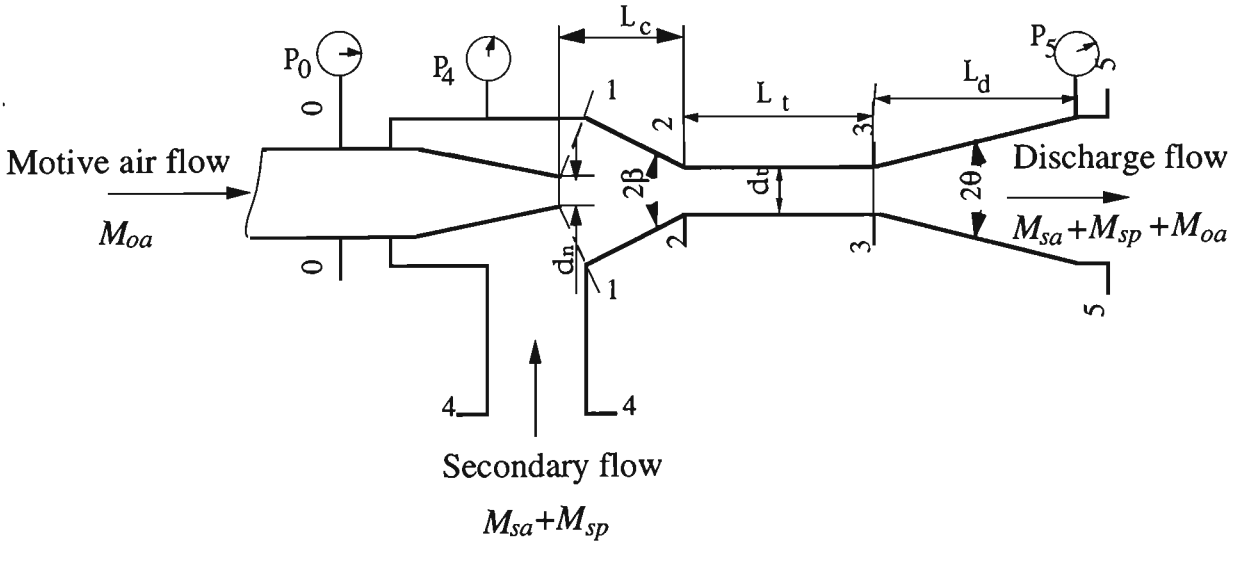

Fig. 3.1 Central air-jet pump schematic used for performance modelling

3.2 Performance Representation

3.2.1 Background Information

Fig. 3.1 shows the variables which define the operating condition of an air-jet pump. It can be seen from this figure that for an air-jet pump with fixed geometry, either to represent the pump characteristics or to determine the operating point of an air-jet pump, five variables are involved, i.e. motive pressure or motive air mass flow rate (actually, for a given nozzle geometry, air mass flow rate is determined by the motive pressure), suction mass flow rate and pressure, delivery pressure and discharge mass flow rate.

The performance of air-solids jet pumps is commonly represented by plotting the mass flow rate of solids against either the motive pressure under atmospheric discharge condition, as shown in Fig. 3.2 [36, 38, 101] or the delivery pressure for a given motive pressure/mass flow rate [28], as shown in Fig. 3.3.

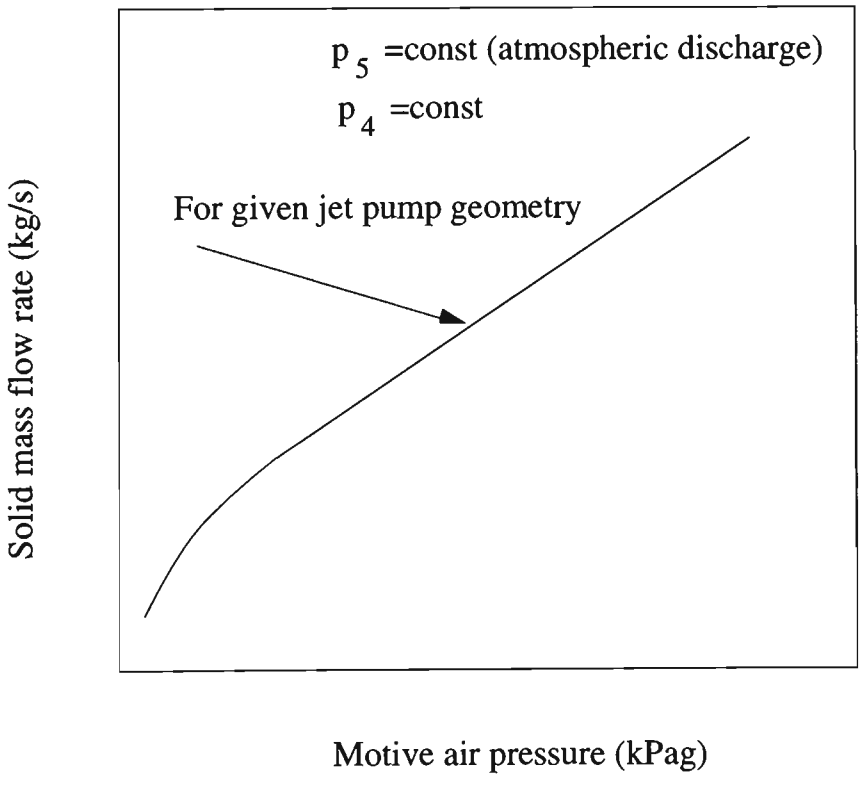

Fig. 3.2 Solid mass flow rate against motive pressure plot

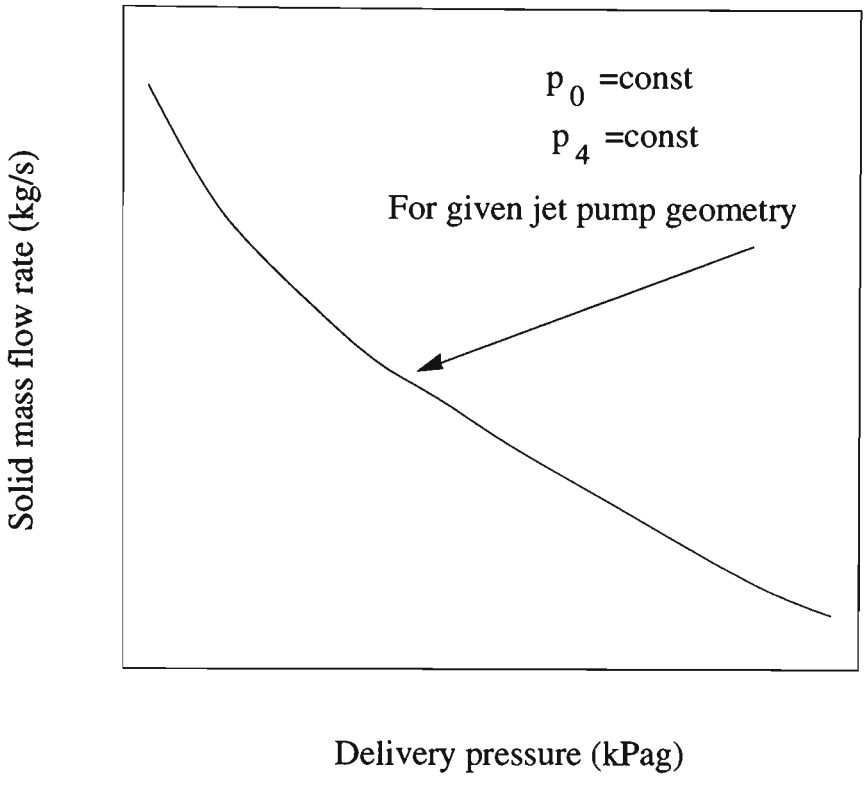

Fig. 3.3 Solid mass flow rate against delivery pressure plot

The suction solid mass flow rate against the motive pressure plot is only meaningful to a particular conveying pipeline system for a given air-jet pump, as the pipeline configuration (layout, length and diameter) affects the solid mass flow rate discharged under atmospheric condition. For example, the air-jet pump performance reported in [38] was obtained from such a conveying pipeline system, with a pipeline 45 m in length containing 3 long radius elbows. Also, this representation of jet pump characteristics doesn't reflect the influence of the variation of delivery pressure (or back pressure of the conveying system) and the suction pressure on solid mass flow rate.

The delivery pressure via solid mass flow rate plot was introduced to represent the variation of secondary mass flow rate with delivery pressure for a given motive pressure. However, this performance representation also doesn't show the influence of suction pressure on the secondary mass flow rate.

Actually, for a given air-jet pump conveying system to meet an application requirement, motive pressure is the unique parameter that can be controlled easily. From this point of

view, performance representation for a given motive pressure is more convenient when designing/selecting and operating a jet pump conveying system. That is, for a given motive pressure, there is an unique relationship between secondary mass flow rate and the difference between the delivery pressure and the suction pressure. Hence, as an improvement, pressure difference $\overline{p_5}$ - $\overline{p_4}$ is introduced in this section to include the influence of suction pressure on secondary mass flow rate.

To relate all the five variables depicted in Fig. 3.1, non-dimensional parameters are defined and used in non-dimensional characteristic plot. Efficiency also is introduced to assess the energy-effectiveness of an air-jet pump. The parameters defined in this section are used to present the experimental results on both the central air-jet pumps and the annular multi-hole jet pumps.

3.2.2 Definition of Dimensional Parameters

Total pressure is defined as the sum of static pressure and dynamic pressure. At the jet pump nozzle inlet, suction port and delivery port, total pressures $\overline{p_0}$, $\overline{p_4}$ and $\overline{p_5}$ are expressed by

$$\overline{p_0} = p_0 + \frac{\rho_{a0} v_0^2}{2} \tag{3.1}$$

$$\overline{p_4} = p_4 + \frac{\rho_{m4} v_4^2}{2} \tag{3.2}$$

$$\overline{p_5} = p_5 + \frac{\rho_{m5} v_5^2}{2} \tag{3.3}$$

3.2.3 Definition of Non-Dimensional Parameters

Area ratio:

$$m = A_2 / A_n \tag{3.4}$$

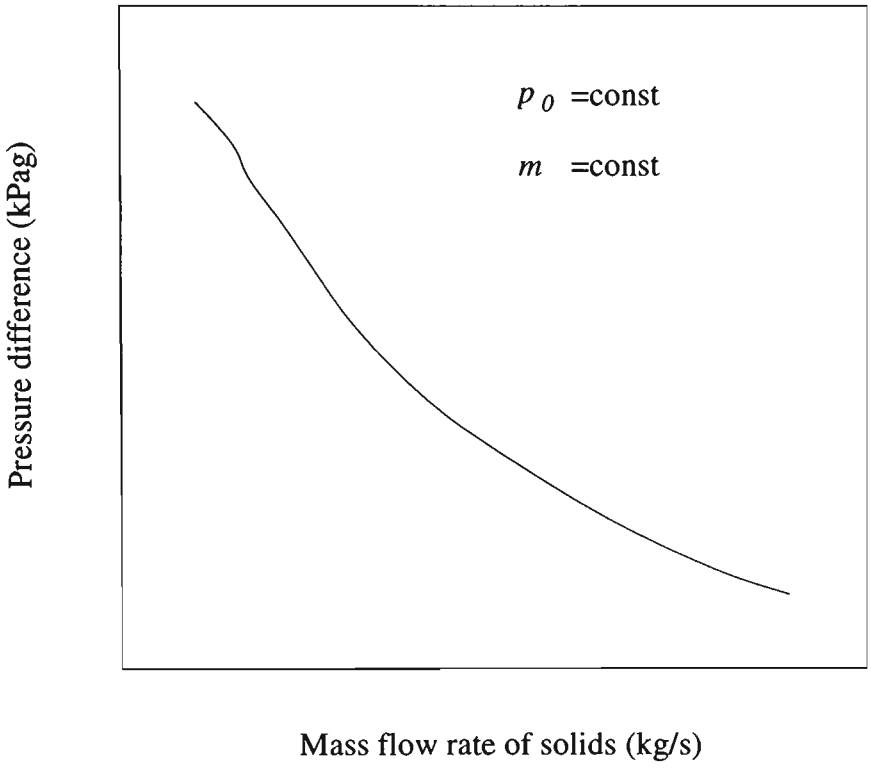

Fig. 3.4 Graphic representation of dimensional jet pump characteristics

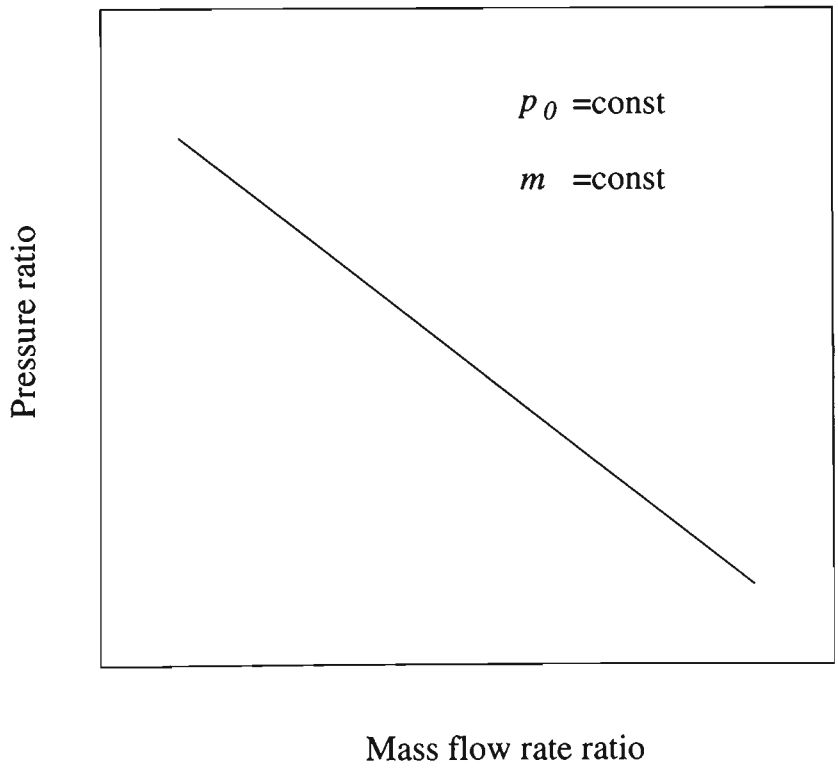

Fig. 3.5 Graphical representation of non-dimensional air-jet pump characteristic

where A_n is the flow area at nozzle outlet. For a converging nozzle, $A_n = \pi d_n^2/4$; for a multi-hole ring nozzle, $A_n = N\pi d_h^2/4$, where N represents the number of holes and d_h stands for the hole diameter.

Mass flow rate ratio:

$$x = \frac{M_{sa} + M_{sp}}{M_{oa}} = \frac{\rho_{4a}}{\rho_{o1}} q_a + \frac{\rho_p}{\rho_{o1}} q_p \tag{3.5}$$

where $q_p = Q_{sp}/Q_{o1}$ and $q_a = Q_{sa}/Q_{o1}$.

Pressure ratio:

$$h = (\overline{p_5} - \overline{p_4})/(\overline{p_0} - \overline{p_4}) \tag{3.6}$$

3.2.4 Pump Characteristics

Both air-solids and air-only jet pump performance can be represented by either the dimensional or non-dimensional parameters defined above for a given jet pump configuration. As shown in Fig. 3.4, the dimensional air-solid jet pump performance plot shows the variation of suction solid mass flow rate M_{sp} with respect to the pressure difference $\overline{p_5} - \overline{p_4}$. Non-dimensional pump performance is represented by a pressure ratio h via mass flow rate ratio x plot for a given air-jet pump configuration represented by area ratio m, as shown in Fig. 3.5. It can be seen from this figure that five variables affecting the jet pump operating condition can be related by using a h -x plot.

3.2.5 Conversion Relations

For a jet pump operating under a given operating condition, p_0, M_o and p_4 are given. To assess the pump characteristics in the process of jet pump design, the dimensional performance plot can be obtained from the non-dimensional characteristic parameters by the following conversion relations if the dependence of h on x is known for a specific jet pump geometry.

$$\overline{p_5} - \overline{p_4} = h(\overline{p_0} - \overline{p_4}) \tag{3.7}$$

$$M_{sp} = xM_{oa} \tag{3.8}$$

where M_{oa} can be calculated by using the mathematical method presented in Section 3.4. Therefore, the performance modelling work presented in this chapter concentrates on the non-dimensional performance.

3.2.6 Efficiency

As in any pneumatic conveying system, there is a need to minimise operating costs. It is therefore important to introduce efficiency as a parameter to measure the energy-effectiveness of an air-jet pump so as to establish options to improve air-jet pump performance by comparing its performance with different configurations and/or operating conditions and to determine an optimum design of air-jet pump conveying system.

For an air-jet pump operating under air-only conditions, the efficiency is considered as the ratio of power obtained by the secondary flow to that consumed by the motive air flow. Assuming that suction air is compressed isothermally from suction pressure to delivery pressure, an isothermal compression efficiency is introduced as a measurement of the energy-effectiveness of air-jet pumps. This isothermal efficiency is defined as

$$\eta_a = \frac{x \ln(p_5/p_4)}{\ln(p_0/p_5)} \tag{3.9}$$

To measure how effectively the motive air flow is converted into useful work for an air-solids jet pump conveying bulk solids from the feeding hopper, different parameters were defined and adopted in the literature. Davies *et al.* [26] suggested that the power consumption per unit solids mass flow rate be a promising basis for the comparison of different jet pump configurations. The power input to an air-jet pump was defined as the combination of motive pressure and motive air mass flow rate. Salam [79] defined the

efficiency for an air-jet pump to transport solids as the ratio of pressure difference p_5 -p_4 to the motive pressure at nozzle inlet. Between these two parameters, the first definition only applies to a given delivery pressure. As a matter of fact, for a given motive flow condition, the efficiency varies with delivery pressure. Hence, this definition is not suitable to assess the energy-effectiveness of air-jet pumps over the possible range of operating conditions. Although the variation of delivery and suction pressure are included in the definition, the latter is incomplete due to the lack of suction mass flow rate. For instance, as delivery pressure increases, the suction solids mass flow rate approaches zero, the efficiency calculated by this definition might indicate maximum value. In fact, for solid transportation, the efficiency should be zero when no solids are conveyed. Also, the solids mass flow rate may achieve the maximum by reducing the delivery pressure, while the efficiency according to this definition may be zero. Therefore, this definition can't be applied to evaluate the energy effectiveness of the air-jet pump. To avoid confusion, it should be noted that the efficiency discussed in this section should be distinguished from the energy transformation efficiency used by Bohnet [1-13] to consider the pressure loss in jet pump components such as the throat tube and diffuser while modelling the air-jet pump performance. Actually, efficiency was not introduced in Bohnet's work to assess the energy-effectiveness of the air-jet pump.

In the present research, *Efficiency* for a jet pump operating under air-solids flow condition is considered as a ratio of the combination of solids mass flow rate with pressure difference to the power consumed by the motive air flow through the jet pump. Assuming that the motive air in the jet pump undergoes an isothermal process, the theoretical power consumed for motive air to expand from the pressure at the nozzle inlet p_0 to the pressure at the jet pump exit p_5 can be calculated by

$$N_{cs} = M_{oa} R T_0 \ln(p_0/p_5) \tag{3.10}$$

The combination of mass flow rate with pressure difference can be determined by dimensional analysis. As the combination should take the dimension of power, one of the possible options is $\left(M_{sp}+M_{sa}\right)\left(p_5-p_4\right)/\rho_{a5}$. Based on this combination and Eq. (3.10), the efficiency for an air-jet pump to transport bulk solids can be expressed by

$$\eta=\frac{x(\overline{p_5}-\overline{p_4})}{p_5\ln(\frac{p_0}{p_5})} \tag{3.11}$$

It can be seen from Eq. (3.11) that the efficiency increases with either mass flow rate ratio or pressure difference. As the pressure difference increases with reducing mass flow rate ratio for a given motive pressure, there must be a compromise between the pressure difference and the mass flow rate ratio to achieve maximum efficiency.

It should be noted that the efficiency calculated by using Eq. (3.11) may be greater than 100% for some special cases where the solid has a high density. This results from the use of air density at the delivery pressure in calculating the power obtained by the secondary flow. As the power is calculated from the product of mass flow rate and pressure difference divided by density, using air density at the delivery pressure may enlarge the amount of power acquired by the secondary flow. An alternative may be to use the density of the air-solids mixture instead of air density in the combination of mass flow rate with pressure difference to determine the power obtained by the secondary flow. This modification results in

$$\eta_m=\frac{x}{(1+x)}\frac{(\overline{p_5}-\overline{p_4})}{p_5\ln(\frac{p_0}{p_5})} \tag{3.12}$$

Comparing Eqs. (3.11) and (3.12) leads to

$$\eta_m=\eta/(1+x) \tag{3.13}$$

As the common variation range of mass flow rate ratio for jet-pumps transporting bulk solids is between 3 and 10, the efficiency calculated from Eq. (3.12) is much smaller than that determined using Eq. (3.11). However, whether greater or smaller, the efficiency determined by either Eq. (3.11) or Eq. (3.12) is meaningful when comparing the performance of different jet pumps. It is true that the higher the efficiency calculated by using either Eq. (3.11) or Eq. (3.12), the better (more energy-effective) the jet pump is. In Chapters 5 and 6, for the sake of convenience and simplicity, the efficiency defined by Eq. (3.11) is applied to present and discuss the experimental results.

3.3 Discharge Performance of Nozzle

3.3.1 Governing Equations

The motive air flow through a nozzle may be considered as isentropic because there is very little heat transfer and also fluid friction effects are small. The resulting equation to express the relationship between the ideal mass flow rate through the nozzle and the motive pressure may be derived by integrating the Euler equation (Eq. 3.14) along a stream tube, while noting that $p\rho^{-\kappa} = \text{constant}$.

$$dp/\rho + vdv = 0 \tag{3.14}$$

For subsonic flow at the nozzle throat,

$$M_{oai} = A_n \sqrt{2\frac{\kappa}{\kappa-1}\rho_{a0}p_0\left(\frac{p_n}{p_0}\right)^{\frac{2}{\kappa}}\frac{1-(p_n/p_0)^{(\kappa-1)/\kappa}}{1-(A_n/A_0)^2(p_n/p_0)^{2/\kappa}}} \tag{3.15}$$

The rate of flow through the nozzle when sonic flow exists at the throat may be determined by substituting the critical pressure ratio into Eq. (3.15). The critical pressure ratio is defined as the ratio of the pressure at the nozzle throat to the pressure at the nozzle inlet. The resulting equation [9] to determine the critical pressure ratio is

$$\left(\frac{p_n}{p_0}\right)^{(1-\kappa)/\kappa} + \frac{\kappa-1}{2}\left(\frac{A_n}{A_0}\right)^2\left(\frac{p_n}{p_0}\right)^{2/\kappa} = \frac{\kappa+1}{2} \tag{3.16}$$

If the velocity of approach is negligible, Eq. (3.16) may be simplified as

$$\frac{p_n}{p_0} = \left(\frac{2}{\kappa+1}\right)^{\kappa/(\kappa-1)} \tag{3.17}$$

Substituting Eq. (3.17) into Eq. (3.15) results in

$$M_{oai} = A_n\sqrt{p_0\rho_{a0}\kappa\left(\frac{2}{1+\kappa}\right)^{(\kappa+1)/(\kappa-1)}} \tag{3.18}$$

Introducing $p_0 = \rho_0 R T_0$, Eq. (3.18) may also be expressed as

$$M_{oai} = \frac{A_n p_0}{\sqrt{T_0}}\sqrt{\frac{\kappa}{R}\left(\frac{2}{1+\kappa}\right)^{(\kappa+1)/(\kappa-1)}} \tag{3.19}$$

It can be seen from Eq. (3.19) that the flow rate is directly proportional to p_0.

Due to viscous friction and boundary variations, the actual flow rate through a nozzle is slightly less than the ideal flow rate given by the above equations. To allow for these effects, Eq. (3.15) can be modified by introducing the discharge coefficient c and an expansion factor Y. The resulting expression for the actual mass flow rate of air is

$$M_{oa} = cA_n Y\sqrt{2\rho_{a0}\frac{(p_0 - p_n)}{1-(A_n/A_0)^2}} \tag{3.20}$$

where p_n is the pressure at the nozzle outlet;

$$Y = \sqrt{\frac{[\kappa/(\kappa-1)](p_n/p_0)^{2/\kappa}\left[1-(p_n/p_0)^{(\kappa-1)/\kappa}\right]}{1-(p_0/p_n)}}\sqrt{\frac{1-(A_n/A_0)^2}{1-(A_n/A_0)^2(p_n/p_0)^{2/\kappa}}}.$$

For sonic flow, the equation to calculate the actual mass flow rate of air may be obtained in a similar way by modifying Eq. (3.19):

$$M_{oa} = \frac{cA_n p_0}{\sqrt{T_0}} \sqrt{\frac{\kappa}{R}\left(\frac{2}{1+\kappa}\right)^{(\kappa+1)/(\kappa-1)}} \tag{3.21}$$

Eqs. (3.20) and (3.21) suggest that the air mass flow rate be calculated for a particular nozzle once the motive pressure is given. The verification of these equations by experimental data is presented in Sections 5.3 for central nozzle and 6.3.3 for annular multi-hole nozzle.

3.3.2 Nozzle Discharge Coefficient

The discharge coefficient is defined as the ratio of the actual flow rate to the ideal flow rate and is generally a function of nozzle geometry, Reynolds number, and for compressible flow, Mach number. It can be determined from experimental data by Eq. (3.20) for subsonic flow and Eq. (3.21) for sonic flow at the nozzle throat. The calculated values of discharge coefficient using Eq. (3.20) and Eq. (3.21) based on the measured pressures and air flow rates are given in Table 3.1 for central nozzle and Table 3.2 for multi-hole ring nozzle.

It can be seen from Table 3.1 that the calculated discharge coefficients for each converging nozzle with straight-tip are around 1, and from Table 3.2 around 0.87. These results agree with that of the same type of nozzle for incompressible flow [25]. The reason is that Eq. (3.20) converts to the equation to calculate mass flow rate for incompressible flow if the expansion factor Y=1. Therefore, the discharge coefficient for compressible flow has the same value as for an incompressible fluid at the same Reynolds number. The air mass flow rates determined by Eq. (3.20) and Eq. (3.21) compare favourably with the experimental results, as shown in Figs. 5.1 and 6.6.

Table 3.1 Discharge coefficients of central nozzle

d_n=4.85mm		d_n=5.8mm		d_n=8.3mm		d_n=14.01mm		d_n=11.95mm	
p_0(kPa g)	c	p_0 (kPa g)	c	p_0 (kPa g)	c	p_0 (kPa g)	c	p_0 (kPa g)	c
200	0.986	539	0.98	212	0.978	20.4	0.985	148	0.984
135	0.985	488	0.98	259	0.968	39.8	0.985	101	0.985
97	0.989	421	0.98	309	0.979	37.4	0.985	130	0.980
248	0.982	375	0.98	343	0.967	48	0.980	92	0.980
303	0.967	304	0.96	155	0.980	71.8	0.986	117	0.985
404	0.969			107	0.967	93.7	0.989	15	0.976
502	0.986			81	0.971	115.5	0.984	30	0.998
667	0.978					139.1	0.991	52	0.973
603	0.981							72	0.982

Table 3.2 Discharge coefficients of multi-hole ring nozzle

d_h=1.55mm, N=8		d_h=1.55mm, N=16		d_h=2.38mm, N=12	
p_0(kPa g)	c	p_0(kPa g)	c	p_0(kPa g)	c
64	0.855	494	0.862	503	0.867
115	0.866	419	0.851	509	0.867
198	0.881	369	0.857	457	0.854
305	0.878	315	0.853	405	0.860
405	0.883	241	0.866	358	0.856
492	0.896	193	0.891	307	0.857
682	0.884	128	0.935	260	0.851
598	0.881	164	0.903	106	0.879

3.4 Properties of Air-Solids Two-phase Flow

In an air-jet pump used for bulk solids conveying, the secondary flow from section 4-4 to section 1-1 and the combined flow from section 1-1 to section 5-5 should be considered as air-solids two-phase flow. Some properties of the air-solids two-phase flow pertinent

to the performance modelling are defined and expressed in this section. The properties of bulk solids are discussed in Section 4.5.

Volumetric concentration is defined as the ratio of volume occupied by particles to total volume. For secondary flow between sections 4-4 and 1-1, this parameter can be expressed by

$$c_{vs} = \frac{V_{sp}}{V_{sp} + V_{sa}} = \frac{q_p}{q_p + q_a} \tag{3.22}$$

Generally, for the combined flow between sections 1-1 and 5-5, the volumetric concentration can be calculated by

$$c_{vk} = \frac{V_p}{V_p + V_a} = \frac{q_p}{1 + q_p + q_a \dfrac{p_4}{p_k}} \tag{3.23}$$

where subscript k stands for sections 1-1, 2-2, 3-3 and 5-5.

Volumetric concentration can also be represented by the densities of gas, particle and bulk solids. Considering mass conservation of the secondary bulk solids flow,

$$\rho_b V_{sb} - \rho_p V_{sp} = \rho_{4a} V_{sa} \tag{3.24}$$

According to Eq. (3.22), $V_{sp} = c_{vs} V_{sb}$ and $V_{sa} = (1 - c_{vs}) V_{sb}$. Therefore,

$$c_{vs} = \frac{\rho_b - \rho_a}{\rho_p - \rho_a}. \tag{3.25}$$

If $\rho_a / \rho_p \approx 0$ and $\rho_a / \rho_b \approx 0$, then

$$c_{vs} \approx \rho_b / \rho_p \tag{3.26}$$

Void fraction is defined as the ratio of volume occupied by gas to total volume. For the motive and secondary mixture flow,

$$\varepsilon_k = \frac{V_a}{V_a + V_p} = 1 - c_{vk} \tag{3.27}$$

For secondary air-solids flow,

$$\varepsilon_s = 1 - c_{vs} \tag{3.28}$$

Density of air-solid mixture can be expressed by volumetric concentration or void fraction. For the combined mixture flow,

$$\rho_{mk} = \rho_p c_{vk} + \rho_{ak}(1 - c_{vk}) \tag{3.29}$$

or expressed by void fraction as

$$\rho_{mk} = \rho_p(1 - \varepsilon_k) + \rho_{ak}\varepsilon_k \tag{3.30}.$$

For secondary air-solids flow, the mixture density is expressed by volumetric concentration as:

$$\rho_{s4} = \rho_p c_{vs} + \rho_{4a}(1 - c_{vs}) \tag{3.31}$$

or expressed by void fraction as

$$\rho_{s4} = \rho_p(1 - \varepsilon_s) + \rho_{4a}\varepsilon_s \tag{3.32}$$

3.5 Determination of Suction Air Mass Flow Rate

As an air-jet pump operates to convey bulk solid from an open feeding hopper to a pipeline, air may be sucked in with the bulk solid or blown out depending on the operating conditions. However, if the motive air blows out through the suction port, the air-jet pump does not work properly and the pumping effect deteriorates. Therefore, only the case where air actually is sucked into the pump through the suction port is considered for the modelling of the air-jet pump performance.

The density of secondary air-solid two-phase flow can also be expressed by

$$\rho_{s4} = \frac{(\rho_p Q_{sp} + \rho_{4a} Q_{sa})}{(Q_{sp} + Q_{sa})}$$

$$= \frac{\rho_p q_p + \rho_{4a} q_a}{q_p + q_a} = \rho_p \frac{q_p}{q_p + q_a} + \rho_{4a}(1 - \frac{q_p}{q_p + q_a}) \tag{3.33}$$

If there is no slip between the solids and air, $\rho_{s4} = \rho_b$.

Comparing with Eq. (3.31), $c_{vs} = q_p/(q_a + q_p)$. That is,

$$q_a = (\frac{1 - c_{vs}}{c_{vs}}) q_p \qquad (c_{vs} > 0) \tag{3.34}$$

From Eq. (3.5),

$$q_p = \frac{1}{\rho_p}(\rho_{o1} x - \rho_{4a} q_a) \tag{3.35}$$

Substituting Eq. (3.35) into Eq. (3.34) results in

$$q_a = \frac{(1 - c_{vs})\frac{\rho_{o1}}{\rho_p} x}{c_{vs} + (1 - c_{vs})\frac{\rho_{4a}}{\rho_p}} \tag{3.36}$$

If there is slip between the solids and air at the suction port, then by considering the mass conservation of secondary flow and assuming the ratio of velocities to be constant:

$$\rho_p c_{vs} v_{4p} A_4 + \rho_{4a}(1 - c_{vs}) v_{4a} A_4 = \rho_{s4}(c_{vs} v_{4p} + (1 - c_{vs}) v_{4a}) A_4 \tag{3.37}$$

This equation can be rearranged as

$$\rho_{s4} = \rho_p \frac{c_{vs}}{c_{vs} + (1 - c_{vs})S} + \rho_{4a} \frac{(1 - c_{vs})S}{c_{vs} + (1 - c_{vs})S} \tag{3.38}$$

where $S = \frac{v_{4a}}{v_{4p}}$ is the velocity slip ratio. Comparing Eq. (3.38) with Eq. (3.33) results in

$$q_a = (\frac{1-c_{vs}}{c_{vs}})Sq_p \qquad (c_{vs} > 0) \tag{3.39}$$

Substituting Equation (3.35) for q_p in Eq. (3.39), it can be obtained that

$$q_a = \frac{(1-c_{vs})S\frac{\rho_{o1}}{\rho_p}x}{c_{vs} + (1-c_{vs})S\frac{\rho_{4a}}{\rho_p}} \tag{3.40}$$

It can be seen by comparing Eqs. (3.36) and (3.40) that the suction air mass flow rate depends on the volumetric concentration, velocity slip ratio and solid mass flow rate for a given motive mass flow rate. If there is no or little velocity slip ($S \approx 1$), Eq. (3.40) reduces to Eq. (3.36).

The suction air mass flow rate can be easily calculated from the definition of $q_a = Q_{sa}/Q_{o1}$ for a given motive air mass flow rate (see Section 3.2.3), once q_a is determined.

3.6 Air-Solids Jet Pump Performance Formulation

Analyses on each component of the jet pump are carried out based on the principles of fluid dynamics and those assumptions given in Section 3.6.1. It should be noted that only the major or final equations are presented here due to the lengthy derivations involved. More details on the derivations of these equations are included in Appendix A.

3.6.1 Fundamental Assumptions

The main underlying assumptions in the formulation of the air-solids jet pump performance prediction model are:

1. Both solids and air phase behave macroscopically as continua;
2. Neither the secondary air-solids mixture nor the motive air undergoes any phase change;

3. No solid attrition occurs in the flow through the jet pump;
4. The air-solids mixture flow in the jet pump throat and diffuser is homogeneous;
5. The air-jet operates isothermally and under steady-state conditions.

3.6.2 Motive Nozzle

Application of the macroscopic mass and energy balance for the motive air flow through the nozzle leads to

$$p_1 \ln(\frac{p_0}{p_1}) = (1+k_{01})z \tag{3.41}$$

where $z = \rho_{o1} v_{o1}^2 / 2$.

Note that for sonic flow at the nozzle throat, p_n determined by Eq. (3.16) or (3.17) should be used instead of p_1 in Eq. (3.41).

3.6.3 Suction Chamber and Throat Entry

Application of the macroscopic mass and energy balance approaches to the secondary air-solid two-phase flow between the suction port (section 4-4) and the inlet of the throat entry (section 1-1), as shown in Fig. 3.1, leads to the following equations:

$$\overline{p_4} - p_1 = (1+k_{41})\frac{\rho_{s1} v_{s1}^2}{2} \tag{3.42}$$

where $\overline{p_4} = p_4 + \frac{\rho_{s4} v_{s4}^2}{2}$. Dividing both sides of Eq.(3.42) by z results in

$$\frac{\overline{p_4} - p_1}{z} = (1+k_{41})\frac{C^2(q_a \frac{p_4}{p_1} + q_p)^2}{(m-1)^2}\frac{\rho_{s1}}{\rho_{o1}} \tag{3.43}$$

where $C = \frac{A_3 - A_n}{A_{s1}}$ is defined as the suction area ratio.

The suction area ratio C is a ratio of the flow area occupied by the secondary flow at section 3-3 to the flow area of secondary flow at section 1-1. For the jet pump shown in

Fig. 3. 1, based on the geometrical relationship, the following expression to determine the suction area ratio can be obtained:

$$C=\frac{m-a_n{}^2}{(\frac{2L_c}{d_n}\tan\beta+\sqrt{m}-a_n)\cos\beta[2a_n+(\frac{2L_c}{d_n}\tan\beta+\sqrt{m}-a_n)\cos^2\beta]} \tag{3.44}$$

where $a_n=d_w/d_n$ is a coefficient to take into consideration the thickness of nozzle outlet and d_w is the external diameter of the nozzle outlet.

Using the energy balance approach for the motive and secondary streams between the throat entry (inlet section 1-1 and throat inlet section 2-2 shown in Fig. 3.1) leads to,

$$p_2-p_1=\frac{(\rho_{o1}Q_{o1}\frac{\rho_{o1}v_{o1}^2}{2}+\rho_{s1}Q_{s1}\frac{\rho_{s1}v_{s1}^2}{2})-(1+k_{12})(\rho_{o2}Q_{o2}\frac{\rho_{o2}v_{o2}^2\zeta_{o2}}{2}+\rho_{s2}Q_{s2}\frac{\rho_{s2}v_{s2}^2\zeta_{s2}}{2})}{\rho_{o1}Q_{o1}+\rho_{s1}Q_{s1}} \tag{3.45}$$

By means of some substitutions and calculations, Eq. (3.45) can be re-written as

$$\frac{p_2-p_1}{z}=\frac{(m-1)^2+x^2(q_a\frac{p_4}{p_1}+q_p)C^2-(1+k_{12})\{\zeta_{o2}(m-1)^2+x^2(q_a\frac{p_4}{p_2}+q_p)\zeta_{s2}\}}{(1+x)(m-1)^2} \tag{3.46}$$

3.6.4 Throat Tube

The application of mass and momentum balances for the motive and secondary mixture between the throat inlet and outlet results in

$$(p_3-p_2)A_2=\rho_{s2}v_{s2}Q_{s2}\zeta_{s2}+\rho_{o2}v_{o2}Q_{o2}\zeta_{o2}-\rho_{m3}Q_3v_3(\mu_3+\frac{k_{23}}{2}) \tag{3.47}$$

This equation can be transformed to

$$\frac{p_3-p_2}{z}=\frac{2x(q_p+q_a\frac{p_4}{p_2})\zeta_{s2}}{m(m-1)}+\frac{2\zeta_{o2}}{m}-\frac{(1+x)(\frac{p_1}{p_3}+q_a\frac{p_4}{p_3}+q_p)(2\mu_3+k_{23})}{m^2} \tag{3.48}$$

3.6.5 Diffuser

Application of the macroscopic mass and energy balance for air-solid mixture flow between the diffuser inlet and outlet results in:

$$\overline{p_5} = p_3 + \frac{(1-k_{35})\rho_{m3}v_3^2}{2} \tag{3.49}$$

Introducing the mass conservation relationship and substituting for velocity result in

$$\frac{\overline{p_5} - p_3}{z} = \frac{(1-k_{35})(1+x)}{m^2}\left(\frac{p_1}{p_3} + q_a\frac{p_4}{p_3} + q_p\right) \tag{3.50}$$

3.7 Determination of Coefficients

Coefficients k_{01}, k_{12}, k_{41}, k_{23} and k_{35} are involved in the performance modelling to account for the influence of the friction and variation of flow passage on performance. By introducing ψ to represent the mass flow ratio of particle to gas in the jet pump,

$$\psi = \frac{M_p}{M_a} = \frac{q_p\rho_p/\rho_{o1}}{1+q_a p_4/p_1} \tag{3.51}$$

and

$$\xi_d = \left\{\frac{\lambda_a + \psi\lambda_p}{8\tan(\theta)} + \frac{m_d - 1}{m_d + 1}\sin(2\theta)\right\}\left(1 - \frac{1}{m_d^2}\right) \tag{3.52}$$

where Eq. (3.52) is modified for two-phase flow from that appeared in [1], those terms related to coefficients k_{12}, k_{23} and k_{35} in Eqs. (3.45), (3.47) and (3.49) also can be expressed by using λ_a and λ_p. Considering that the momentum or energy losses due to friction expressed in terms of coefficient k_{12}, k_{23} and k_{35} and that expressed by using λ_a and λ_p should be equal leads to the following expressions:

$$k_{12}\left(\rho_{o2}Q_{o2}\frac{\varsigma_{o2}\rho_{o2}v_{o2}^2}{2} + \rho_{s2}Q_{s2}\frac{\varsigma_{s2}\rho_{s2}v_{s2}^2}{2}\right) = (\lambda_a + \psi\lambda_p)\frac{L_c}{d_n}\rho_2 Q_2\frac{\rho_{a2}v_{a2}^2}{2} \tag{3.53}$$

$$k_{23}\frac{\rho_{m3}v_3^2}{2} = (\lambda_a + \psi\lambda_p)\frac{L_t}{d_3}\frac{\rho_{a3}v_{a3}^2}{2} \tag{3.54}$$

$$k_{35}\frac{\rho_{m3}v_3^2}{2}=\xi_d\frac{\rho_{a3}v_{a3}^2}{2} \tag{3.55}$$

Transforming Eqs. (3.53), (3.54) and (3.55) results in that k_{12}, k_{23} and k_{35} can be determined by using the following expressions:

$$k_{12}=\frac{(\lambda_a+\psi\lambda_p)\frac{L_c}{d_n}(1+q_a\frac{p_4}{p_1})^2(1+x)}{\zeta_{o2}(m-1)^2+\zeta_{s2}x^2(q_p+q_a\frac{p_4}{p_2})} \tag{3.56}$$

$$k_{23}=\frac{(\lambda_a+\psi\lambda_p)L_t/d_t}{(1+\frac{\rho_p q_p/\rho_{o1}}{1+\rho_{a4}q_a/\rho_{o1}})(1+\frac{q_p}{q_a p_4/p_3+p_1/p_3})} \tag{3.57}$$

$$k_{35}=\frac{\xi_d}{(1+\frac{\rho_p q_p/\rho_{o1}}{1+\rho_{a4}q_a/\rho_{o1}})(1+\frac{q_p}{q_a p_4/p_3+p_1/p_3})} \tag{3.58}$$

Hence, k_{12}, k_{23} and k_{35} are related to air friction λ_a and particle friction λ_p, where air friction is pipe friction due to air-only flow, and particle friction means pipe friction due to solid particles. Air friction factor is available in common fluid mechanics textbook and handbook, such as [9, 25] and experimental data on particle friction factor λ_p of various product flows in pipe are available in the literature [100]. Although there is some difference between the friction in the pipe and that in the jet pump, this kind of difference is negligible when the readily available pipe friction factor is applied to the very short length of throat tube.

Coefficient k_{01} is introduced to allow for pressure loss due to viscous friction, turbulence and boundary variations while motive air flows through the nozzle. For a convergent nozzle with straight-tip, k_{01}=0.06 to 0.11 [9]. Other investigators recommend k_{01}=0.03 to 0.05 [111] and k_{01}=0.1 [112]. Coefficient k_{41} is introduced to account for the pressure loss for secondary flow from the suction port (section 4-4) to section 1-1 shown in Fig. 3.1. This coefficient can be determined approximately by treating the flow passage as a combining tee (*i.e.* one stream of fluid flows straight into the tee and the other flows into

the tee at right angle to the straight-flowing fluid, two streams combine and flow out of the tee at the direction of the straight-flowing fluid [9]). Coefficients ζ_{o2}, ζ_{s2} and μ_3 are introduced to account for the effects of non-uniform velocity distribution over the controlling sections. Assuming that the average motive jet velocity is maintained between the nozzle outlet and the throat inlet, the momentum modification coefficients due to the variation of motive air-jet profile and velocity distribution from nozzle outlet to throat inlet become unity, *i.e.* $\zeta_{o2}=1$, $\zeta_{s2}=1$. With the assumption that the motive and secondary fluids are perfectly mixed at the throat tube exit, the momentum modification coefficient due to velocity slip between particles and air at throat outlet (section 3-3) becomes unity, *i.e.* $\mu_3=1$.

3.8 Outline of Solution Method

Substituting Eq (3.42) for p_1 into (3.41) results in

$$(\overline{p_4}-(1+k_{41})\frac{\rho_{s1}v_{s1}^2}{2})\ln(\frac{p_0}{p_1})=(1+k_{01})\frac{\rho_{o1}v_{o1}^2}{2} \tag{3.59}$$

By introducing a throat entry function defined as

$$\alpha=\frac{\dfrac{\overline{p_4}}{p_0-p_4}\ln(\dfrac{p_0}{p_1})}{1+\ln(\dfrac{p_0}{p_1})\dfrac{C^2(q_a p_4/p_1+q_p)^2(1+k_{41})\rho_{s1}/\rho_{o1}}{(m-1)^2(1+k_{01})}} \tag{3.60}$$

Eq. (3.59) can be transformed to

$$v_{01}=\frac{1}{\sqrt{1+k_{01}}}\sqrt{\frac{2(\overline{p_0}-\overline{p_4})\alpha}{\rho_{o1}}} \tag{3.61}$$

Combining Eq. (3.6) with Eq. (3.61), the pressure ratio can be expressed by the throat entry function as

$$h=\frac{\alpha(\overline{p_5}-\overline{p_4})}{(1+k_{01})z} \tag{3.62 (a)}$$

Eq. (3.62) (a) can be rearranged as

$$h = \frac{\alpha}{(1+k_{01})}\left(\frac{\overline{p_5} - p_3}{z} + \frac{p_3 - p_2}{z} + \frac{p_2 - p_1}{z} + \frac{p_1 - \overline{p_4}}{z}\right) \tag{3.62}$$

The solution to Eq. (3.62) showing the variation of pressure ratio h with mass flow rate ratio x can be obtained by combining Eq. (3.62) with Eqs. (3.43), (3.46), (3.48) and (3.50) and expressed as the following general form:

$$h = f(m, x, C, \rho_{o1}, \rho_p, \rho_b, \rho_{4a}, p_0, p_4, p_5) \tag{3.63}$$

It can be seen from Eq. (3.63) that the characteristics of an air-solid jet pump is determined by the geometric parameters m and C, and also related to the operating conditions expressed by $x, \rho_p, \rho_b, \rho_{4a}, \rho_{o1}, p_0, p_4$ and p_5. Therefore, to obtain the relationship between h and x for a jet pump with fixed geometry and operating under a given motive pressure, the performance prediction model expressed by Equations (3.40), (3.43), (3.46), (3.48), (3.50), (3.51), (3.52), (3.56) to (3.58), (3.60) and (3.62) must be solved simultaneously. This equation set is non-linear transcendental and can be solved by iteration method for specific primary and suction pressures. The calculation procedure is outlined in Fig. 3.6.

3.9 Shut-Off Pressure Ratio

Shut-off pressure ratio is referred as the pressure ratio at which secondary flow ceases. In this case, the motive air jet is impinging on a moving column of fluid in the throat tube, and there is ideally no other fluid entering or leaving the moving fluid column. Hence, this situation is basically single-phase flow with sudden expansion and $p_4 = p_1 = p_2$. Applying the momentum approach and neglecting frictional losses between section 1-1 and section 2-2, it can be obtained that

$$h_u = \frac{2\alpha}{m(1+k_{01})}\left(1 - \frac{1 + k_{35} + \lambda_a L_t / d_t}{2m}\right) \tag{3.64}$$

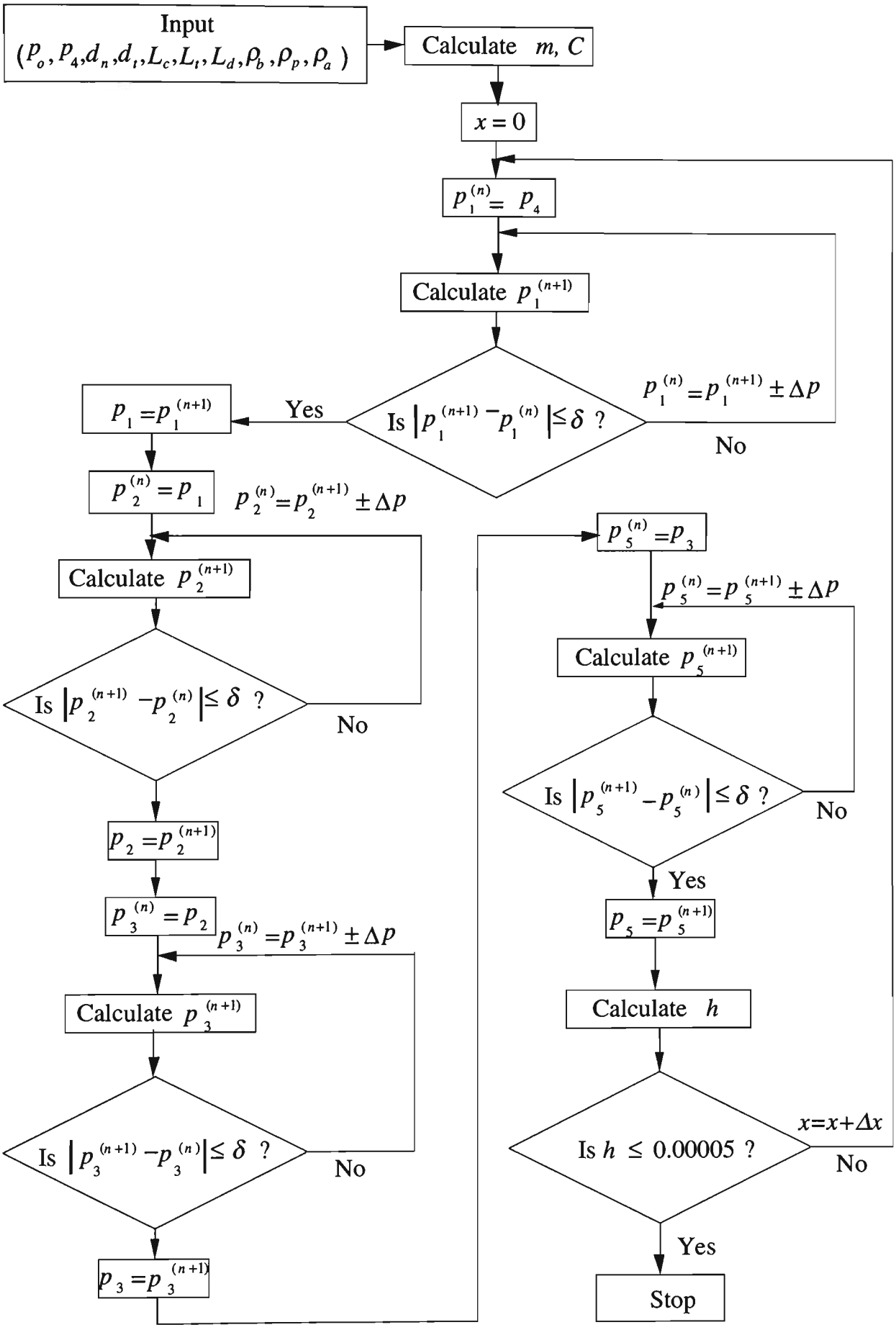

Fig. 3.6 Outline of performance prediction model solving procedure

The value of area ratio corresponding to the maximum shut-off pressure ratio can be determined by:

$$\frac{\partial h_u}{\partial m} = 0 \tag{3.65}$$

Combining Eqs. (3.64) and (3.65) leads to

$$m_u = 1 + k_{35} + \lambda_a L_t / d_t \tag{3.66}$$

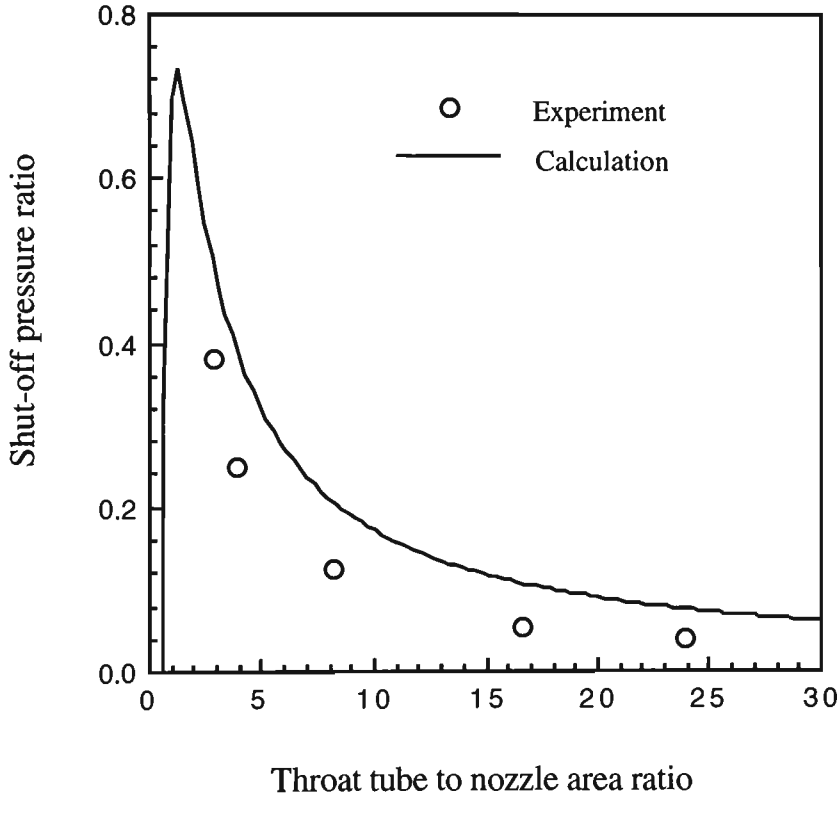

Fig. 3.7 The variation of shut-off pressure ratio with area ratio

The graphical expression of Equation (3.64) for $k_{35} = 0.1$, $\lambda_a = 0.025$ and $L_t/d_t = 5.6$ is shown in Fig. 3.7. It can be seen from this figure that the maximum shut-off pressure ratio can be reached if the area ratio is around 1.5. It should be noted from Eq. (3.66) that the area ratio corresponding to the maximum shut-off pressure ratio is related to friction losses which depend on the geometry of jet pump. It can also be clearly seen from Fig.

3.7 that shut-off pressure ratio decreases quite rapidly as the area ratio increases up to approximately 25 and that a further increase in area ratio will have little influence on the shut-off ratio. Therefore, an effective area ratio should be selected in the range of 1.5 and 25. Experimental data also have been plotted in this figure for comparison with the predictions by using Eq. (3.6.4). It can be seen clearly that the trends of shut-off pressure ratio varying with area ratio is well modelled by Eq. (3.64). The over-evaluation of the shut-off pressure ratio might arise from an under-evaluation of the pressure loss across the jet pump.

3.10 Comparison between Theory and Experimental Results

For a given m and C, the solution to the performance prediction model of an air-solids jet pump can be obtained. This solution provides dimensionless air-solids jet pump characteristics and can be illustrated by a graph of h versus x for different m. A comparison between predicted and experimental results is made to demonstrate the validity of the performance prediction model developed in this chapter for different jet pump geometries (represented by area ratio), operating conditions (represented by motive and delivery pressures) and bulk solids (*i.e.* plastic pellets, wheat, sorghum - see Table 4.3). Note that except for Dawson and others which are referenced, all the data used to demonstrate the theoretical modeling are from the author's own test work. Explanations on the test rig and how these data were obtained are presented in Chapters 4 and 5.

3.10.1 Area Ratio

Figs. 3.8 to 3.13 show the comparison between theoretical predictions by using the theoretical model developed in this chapter and experimental results for different area ratios. It can be seen from these figures that the non-dimensional characteristic curve becomes flatter as m increases. This suggests that the larger area ratio jet pump suits the application condition of lower back pressure and larger mass flow rate of product, and vice versa.

To illustrate the calculation of the predicted results plotted on Figs. 3.8 to 3.14 by using the theoretical model developed in this chapter, a workable example is provided below.

To predict the performance of a jet pump with m =2.86 to convey wheat into a pipeline system, all the coefficients and input data required are listed in Table 3.3. In this table, the determination of k_{o1}, ς_{o2}, ς_{s2} and μ_3 has been explained in Section 3.7. The value of λ_a was obtained from [9] and λ_p was calculated from the equations presented by Weber [100]. Regarding the determination of slip ratio S, observations from experiment show that the bulk solid moves into the suction chamber of the pump very slowly, and very little air is sucked in through the voidage of the material (see also Section 5.6.1). Hence , it is assumed that no slip occurs between the suction air and solid particles, that is S = 1. However, it should be noted that the analytical model developed and presented in this thesis can be easily extended to the case where S = const, once the slip ratio is determined from experiment by using other approaches.

The calculation procedure to solve the performance prediction model (*e.g.* Eq. (3.62) and associated equations) is outlined in Section 3.8. A computer program written using Fortran 77 for this calculation is included in Appendix B. The calculation starts at x = 0 and is stopped when h is less than a pre-assigned value. The predicted results are given in Table 3.4 and plotted on Fig. 3.9 for a comparison with the experimental data.

Table 3.3 List of coefficients and initial data required

Coefficients	Initial data
k_{o1}=0.11	m =2.86
λ_a=0.025	p_o = 40 kPag
λ_p =0.00175	p_4 = 0 kPag
S =1.0	L_t/d_t = 5.6
ζ_{o2} = 1	L_c/d_n = 3.6
ζ_{s2} = 1	m_d = 2
μ_3 = 1	ρ_b = 793 kgm^{-3}
	ρ_p = 1424 kgm^{-3}
	θ = 7.23°
	β = 15°

Table 3.4 List of calculation results for m =2.86

x	h	k_{12}	k_{23}	k_{35}	p_1 (Pag)	p_2 (Pag)	p_3 (Pag)	p_5 (Pag)	ψ
0.5	0.393	0.048	0.1133	0.0815	-0.039	2199	11130	15700	0.4997
1	0.3613	0.0655	0.0962	0.0822	-0.1639	1419	8195	14450	0.9993
1.5	0.3372	0.0846	0.0843	0.0828	-0.3726	940	5471	13487	1.4986
2	0.3163	0.1046	0.0755	0.0835	-0.6647	612	2786	12651	1.9978
2.5	0.2968	0.1257	0.0687	0.0841	-1.0403	371	56	11871	2.4967
3	0.2777	0.1476	0.0634	0.0848	-1.4993	184	-2777	11108	2.9955
3.5	0.2584	0.1703	0.0591	0.0854	-2.0418	34	-5771	10334	3.4941
4	0.2381	0.1938	0.0555	0.0861	-2.6678	-89	-8987	9525	3.9925
4.5	0.2163	0.2179	0.0525	0.0867	-3.3773	-193	-12511	8652	4.4908
5	0.1919	0.2424	0.0499	0.0874	-4.1702	-281	-16482	7677	4.9888
5.5	0.1632	0.2673	0.0477	0.088	-5.0467	-358	-21163	6526	5.4867
6	0.1254	0.2923	0.0458	0.0886	-6.0066	-424	-27230	5016	5.9843

3.10.2 Motive Pressure

Comparisons between theoretical calculations of non-dimensional pump performance for jet pumps with area ratios of 2.86, 8.14 and 23.84 and experimental results for different motive pressures are shown in Fig. 3.11. It can be seen that for a given area ratio, the performance line corresponding to higher motive pressure is always underneath that for lower motive pressure.

3.10.3 Properties of Bulk Solids

Three kinds of materials have been used to demonstrate the performance prediction model. The comparisons between predicted and experimental results are presented in Figs. 3.8 to 3.13. Experimental data available in the literature [28] also have been used to verify the performance prediction model. Fig. 3.14 shows the comparison of the predicted dimensional pump performance with the experimental data obtained by Dawson *et al.* [28].

It can be seen from all the comparisons shown in Figs. 3.8 to 3.14 that the predicted result is in good agreement with the experimental data, except for the case for m=2.86 in Fig. 3.12. The scatter shown here may be due to material deposition, because the motive pressure may have been too low to ensure proper dilute-phase flow. Slugs actually were observed during these experiments. As shown by Figs. 3.8 to 3.14, the good comparison between theoretical predictions and experimental data leads to a conclusion that the performance prediction model developed in this chapter can predict well the performance of air-jet pumps with different pump geometry (*i.e.* a wide range of area ratio) and operating under a wide range of motive pressure and delivery pressure to convey different materials. Based on this model, the design of air-jet pumps and associated systems is formulated and presented in Chapter 7.

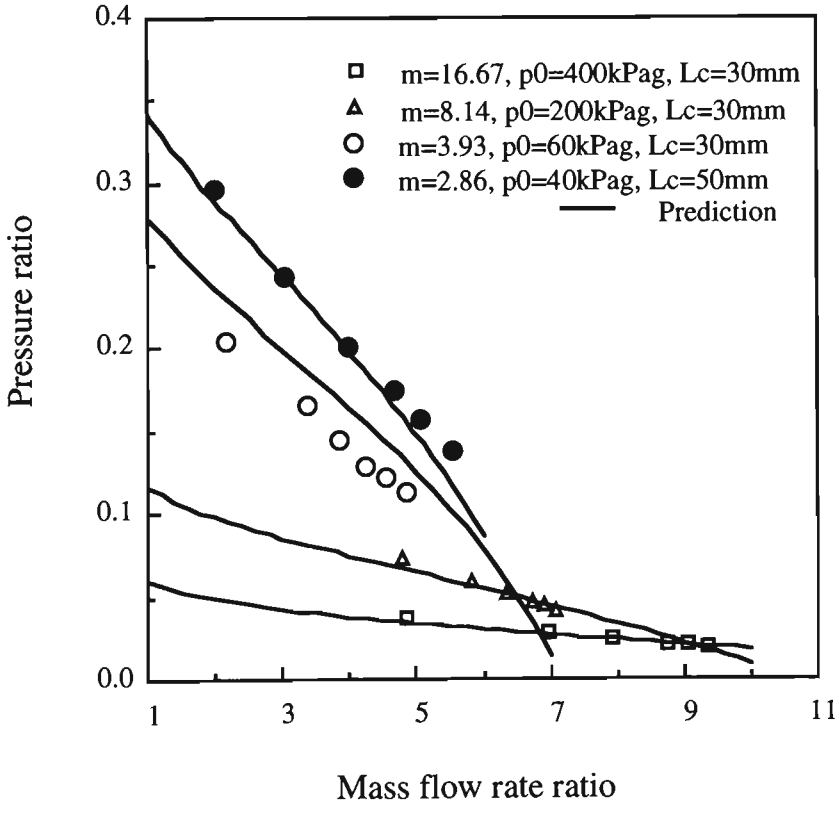

Fig. 3.8 Comparison between predicted and experimental results (plastic pellets, $L_t/d_t = 5.6$, ρ_b=530 kg m^{-3}, ρ_p=893kg m^{-3})

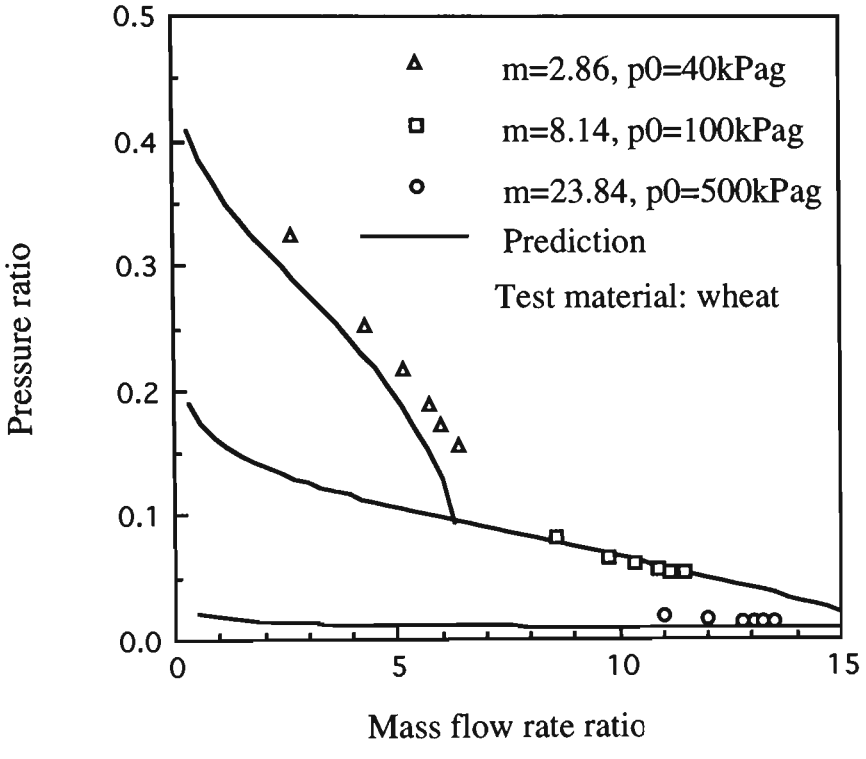

Fig. 3.9 Comparison between predicted and experimental results

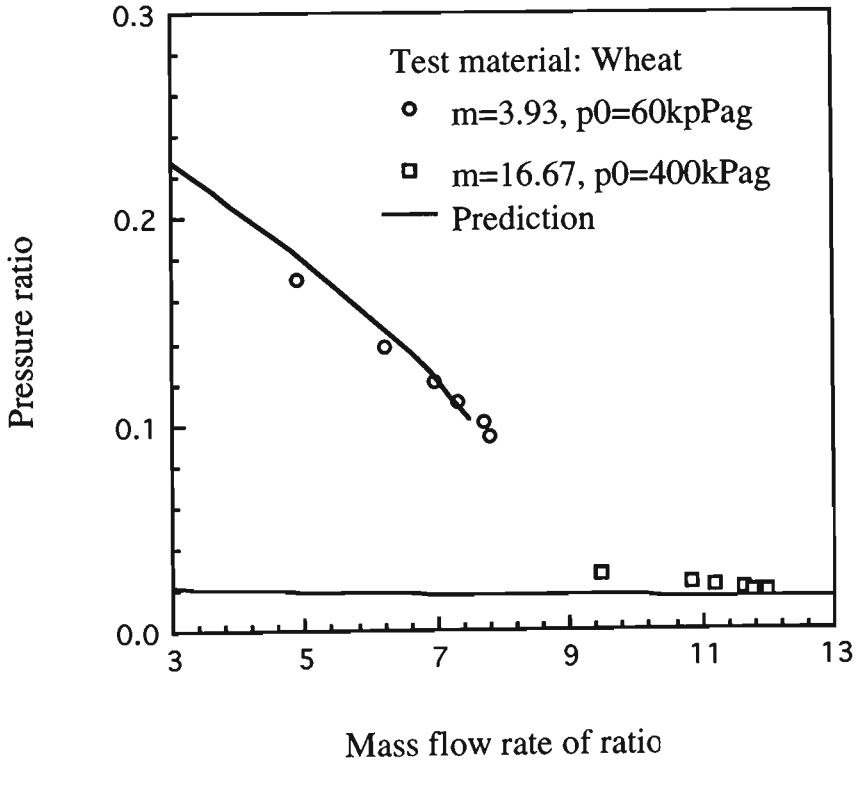

Fig. 3.10 Comparison between predicted and experimental results

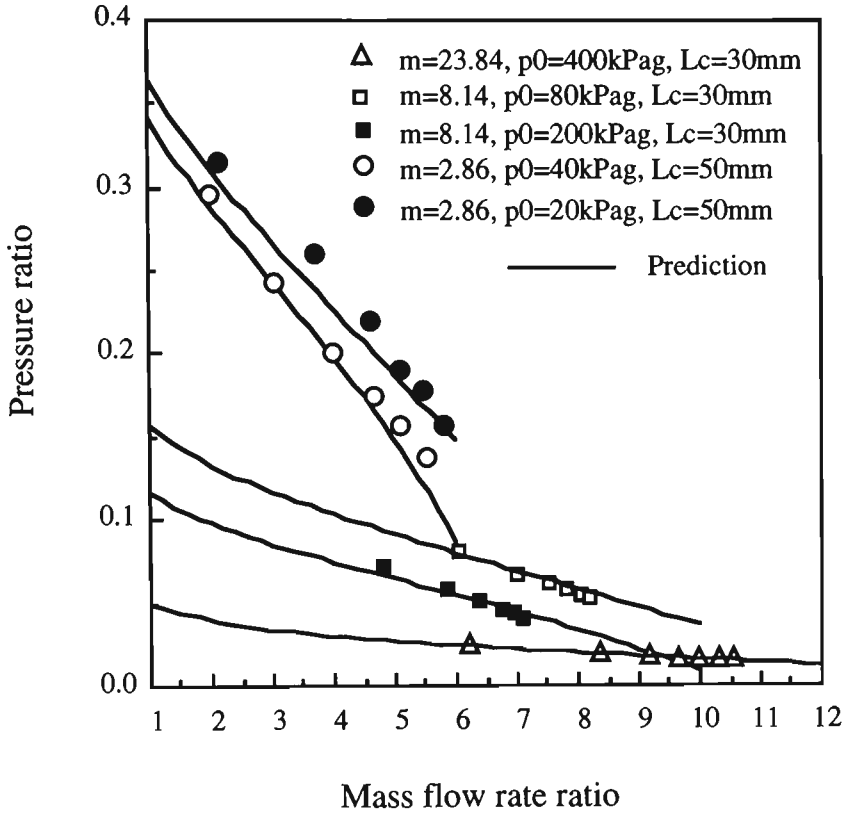

Fig. 3.11 Comparison between predicted and experimental results (plastic pellets, $L_t/d_t = 5.6$, ρ_b=530 kg m^{-3}, ρ_p=893kg m^{-3})

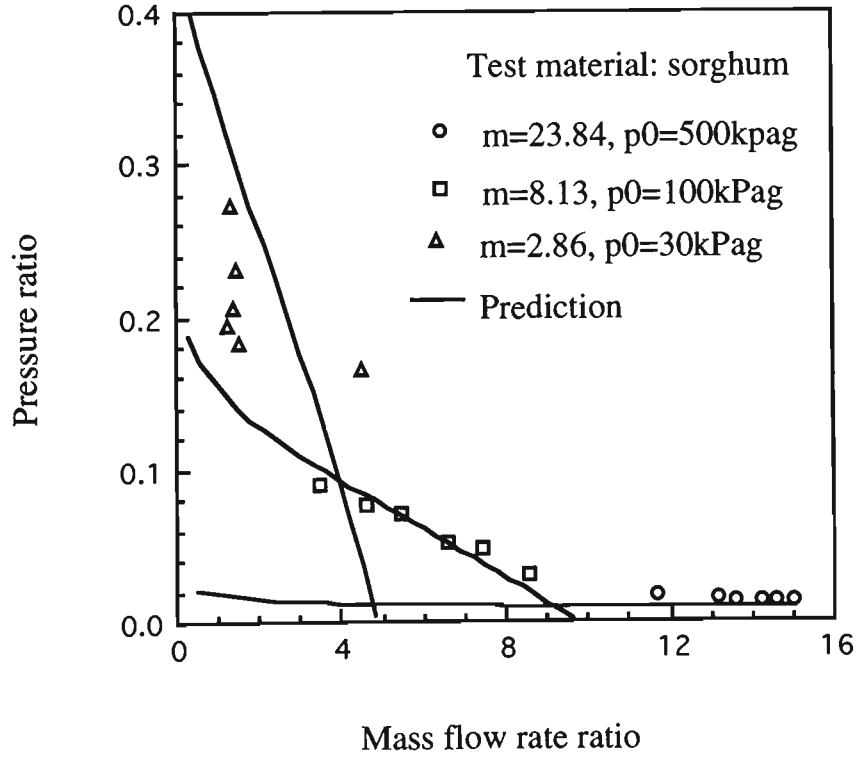

Fig. 3.12 Comparison between predicted and experimental results

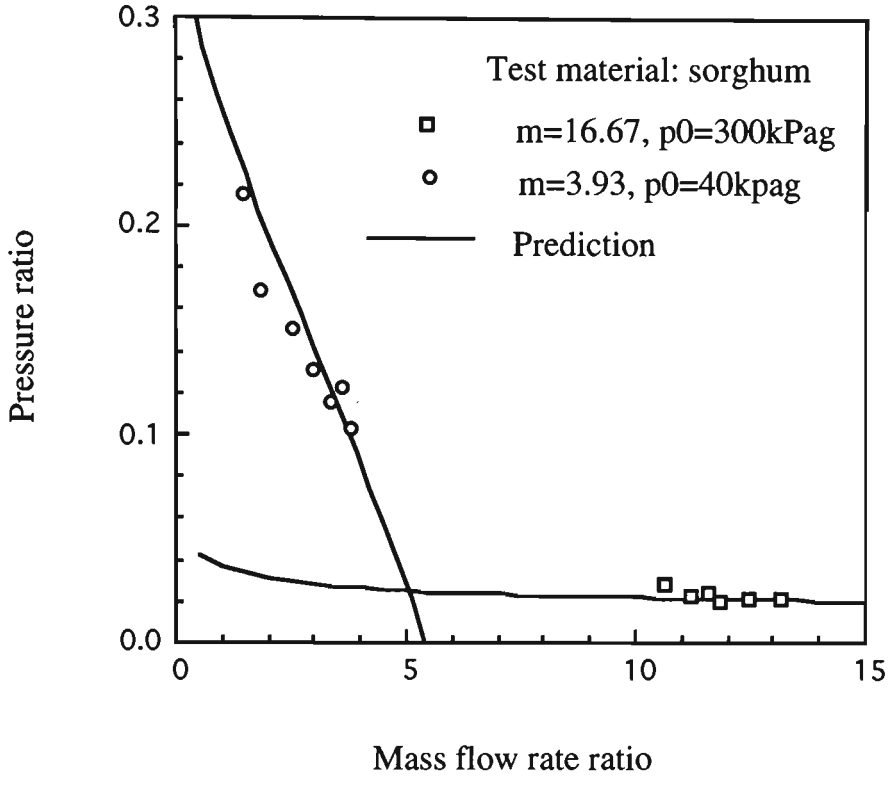

Fig. 3.13 Comparison between predicted and experimental results

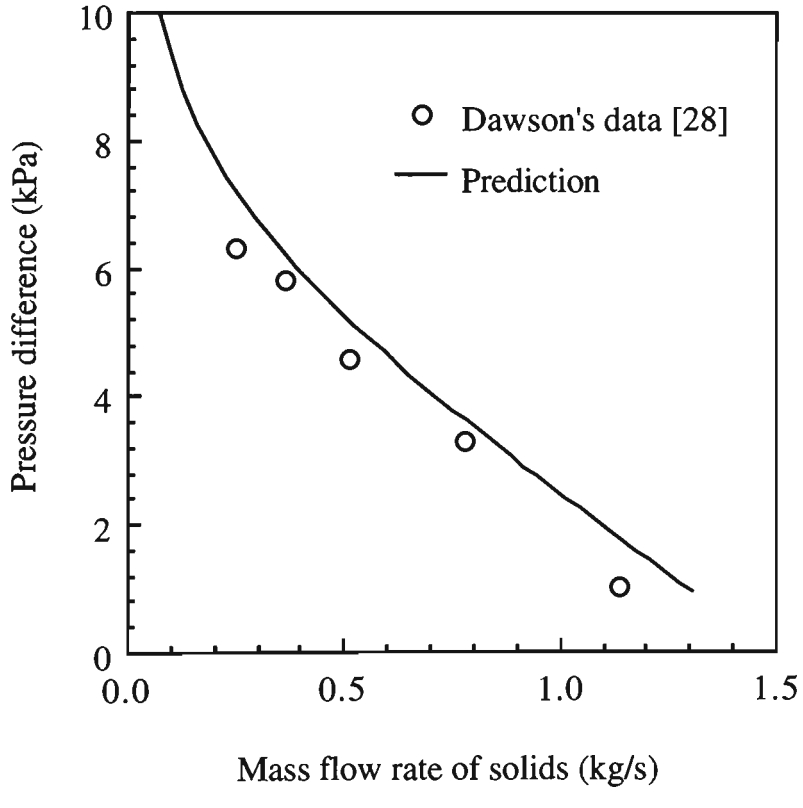

Fig. 3.14 Comparison between predicted dimensional performance and experimental data (d_t=76mm, d_n = 21mm, L_t / d_t=3, Sand:ρ_b=1350 kg/m^3,ρ_p=2631kg/m^3 , p_0=168 kPa)

3.11 Effect of Throat Entry Geometry

Having demonstrated the validity by experiment, the performance prediction model can be used to analyse the influence of the effect of the throat entry geometry on jet pump performance. The throat entry geometry is described by the suction area ratio C, which influences the performance via throat-entry function. Therefore, the effect of the geometry of throat entry on performance can be analysed by Eq. (3.60) for a specific area ratio. It can be seen from Equation (3.62) that the pressure ratio is proportional to the value of throat entry function. This means that jet pump performance can be improved by increasing the value of the throat entry function. From Eq. (3.60) it can be seen that for given p_o, p_4 and m, the value of the throat entry function increases as the suction area ratio C is reduced. Therefore, reducing suction area ratio may result in an improvement in pump performance.

Eq. (3.44) illustrates that C can't be zero and can only become smaller by the increase of nozzle-throat gap and contracting angle from the diameter of the suction chamber to that of the throat tube for a specific area ratio m as shown in Fig. 3.15. However, the increase of nozzle-throat gap and contracting angle will be limited practically by manufacturing and flow friction conditions. Also, extra nozzle-throat gap may cause more pressure losses due to friction and mixing. Experimental investigations into the influence of nozzle-throat gap are presented in Chapter 5. The variation of suction area ratio with contracting angle β and L_c / d_n for a given m is shown in Fig. 3.15. This figure illustrates that the value of L_c / d_n should be between 3 and 5 to obtain smaller values of C and larger values of the throat entry function. Experimental results presented in Chapter 5 also support this point. It can also be seen from this figure that the contracting angle should be in the range from 40° to 60° to obtain a more efficient pumping effect.

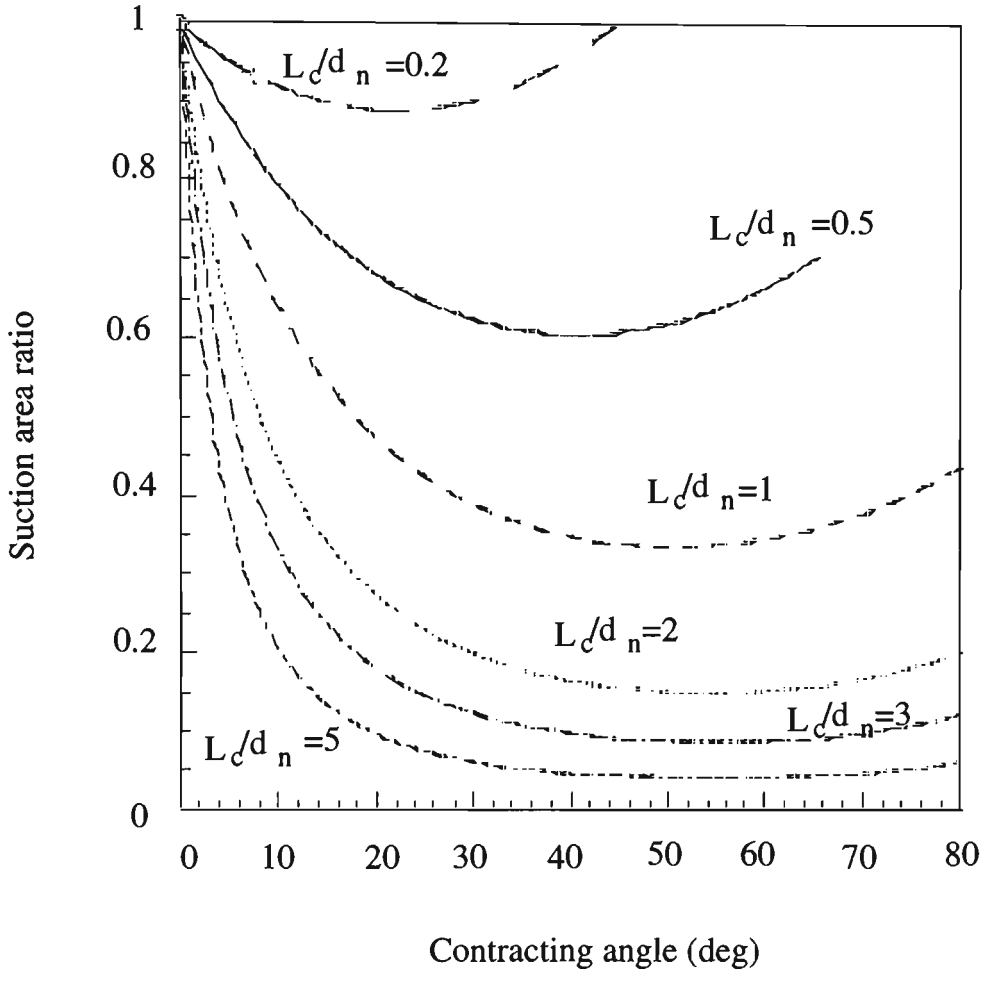

Fig. 3.15 Variation of suction area ratio with contracting angle and nozzle-throat gap L_c / d_n

CHAPTER 4

EXPERIMENTAL FACILITY AND TECHNIQUES

Experimental investigations have been undertaken to understand the influence of geometrical parameters and operating conditions on air-jet pump performance. The experimental work also is aimed at demonstrating the theoretical analysis and the performance prediction model developed in Chapter 3.

4.1 Description of Test Rig

The air-jet pump test rig, as depicted in Figs. 4.1 and 4.2, was designed and fabricated to monitor the performance of different types of air jet pump (such as central air-jet pump and annular air-jet pump with multi-hole ring nozzle) subjected to different motive pressures, delivery pressures and nozzle geometries. The test rig also allows materials to be changed easily. The four primary components of the test rig are: the air supply, the air jet pump to be tested, the receiving hopper and the feeding hopper.

4.1.1 Air-Supply and Control

The air supply consists of a compressor, air dryer and air receiver, and provides the high pressure air for the motive air flow in the jet pump. The major consideration in the selection of an air supply plant for the experimental investigation is to provide sufficient air for all experiments. In the Bulk Solids Handling Laboratory, air at a maximum pressure head of 800 kPag is available, supplied from the following rotary screw compressors:

- Atlas Copco electric-powered Model GA-308, 3.1 m^3 min^{-1} free air delivery.
- Ingersoll Rand diesel-powered Model P374-WP, 10.6 m^3 min^{-1} free air delivery.

- Ingersoll Rand diesel-powered Model P840-WGM, 24.1 $m^3 min^{-1}$ free air delivery.

To monitor the performance of jet pumps with numerous configurations and operating at various combinations of motive pressure and different nozzle flow areas, any combination of the above compressors can be employed for the test rig. The compressors are connected to an after-cooler, two refrigerated air dryers and two air receivers (1.74 and 6.0 m^3 volumetric capacity). Various filters and separators are installed in series with these compressors to ensure a dry and oil-free air supply. Fig. 4.3 shows a general arrangement of the air supply system.

As shown in Figs. 4.1 and 4.2, cooled, dried and oil-free air is introduced into the air-jet pump and then the conveying pipeline through an orifice plate or annubar where the air flow-rate is measured. A pressure regulator that maintains a fairly constant pressure upstream of the nozzle is used to control the motive air flow through the jet pump.

4.1.2 Feeding Hopper and Receiving Silo

A feeding hopper with a discharge valve mounted on the bottom of the vessel supplies the material to be conveyed. It is supported by load cells (see Figs. 4.1 and 4.2). The mass of material discharged from the hopper can be measured by the load cells. The hopper is connected to the suction port of the jet pump. A valve is mounted on the top of the hopper to allow connection to atmosphere.

The air-solid mixture discharging from the air jet pump then enters the pipeline and eventually the receiving silo where the solids fall out of suspension and the air exits to atmosphere via the annubar flow meter, which measures the air mass flow rate discharged from the receiving silo. The mass of the received material can be measured by

the load cells which support the receiving silo. The pressures in the receiving hopper (and at the exit of the air-jet pump) can be varied by selecting 6 different diameters of orifice plate mounted at the exit of the receiving hopper. In this way, varying lengths of pipeline can be simulated.

Two valves are installed between the receiving silo and the feeding hopper to enable proper isolation. A flexible tube is used between these two valves so that the mass of material conveyed can be measured separately.

4.1.3 Conveying Pipeline

The conveying pipeline consists of a 52 mm internal diameter mild steel pipe 3 metres in length and a 50 mm internal diameter glass pipe 13 metres in length. Pressure tappings are located along the mild steel pipe at 200 mm intervals to enable static pressure distribution measurements.

4.2 Air Jet Pump Design

Figs. 4.4 and 4.5 show the general configuration of the air-jet pump tested. These jet pumps and associated connections were designed to provide easy changing of the nozzle configuration and/or nozzle geometry. Table 4.1 and 4.2 provide the detailed dimensions of each jet pump configuration tested.

Table 4.1 Dimensions of annular air-jet pumps with multi-hole ring nozzle

Nozzle No.	Area ratio	Number of holes	Diameter of hole (mm)	Diameter of mixing tube (mm)
52	130	8	1.55	50
107	65	16	1.55	50
175	36.8	12	2.38	50

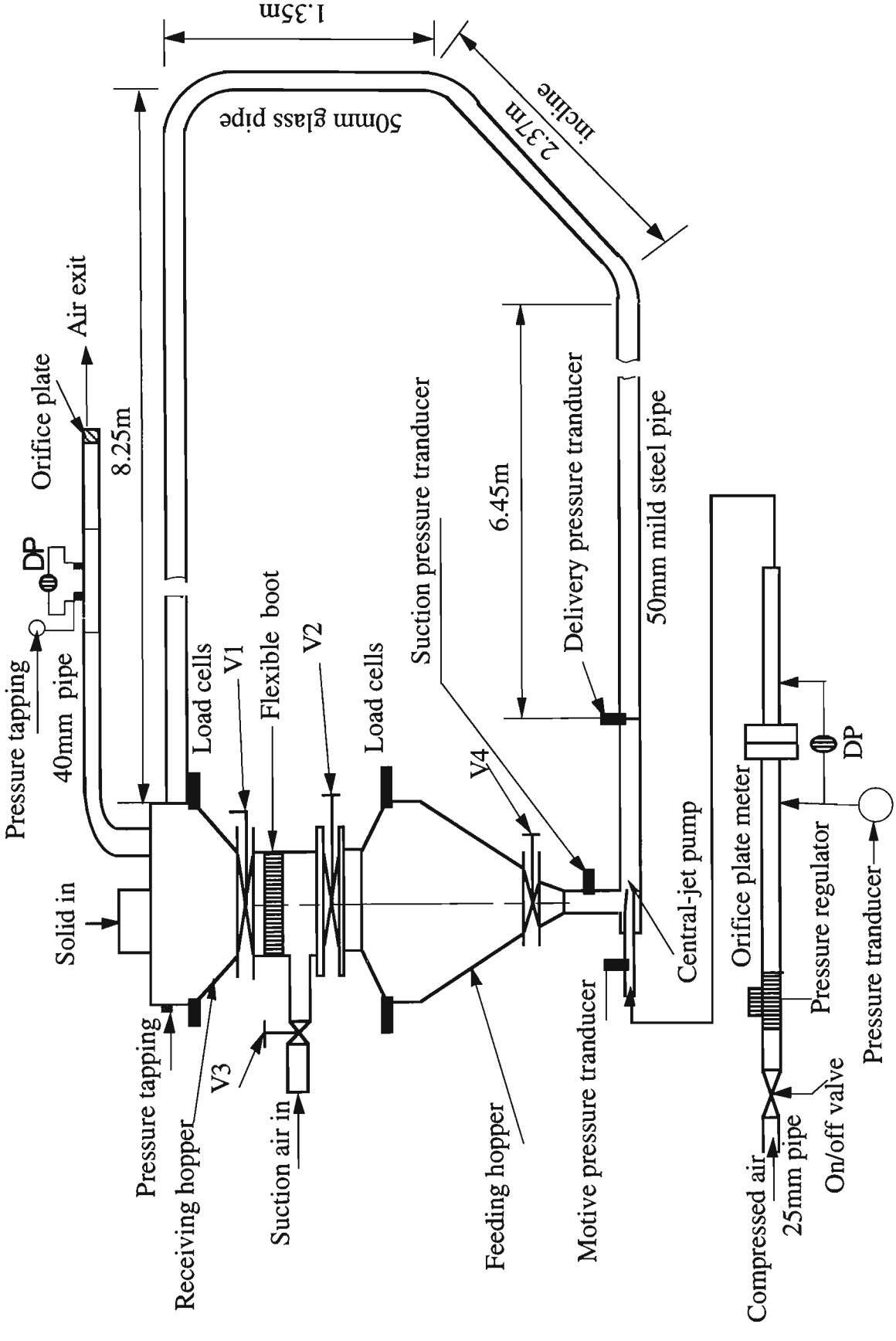

Fig. 4.1 General layout of central air-jet pump test rig
(DP = Diff. press. meter, V = Valve.)

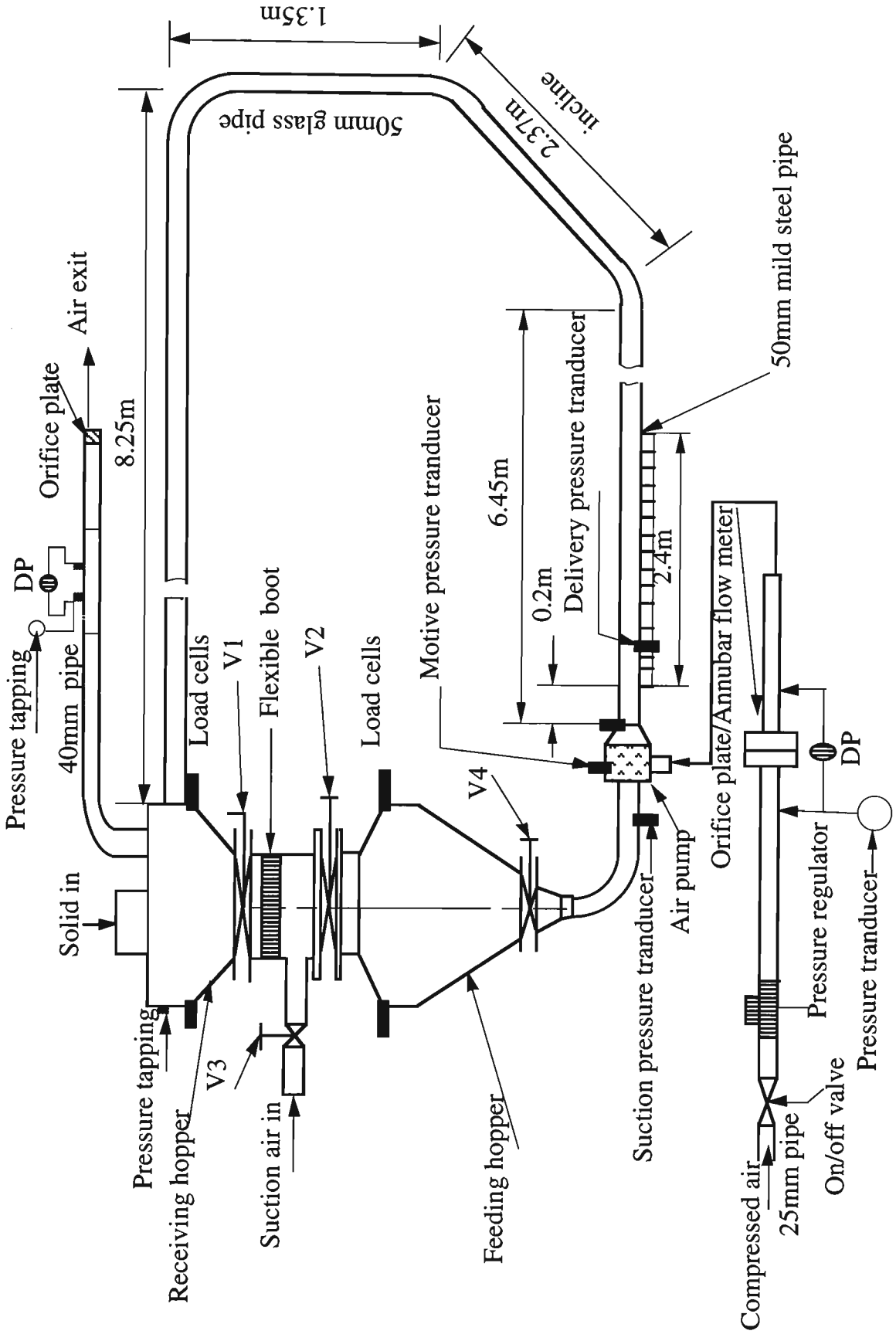

Fig. 4.2 General layout of annular air-jet pump test rig

(DP = Diff. press. meter, V = Valve.)

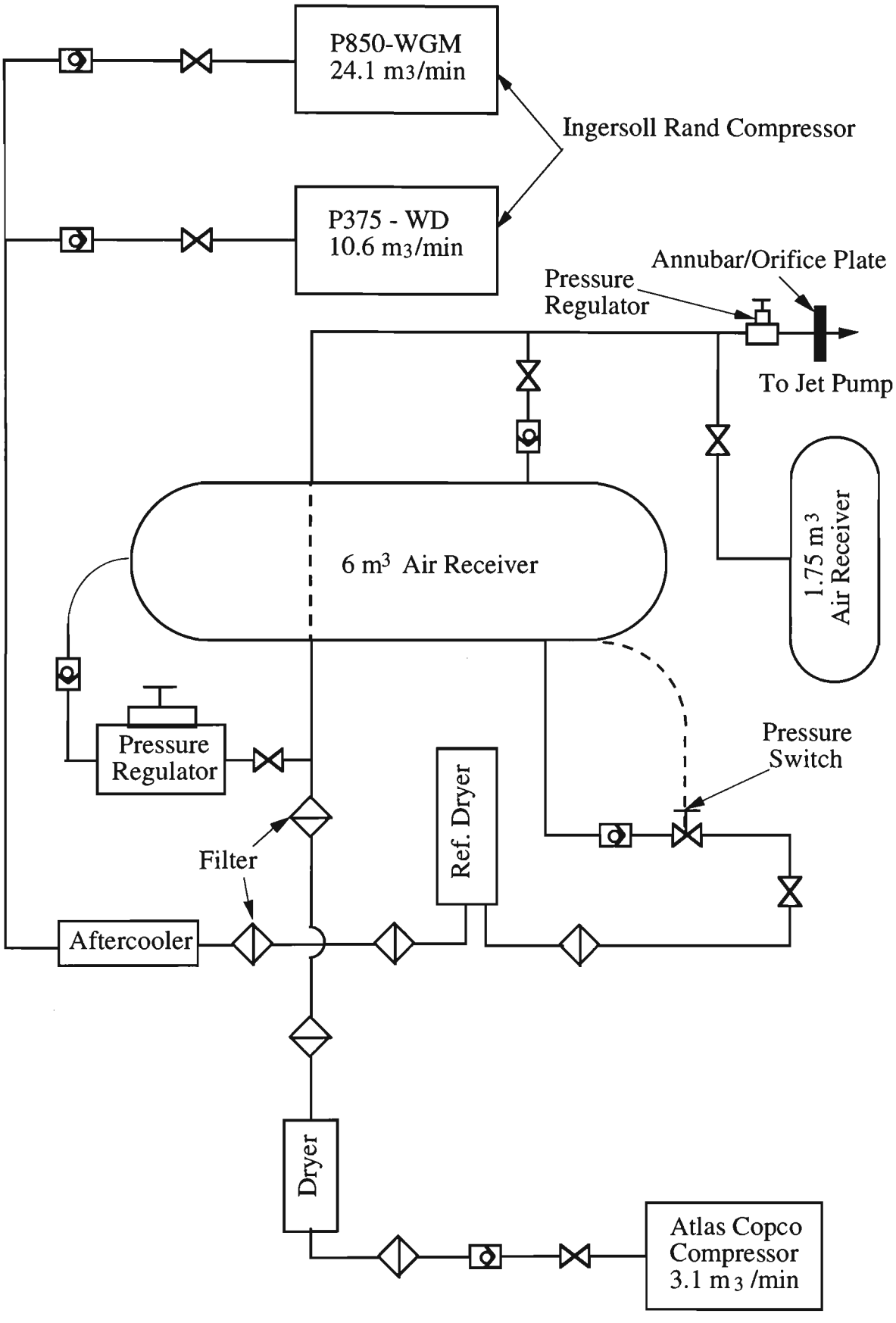

Fig. 4.3 General arrangement of compressed air supply

Table 4.2 Dimensions of central air-jet pumps

Area ratio *m*	Diameter of nozzle outlet (mm)	Diameter of mixing tube (mm)	Nozzle-throat gap (mm)
2.86	14.01	23.68	30, 50, 70, 87
3.96	11.95	23.68	30, 50, 70, 87
8.14	8.30	23.68	30, 50, 70, 87
16.67	5.80	23.68	30, 50, 70, 87
23.84	4.85	23.68	30, 50, 70, 87

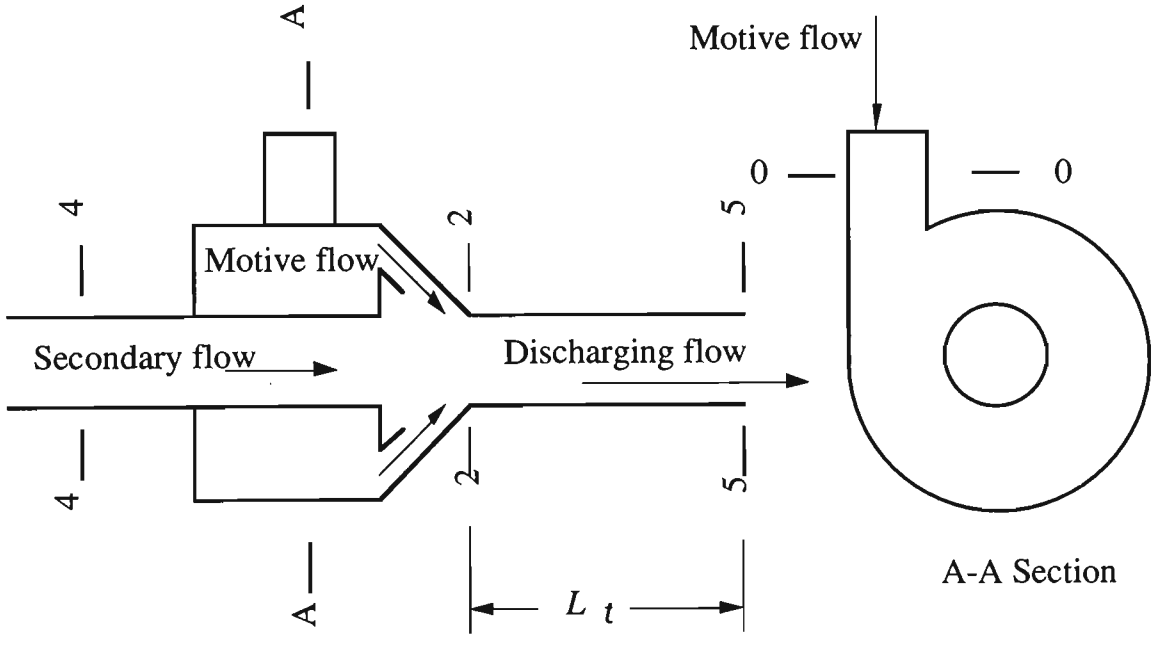

Fig. 4.4 General configuration of annular air-jet pump for testing

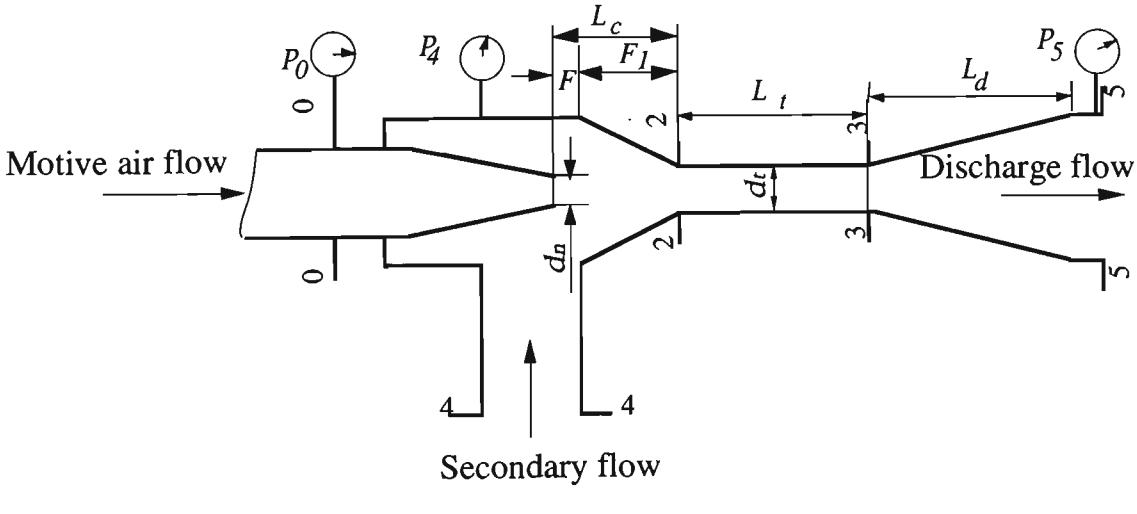

Fig. 4.5 General configuration of central air-jet pump for testing

4.3 Instrumentation and Data Acquisition

The instrumentation is designed to measure directly the following parameters during the experiments on jet pump performance:

- mass flow rate of solids (M_{sp}),
- mass flow rate of air (M_{oa}),
- static air pressures at various points of the system (p),
- pressure differentials between the suction port and the delivery port, and between delivery port and pipeline exit;
- mass flow rate of sucked air (M_{sa}).

The following sections describe the instrumentation used for measurement and data processing procedures.

4.3.1 Mass Flow-Rate of Air

The motive pressure p_0 was set using the regulator and the motive air mass flow rate discharging from the nozzle was measured using a sharp-edged orifice plate or annubar. An orifice plate is simply a thin, flat plate having a central hole. Fig. 4.6 shows the orifice plate device used in this project. A differential pressure (DP) meter was placed across the orifice plate. The DP meter readings were recorded and converted to mass flow rate by using a computer program based on BS 1042, Part 1, 1964. Inserting this device into an air supply pipeline, the flow-rate of air through the device can be calculated from a measurement of the upstream pressure and the difference between the pressures on the wall of the pipe at specified distances upstream and downstream of the orifice plate. The numerical relationship between the flow-rate of air and pressure difference

depends on the shape of the orifice and the positions of the pressure tapping. The orifice plate and positions of the pressure tapping used in this project are designed according to B.S. 1042. The pressure difference is measured by a 80 inch H_2O full-scale DP (differential pressure) transmitter connected to the pressure tapping holes.

An annubar was placed at the exit of the receiving hopper to measure the mass flow rate of air discharging from the hopper. The mass flow rate of air through the suction port was determined by subtracting the motive air mass flow rate from that obtained from the annubar. The annubar and sharp-edged orifice plate flow measurements were cross-checked by flowing the same amount of air through each meter (i.e. by closing valve V4 shown in Figs. 4.1 and 4.2).

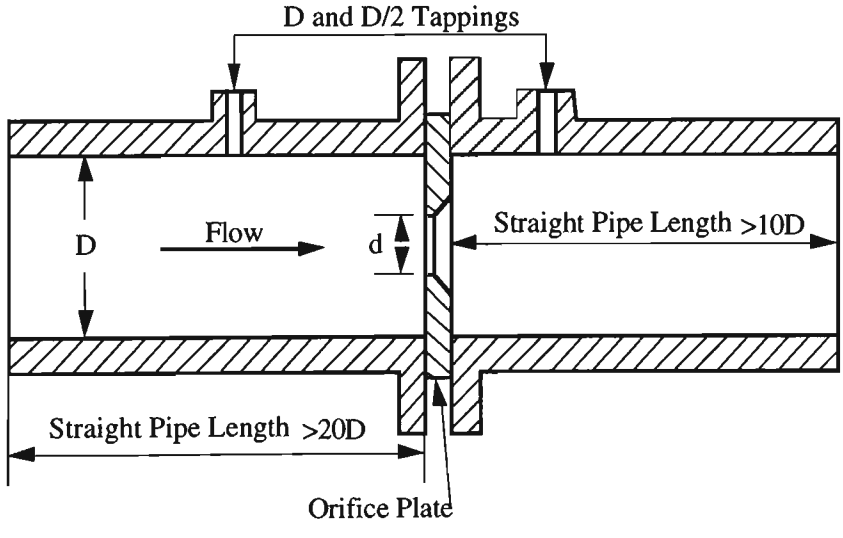

Fig. 4.6 Orifice plate device

4.3.2 Mass Flow-Rate of Solids

Shear-beam-type load cells support the feeding hopper and the receiving silo (see Figs. 4.1 and 4.2). The mass of material discharged from or loaded into these containers over a period of time (e.g. ranging from 50 to 150 seconds) can be measured by these load cells. An average mass flow-rate of solids is obtained by calculating the gradient of the line of best fit.

4.3.3 Static Pressure

Static air pressures at different locations such as nozzle inlet, upstream of orifice plate or/and annubar and delivery port are measured simply with strain-gauge pressure transducers (range 0-6 bar and range 0-1 bar), see Figs. 4.1 and 4.2. The pressure tapping details are similar to those adopted by Wypych and Arnold [105]. Refer to Fig. 4.7 for an exploded view of a typical pipeline air pressure tapping location. The pressure transducer is connected to the pipe socket by a quick connector.

The pressures upstream of the orifice plate and the nozzle were monitored using pressure gauges with an accuracy of ±1% and pressure transducers with an accuracy of ±0.5%. The pressures at the inlet of annubar and at the exit of the air jet pump were monitored using pressure transducers and a water manometer to ensure good accuracy. The pressure differentials between the suction port and the exit of the air pump and between the exit of the air pump and the receiving hopper were measured using DP meters. A DP meter was used also to monitor the pressure differential across the annubar. All the DP meters used in the experimental work were cross-checked with a water manometer. The vacuum generated by the air jet pump was monitored using a water manometer. The pressure at suction port was also measured by using the water manometer. The pressure difference between the suction port and the delivery port (inlet of pipeline) was measured by using DP transducers.

4.3.4 Data Acquisition System

A computer based data acquisition system (DAS), as shown in Fig. 4.8 was used to collect the experimental data.

This DAS consisted of an IBM-PC/AT compatible computer and an AX5621 board plugged into an expansion slot of the computer. The AX5621 board is a high-speed,

high-resolution analog-digital converter. Signal scanning was carried out by the board. A computer program named "logger" was designed to control the operation of the board and arrange the collection and storage of the data. All time history signals sampled by DAS were stored finally onto floppy diskettes as data files in ASCII format.

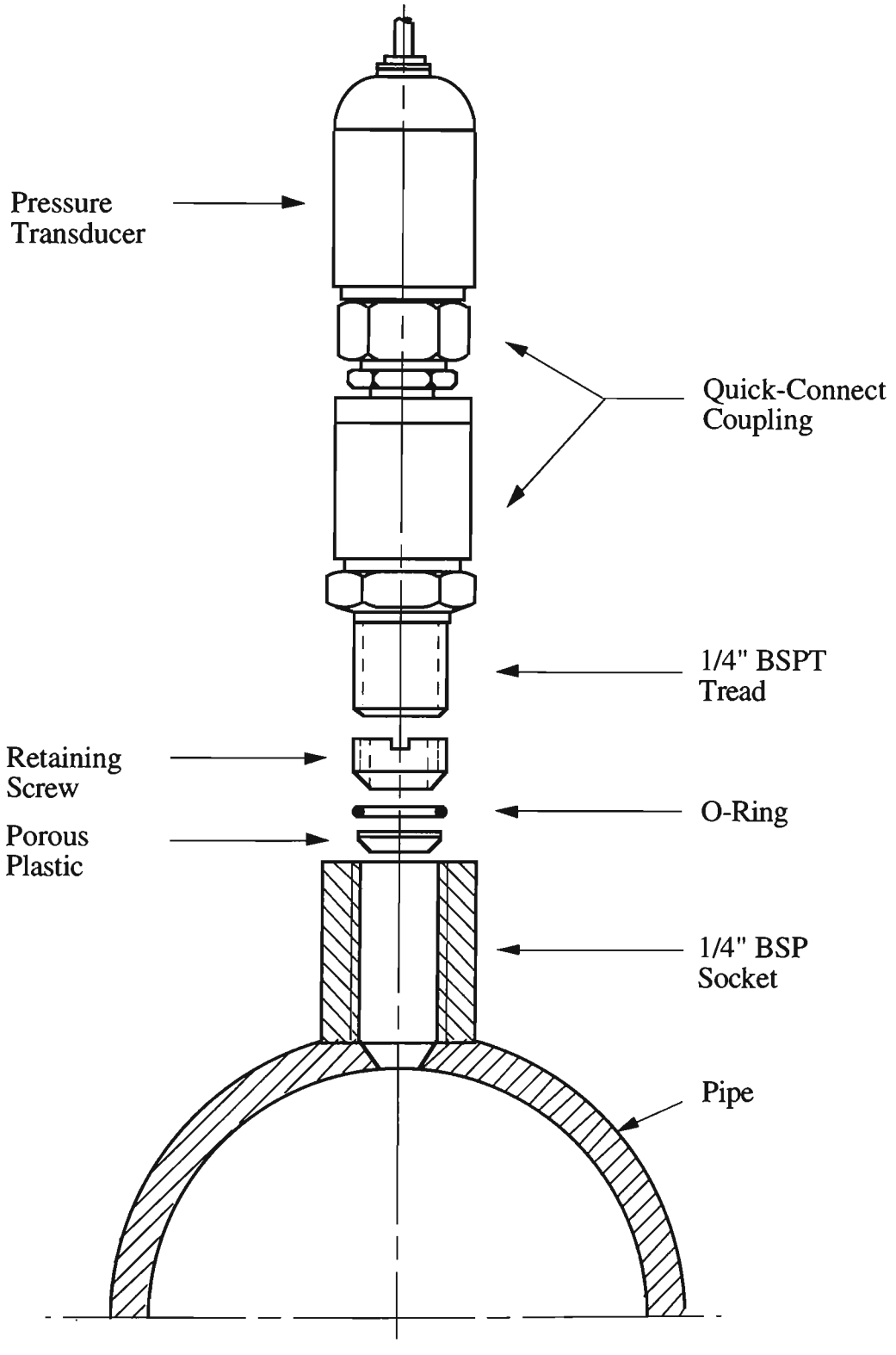

Fig. 4.7 Exploded view of typical air pressure tapping location

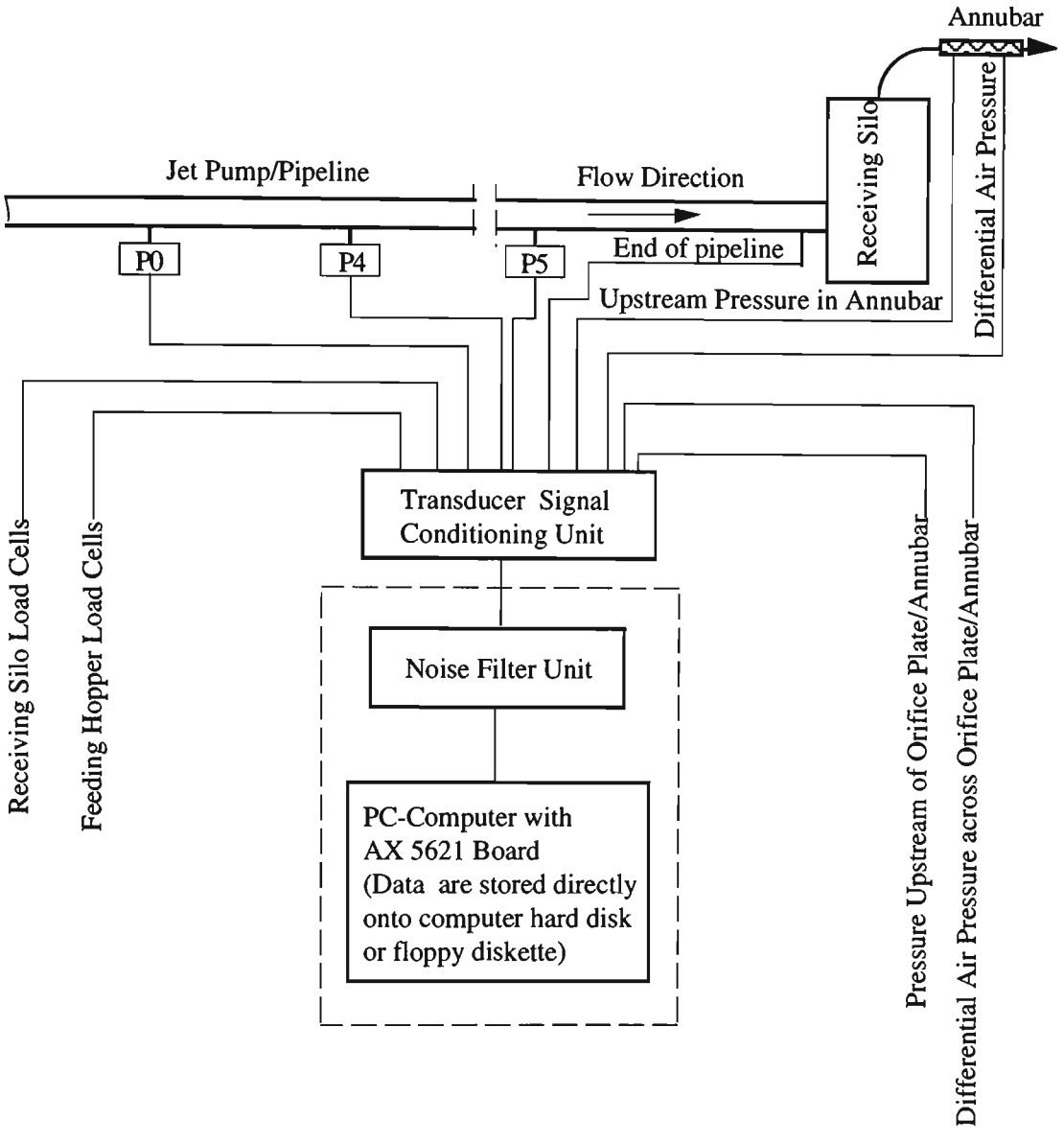

Fig. 4.8 Data acquisition systems

4.3.5 Data Processing

A data processing program "HPPLT" developed by previous researchers of the Bulk Solids Handling Research group based on a compatible IBM-PC/XT or AT computer was used to process the data collected by the DAS. The software supporting this processing was PLOT PACKAGE, which was developed by the University of Wollongong. This data processing program can read the data files directly from the diskettes, and then display the signals as required or carry out further calculations on the signals. The major functions of "HPPLT" are listed below:

(i) Plot multiple pipeline transducer responses

(ii) Calculate and plot mass flow-rate of air with respect to cycle time

(iii) Calculate flow characteristics (e.g. average pressure, solid mass flow rate)

(iv) Plot multiple pipeline transducer responses and mass flow-rate of air onto one screen

Functions (i) and (iv) are similar, but Function (i) only displays one type of transducer response (*e.g.* air pressure), whereas Function (iv) allows several types of transducer response (*e.g.* air pressure, mass flow-rate of air etc.) to be shown simultaneously for ease of comparison. Typical graphical outputs generated by Function (iv) are repeated in Fig. 4.9. Function (iv) is used to calculate the mass flow-rate of air according to the orifice plate/annubar equation using the values of differential pressure and upstream pressure of the orifice plate/annubar. These calculated results can also be presented by Function (iv), see Fig. 4.9. In Fig. 4.9, CH. 5 is the motive pressure; CH. 11 and CH. 13 represent the delivery pressure of jet pump and the back pressure in the receiving silo respectively; CH. 1 and CH. 3 illustrate the variation of the mass of the product discharged from the feeding hopper and loaded into the receiving silo; and the motive air mass flow rate also is presented. It also can be seen that the operation condition of the air-jet pump tested is quite stable.

Function (iii) is used for the statistical calculation of some major parameters, including the average value of the mass flow-rate of air in a specific time range, average static pressures and solid mass flow rate discharged from the feeding hopper and receiving silo, etc.

To obtain the dimensional and non-dimensional performance characteristics and efficiency using the average pressures and mass flow rates produced by using HPPLT, a computer program was developed by the author based on the definition presented in

Section 3.2. This program generates data files so that non-dimensional and dimensional performance plots and efficiency plots can be produced by using a commercial graph software package (e.g. Cricket Graph).

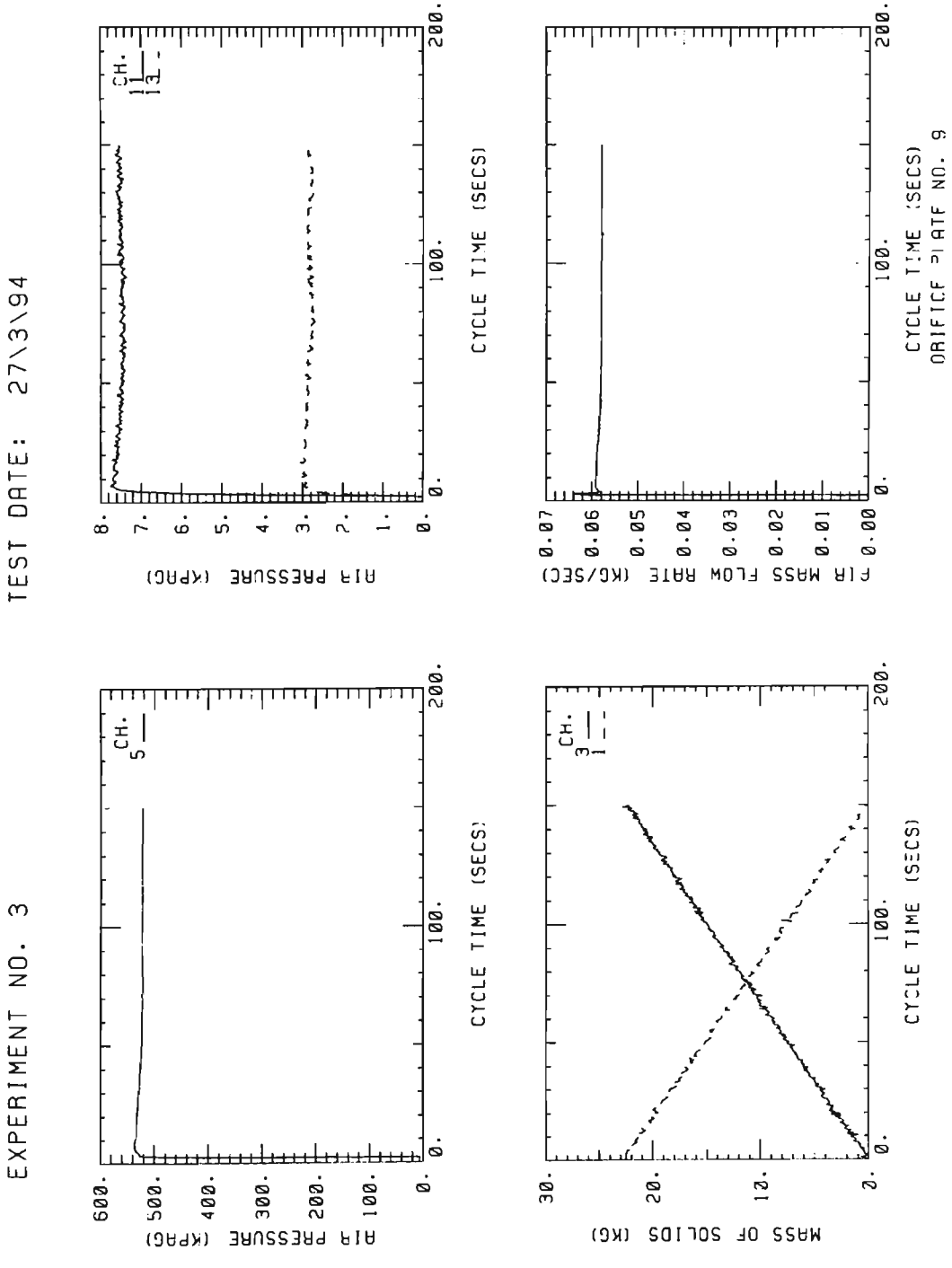

Fig. 4.9 Typical experimental result plot created by using HPPLT

4.4 Calibration

Transducers sense physical phenomena and provide electrical signals that a data acquisition system can accept. For example, load cells convert force into an analog electrical signal that the A/D converter (ADC) can measure and record. Other examples include pressure transducers and flow transducers which measure pressure and flow-rate, respectively. Although all the physical quantities are measured through different sensors, e.g. mass via load cells and air pressure via strain-gauge transducers, the actual engineering value cannot be read directly from the recorded values since they are all in the form of electrical output.

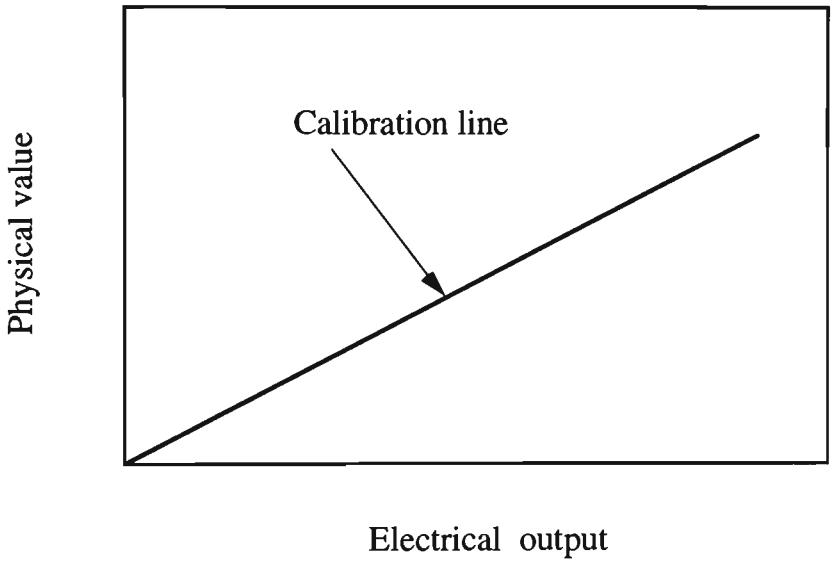

Fig. 4.10 Linear relationship between physical phenomena and electrical signal

The electrical output of a good sensor should provide a linear relationship with the actual measuring quantity, as shown in Fig. 4.10. The linearity represents the quality of the sensor. The slope of the line called the calibration factor of the transducer represents the sensitivity of the transducer. To obtained accurately the actual values of the measured quantities, the linear relationship must be determined by calibration. Generally, the calibration factor of a transducer is constant. However, variations in some environmental factors such as temperature, pressure, etc. will affect the characteristics of the sensor.

Hence, it is required to calibrate various transducers periodically, especially before a new set of experiments. Standardised calibration procedures have been developed for load cells and pressure transducers by the Bulk Solids Handling Research group.

4.4.1 Pressure Transducer Calibration

All the pressure transducers used in the test program are calibrated by maintaining a constant pressure in the pipeline and recording simultaneously the voltage responses of the transducers. The calibration procedures can be summarised as follows.

(i) Connect pressure transducers and a high accuracy pressure meter to the pipeline via pressure tappings.

(ii) Purge the pipeline with a high flow-rate of air, close the discharge valve at the bottom of the feeding hopper and block the pipe at the exit of the 40 mm diameter annubar with a steel plate (refer to Figs. 4.1 and 4.2).

(iii) Open the air supply valve, blow air into the pipeline until the pipeline pressure arrives at a designated value (e.g. 40 kPag), then close the air supply valve.

(iv) Record the pressure value monitored by the pressure meter and the voltage responses of all the transducers after the pipeline pressure becomes stable.

(v) Repeat steps (iii) and (iv) until the highest designated static pressure (i.e. a pressure slightly higher than the highest expected pressure occurring in the subsequent test program) is obtained.

A typical calibration line of a pressure transducer is presented in Fig. 4.11. The calibration factor of the transducer is 30.726 kPa/mV.

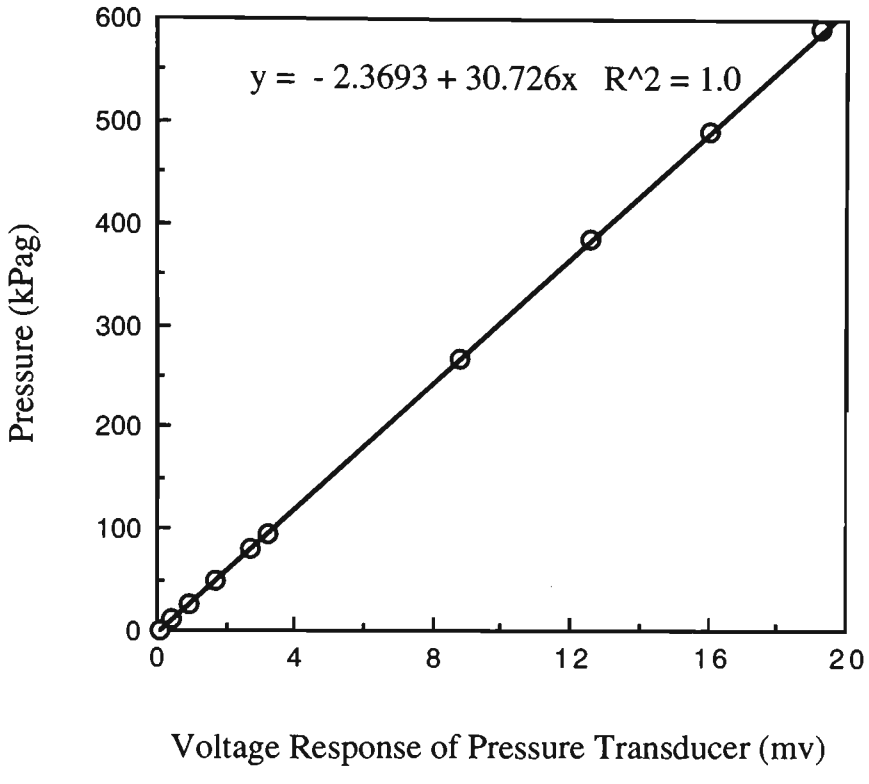

Fig. 4.11 Typical pressure transducer calibration line

4.4.2 Load Cell Calibration

Load cells which are used to support the feeding hopper, and product receiving silo, monitor the mass of material loaded in or discharged from these containers. Calibration of load cells is carried out by filling a known mass of product into the feed hopper. The detailed steps are:

(i) Remove any previously conveyed material from the pneumatic conveying test rig and purge the rig with a high flow-rate of air until the pipeline and rig are believed clean. Record the voltage output of all load cells.

(ii) Load a given mass of a product (say 40 kg) into the feed hopper. Record the voltage output of the load cells which support the feeding hopper.

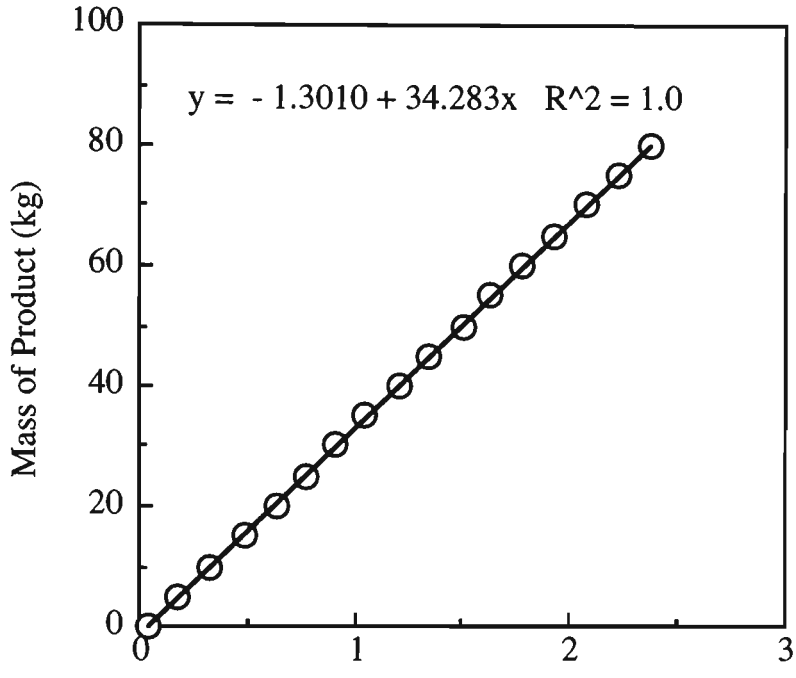

(a) Feeding hopper load cells

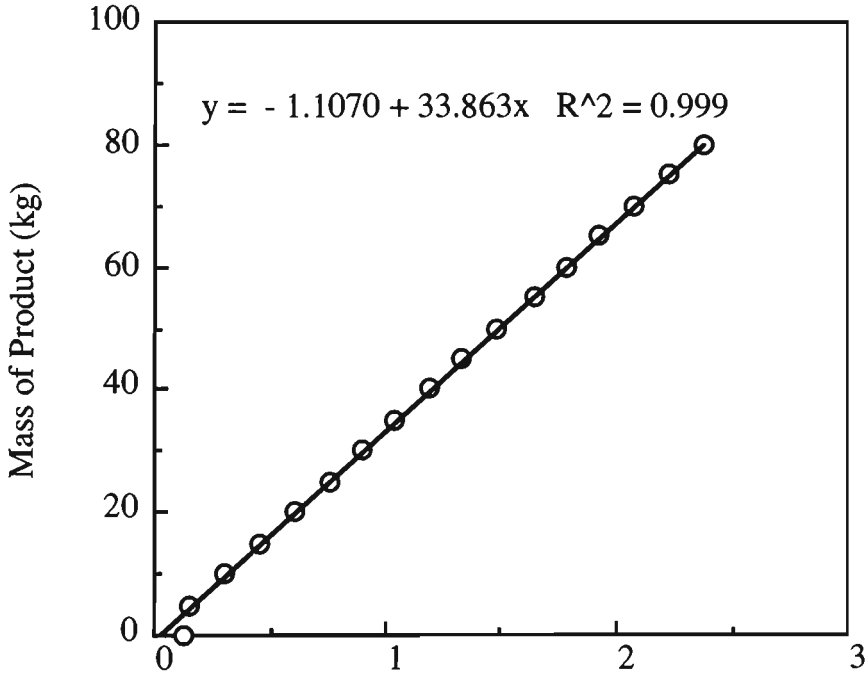

(b) Receiving silo load cells

Fig. 4.12 Calibration of load cells

(iii) Transport this material to the receiving silo (using a high flow-rate of air to ensure no product is left in the pipeline) and record the voltage output from the load cells of the receiving silo.

(iv) Discharge all the product from the receiving silo to the feed hopper (ensuring no product is left in the receiving silo). Then add another given mass of product into the hopper and record the voltage.

(v) Repeat steps (iii) and (iv) until all the designated product is loaded in the hopper.

The calibration results of the load cells are presented in Fig. 4.12. The linearity is quite good for each set of load cells. The calibration factors for the load cells of the feed hopper and receiving silo are 34.283 kg/mv and 33.863 kg/mv, respectively.

4.5 Test Materials and Their Properties

4.5.1 Test Materials

As analysed in Chapter 3, air-jet pump performance is influenced by the properties of the materials to be conveyed. Hence for an air-jet pump conveying system to be designed to ensure satisfactory and efficient operation, the influence of the properties of the materials must be considered properly. There are many terms used to describe the properties of bulk solids. Many of these properties are used in qualitative, descriptive and empirical ways. They are often difficult to define precisely and even more difficult to measure. In this work, attention is paid particularly to dilute air-solids flow in the jet pump and pipeline system. The properties considered here include particle size and distribution, density and voidage. The following sections introduce these properties and their measurement method. Three materials were chosen to examine the influence of material properties on the air-solid performance of the jet pump. Table 4.3 lists the physical

properties of these materials. In this table, bulk density and voidage are for a loose-poured condition.

Table 4.3 Properties of product tested

Name of Material Tested	Bulk Density (kg m^{-3})	Particle Density (kg m^{-3})	Particle Diameter (mm)	Void Fraction
Sorghum	772	1370	3.8	0.44
Wheat	793	1424	3.6	0.44
Plastic pellets	530	893	3.7	0.41

4.5.2 Particle Size and Distribution

Particle size and distribution are the most often used characteristics of a bulk material. However, it is often difficult to define particle size. For the spherical particle, see Fig. 4.13(a) , the size can be defined easily as the diameter. However, for cubic and irregular shaped particles, see Figs. 4.13 (b) and (c), terms such as length, thickness and diameter have little meaning as many different values for each can be determined from each single particle. In an attempt to represent the size of an irregularly shaped particle by a single quantity, the term most often used is equivalent diameter. This refers to the diameter of a sphere that exhibits the same behaviour as the particle when subjected to the same sizing technique, e.g. the sphere that has the same projected area or mass or that just passes through a mesh aperture. Thus the measurement of the size (equivalent diameter) of particles is dependent on the method used to determine that parameter.

The particle size mentioned above actually indicates single particle size. The size and shape of particles that randomly make up a real bulk solid usually vary quite widely. In this case, a mean particle size is needed to represent the size nature of the bulk solid. Only

after knowing the single particle size and distribution of a bulk solid, the mean particle size (equivalent diameter) of the bulk solid may be calculated by an appropriate method, such as the methods of arithmetic mean, geometric mean and log geometric mean, etc. Hence the size range (distribution) of the bulk solids also is an important parameter that defines the size nature of the bulk solid. There are many methods that can be used for determining the size distribution of particulate materials, such as mechanical sieving, sedimentation, microscopy, electron microscopy, scanning electron microscopy, advanced optical methods (e.g. laser diffraction).

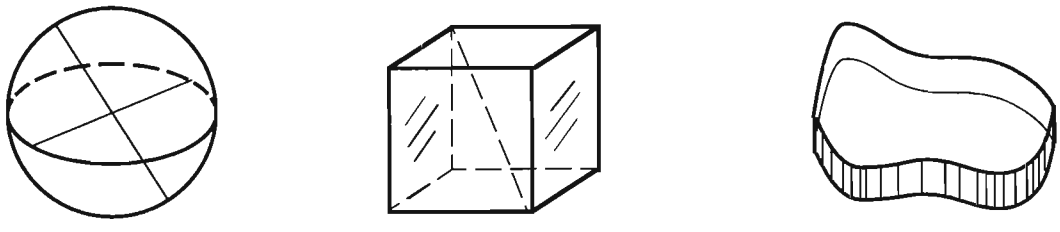

(a) (b) (c)

Fig. 4.13 Regular and irregular shaped particles

Among them, mechanical sieving is the most widely used method for determining the size distribution of a bulk solid and is a process well known to most researchers and engineers, as it covers the range of particle sizes that are of considerable industrial importance. With this method, a bulk solid sample is placed on a nest of screens with precisely defined apertures. These sieves are either manually or mechanically shaken for a designated period of time, resulting in a proportion of granules being retained on each screen. The particle size and distribution, as measured by sieving, can be defined by quoting the aperture of the two screens, one through which the particles pass and the other on which they are retained.

The most useful approach to present the particle size and distribution data is to plot the particle size or equivalent diameter against the mass percentage of the sample under a

certain size graphically. Such information gives an appreciation of the range of particle size constituting the bulk solid. A commonly used method for assigning a characteristic figure to this information is by quoting the median size. This is defined as the particle size which represents 50 % of the sample by mass.

In the case of monosized or nearly monosized particles, mean equivalent spherical size by mass is often employed. For large size particles like polyethylene pellets, the mean equivalent spherical size can be determined by the following equation as the numbers of known mass particles can be counted,

$$d_p = \sqrt[3]{\frac{6\,\dot{m}_p}{\pi \rho_p n_p}} \tag{4.1}$$

where d_p is the mean equivalent particle diameter, $\dot{m}_p$ is the mass of particles, n_p is the number of the particles of the known mass, ρ_p is the particle density.

4.5.3 Bulk Density

The mass of a bulk solid divided by the total volume of the particles and voids contained in the bulk solids is defined as bulk density. For a particular bulk solid, the bulk density does not have an unique value and varies with the condition of the bulk solid. It is dependent on the particle density, particle shape and how the particles are packed or positioned with respect to one another. For example, a bulk solid that has been conveyed pneumatically may be aerated and have a lower bulk density than if it had been allowed to de-aerate. It is not always easy to determine the bulk density of a product under changing consolidation conditions. In an air-jet pump conveying system, as the bulk solids often flow under gravity into the suction chamber of the jet pump, it is considered that the bulk solid at the suction port and suction chamber is approximately equal to a loose-poured condition. Hence, only the loose-poured bulk density is discussed here (*i.e.* compacted, tapped bulk densities, etc. are not considered).

Loose-poured bulk density usually is obtained by the following steps:

(i) Pour carefully and gently a certain volume of bulk solid into a measuring cylinder. Note that the measuring cylinder must be held at an angle of 45° to the horizontal when pouring to avoid compaction.

(ii) Bring the cylinder upright and note the volume occupied by the bulk solid.

(iii) Weigh the cylinder and bulk solid and deduce the mass of the bulk solid.

(iv) Determine the loose-poured bulk density by dividing the mass by the poured volume of the bulk solid.

4.5.4 Particle Density

A bulk solid consists of many randomly grouped particles. Besides the bulk density, each particle that makes up the bulk solid has particle density. Particle density is defined as the average mass of a single particle divided by its volume. It can often be measured using an air comparison pycnometer or stereo pycnometer. In this study, a stereo pycnometer is used for most measurements of particle density. It employs Archimedes principle of fluid displacement to determine the volume of the solid objects. The displaced fluid is a gas which can penetrate the finest pores to assure maximum accuracy. A diagram displaying the principle of the stereo pycnometer is presented in Fig. 4.14.

The device consists of two cells (i.e. the sealed sample cell and added cell) with volumes V_c and V_a connected through a selector valve. A pressure transducer is installed in the sample cell to allow accurate monitoring of the system pressure. The basic operating procedures are stated below:

(i) Open the vent valve and selector valve to bring the system to ambient pressure, then close the selector valve carefully.

(ii) Place a given volume of bulk solid sample in the sample cell, then close the vent valve and seal the sample cell.

(iii) Open the air flow valve and pressurise the sample cell to a designated pressure p_{x1} (e.g. 17 psig) above ambient.

(iv) Open the selector valve to connect the added cell with the sample cell. The air in the sample cell flows into the added cell and the pressure will fall to a lower value p_{x2}.

(v) Calculate the particle volume according to the following equation:

$$V_p = V_c + \frac{V_a}{1 - p_{x1}/p_{x2}} \tag{4.2}$$

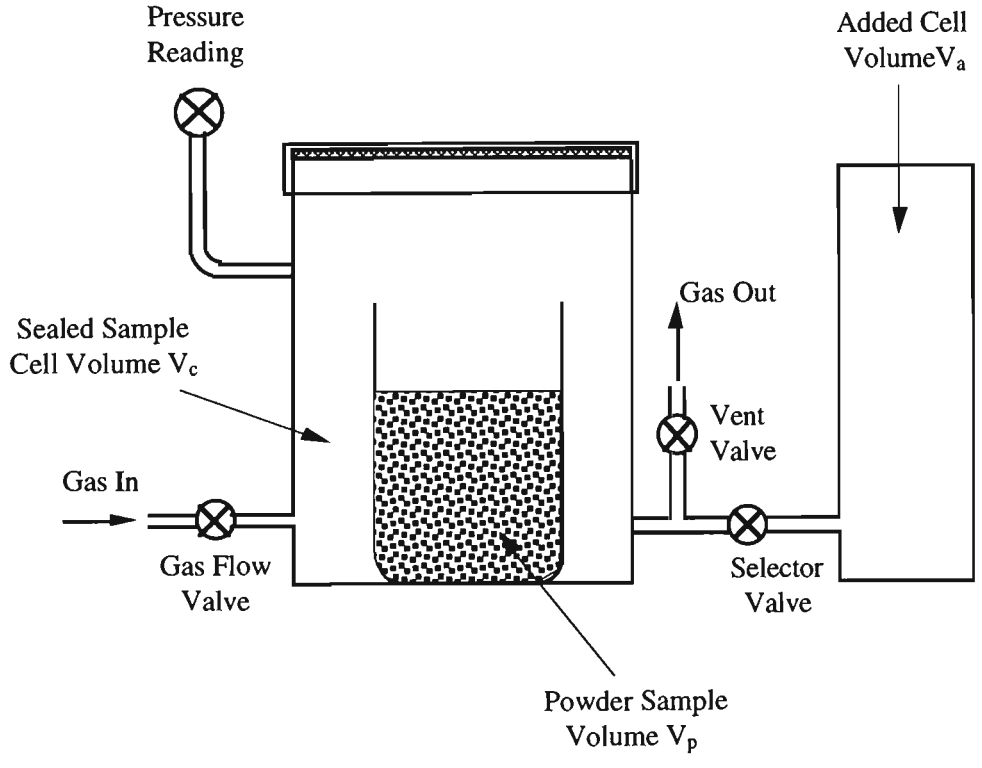

Fig. 4.14 Schematic of stereo pycnometer

The pycnometer yields the apparent particle density which is the mass of product divided by the occupied volume including closed pores but excluding open pores. It should be

noted that a stereo-pycnometer only measures the average particle density of a bulk solid. The densities of different constituent particles in a blended product may be determined by measuring them before mixing.

4.5.5 Bulk Voidage

The volume of a bulk material is not occupied completely by the particles. Part of the space is filled by voids. The volume ratio of the total voids to the bulk material is defined as the bulk voidage of the material. The bulk voidage can be calculated theoretically by using geometry for the bulk material which only consists of mono-sized spherical particles. However, due to the different arrangements of the particles, the bulk voidage can vary within a wide range even though the particle size does not change, as shown in Fig. 4.15. Also for multi-sized particles, many other factors such as size, shape and distribution of particles and degree of consolidation affect the value of bulk voidage. Hence, it is very difficult to calculate bulk voidage directly from geometry.

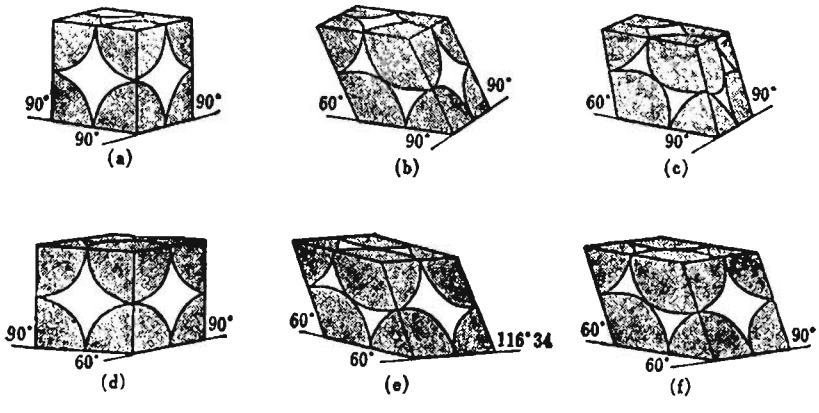

Fig. 4.15 Different arrangements of particles [74]

However, according to the definition of the bulk voidage, the bulk density and the particle density, the bulk voidage can be obtained from

$$\varepsilon = 1 - \frac{\rho_b}{\rho_p} \tag{4.3}$$

Hence the bulk voidage of a bulk solid is often calculated from the above equation after measuring the bulk density and particle density of the bulk solid.

4.6 Experimental Procedure

After all the instruments are installed and calibrated as required, a system check was conducted to ensure the test rig and experimental work ran smoothly and correctly. After completing all the necessary checks, experiments were carried out using the procedures described in the following section.

The principal variables measured in the experiments were motive and back pressure for each nozzle geometry. The experimental work for each nozzle geometry was divided into three distinct sections of work as detailed below.

4.6.1 Shut-Off Vacuum Generated and Nozzle Discharging Performance

This test was carried out by running air through the system at a given motive pressure. The receiving hopper was fully open to atmosphere. The feeding hopper was empty and sealed by closing either valve V2 or valve V1 and V3 (refer to Figs. 4.1 and 4.2). Motive air flow rate was monitored by the orifice plate and annubar and the corresponding vacuum generated in the feeding hopper was recorded. Motive pressure was varied to determine its effect on the vacuum generated and the relationship between the motive pressure and the motive mass flow rate. Furthermore, the relationship between the vacuum and the pressure at the exit of the jet pump was tested for each motive pressure. This was done by mounting an orifice plate at the exit of the receiving hopper (i.e. to vary the back-pressure inside the receiving hopper). The diameter of this orifice plate was changed to achieve a wide range of back-pressures.

4.6.2 Air-Only Performance

This test was carried out by running the motive air flow through the system at a given motive pressure and a given pressure at the exit of the air jet pump. The feeding hopper was empty. The valve V1 was closed and valves V2 and V3 opened to allow air to be sucked in. The pressure differences across the orifice plate flow meter and the annubar were monitored and recorded. The pressures at the nozzle inlet, upstream of the orifice plate flow meter, suction port and exit of the air-jet pump and the inlet of the annubar also were measured. The pressure at the exit of the air jet pump was varied by selecting 6 different diameters of orifice plate mounted at the exit of the receiving hopper. This allowed the determination of the relationship between the suction air mass flow rate and the pressure at the exit of the air jet pump. For some experiments conducted on the annular air-jet pump with multi-hole ring nozzle, the pressure distribution along the mixing section was monitored using a bank of water manometers. The motive pressure then was varied to observe the influence of motive pressure on air-jet pump performance.

4.6.3 Air-Solids Performance

This test was similar to the air-only performance test except that bulk solids were introduced into the suction port. In addition to repeating the measurements made in the air-only performance test, the mass variations of the feeding and receiving hoppers were monitored using load cells to allow the determination of conveying rate.

To eliminate the influence of the feeding hopper design on the results of monitoring the air-solids performance of the jet pump, the maximum discharge capacity of the feeding hopper under atmospheric condition must be greater than the maximum solid mass flow rate through the jet pump under all test conditions. Hence, the maximum capacity of the feeding hopper under atmospheric condition must be measured for each material. These results are listed in Table 4.4.

Table 4.4 Maximum atmospheric discharge capacity of the feeding hopper

Material	Test 1 (kg/s)	Test 2 (kg/s)	Test 3 (kg/s)	Average (kg/s)
Plastic pallets	0.402	0.406	0.401	0.403
Sorghum	0.594	0.587	0.579	0.586
Wheat	0.782	0.787	0.805	0.788

The operating procedures of the air-solids performance test are summarised below:

(i) Open the silo valve V1 and load sufficient material into the feeding hopper, see Figs. 4.1 and 4.2, then close the valve after loading.

(ii) Select and mount an orifice plate at the exit of annubar on the top of the receiving silo.

(iii) Regulate the motive pressure to the designated value.

(iv) Set the data acquisition system to scan the required channels at a suitable sampling rate.

(v) Start the data acquisition system.

(vi) After about 10 seconds, open the motive air valve to introduce air into the jet pump.

(vii) Open the discharge valve of the feeding hopper to feed the material into the suction chamber of the air-jet pump.

(viii) After all the material in the hopper has been conveyed into the silo, turn off the discharge valve of the feeding hopper.

(ix) Keep the air blowing until all the material left in the jet pump and pipeline returns to the silo, then close the air supply valve.

An air-jet pump characteristic could be obtained by varying the back pressure and repeating steps from (i) to (ix). A wide range of back pressure variation was achieved by choosing different diameters of orifice plate at the exit of the receiving silo.

In order to ensure good accuracy of results, all the above tests were performed under steady-state conditions and checked for repeatability.

CHAPTER 5

EXPERIMENTAL INVESTIGATION INTO CENTRAL AIR-JET PUMPS

5.1 Introduction

Central air-jet pumps have been commercially available for pneumatic conveying for many years. In engineering practice, the determination of the ability of this type of equipment to induce a solid flow from a feeding hopper and the parameters that affect conveying rate and pressure should be the first step in designing/selecting an air-jet pump system.

Despite an abundance of experimental work [10-13, 20, 26, 28, 36, 37, 58, 60, 73, 101], to date the understanding of the relationship between the conveying capacity and related factors is far from adequate. The main reason is there is a shortage of systematic experimental data relating both geometrical parameters and operating conditions to performance. As a result, the design of this type of equipment and associated system still rely heavily on experience and trial-and-error. Hence, it is essential to investigate the effect of air-jet pump geometry and operating conditions on pump performance so that a design strategy can be formulated and options to improve efficiency can be determined.

During the present research, a systematic experimental program has been designed and undertaken in the Bulk Solids Handling Laboratory at the University of Wollongong to strengthen jet pump data base. The investigation was aimed at examining the factors that influence air-jet pump performance. The results obtained from this work also are used to verify the theoretical model developed in Chapter 3. The experiments were conducted by varying nozzle-throat gap, motive pressure and back pressure for each particular air-jet pump design to observe the effect of operating conditions and geometrical parameters on

the air-jet pump performance. In this chapter, the experimental results are presented using dimensional and non-dimensional characteristics defined in Section 3.2. Compared with the experimental work reviewed in Section 2.3, the present experimental investigation possesses the following distinct features:

- Efficiency has been introduced to assess the energy-effectiveness of an air-jet pump for transporting bulk solids in a pipeline;
- The influence of nozzle-throat gap on pump characteristics has been examined in detail for five different area ratios and different motive pressure;
- Wider motive pressure variation range has been tested for each air-jet pump configuration to monitor the influence of motive pressure on pump performance;
- Area ratio has been used as a geometry factor to describe pump geometry; a wide area ratio range also has been tested by varying the nozzle diameter for a given throat tube diameter;
- Both air-only and air-solids performance have been monitored so as to better understand the factors influencing pump performance;
- Both dimensional and non-dimensional characteristics have been used to present the experimental results.

5.2 Experimental Scheme

The general configuration of the air-jet pump tested has been shown in Fig. 4.5. This jet pump was designed to provide easy changing of the nozzle configuration and/or nozzle geometry. Different combinations of motive pressure, nozzle-throat gap, nozzle outlet diameter and jet pump exit pressure were investigated by considering the variation of one parameter with respect to the others, so as to monitor the air-only and the air-solids

characteristics. These combinations are summarised in Table 5.1. It should be noted that the pump exit pressure also was varied 6 times by selecting different diameters of orifice plate mounted at the exit of the receiving silo for each experiment set-up (combination of area ratio, nozzle-throat gap and motive pressure), so that the relationship between suction mass flow rate and the delivery pressure can be determined. The majority of the experiments were conducted using white plastic pellets as the test material. Wheat and sorghum also were used to investigate the influence of material properties on pump performance. The properties of these three materials have been listed in Table 4.3. The experimental procedure is detailed in Section 4.6. The detailed dimensions of each jet pump configuration tested have been provided in Table 4.2.

5.3 Motive Air Mass Flow Rate

The dependency of motive air mass flow rate on motive pressure for 5 different nozzles is shown in Fig. 5.1. This figure illustrates that the mass flow rate of air through each nozzle is proportional to the motive pressure. Also, for a given motive pressure, the mass flow rate of air obviously increases with nozzle size (i.e. flow area).

The air mass flow rates determined by Eq. (3.20) and Eq. (3.21) using c=0.98 also have been plotted in Fig. 5.1 for comparison. It can be seen in this figure that the calculation results agree favourably with the experimental results.

5.4 Shut-Off Vacuum

Shut-off vacuum refers to the vacuum at the suction port generated by the air-jet pump discharging to atmosphere when the feeding hopper is closed. The shut-off vacuum is proportional to the motive pressure as shown in Fig. 5.2. This figure also shows the influence of area ratio on shut-off vacuum. As the area ratio increases, the shut-off

vacuum decreases for a given motive and delivery pressure. The influence of delivery pressure on the shut-off vacuum is shown in Fig. 5.3. It can be seen that the shut-off vacuum for a given motive pressure decreases as the delivery pressure increases. If the delivery pressure reaches a certain value, the shut-off vacuum will become zero. If the delivery pressure increases further, the pressure in the suction port will become positive. This means that the motive air flow will discharge partly via the suction port of the jet pump. Thus, the suction effect will deteriorate.

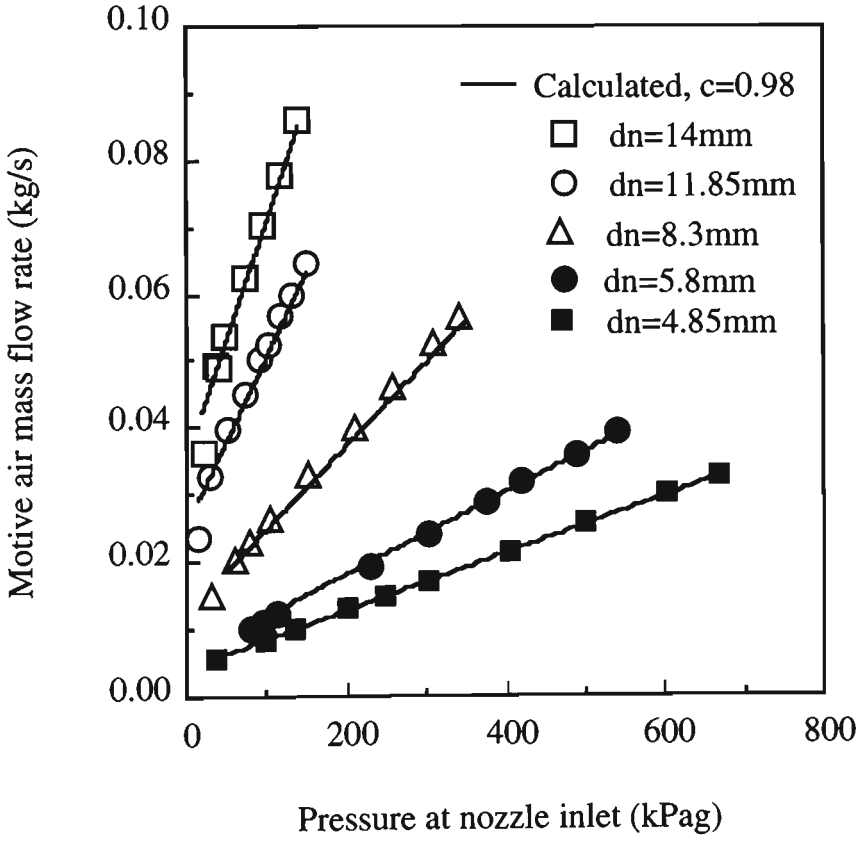

Fig. 5.1 Variation of motive air mass flow rate with motive pressure

Table 5.1 Summary of experimental set-up for central air-jet pump

Area ratio	Nozzle-throat gap (mm)	Motive Pressure for Air-only Performance Test (kPag)	Motive Pressure for Air-Solid Performance Test (kPag)		
			plastic pellets	wheat	sorghum
2.86	30	40	40 20		
2.86	50	40 100	100 80 60 40 20	40	30
2.86	70	40	40 20		
2.86	87	40	40 20		
3.93	30	60	60		
3.93	50	60 100	60 40	60	40
3.93	70	60	60		
3.93	87	60	60		
8.14	30	100 200	80 100 150 200		
8.14	50	100 200	100 200	100 200	100
8.14	70	100 200	100 200		
8.14	87	100 200	100 200		
16.67	30	400	400		
16.67	50	400	300	400	300
16.67	70	400	400		
16.67	87	400	400		
23.84	30	400 200	200 400 600		
23.84	50	400	400	500	500
23.84	70	400	400		
23.84	87	400	400		

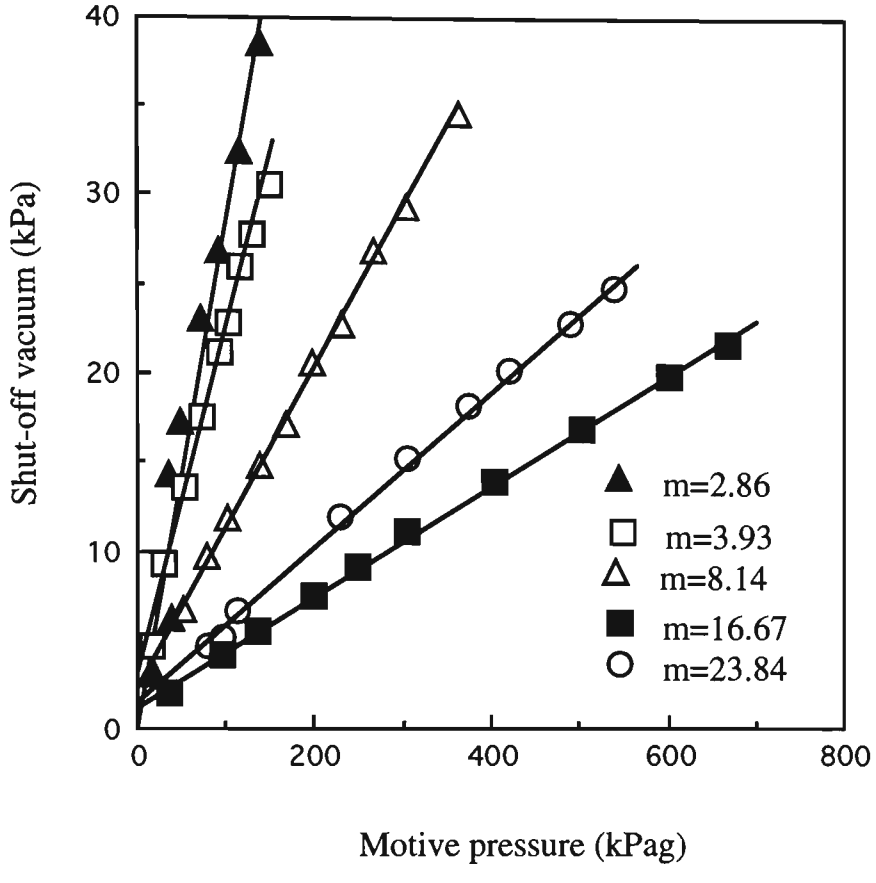

Fig. 5.2 Variation of shut-off vacuum with motive pressure and area ratio (L_c = 30 mm)

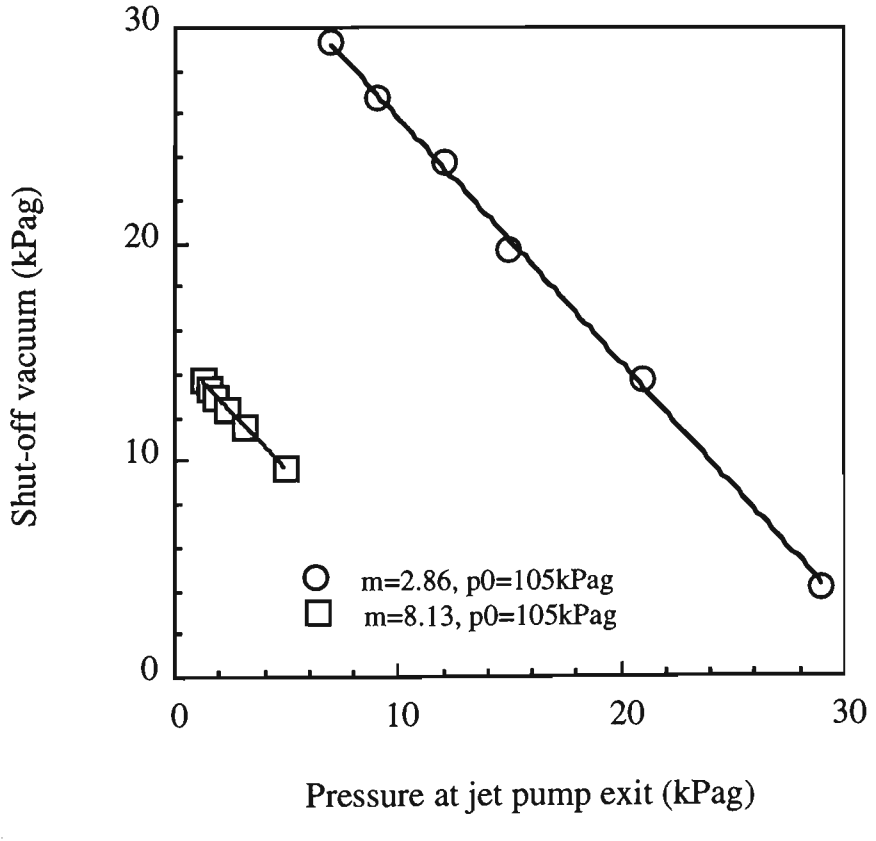

Fig. 5.3 Influence of delivery pressure on shut-off pressure (L_c = 30 mm)

5.5 Air-Only Pump Characteristics

5.5.1 Dimensional Characteristics

Dimensional air-only performance of air-jet pumps represents the variation of mass flow rate with pressure difference $\overline{p_5} - \overline{p_4}$. This relationship is influenced by pressure (motive pressure, suction pressure and receiving hopper pressure) and nozzle throat gap, as detailed below.

5.5.1.1 Influence of Pressure

The influence of pressure difference $\overline{p_5} - \overline{p_4}$ on suction air mass flow rate is shown in Fig. 5.4. It can be seen clearly that for a given motive pressure, as the pressure difference increases, the suction air mass flow rate decreases, and vice versa.

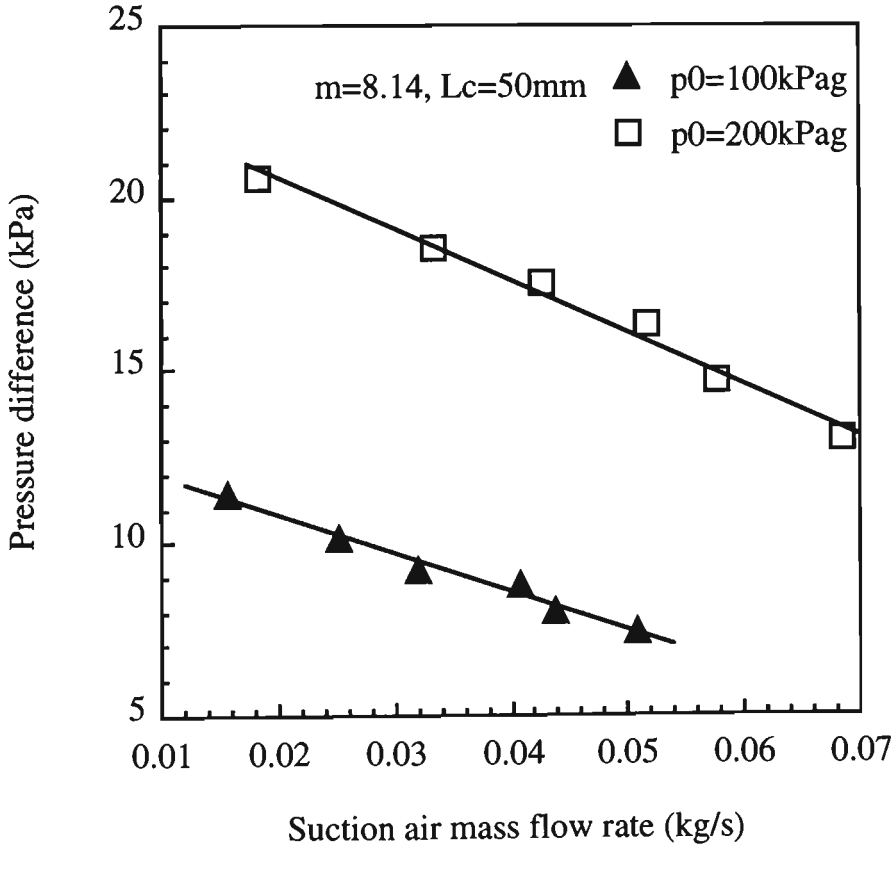

Fig. 5.4 Influence of motive pressure on dimensional pump performance

A variation in motive pressure affects the pressure difference and suction air mass flow rate. It can also be seen from Fig. 5.4 that for a given suction mass flow rate, the pressure difference created by the air-jet pump increases with motive pressure, and for a given pressure difference, the suction air mass flow rate increases as the motive pressure increases.

As shown in Fig. 5.5, the influence of delivery pressure on suction mass flow rate is similar to the influence of pressure difference $\overline{p_5} - \overline{p_4}$ on suction mass flow rate. For a given motive pressure, the suction mass flow rate decreases as the delivery pressure increases. If the delivery pressure becomes too large, the suction mass flow rate will tend to zero. The delivery pressure is affected by the pressure in the receiving hopper in an air-jet pump conveying system. For a given motive pressure, as shown in Fig. 5.6, an increase in the receiving hopper pressure decreases the suction mass flow rate, and vice versa. In fact, the delivery pressure required by a conveying system is the sum of the pressure in the receiving hopper and the pressure drop across the conveying pipeline. An increase in the receiving hopper pressure increases the delivery pressure of the air-jet pump and pressure difference required by the conveying system for a given suction pressure.

Figures 5.5 and 5.6 also show that the variation of the motive pressure may also influence the delivery pressure and the receiving hopper pressure generated by the air-jet pump. For example, it can be seen clearly that an increase in motive pressure may increase the delivery pressure and the receiving hopper pressure; for a given delivery pressure and receiving hopper pressure, an increase in motive pressure may cause an increase in suction air mass flow rate. Fig. 5.7 shows that the suction pressure is dependent on the suction mass flow rate. The suction pressure decreases as the suction mass flow rate increases. The reason is that the pressure drop between the inlet of the feeding hopper and suction port increases with suction air mass flow rate.

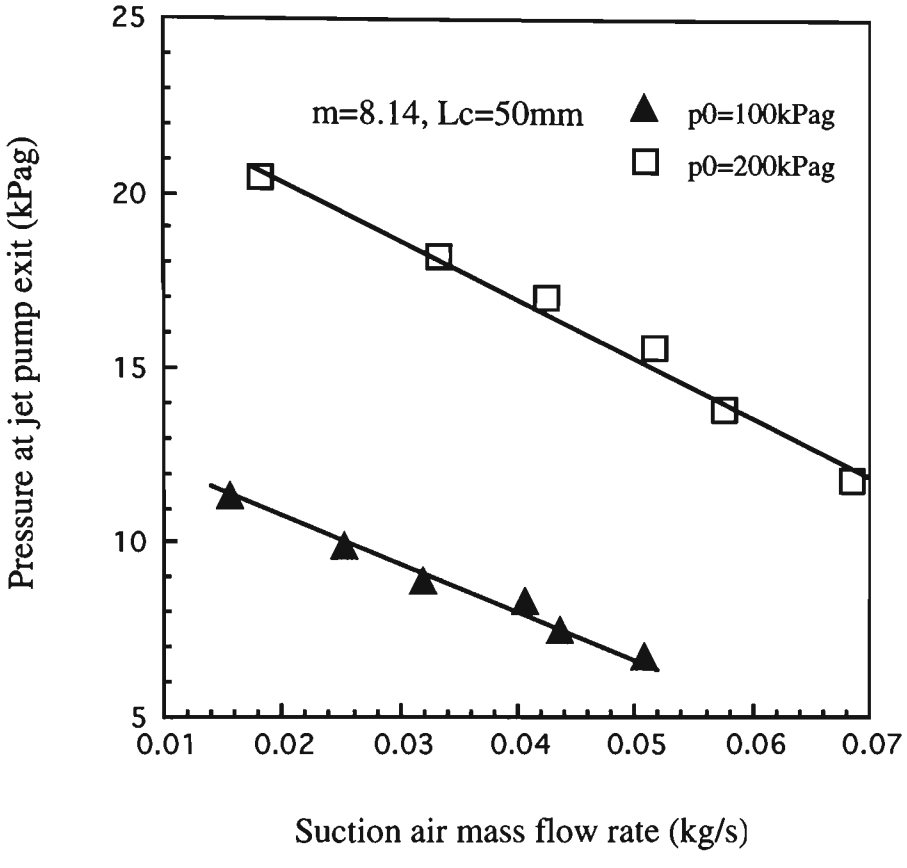

Fig. 5.5 Influence of motive pressure on delivery pressure

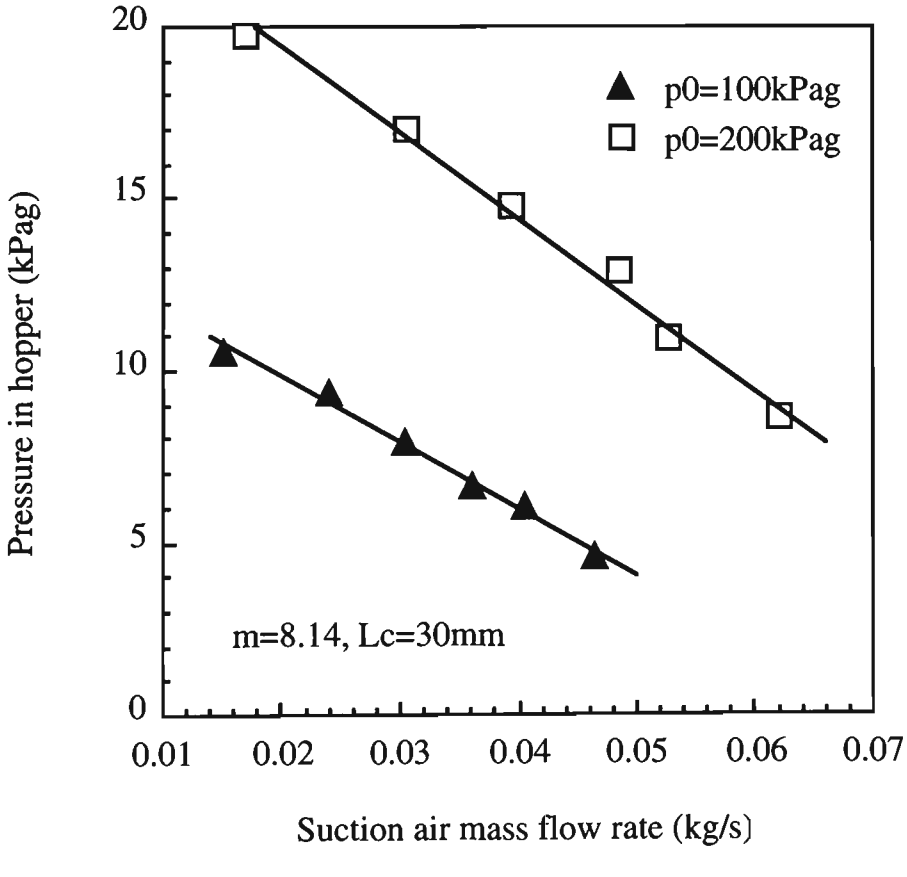

Fig. 5.6 Influence of motive pressure on receiving hopper pressure

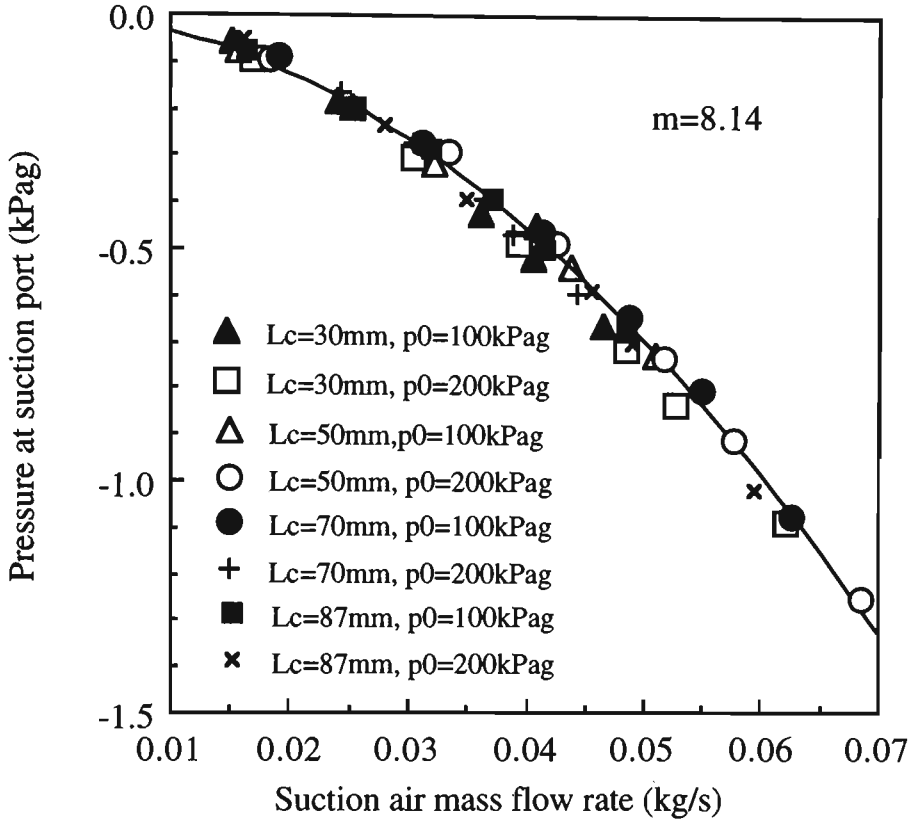

Fig. 5.7 Variation of suction pressure with suction air mass flow rate

5.5.1.2 Influence of Nozzle-throat Gap

Nozzle-throat gap is expressed by some researchers [20, 28, 101] as the distance F shown in Fig. 4.5. However, the flow area of the motive air-jet at the throat entry section 2-2, which contributes to the performance of the air-jet pump, is determined by the distance L_c rather than F. Therefore, F can not really reflect the influence of motive air-jet expansion from the nozzle exit to the throat entry section on performance. In this thesis, nozzle-throat gap is defined as the distance L_c between the nozzle exit section and the throat inlet section, as shown in Fig. 4.5. The difference between L_c and F is 30 mm for the jet pump designs considered in this study. Fig. 5.8 shows the influence of nozzle-throat gap on air-only pump characteristics. It can be seen from this figure that for a given suction air mass flow rate, the pressure difference decreases as the nozzle-throat gap

increases from 30 mm to 50 mm to 70 mm and then 87 mm (for a given motive and suction pressure). The maximum pressure difference over all the variation range of the suction air mass flow rate for m =2.86 has been obtained by using a nozzle-throat gap of 50 mm.

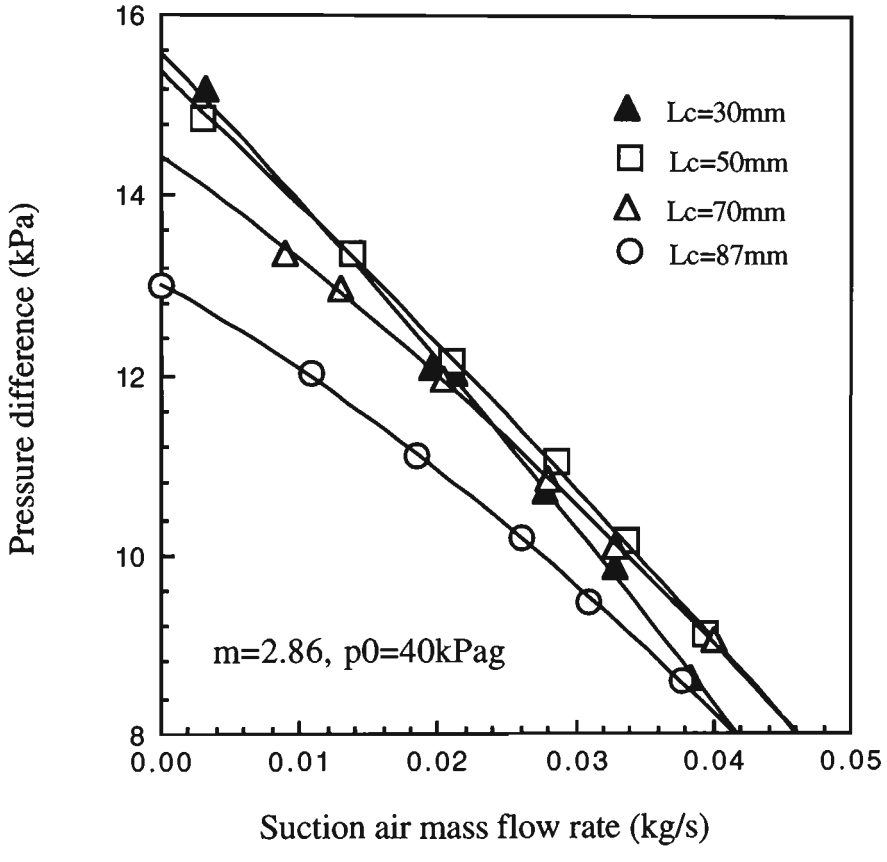

Fig. 5.8 Influence of nozzle-throat gap on dimensional pump performance

The influence of throat tube length has not been investigated, and L_t/d_t =5.5 was used in this experimental work for both air-only and air-solid performance monitoring. However, it has been reported that the optimum value of L_t/d_t = 6 to 8.5 [48], which is close to $L_t/d_t \approx 7$ observed in a water jet pump of similar design, although mixing tube lengths as short as 5.7 d_t and as long a l0 d_t also have yielded good performance [14, 46, 69, 83].

5.5.2 Non-Dimensional Pump Characteristics

Non-dimensional air-only pump performance is represented using the non-dimensional parameters defined in Section 3.2. Based on the present experimental investigation, non-dimensional performance is influenced by the motive pressure, nozzle-throat gap and area ratio.

5.5.2.1 Influence of Motive Pressure

The influence of motive pressure on non-dimensional air-only pump performance is shown in Fig. 5.9. It can be seen that for a given mass flow rate ratio, the pressure ratio decreases as the motive pressure increases, and vice versa; for a given pressure ratio, the mass flow rate ratio increases as the motive pressure decreases, and vice versa. For a given delivery pressure, a variation in motive pressure causes a change in h, so the secondary flow rate will change to maintain a mass flow rate ratio x with respect to h. However, the pressure drop in the conveying system increases with mass flow rate. For a given pressure in the receiving hopper, an increase in pressure drop requires an increase in delivery pressure. For given motive pressure and suction pressure, increasing the delivery pressure will increase h and decrease x and the suction mass flow rate.

From Eq. (3.6), it can be seen that an increase in pressure ratio h for a given delivery pressure suggests that the motive pressure can be reduced for a given jet pump geometry. However, as mentioned above, an increase in pressure ratio h reduces the mass flow rate ratio x. From Eq. (3.5), a reduction in x requires an increase in motive mass flow rate for a required suction air mass flow rate. For a given nozzle geometry, increasing the motive mass flow rate in turn requires an increase in motive pressure. Hence, there must be a compromise of motive pressure between h and x for a given area ratio to minimise the power input required, or an optimum motive pressure for a given area ratio.

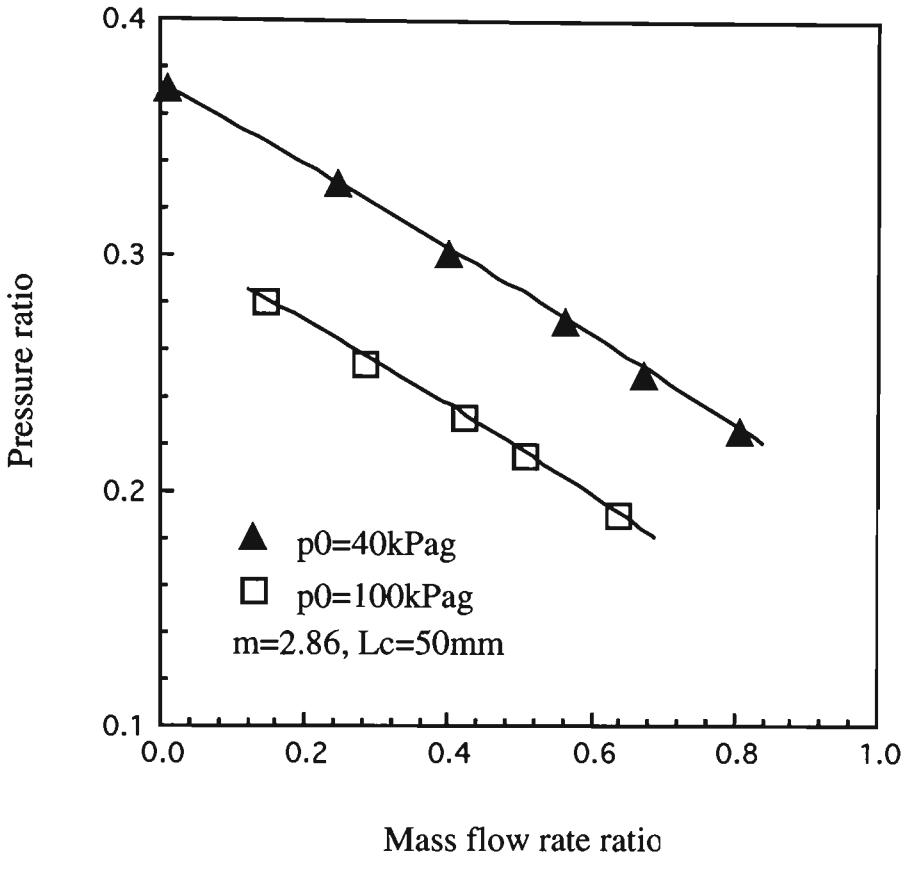

Fig. 5.9 Influence of motive pressure on non-dimensional pump performance

5.5.2.2 Influence of Area Ratio

Fig. 5.10 shows the non-dimensional air-only pump performance curves with five different area ratios. From this figure it can be seen that the *h*-*x* lines become flatter as *m* is increased and steeper as *m* is decreased. This means that *x* may increase or decrease by varying *m* for a given *h*, and for a given *x*, *h* may increase or decrease. This suggests that reducing *m* produces a steeper *h*-*x* characteristic line and an increased pressure ratio. From Eq. (3.6), an increase in h requires an increase in p_5 if p_0 and p_4 are kept constant. This suggests that a small *m* suits the application of a high delivery pressure, and vice versa. It also can be seen that the maximum mass flow ratio corresponding to a minimum pressure ratio value (i.e. delivery pressure as small as possible for a given motive pressure) increases with area ratio. The reason is that an increase in area ratio for a given throat tube diameter can only be gained by decreasing the flow area of the motive fluid. For a given motive pressure, the motive flow rate decreases with a decrease in

motive flow area. That is, the motive mass flow rate decreases with an increase in area ratio. The flow area of secondary stream increases with an increase in area ratio for a given throat tube diameter. The suction air mass flow rate increases as the flow area increases for a given suction pressure. The increase in maximum suction mass flow rate and the decrease in motive mass flow rate cause the maximum mass flow ratio to increase with area ratio.

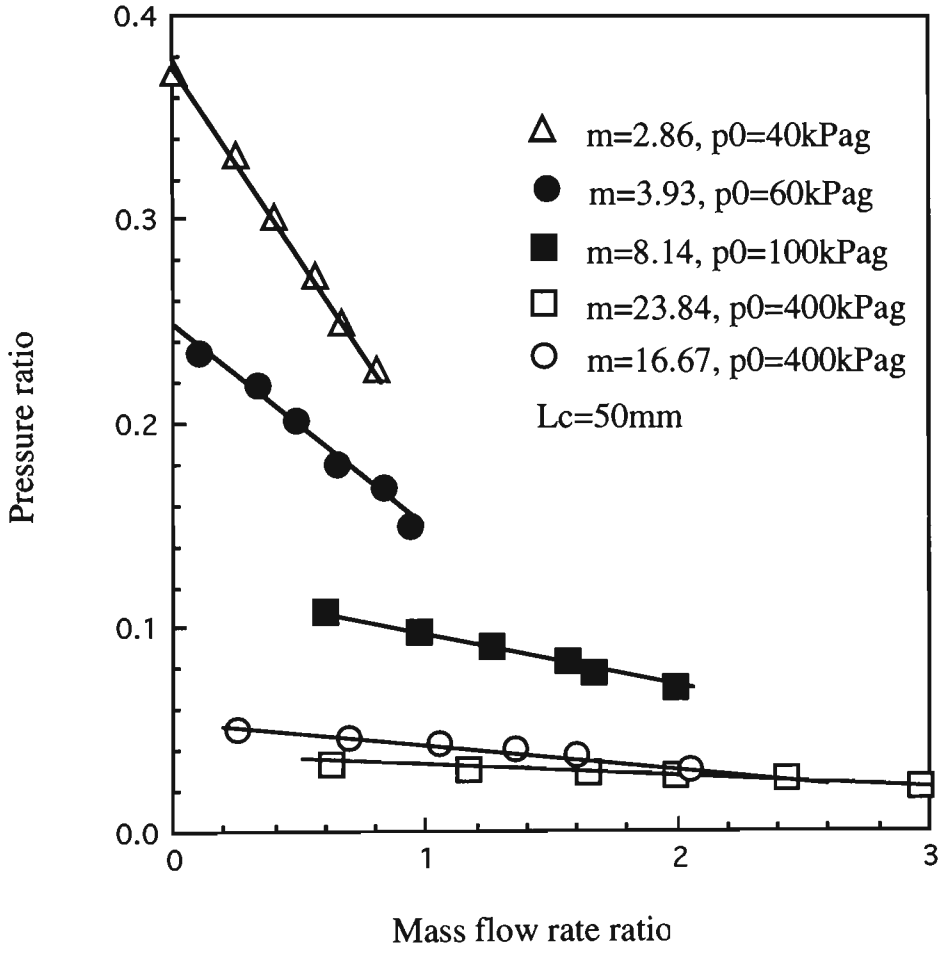

Fig. 5.10 Influence of area ratio on non-dimensional pump performance

Fig. 5.10 also shows that the one pressure ratio or mass flow rate ratio value can be obtained using air-jet pumps with different area ratio m. Different values of m represent different relationships between h and x, and require different power input. Therefore, there must be an optimum area ratio for a given operating condition.

5.5.2.3 Influence Of Nozzle-Throat Gap

Fig. 5.11 shows the influence of nozzle-throat gap L_c on non-dimensional pump performance. It can be seen that the mass flow rate ratio for a given pressure ratio decreases as the distance L_c is increased. For a given motive pressure, a specified h results in a given delivery pressure (suction pressure varies very little); an increase in mass flow rate ratio x means an increase in suction mass flow rate and vice versa. Therefore, it is preferred to use $L_c \approx 30$ to 50 to obtain the greatest air mass flow rate ratio for a given pressure ratio for all the jet pump designs tested.

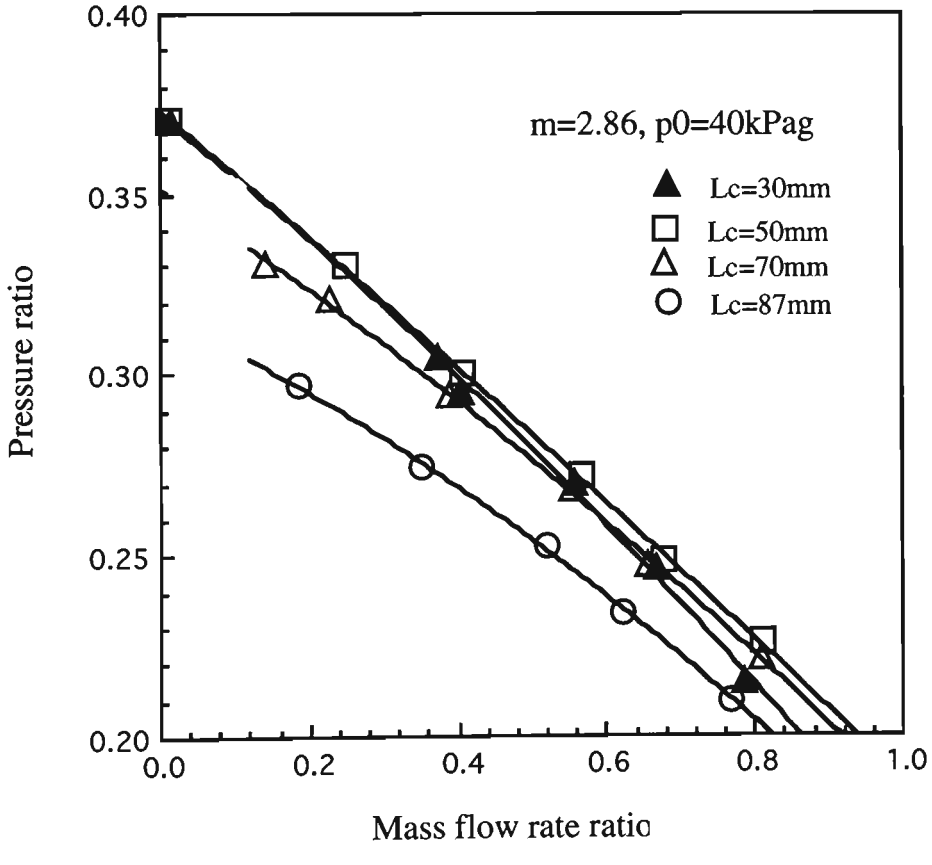

Fig. 5.11 Influence of nozzle-throat gap on non-dimensional performance

5.5.3 Air-Only Efficiency

Efficiency defined by Eq. (3.9) is introduced to measure how effectively the motive air flow is used to compress the suction air isothermally. Factors influencing air-only efficiency is presented and discussed as follows.

5.5.3.1 Motive Pressure

Figs. 5.12 and 5.13 show the influence of the motive pressure on efficiency. It can be seen clearly from these figures that for a given mass flow rate ratio the efficiency increases with decreasing motive pressure. This suggests that a lower motive pressure should be employed to improve efficiency. However, it should be noted that a decrease in motive pressure will decrease the motive mass flow rate for a given nozzle geometry and increase the pressure ratio h and decrease x (for a given delivery pressure).

5.5.3.2 Area ratio

The relationship between area ratio m, mass flow rate ratio and efficiency is shown in Fig. 5.14. It can be seen from this figure that there must be an optimum area ratio for a given mass flow rate (to obtain maximum efficiency). For example, for x=1, the optimum value of m is 3.93, and 23.84 for x=3. This suggests that the efficiency of an air-jet pump conveying system can be improved by optimising the area ratio m for a given set of operating conditions.

5.5.3.3 Nozzle-Throat Gap

The influence of nozzle-throat gap on efficiency is shown in Fig. 5.15. It can be seen that there is not much difference between the efficiency curves for a given operating condition as the nozzle-throat gap L_c increases from 30 mm to 70 mm. However, a significant decrease in efficiency occurs for L_c=87 mm. Therefore, in terms of efficiency, an optimum nozzle-throat gap exists for a given jet pump. The optimum value of L_c for all

the jet pump designs tested in this work is in the range of 30 mm to 50 mm, which may be expressed as L_c/d_t =1.25 to 2.1. Ichiro [48] is one of the few researchers that deals with the influence of nozzle-throat gap on air-only pump performance. The optimum value of L_c for an air-jet pump with a design similar to that used in present work was found by Ichiro [48] to be 15 mm, which corresponds to L_c/d_t =1.57. Similar work concerning the nozzle-throat gap was conducted by Watson [113] on steam ejectors. The optimum value was found to be L_c/d_t =2.0 [113]. Hence, the present results regarding the optimum values of L_c agree fairly well with those presented by previous researchers.

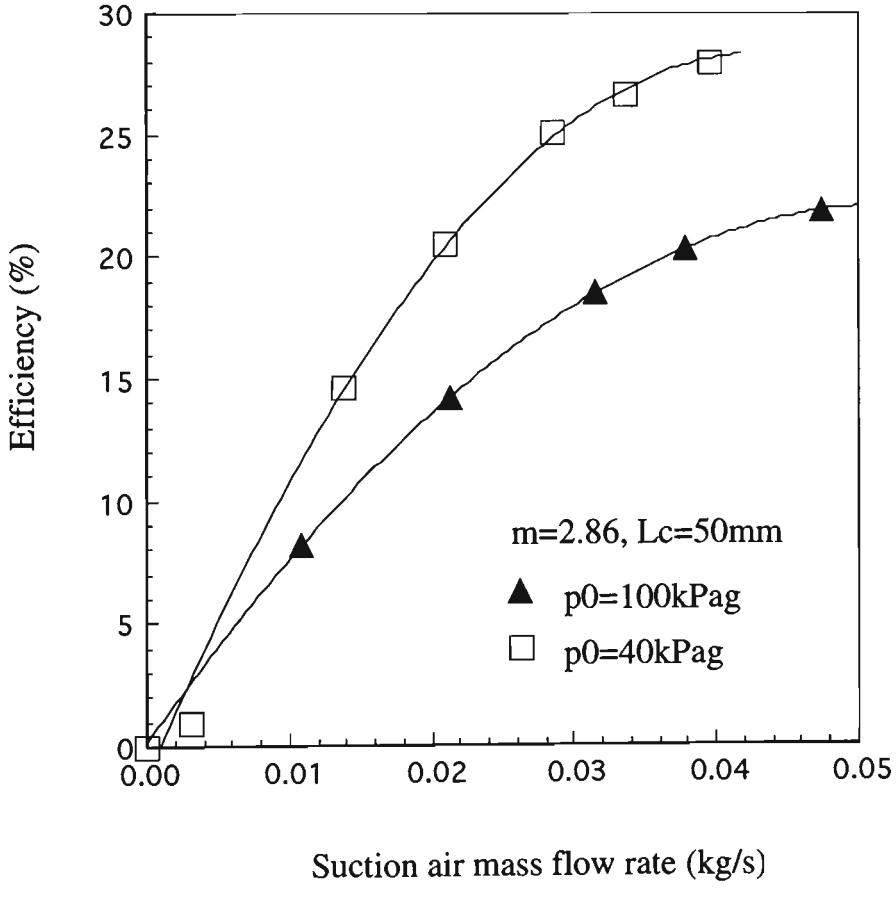

Fig. 5.12 Influence of motive pressure on efficiency and suction mass flow rate

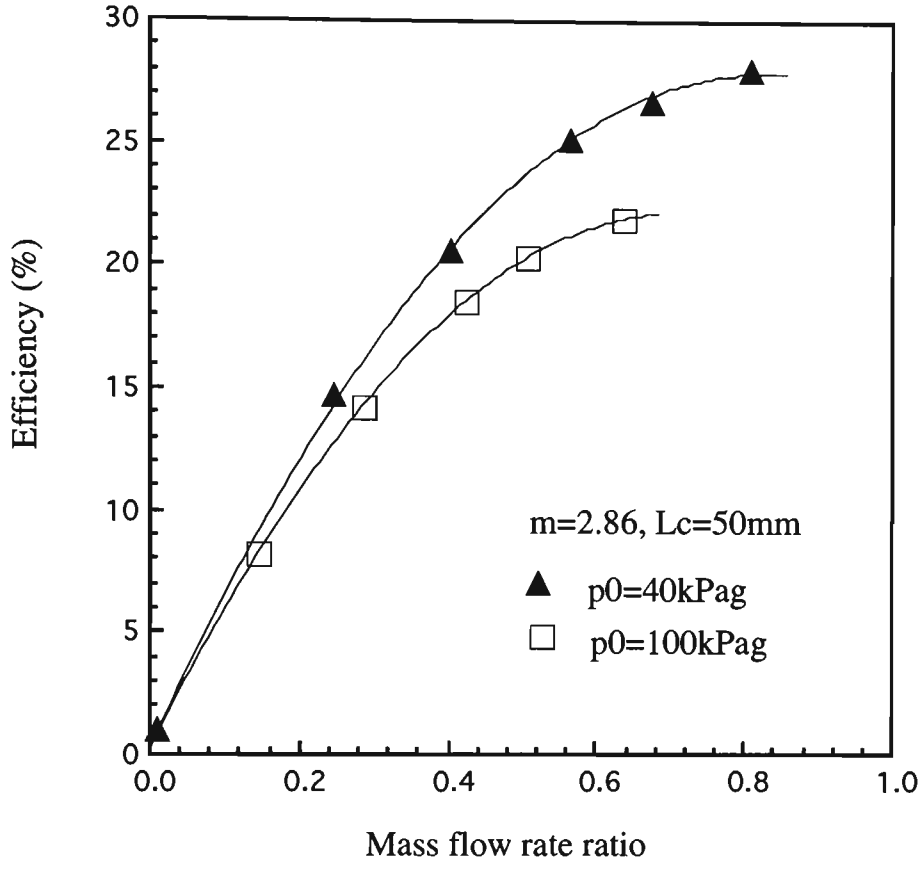

Fig. 5.13 Influence of motive pressure on efficiency and mass flow rate ratio

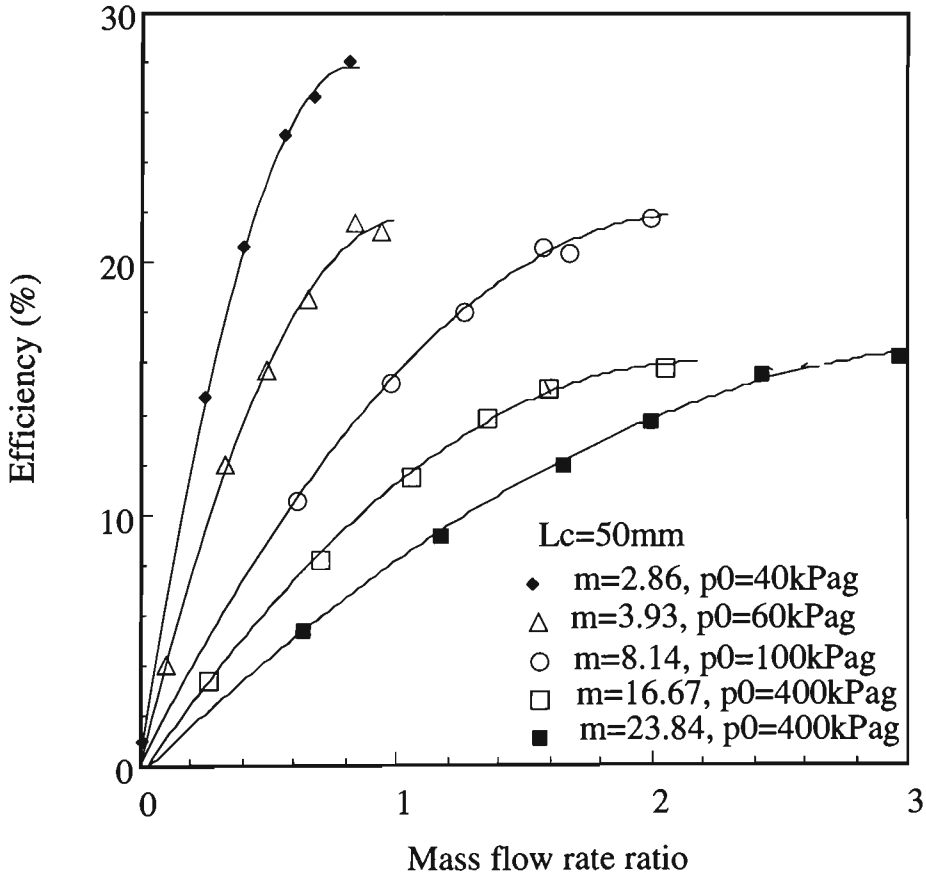

Fig. 5.14 Influence of area ratio on efficiency

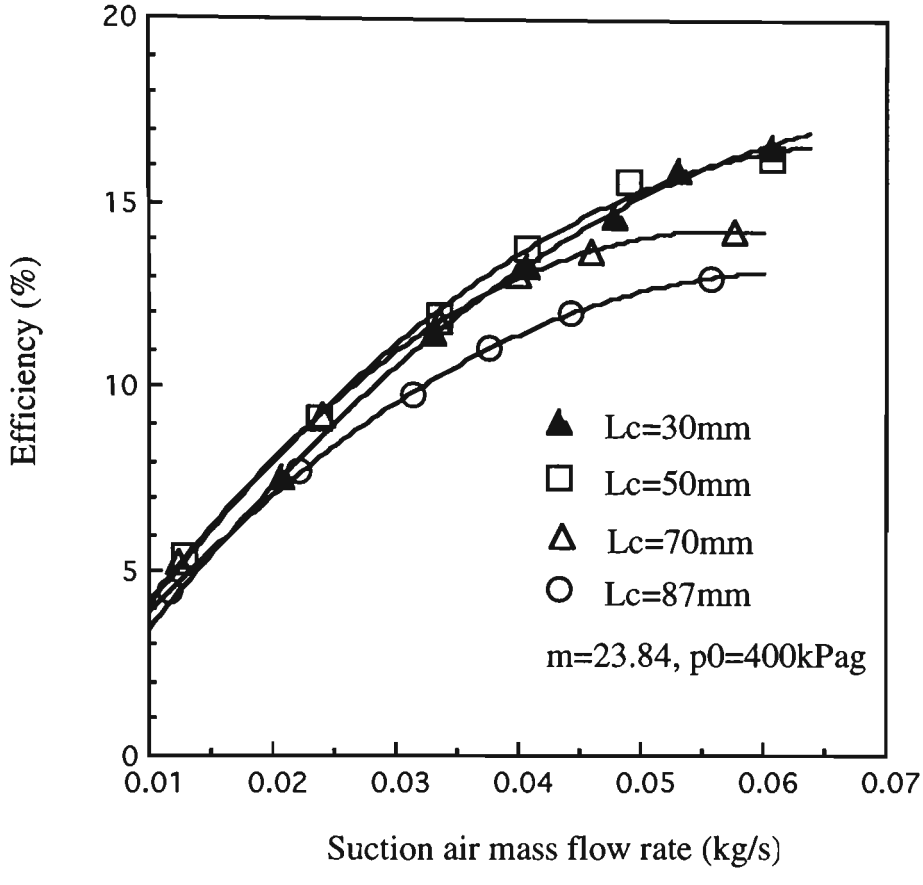

Fig. 5.15 (a) Influence of nozzle-throat gap on efficiency and suction mass flow rate

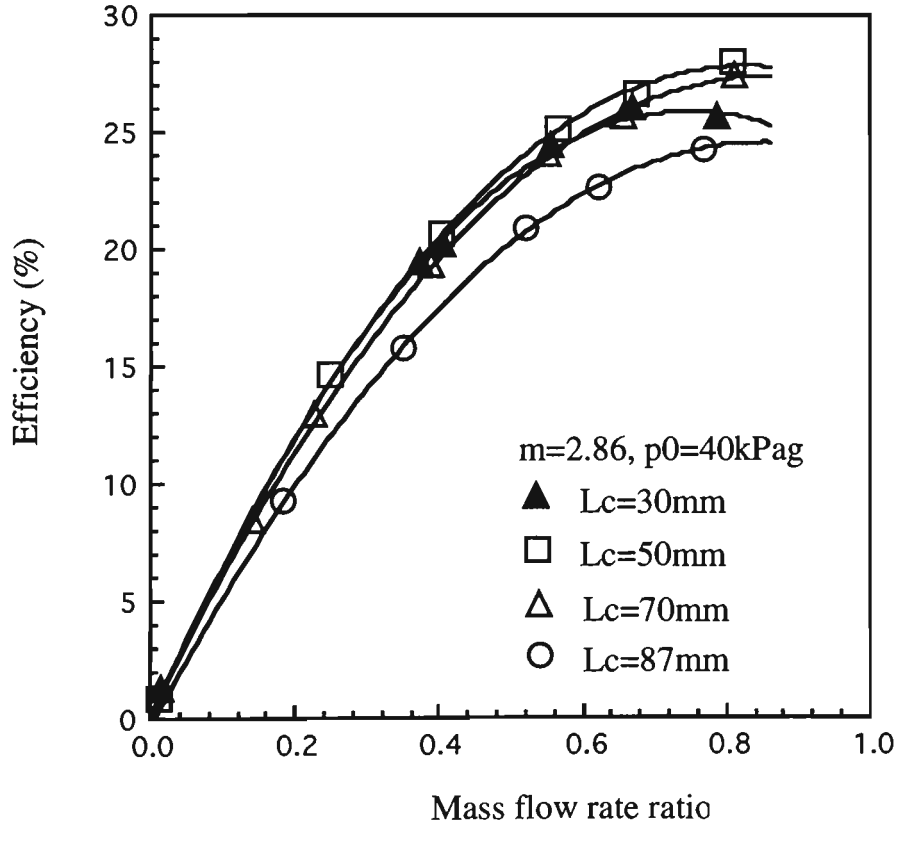

Fig. 5.15 (b) Influence of nozzle-throat gap on efficiency and mass flow rate ratio

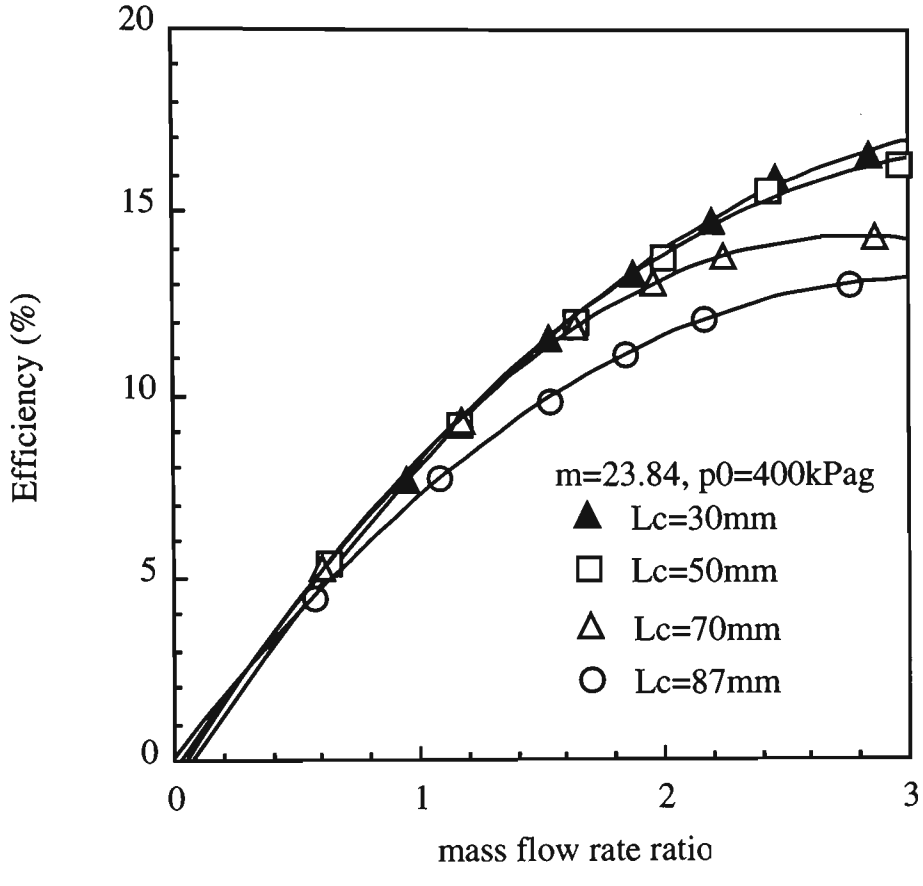

Fig. 5. 15 (c) Influence of nozzle-throat gap on efficiency and mass flow rate ratio

5.6 Air-Solids Pump Characteristics

5.6.1 Dimensional Characteristics

Dimensional air-solid performance also is represented by the relationship between the pressure difference $\overline{p_5} - \overline{p_4}$ and the mass flow rate of solids. The influence of pressure difference $\overline{p_5} - \overline{p_4}$ on suction solid mass flow rate for a given motive pressure is shown in Fig. 5.16. For a given motive pressure, it can be seen that as the pressure difference increases, suction solid mass flow rate decreases. Factors affecting this relationship are discussed below. Note unless stated otherwise, all test results are relevant to plastic pellets (see Table 4.3).

5.6.1.1 Motive Pressure

A variation in motive pressure affects pressure difference and solid mass flow rate, as shown in Fig. 5.16. It can be seen clearly from this figure that over all the variation range of suction solids mass flow rate, the pressure difference created by the air-jet pump increases with motive pressure, and for a given pressure difference, the suction solids mass flow rate increases as motive pressure increases.

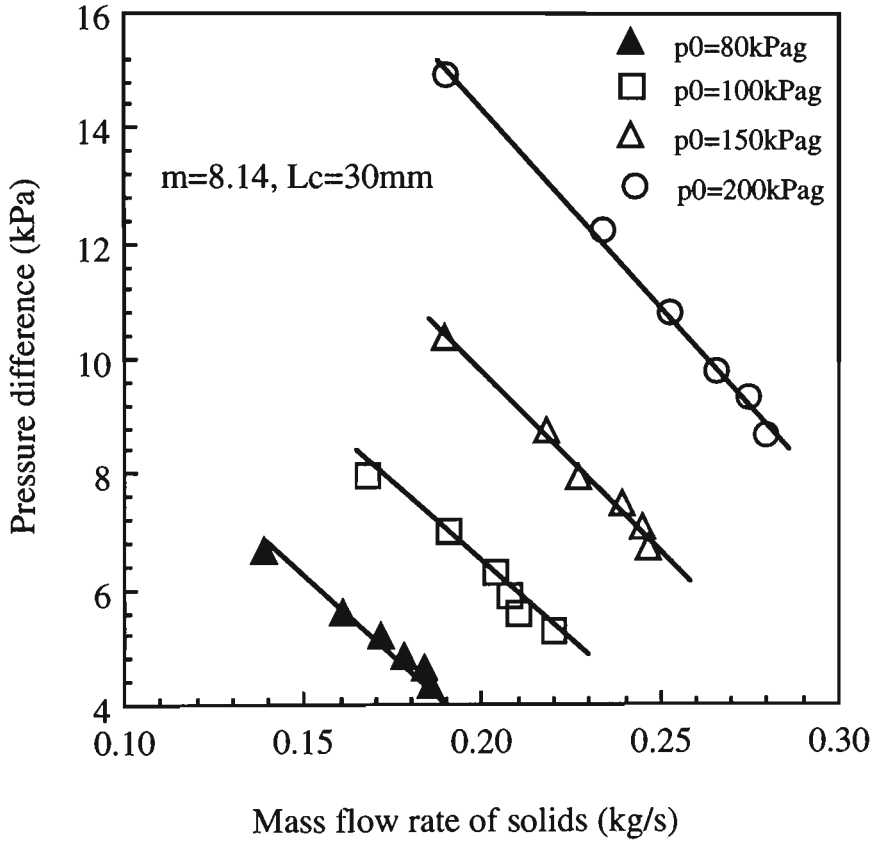

Fig. 5.16 Variation of pressure difference $\overline{p_5} - \overline{p_4}$ with motive pressure

5.6.1.2 Delivery Pressure and Receiving Hopper Pressure

As shown in Fig. 5.17, the influence of delivery pressure on suction solid mass flow rate is similar to the influence of pressure difference $\overline{p_5} - \overline{p_4}$ on suction solid mass flow rate. For a given motive pressure, the suction solid mass flow rate decreases as the delivery pressure increases. If the delivery pressure is too large, or if the suction pressure is too small, the suction solid mass flow rate will tend to zero and the pumping effect will

deteriorate. The delivery pressure is affected by the pressure in the receiving hopper in an air-jet pump conveying system. For a given motive pressure, as shown in Fig. 5.18, an increase in the receiving hopper pressure decreases the solids conveying rate, and vice versa. Actually, the delivery pressure required by a conveying system is similar to that in air-only flow conditions (that is, the sum of the pressure in receiving hopper and the pressure drop across the conveying pipeline). For a given suction pressure, an increase in the receiving hopper pressure requires an increase in the delivery pressure of the air-jet pump and increases the pressure difference required by the conveying system.

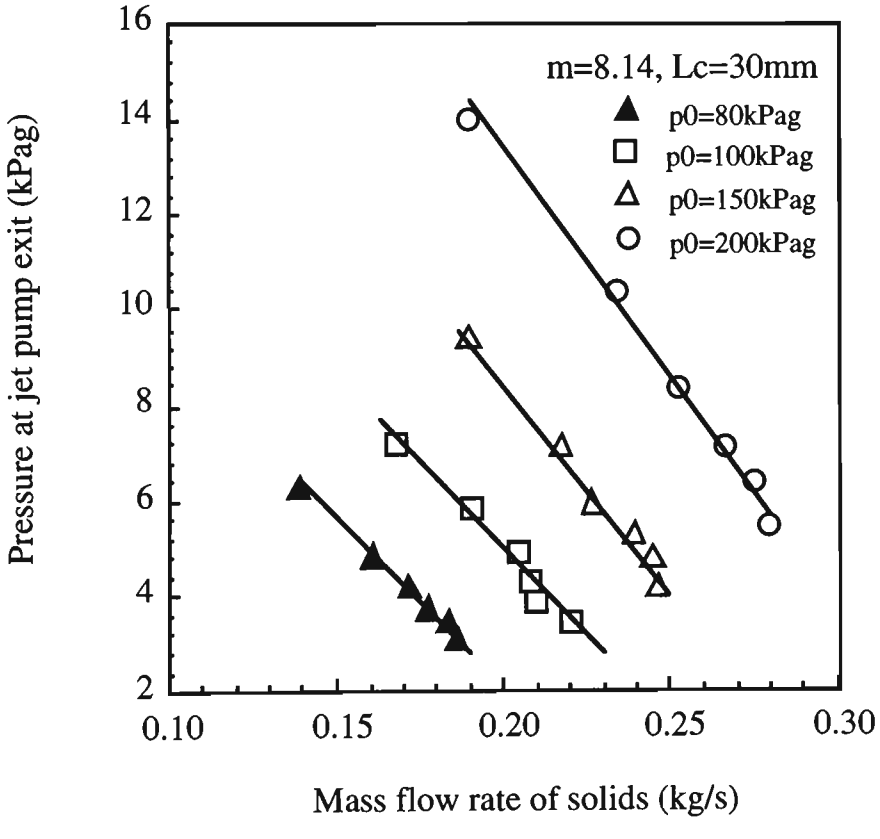

Fig. 5.17 Influence of motive pressure on conveying rate and pressure at exit of jet pump

5.6.1.3 Suction Pressure and Suction Solids Mass Flow Rate

Suction mass flow rate consists of both suction air and suction solids mass flow rate, since the feeding hopper which feeds material into a jet pump suction port is open to atmosphere in an actual air-jet pump conveying system. Therefore, as stated in Sections 4.6.2 and 4.6.3, the valves V2 and V3 shown in Figs. 4.1 and 4.2 were fully opened to

atmosphere to allow air to be sucked in without any manual control. The measurement of suction air mass flow rate has been explained in Section 4.3.1. Since the material completely fills the suction port, air under atmosphere can only be sucked through the voidage between particles. On the other hand, the suction air mass flow rate is determined by the pressure difference between ambient and suction port. As shown in Fig. 5.19, this pressure difference varies with solid mass flow rate and is quite small (generally between -1 and -3 kPag). For the above reasons, the suction air mass flow rate under solid pumping condition is very limited. From the experimental data for the materials tested, this value is, in average, about 0 to 4 percent of the motive air mass flow rate, depending on material properties. Hence, the suction air mass flow rate in solid pumping could be ignored in presenting the experimental data to show the effects of operating and geometrical parameters on pump performance. Similar treatment can be found in the literature regarding presentation of experimental results on air-solid jet pump performance [20, 26, 28, 108].

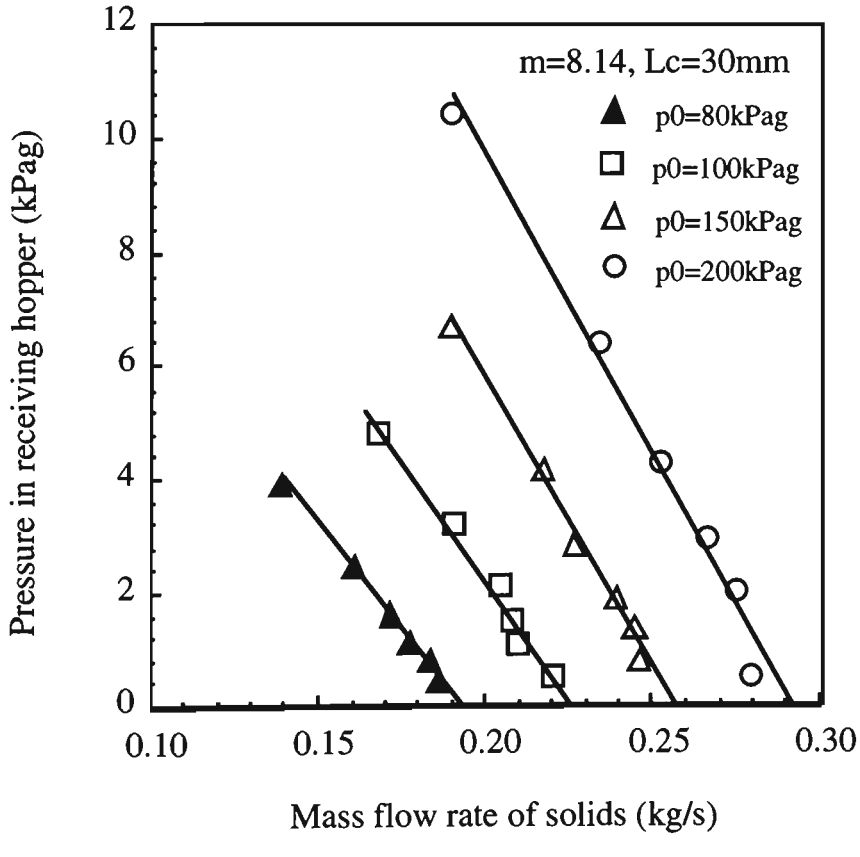

Fig. 5.18 Influence of motive pressure on conveying rate and the pressure in the receiving hopper

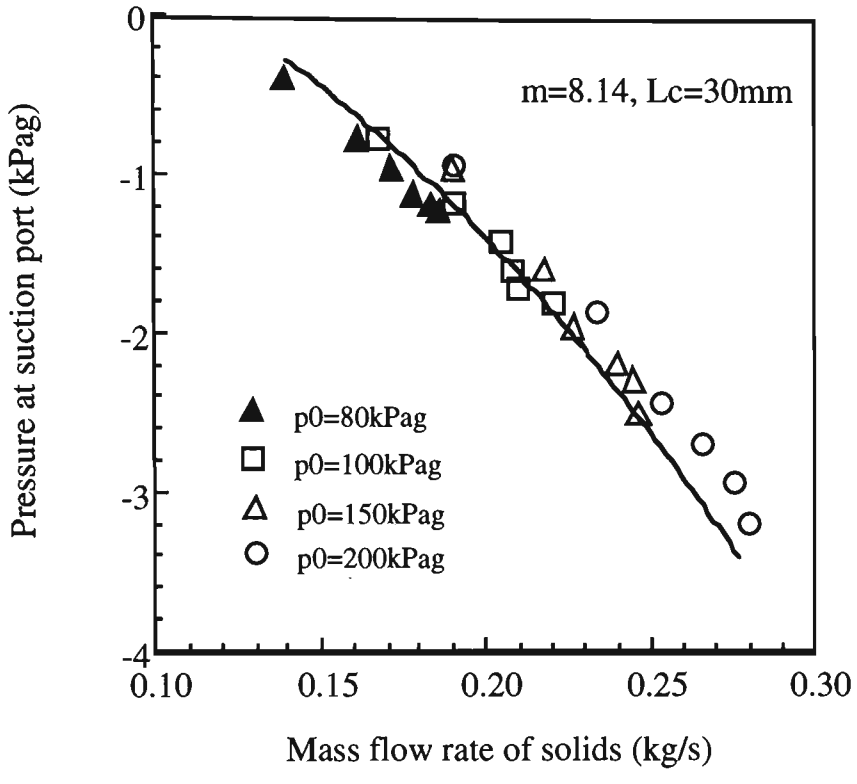

Fig. 5.19 Variation of suction pressure with mass flow rate of solids

It can be seen from Fig. 5.19 that the suction pressure is dependent on the mass flow rate of solids (e.g. the suction pressure decreases as the mass flow rate of solids increases). Note the conveyed mass flow rate is less than the maximum discharge rate of the feed hopper (under atmospheric conditions). The reason is that the pressure drop between the inlet of the feeding hopper and suction port increases with the suction mass flow rate of solids. It has been confirmed by experiment that the maximum discharge capacity under atmospheric condition is 0.4 kg/s for the plastic pellets (refer to Table 4.4). It also can be seen from Fig. 5.19 that although the suction pressure decreases and the suction mass flow rate of solids increases as the motive pressure increases, the variation of suction pressure and suction mass flow rate effectively follow the same relationship.

5.6.1.4 Nozzle Outlet Diameter

Jet pump configuration also has a significant influence on dimensional performance. Fig. 5.20 shows the influence of varying nozzle diameter (for a given throat diameter) on the performance lines. It can be seen from this figure that: to generate a given pressure

difference, a different nozzle diameter requires a different motive pressure and creates a different suction mass flow rate of solids; to obtain a given suction mass flow rate of solids, a different nozzle diameter requires a different motive pressure and creates a different pressure difference because a different air mass flow rate causes a change in the pressure drop across the conveying pipeline. It should be noted that for a given motive pressure, a reduction in nozzle outlet diameter decreases the motive air mass flow rate. Therefore, the motive pressure should be appropriate to the nozzle diameter to avoid pipeline blockage.

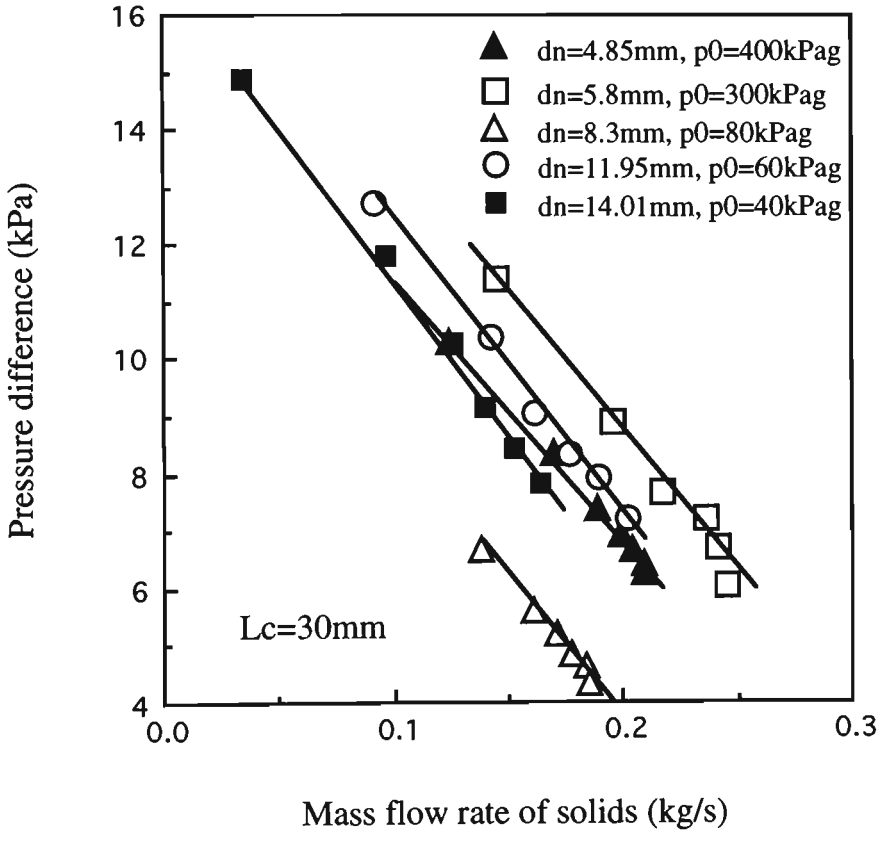

Fig. 5.20 Influence of nozzle outlet diameter on dimensional performance

5.6.1.5 Nozzle-Throat Gap and Throat Tube Length

Fig. 5.21 shows the influence of nozzle-throat gap on pressure difference $\overline{p_5} - \overline{p_4}$. It can be seen from this figure that the performance line becomes flatter as the nozzle-throat gap is increased from 30 to 50, 70 and then 87 mm, and the maximum pressure difference for a given suction solids mass flow rate is obtained for a nozzle-throat gap of 50 mm.

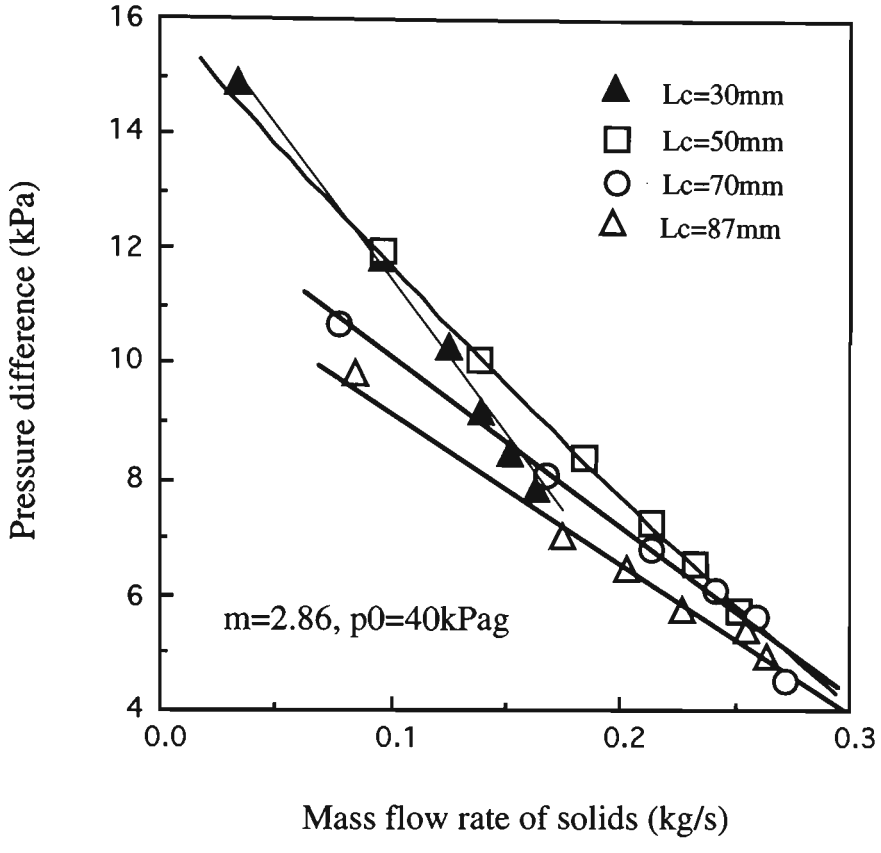

Fig. 5.21 Influence of nozzle-throat gap on dimensional air-solids performance

The influence of throat tube length has not been investigated, but the maximum pressure recovery for a central air-jet pump conveying wheat was found by Chellappan and Ramaiyan [20] to occur in the range L_t/d_t = 7.9 to 9.5. This result is close to $L_t/d_t \approx 7$ observed in a water jet pump of similar design, although mixing tube lengths as short as 5.7 d_t and as long a l0 d_t also have yielded good performance [14, 46, 69, 83]. Also, the influence of the throat tube length on dimensional pump performance was investigated by Dawson *et al.* [28] by varying L_t/d_t from 0, 3, 6 to 9. Based on all these results, it is believed that a value of L_t/d_t = 5 to 9 will not cause a significant influence on central air-jet pump performance.

5.6.1.6 Material Properties

Figure 5.22 shows the influence of material properties on dimensional characteristics. It can be seen clearly that the characteristic lines depend strongly on material properties.

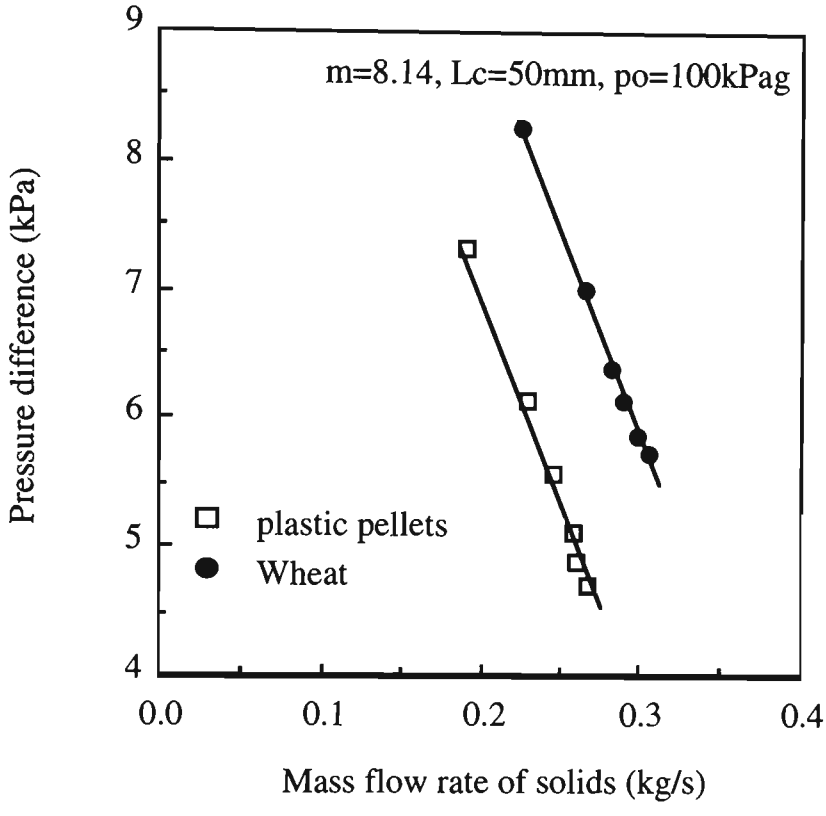

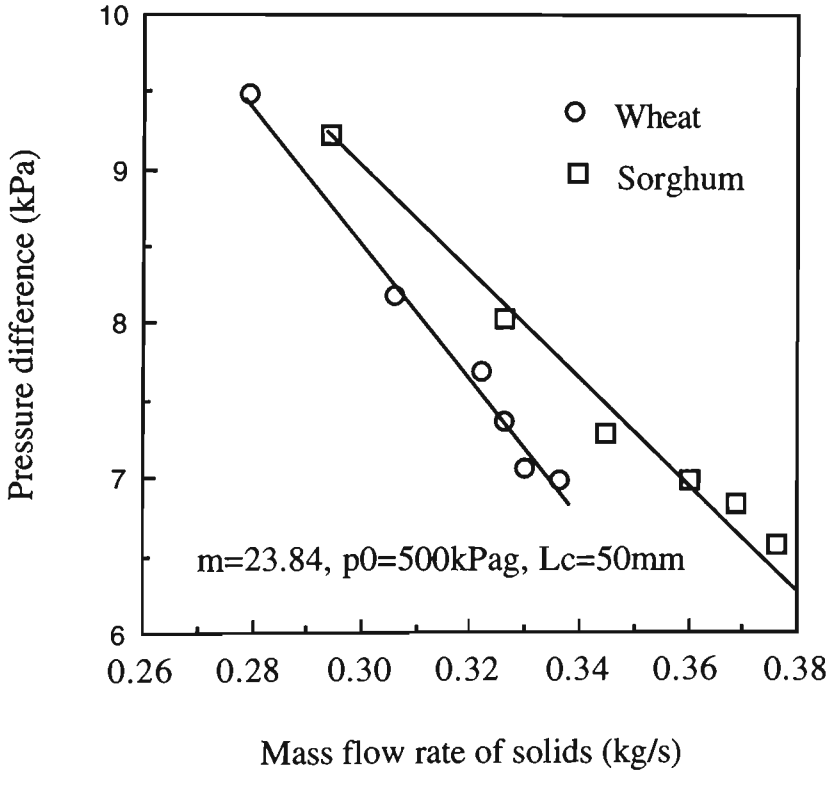

Fig. 5.22 Dimensional characteristics for different materials

5.6.2 Non-Dimensional Performance

The non-dimensional air-solids performance of an air-jet pump is represented by a plot of pressure ratio h against mass flow rate ratio x for a given air-jet pump configuration (represented by area ratio m.) These non-dimensional parameters have been defined in Section 3.2.3

5.6.2.1 Motive Pressure

The influence of motive pressure on non-dimensional air-solids performance is shown in Fig. 5.23 It can be seen that for a given mass flow rate ratio of solids to air, the pressure ratio decreases as the motive pressure increases; for a given pressure ratio, the mass flow rate ratio increases as the motive pressure decreases.

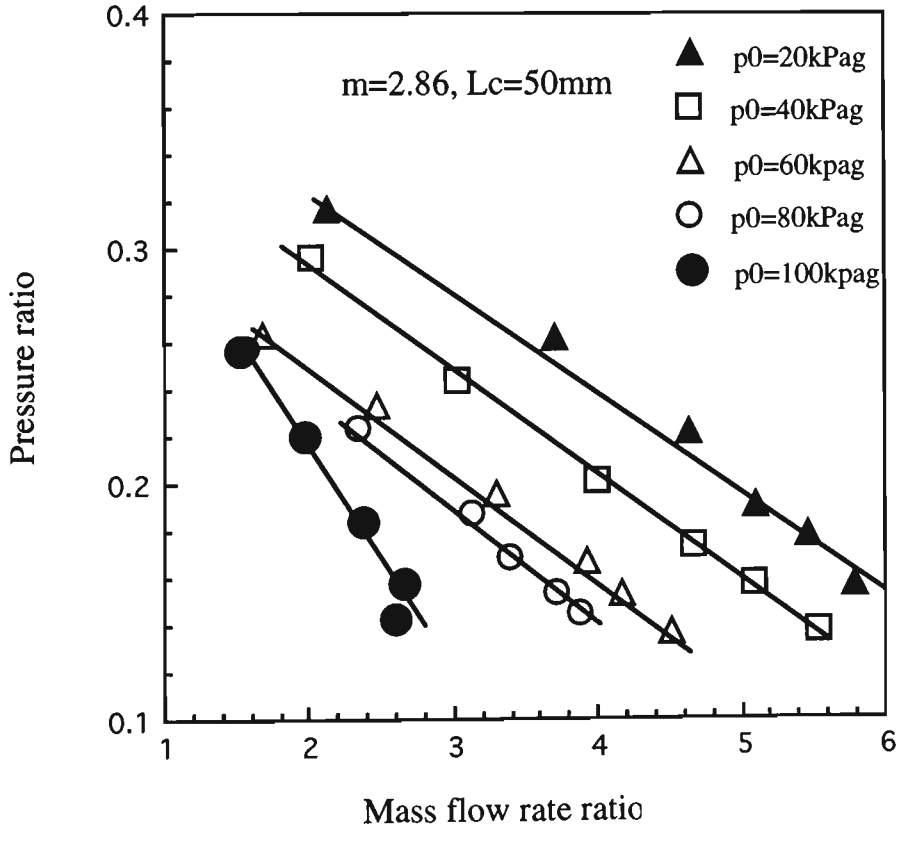

Fig. 5.23 Influence of motive pressure on non-dimensional air-solids performance

5.6.2.2 Area Ratio

Fig. 5.24 shows the non-dimensional performance curves of the air-jet pump with five different area ratios. It can be seen clearly from this figure that the influence of area ratio on non-dimensional air-solids performance is similar to that on air-only performance. For example, the h-x lines become flatter as m is increased and steeper as m is decreased. This means that x may increase or decrease by varying m for a given h, and for a given x, h may increase or decrease, which suggests that increasing m produces a flatter h-x characteristic line, a decreased pressure ratio and an increased mass flow rate ratio. From Eq. (3.6), a decrease in h will decrease $\overline{p_5}$ if $\overline{p_0}$ and $\overline{p_4}$ are kept constant. This suggests that a great m suits the application of a high mass flow rate, and vice versa. It also can be seen from Fig. 5.24 that the maximum mass flow ratio corresponding to a minimum pressure ratio value (i.e. delivery pressure as small as possible for a given motive pressure) decreases with decreasing area ratio. The reason is that a decrease in area ratio for a given throat tube diameter can only be gained by increasing the flow area of motive fluid. For a given motive pressure, the motive flow rate increases with an increase in motive flow area, that is, the motive mass flow rate increases with a decrease in area ratio. As the flow area of secondary stream decreases with a decrease in area ratio for a given throat tube diameter, the suction solids mass flow rate decreases with decreasing flow area for a given suction pressure. The decrease in maximum suction mass flow rate and the increase in motive mass flow rate cause the maximum mass flow ratio to decrease with decreasing area ratio.

For a given area ratio m, the mass flow rate ratio x increases as the pressure ratio h decreases. For a given delivery pressure, a variation in motive pressure causes h to change, so the secondary mass flow rate will change to maintain a mass flow rate ratio x with respect to h. However, the pressure drop in the conveying system increases with mass flow rate. For a given pressure in the receiving hopper, an increase in pressure drop requires an increase in delivery pressure. For a given motive pressure and suction

pressure, increasing the delivery pressure will increase h and decrease x and the suction mass flow rate.

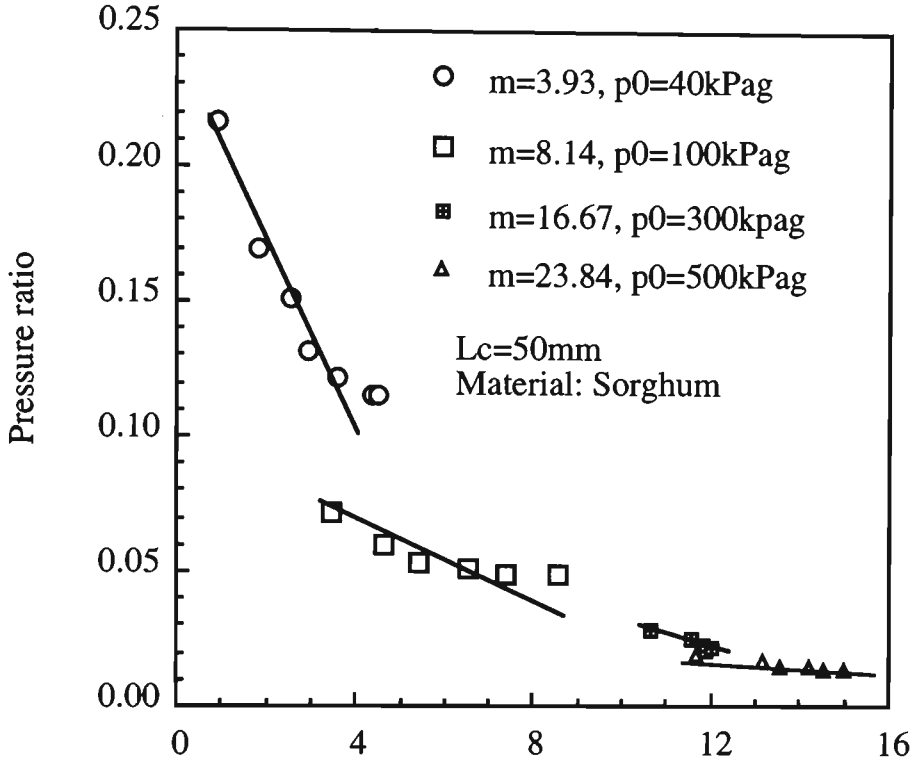

(a) Sorghum

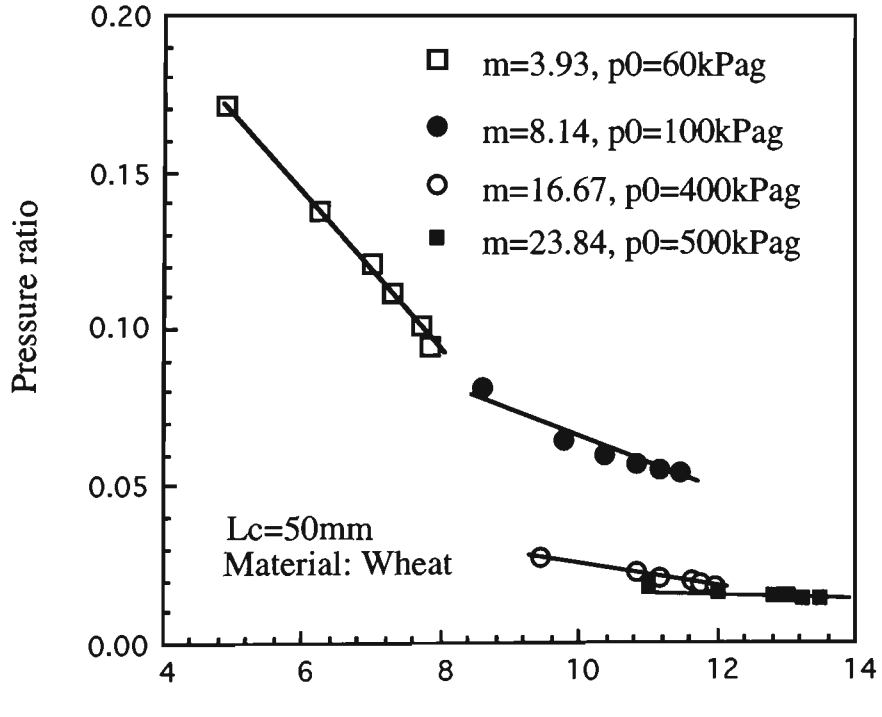

(b) Wheat

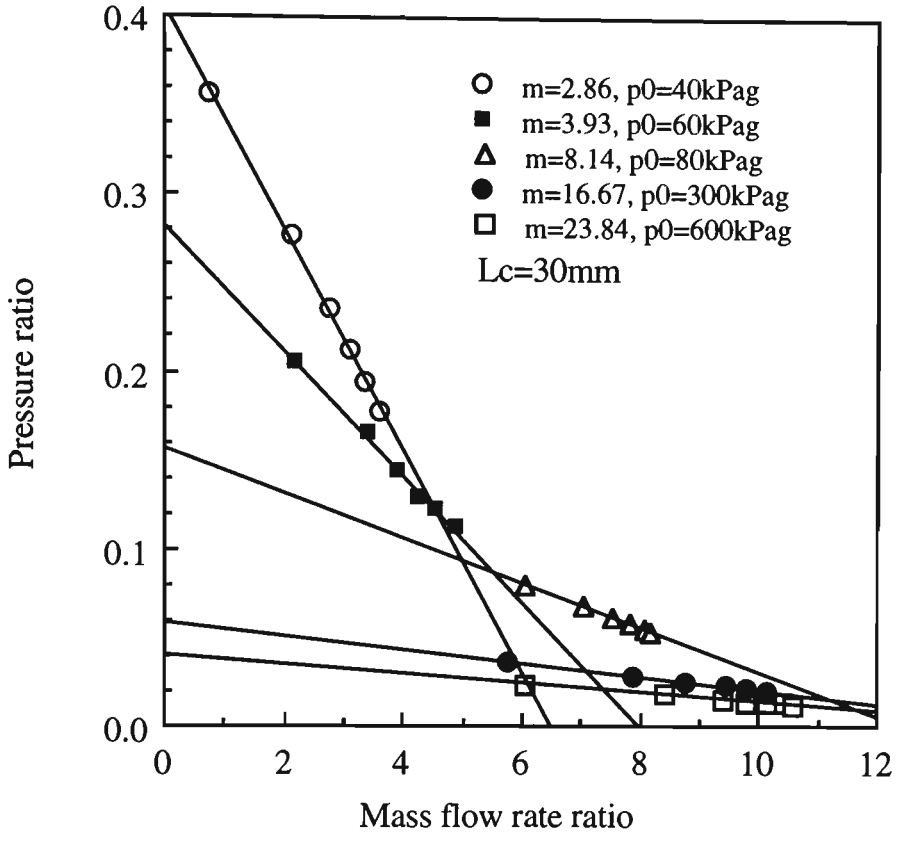

(c) Plastic pellets

Fig. 5.24 Influence of area ratio on non-dimensional air-solids performance

From Eq. (3.6), it can be seen that an increase in pressure ratio h for a given delivery pressure suggests that the motive pressure and the motive mass flow rate can be reduced for a given jet pump geometry, so too the power required by a central air-jet pump. As mentioned above, an increase in pressure ratio h reduces mass flow rate ratio x. From Eq. (3.5), a reduction in x requires an increase in motive mass flow rate for a required conveying rate. For a given nozzle geometry, increasing the motive mass flow rate in turn requires an increase in motive pressure. Therefore, there must be a compromise of motive pressure between h and x for a given area ratio and a required conveying rate to minimise the power required, or an optimum motive pressure for a given area ratio. From Fig. 5.24, it can be seen that one value of pressure ratio or mass flow rate ratio can be produced using air-jet pumps with different area ratio m. For example, to produce x =8, m may be 8.14, 16.67 or 23.84. Different m correspond to different relationships

between h and x, and require different power input. Therefore, there must be an optimum area ratio for a given air-solids operating condition.

5.6.2.3 Nozzle-Throat Gap

Fig. 5.25 shows the influence of nozzle-throat gap L_c on performance. It can be seen that the pressure ratio increases initially as the distance L_c is increased, and that later there is no appreciable increase and then a decrease. Therefore, for normal operation it is preferred to use $L_c \approx 50$ mm ($F \approx 20$ mm) to obtain the greatest conveying rate for a given delivery pressure for all the jet pump designs tested (also refer to Fig. 5.21). For extremely abrasive materials where nozzle wear is a factor, the nozzle-throat gap can be greater than the optimum value at the expense of a modest reduction in conveying rate.

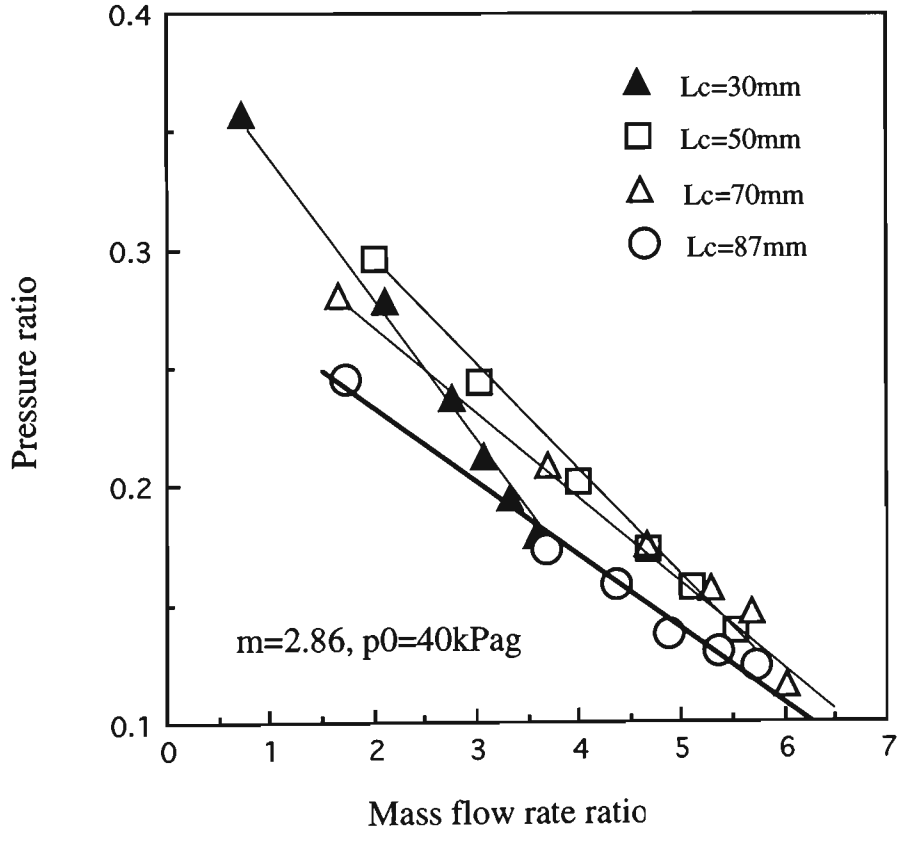

Fig 5.25 Influence of nozzle-throat gap on non-dimensional air-solids performance

The paper by Chellappan and Ramaiyan [20] is one of the few papers that deals with the influence of nozzle-throat gap on performance. The optimum distance F for a central air-

jet pump conveying wheat was found [20] to occur in the range of 10 to 15 mm. Unfortunately, it is not possible to compare the above results with those presented by Chellappan and Ramaiyan [20] due to a lack of information [20] to determine F_1 as shown in Fig. 4.5. F = 25 mm was adopted by Dawson *et al.* [28] although their trials indicated that increasing the distance between the nozzle exit and the throat entry resulted in a small increase in solids mass flow rate. This agrees with the results presented by Chellappan and Ramaiyan [20].

5.6.2.4 Materials

The influence of material properties on non-dimensional performance is illustrated in Fig. 5.26. It can be seen that an air-jet pump of given geometry and operating at the same motive pressure to convey different materials produces different non-dimensional operating characteristics. The reason is that the material properties, such as bulk density, particle density and particle shape, contribute to pump performance. For example, it was found that wheat and sorghum due to their higher bulk and particle densities were able to be conveyed at higher mass flow rate ratios than plastic pellets (i.e. at the same h value).

5.6.3 Efficiency

Efficiency is a measure of how effectively the motive air flow is converted into useful work for conveying bulk solids from the feeding hopper and has been defined in Section 3.2.6 Factors influencing efficiency are discussed as follows.

5.6.3.1 Motive Pressure

Fig. 5.27 shows the influence of the motive pressure on the efficiency defined by Eq. (3.11). It can be seen from this figure that the efficiency increases with decreasing motive pressure. This suggests that a lower motive pressure should be employed to improve efficiency. Also, as shown in Fig. 5.23, a variation in motive pressure will cause the relationship between h and x change. Therefore, the suction mass flow rate of solids

corresponding to maximum efficiency will vary slightly with motive pressure. From Fig. 5.27 it can be seen that a decrease in suction solid mass flow rate corresponding to the maximum efficiency with decreasing motive pressure. It should be noted that a decrease in motive pressure will decrease the motive mass flow rate for a given nozzle geometry, increase the pressure ratio h and decrease x, and vice versa (for a given delivery pressure). If the motive pressure and flow rate are too low to maintain dilute-phase flow in the conveying pipeline, deposition and/or blockage will occur. Therefore, to maximise efficiency, the motive pressure for a central-jet pump should be close to the critical (minimum) pressure for a given nozzle to provide sufficient air to avoid particle deposition in the conveying pipeline.

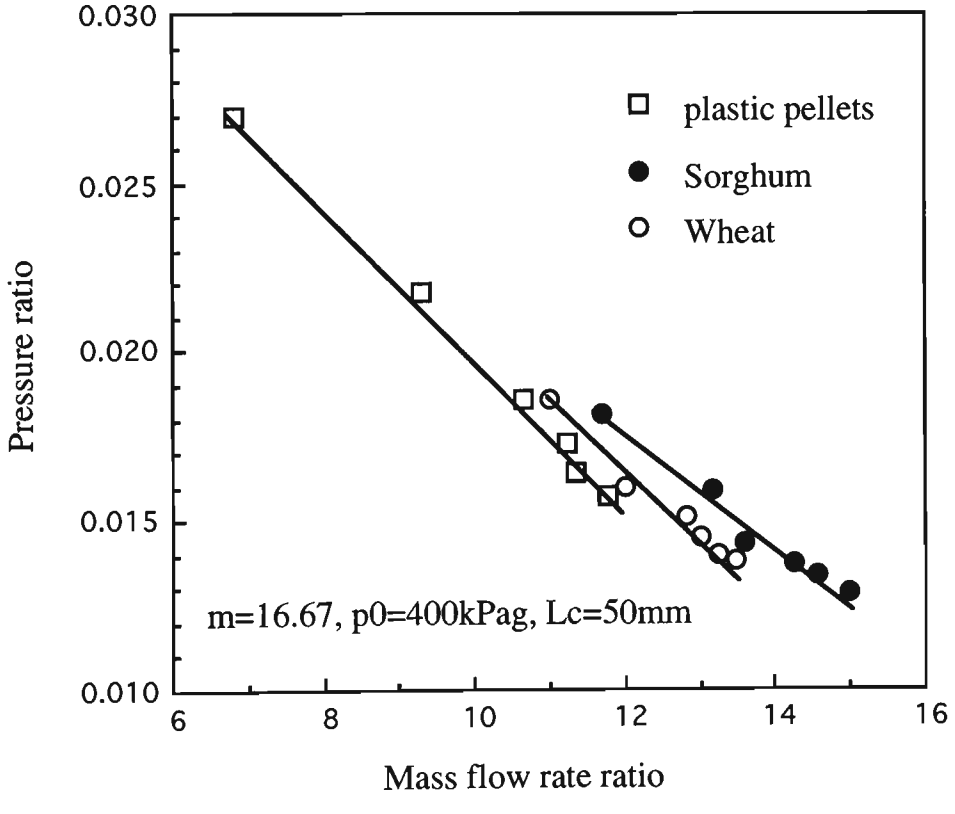

Fig. 5.26 Influence of material on non-dimensional pump characteristics

5.6.3.2 Area Ratio

The relationship between area ratio m, mass flow rate ratio and efficiency is shown in Fig. 5.28. It can be seen from this figure that for a given mass flow rate ratio, the

efficiency is corresponding to area ratio m. That is, there must be an optimum area ratio for a given mass flow rate to obtain maximum efficiency. For example, for x=3, the optimum value of m is 2.86, and for x=6, the optimum value of m is 8.14. This suggests that the efficiency of an air-jet pump conveying system can be improved by optimising the area ratio m for given operating conditions as discussed in Section 5.6.2.2.

5.6.3.3 Nozzle-Throat gap

The influence of nozzle-throat gap on efficiency is shown in Fig. 5.29. It can be seen that the efficiency for a given operating condition increases initially as the nozzle-throat gap L_c is increased, and that later there is no appreciable increase and then a decrease. Therefore, as discussed above, an optimum nozzle-throat gap exists for a given jet pump to obtain better efficiency.

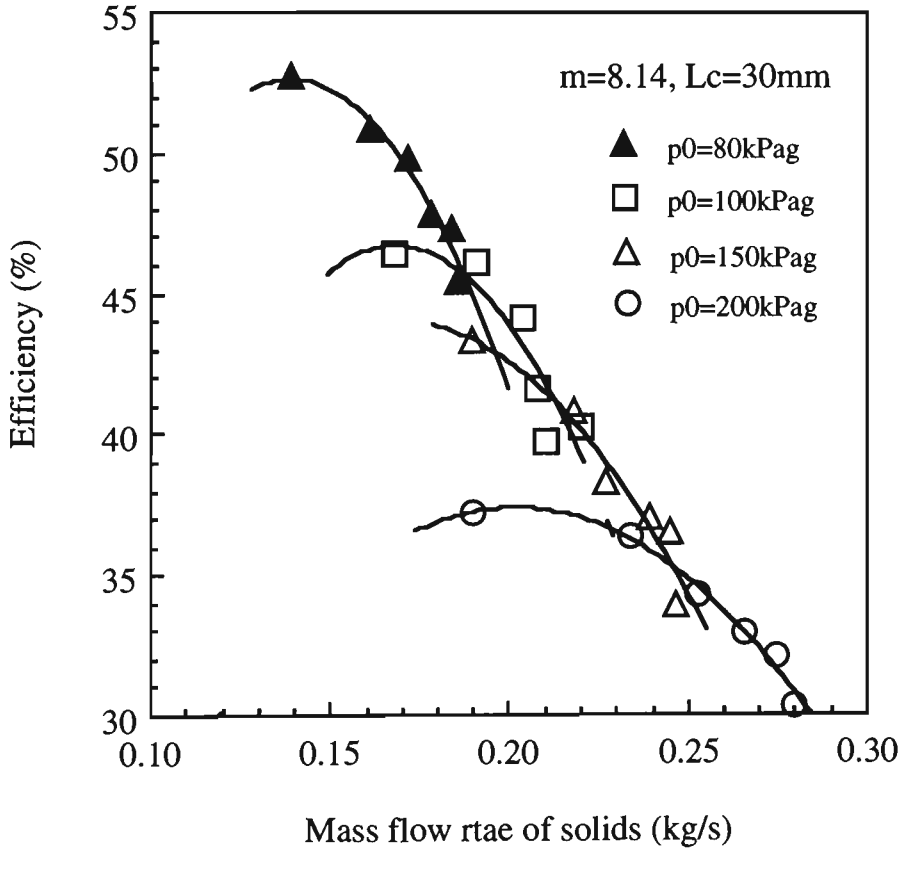

Fig. 5.27 Influence of motive pressure and conveying rate on efficiency

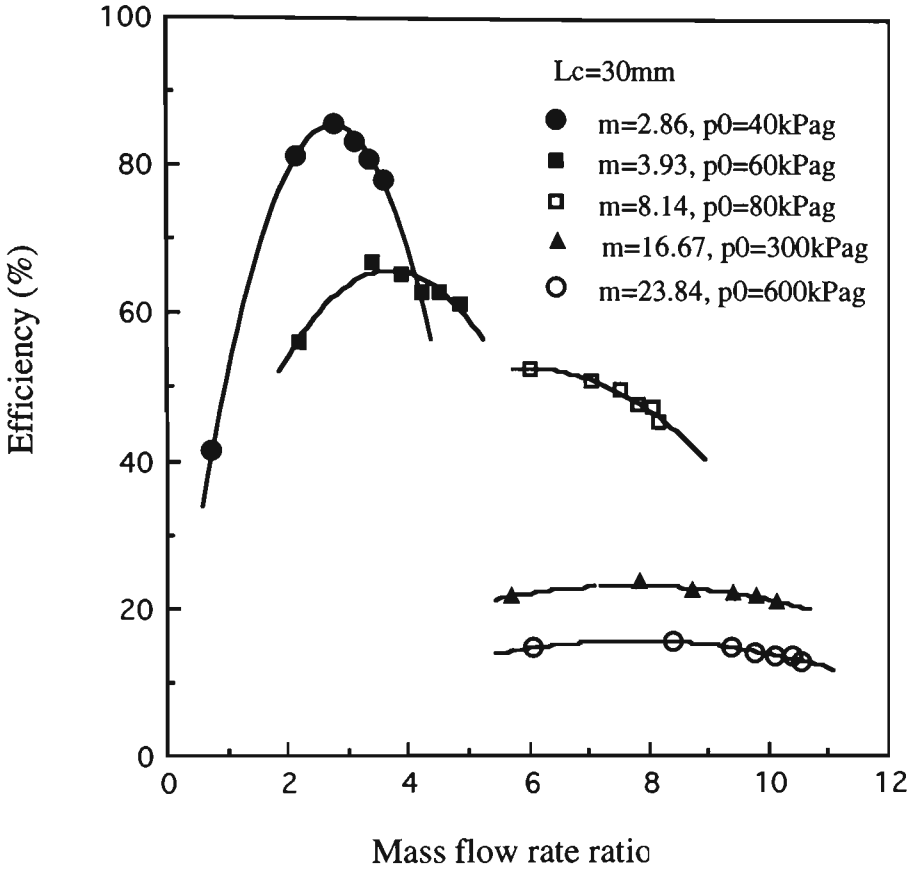

Fig. 5.28 Influence of area ratio on efficiency

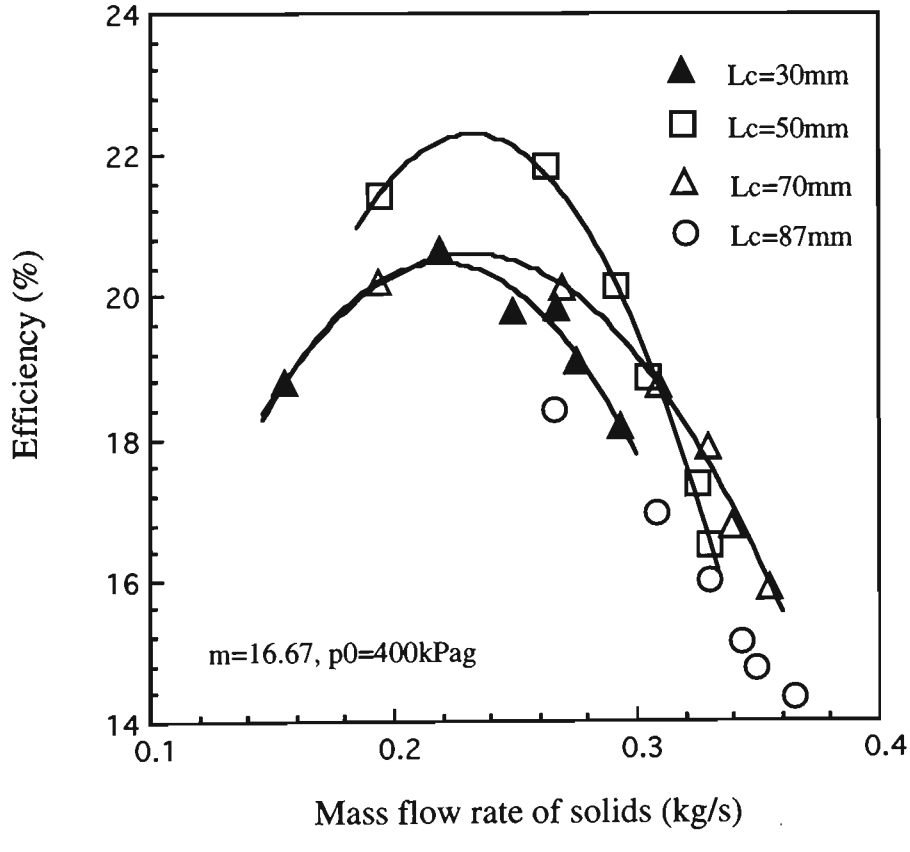

Fig. 5.29 Influence of nozzle-throat gap on mass flow rate and efficiency

5.6.3.4 Material Properties

As shown in Figs. 5.30 and 5.31, for a given air-jet pump configuration, conveying different materials will attain different efficiencies.

5.7 Comparison between Air-Solids and Air-Only Performance

The comparison between non-dimensional air-only and air-solids performance is shown in Fig. 5.32 and the dimensional format is given in Fig. 5.33. It can be seen clearly from these figures that whether using non-dimensional or dimensional characteristics, the air-only performance line always lies underneath the air-solids line. This is due to the difference between the influence of the solid component in air-solids flow and the secondary air-only flow on the frictional losses in the air-jet pump. Both performance lines should converge to the same point as the mass flow rate of solids approaches zero.

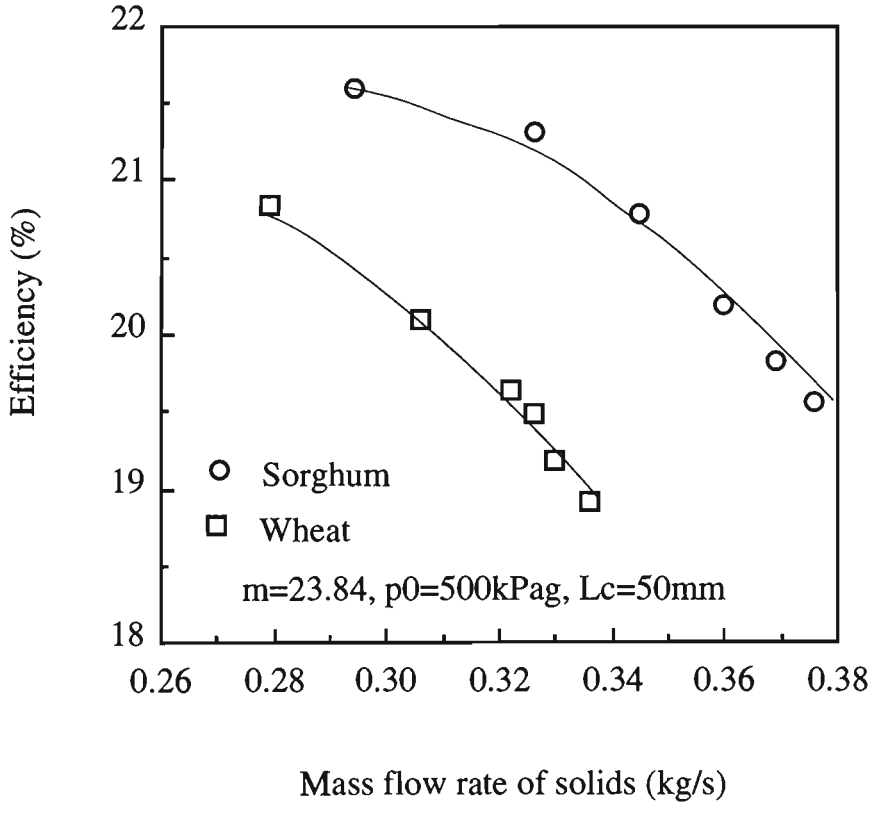

(a) Efficiency via mass flow rate of solids

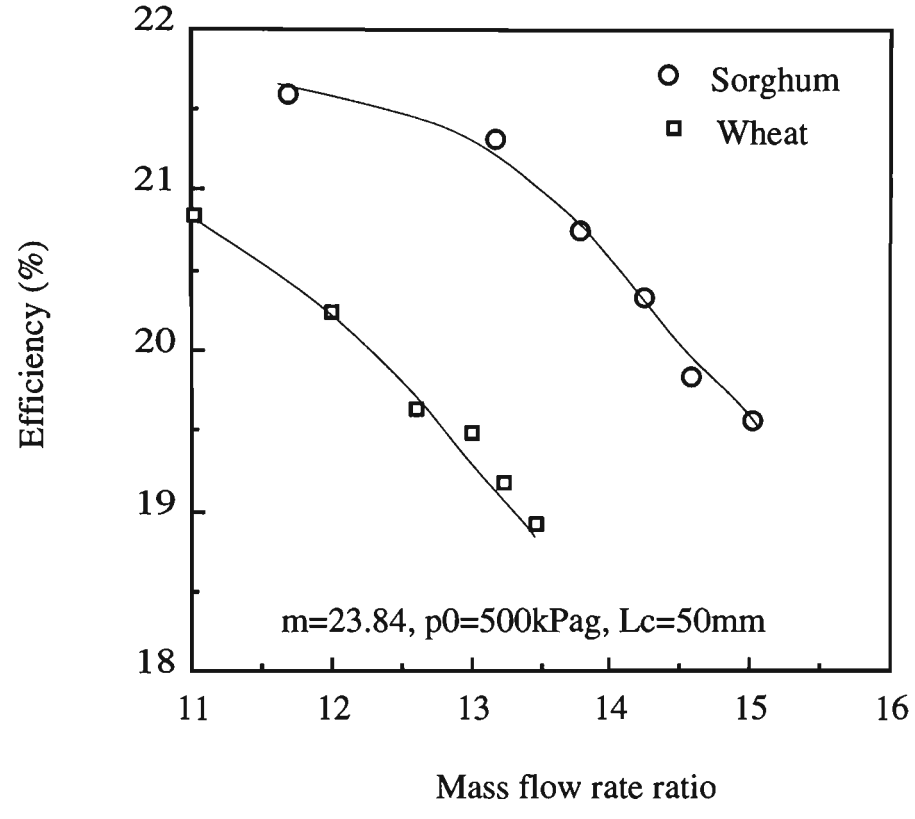

(b) Efficiency via mass flow rate ratio

Fig. 5.30 Comparison of efficiencies for conveying sorghum and wheat

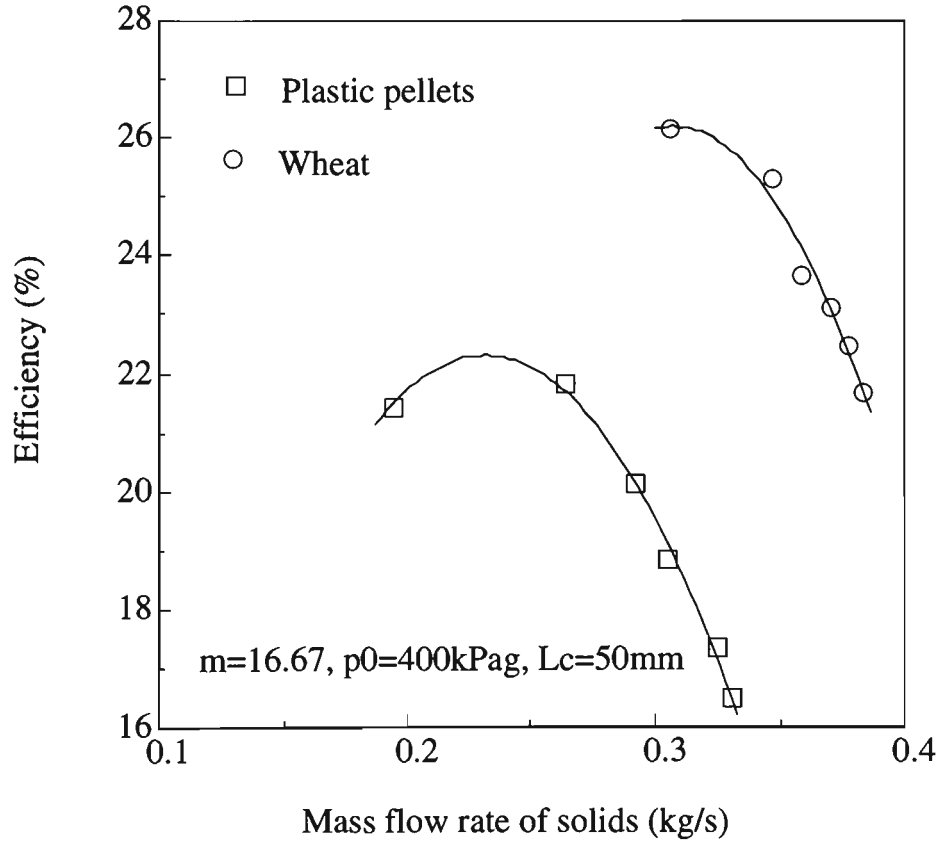

Fig. 5.31 Comparison of efficiencies for conveying wheat and plastic pellets

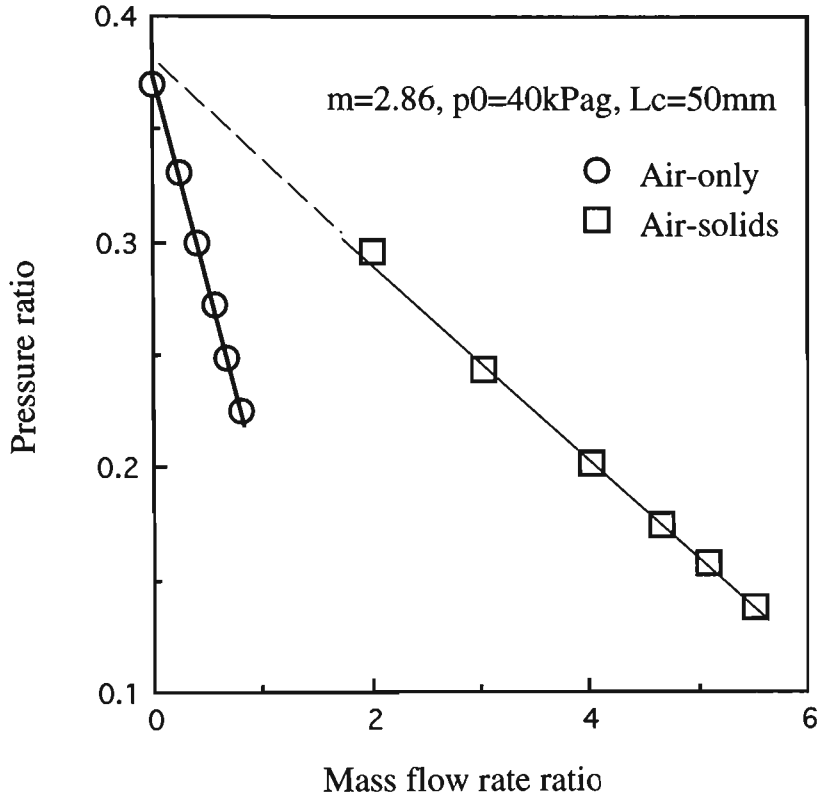

Fig. 5.32 Comparison between air-only and air-solids non-dimensional performance

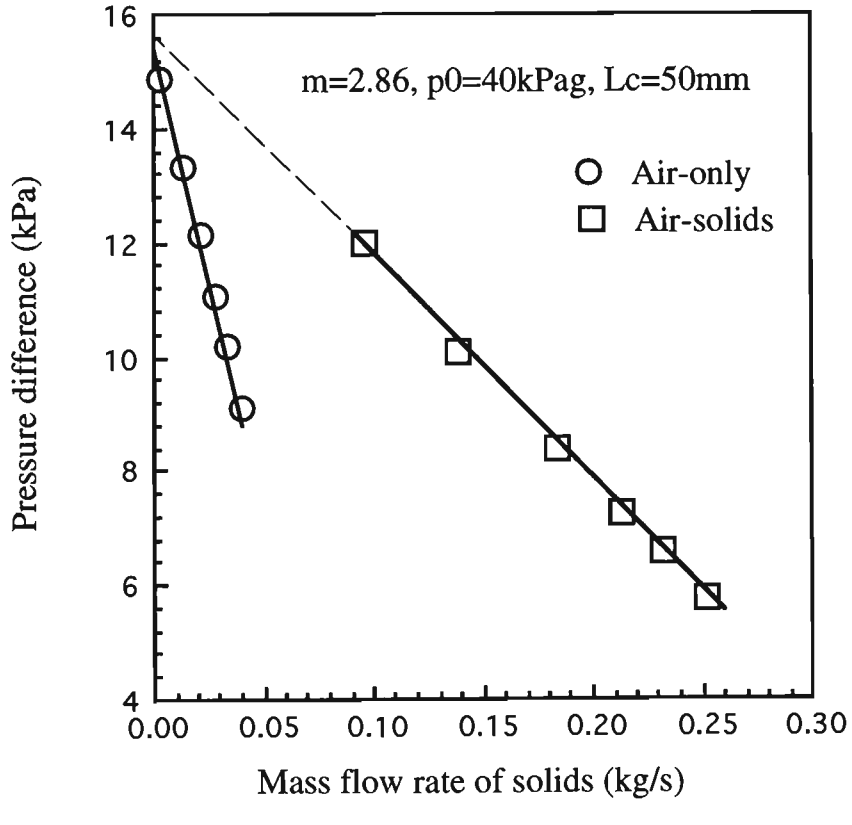

Fig. 5.33 Comparison between air-only and air-solids dimensional performance

CHAPTER 6
EXPERIMENTAL INVESTIGATION INTO ANNULAR AIR-JET PUMPS

6.1 Introduction

In a central air-jet pump, high velocity air and low velocity secondary flow combine in the mixing throat section. Because of the turbulent motion of the solid particles and the expansion of the motive jet in the core, erosion can be a serious problem. A novel solution for reducing surface erosion is to reduce air-particle turbulence. This idea underlies the use of a swirling annular jet to control erosion. An innovative design of annular air-jet pump has been produced by J.S. Melbourne Controls and used successfully in several pneumatic conveying applications over recent years. The difference between this type of annular jet pump and central air-jet pump is that central jet pumps consist of a high velocity jet (motive flow) generated by a convergent nozzle located along the centre-line of the jet pump and an annular (secondary) flow surrounding the central nozzle containing the solid particles to be pumped, while in annular jet pumps the high velocity air-jet flow is introduced around the periphery of the pump and the particles are introduced in the central pipe.

Fig. 4.4 shows a general arrangement of this type of air-jet pump. The basic principle of operation is as follows: motive fluid flows into the annular chamber and then is throttled through a multi-hole ring nozzle; this creates non-intersecting multi-jets flowing at high velocity with swirl; the fast-moving multi-jets with swirl create a low pressure region in the neighbourhood of the multi-jet outlets; material from a feeding hopper is drawn through a central pipe into this multi-jet stream flowing at high velocity and with swirl; the two fluid streams with different velocity and density mix in the mixing section of the

air-jet pump, and then the combined flow discharges into the conveying pipeline at a delivery pressure and velocity. The suction flow also is pumped by means of the momentum of the motive fluid similar to a central air-jet pump. However, the presence of swirl makes the multi-jet spread more rapidly with axial distance and increases the mixing in the mixing section. It is believed also that the paths of the motive air steams (i.e. from the multi-hole nozzle) follow a non-intersecting helix pattern and hence assist in reducing wear and particle attrition.

To date, although this type of air-jet pump is commercially available, there is little information in the literature on performance monitoring and geometrical design. Hence, a systematic experimental investigation has been conducted into the performance of this novel type of air-jet pump under both air-only and air-solids flow conditions. This experimental work is aimed at investigating the effect of geometrical designs and operating conditions on both the air-only and the air-solids performance by varying motive pressure, back pressure and nozzle geometry. Note air-only performance is of considerable importance and usefulness in establishing particular operating parameters and trends (eg shut-off vacuum, efficiency, influence of area ratio, nozzle-throat gap, etc) for the transport of bulk solids in pipelines.

This chapter presents and discusses the influence of jet pump geometry and operating parameters on both air-only and air-solids performance and efficiency based on the results obtained from the above-mentioned investigations. The experimental results also are presented using the dimensional and non-dimensional parameters defined in Section 3.2.

6.2 Experimental Scheme

Various combinations of motive pressure and nozzle dimension were investigated to monitor air-jet pump performance by considering the variation of one parameter while the others are kept constant. Each experiment was carried out by running the motive air flow

through the system at a given motive pressure and a given pressure at the exit of the air-jet pump. The pressure at the jet pump exit was varied by selecting one of 6 different diameters of orifice plate mounted at the exit of the receiving hopper. This allowed the determination of the relationship between the suction solids mass flow rate and the jet pump exit pressure. A detailed description of the test procedure has been presented in Section 4.6. Table 6.1 summarises all the experiments conducted.

Table 6.1 Experimental set-up for air-jet pump performance monitoring

Area Ratio	Number of Holes	Diameter of Hole (mm)	Motive Pressure (kPag)	Flow Condition
36.8 (Nozzle No. 175)	12	2.38	100 200 300 400 480	Air-Only
65 (Nozzle No. 107)	16	1.55	100 200 300 320 400 500	
130 (Nozzle No. 52)	8	1.55	400 500 600	
36.8 (Nozzle No. 175)	12	2.38	207 307 400 485	Air-Solids
65 (Nozzle No. 107)	16	1.55	305 400 535	
130 (Nozzle No. 52)	8	1.55	400 500 600	

In Table 6.1, area ratio is calculated by using Eq. (3.4). The nozzle number indicates the motive air consumption in CFM at 700 kPa (101.6 psi) according to manufacturer's claim.

6.3 Air-Only Performance

6.3.1 Suction Mass Flow Rate and Pressures

The relationship between suction mass flow rate and the pressure at the jet pump exit can be represented by a dimensional characteristic plot for a given jet pump configuration. An air-only characteristic plot shows the variation of suction air mass flow rate M_{sa} with pressure difference $\overline{p_5} - \overline{p_4}$. As shown in Fig. 6.1, for a given motive pressure, as the pressure difference increases, the suction air mass flow rate decreases, and vice versa. The factors influencing the suction air mass flow rate and pressure are illustrated below.

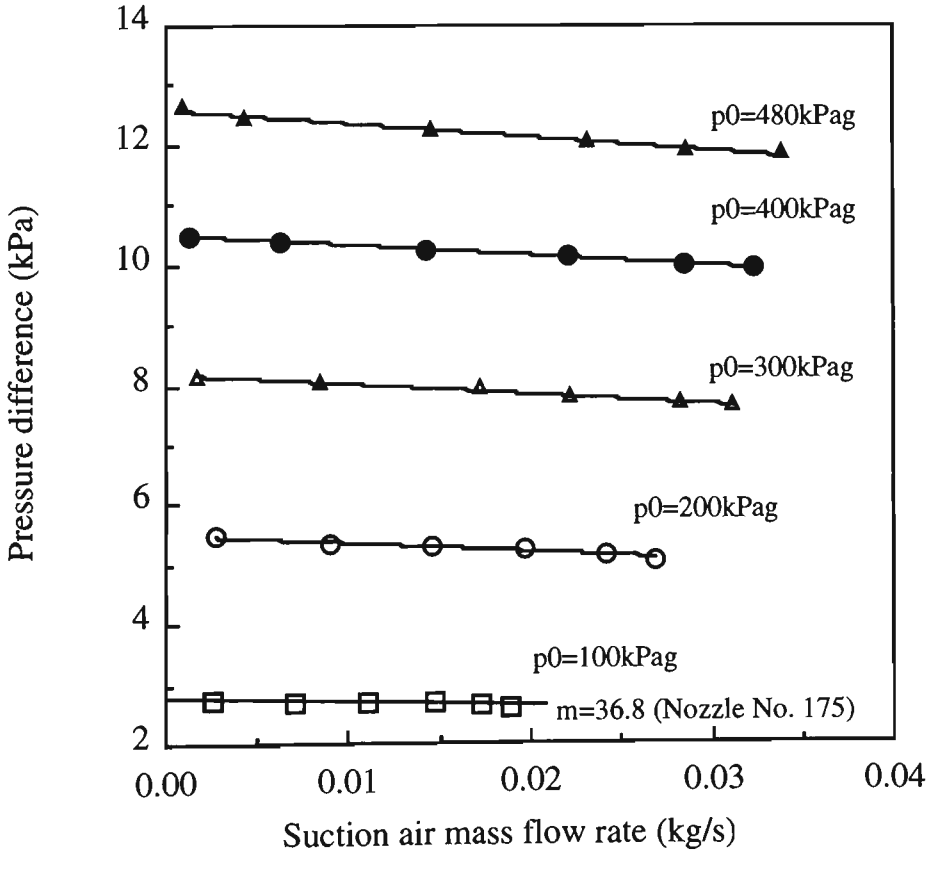

Fig. 6.1 Variation of pressure difference $\overline{p_5} - \overline{p_4}$ with suction air mass flow rate

Fig. 6.1 shows the influence of motive pressure on dimensional characteristics. It can be seen from this figure that a variation in motive pressure affects both the pressure difference and suction air mass flow rate. For example, for a given suction mass flow rate, the pressure difference created by the air-jet pump increases with motive pressure, and for a given pressure difference, suction air mass flow rate increases as motive pressure increases.

Fig. 6.2 shows the dependency of the suction pressure on the suction mass flow rate. The suction pressure decreases slightly as the suction mass flow rate increases. The influence of motive pressure on suction pressure is negligible. The reason is that the pressure drop between the inlet of the feeding hopper and suction port increases with suction air mass flow rate.

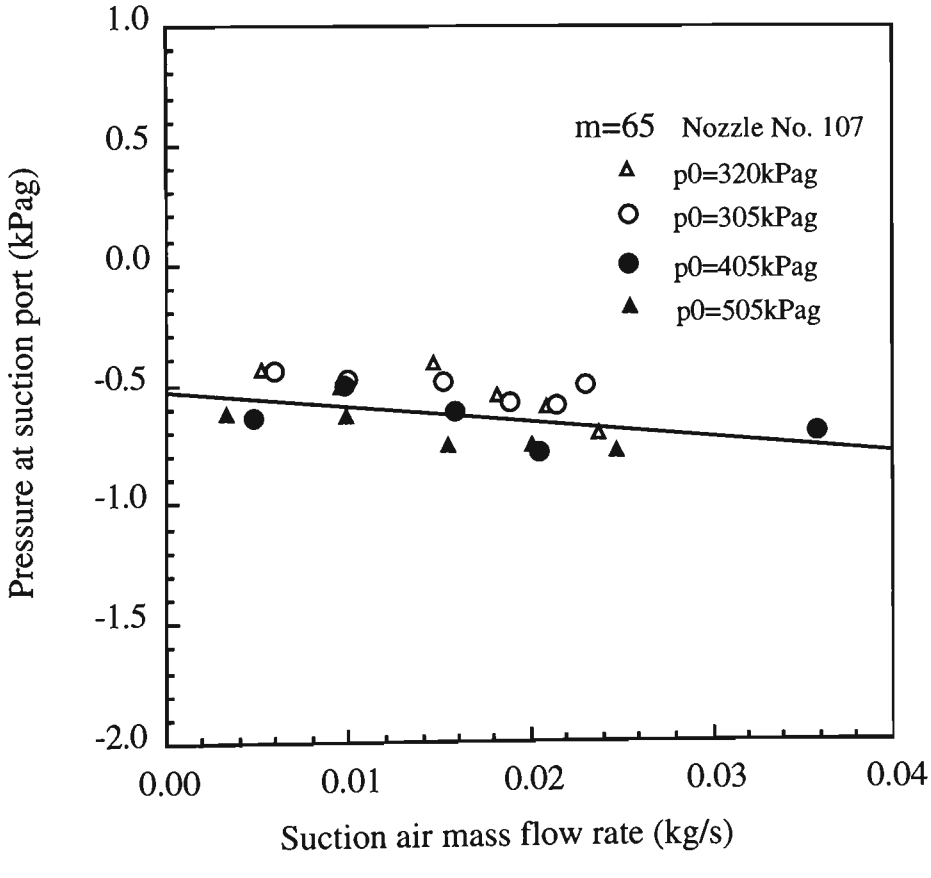

Fig. 6.2 Variation of suction pressure with suction mass flow rate

As shown in Fig. 6.3, the influence of delivery pressure on suction mass flow rate is similar to the influence of pressure difference $\overline{p_5} - \overline{p_4}$ on suction mass flow rate. For a given motive pressure, the suction mass flow rate decreases as the delivery pressure increases. If the delivery pressure is too large, the suction mass flow rate will tend to zero.

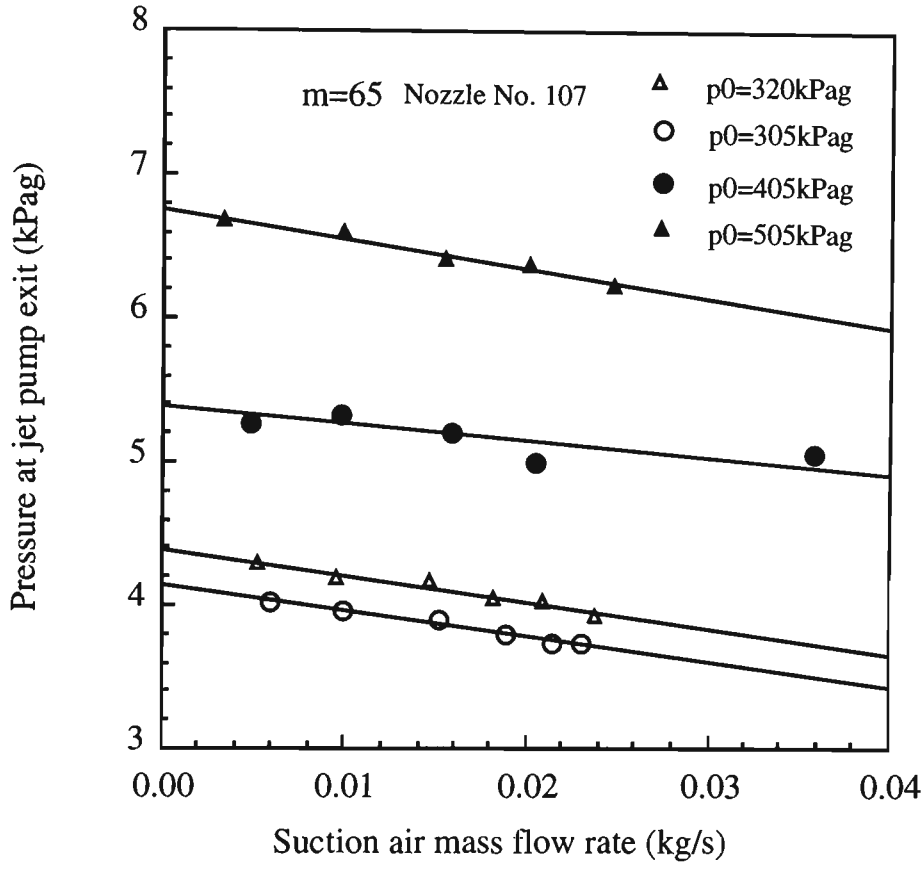

Fig. 6.3 Variation of delivery pressure with suction air mass flow rate

The required delivery pressure is affected by the pressure in the receiving hopper in an air-jet pump conveying system. For a given motive pressure, as shown in Fig. 6.4, an increase in the receiving hopper pressure decreases the suction mass flow rate, and vice versa. Actually, the delivery pressure required by the conveying system is the sum of pressure in the receiving hopper and the pressure drop across the conveying pipeline. An increase in the receiving hopper pressure increases the delivery pressure/pressure difference required by the air-jet pump conveying system for a given suction pressure, and results in a decrease in suction mass flow rate. However, as shown in Figs. 6.3 and

6.4, the pressures both at the jet pump exit and in the receiving hopper are influenced by motive pressure. An increase in motive pressure may increase the delivery pressure generated by the jet pump.

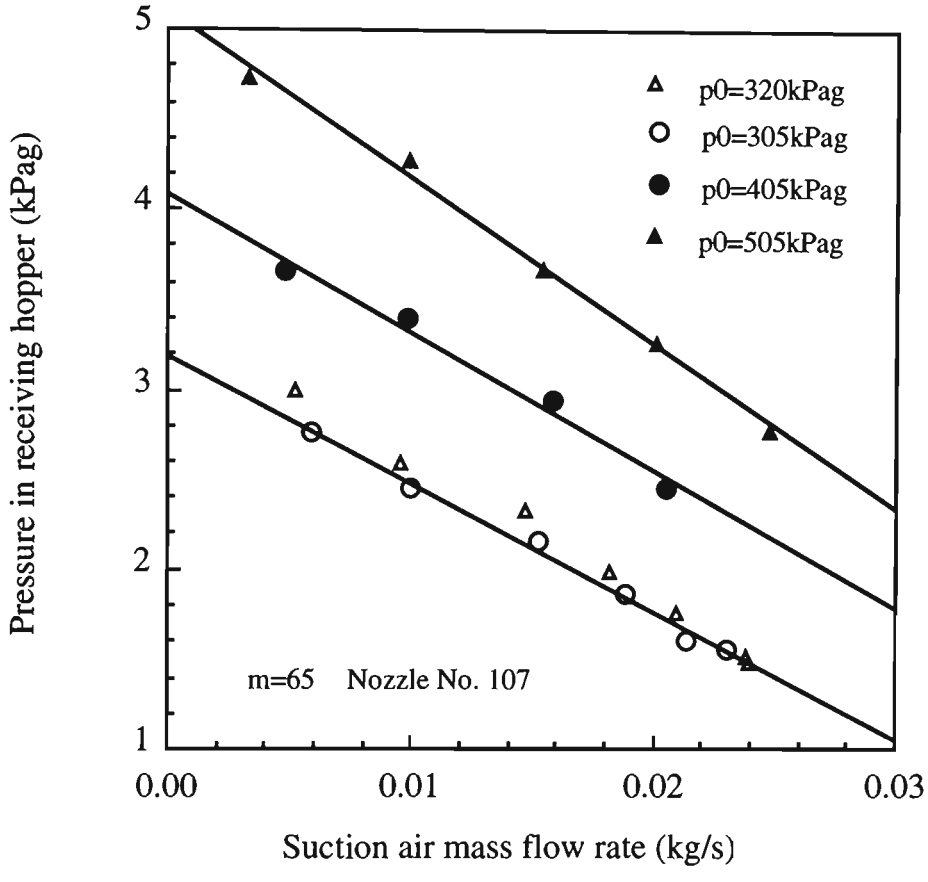

Fig. 6.4 Variation of pressure in receiving hopper with suction air flow rate

6.3.2 Non-Dimensional Air-Only Characteristics

Non-dimensional air-only pump performance is presented using a pressure ratio h versus mass flow rate ratio x plot for a given air-jet pump configuration (represented by area ratio m). Fig. 6.5 shows non-dimensional air-only characteristics with different motive pressures. It can be seen from this figure that the influence of motive pressure on non-dimensional performance is negligible. This potentially supports the representation of air-jet pump performance with such a non-dimensional performance plot.

Fig. 6.5 also shows the influence of three different area ratios on non-dimensional air-only pump characteristics. From this figure it can be seen that the influence of area ratio on annular air-jet pumps is similar to that on central air-jet pumps. For example, for a

given mass flow rate ratio, h increases with decreasing m, and vice versa. This means that for a given x, h may increase or decrease by varying m. From Eq. (3.6), an increase in h will increase p_5 if p_0 and p_4 are kept constant. This suggests that a small m suits the application of a high delivery pressure, and vice versa. It also can be seen from this figure that the maximum mass flow ratio corresponding to the minimum pressure ratio (*i.e.* delivery pressure as small as possible for a given motive pressure) increases with increasing area ratio. The reason is that a variation in area ratio for a given throat tube diameter can only be obtained by adjusting the flow area of motive fluid. For example, a decrease in motive flow area will increase the area ratio. For a given motive pressure, the motive flow rate decreases with a decrease in motive flow area, that is, the motive mass flow rate decreases with an increase in area ratio. The flow area of secondary stream increases with a decrease in motive flow area for a given throat tube diameter, that is, the secondary mass flow rate increases with an increase in area ratio. The increase in maximum suction mass flow rate and the decrease in motive mass flow rate make maximum mass flow ratio increase with increasing area ratio.

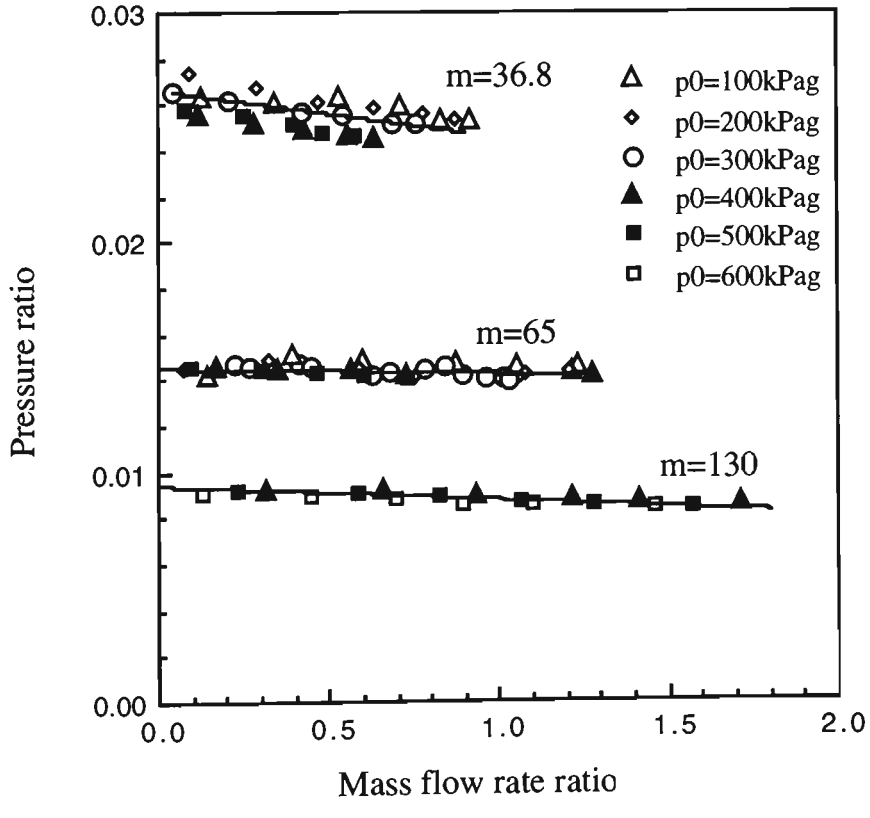

Fig. 6.5 Influence of area ratio on non-dimensional air-only performance

As shown in Fig. 6.5, different area ratios may be used for an annular air-jet pump to produce a given mass flow rate ratio. As different m represent different relationships between h and x, and different requirements of power input, there must be also an optimum area ratio for a given operating condition for annular air-jet pumps.

6.3.3 Motive Mass Flow Rate

The dependency of motive air mass flow rate on motive pressure for three different multi-hole ring nozzles is shown in Fig. 6.6. It can be seen from this figure that the motive air mass flow rate is proportional to the motive pressure for a given nozzle geometry, and also related to the flow area of the nozzle. For a given motive pressure, the larger the flow area, the larger the air mass flow rate. The air mass flow rates determined by Eq. (3.20) and Eq. (3.21) using c=0.87 also has been plotted in Figure 6.6. It can be seen below that the theoretical calculations compare favourably with the experimental observations.

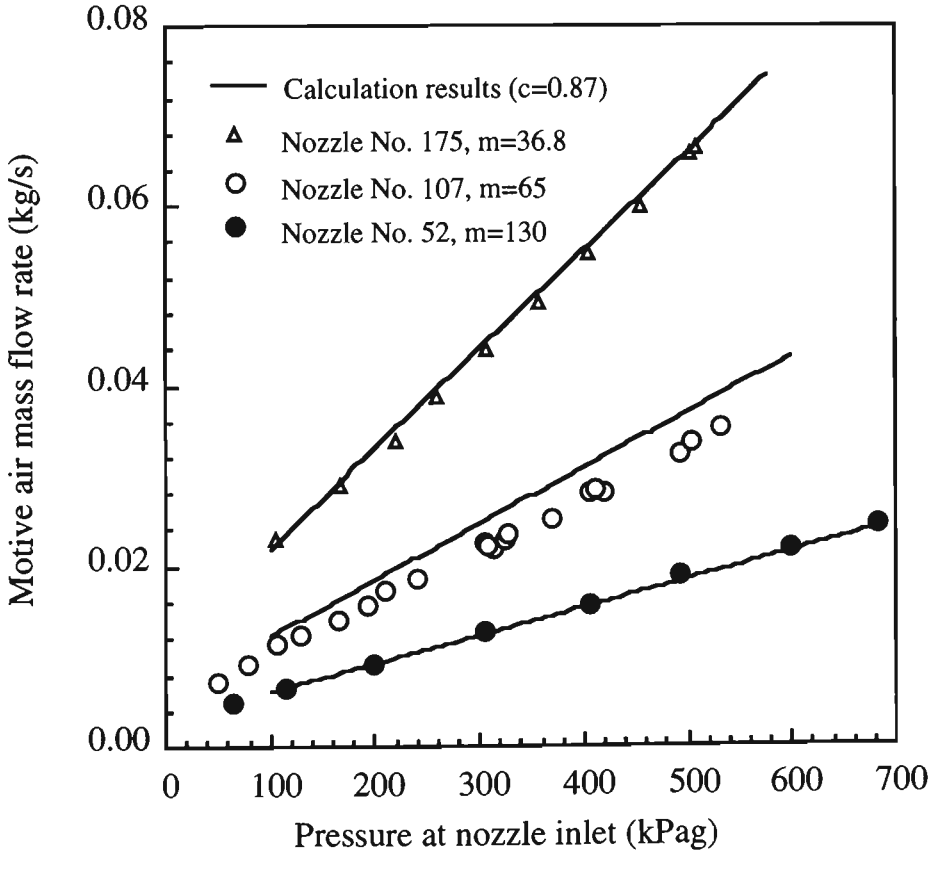

Fig. 6.6 Variation of motive air mass flow rate with motive pressure

6.3.4 Shut-off Vacuum

As mentioned in Section 5.4, shut-off vacuum refers to the vacuum at the suction port generated by the air-jet pump discharging to atmosphere when the feeding hopper is closed. For annular air-jet pumps, the shut-off vacuum is proportional to the motive pressure as shown in Fig. 6.7. This figure also shows the dependency of shut-off vacuum on area ratio. For given motive and delivery pressure, as the area ratio increases, the shut-off vacuum decreases. Fig. 6.8 shows the influence of delivery pressure on the shut-off vacuum. It can be seen from this figure that the shut-off vacuum increases as the delivery pressure decreases for a given motive pressure. If the delivery pressure reaches a certain value, the shut-off vacuum becomes zero. If the delivery pressure increases further, the pressure in the feeding hopper will become positive. This means that the motive air flow will discharge partly via the suction port of the jet pump. Thus, the suction and pumping effect will deteriorate.

6.3.5 Air-Only Efficiency

By considering the definition of efficiency given in Section 3.2.6 as a measure of the energy-effectiveness of the air-jet pump, the factors influencing the air-only efficiency of the air-jet pump are discussed below.

6.3.5.1 Motive Pressure

Figs. 6.9 and 6.10 show the influence of the motive pressure on the efficiency defined by Eq. (3.13). It can be seen from these figures that for a given suction air mass flow rate the efficiency increases with decreasing motive pressure (Fig. 6.9), while for a given mass flow rate ratio the efficiency increases with increasing motive pressure (Fig. 6.10). This suggests that a lower motive pressure should be employed to improve efficiency for the suction air mass flow rate required. However, It should be noted that a decrease in motive pressure will decrease motive mass flow rate for a given nozzle geometry and

increase the pressure ratio h and decrease x (for a given delivery pressure). For a given efficiency, using a larger motive pressure may create a larger suction air mass flow rate, and generate a smaller mass flow rate ratio. This suggests that motive air mass flow rate increases more rapidly than suction air mass flow rate does.

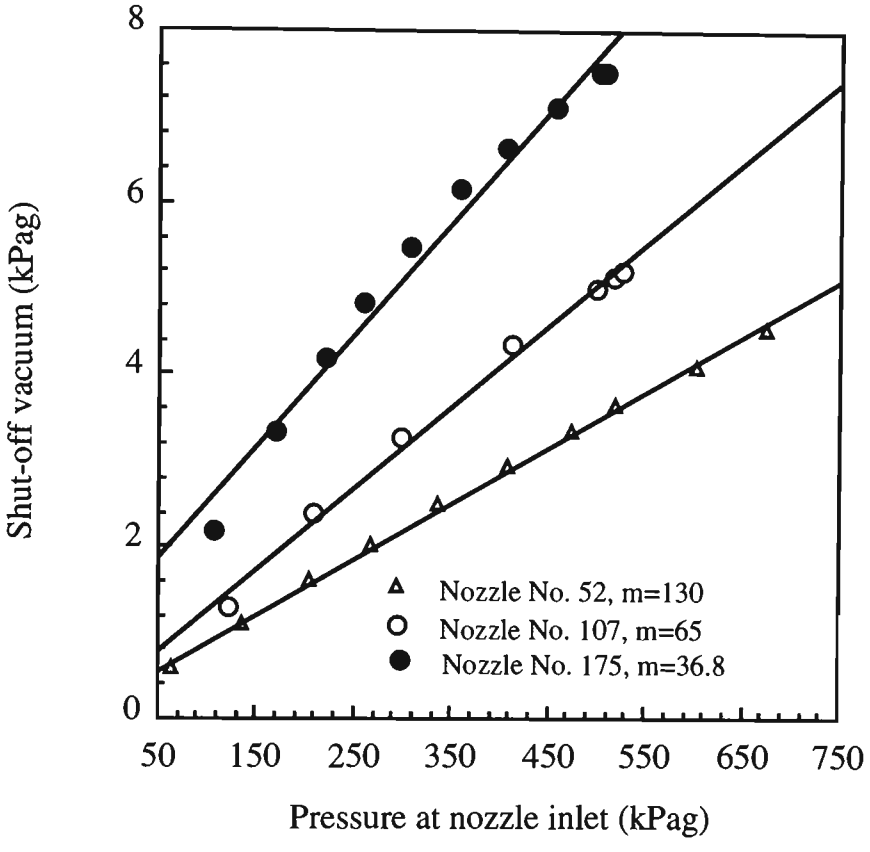

Fig. 6.7 Variation of shut-off vacuum with motive pressure

6.3.5.2 Area Ratio

The relationship between area ratio m, mass flow rate ratio and air-only efficiency is shown in Fig. 6.11. It can be seen from this figure that for a given mass flow rate ratio, the efficiency is corresponding to area ratio m. It also can be inferred that there must be an optimum area ratio for a given mass flow rate ratio to obtain maximum efficiency. Fig. 6.11 implies an obvious option to improve efficiency by reducing area ratio. It can be seen from Fig. 6.11 that the area ratio tested is far from the optimum area ratio (compared with central air-jet pump, the optimum is in the range of 2 to 3, see Fig. 5.14). Therefore, the efficiency can be improved by optimising area ratio m for a given operating condition.

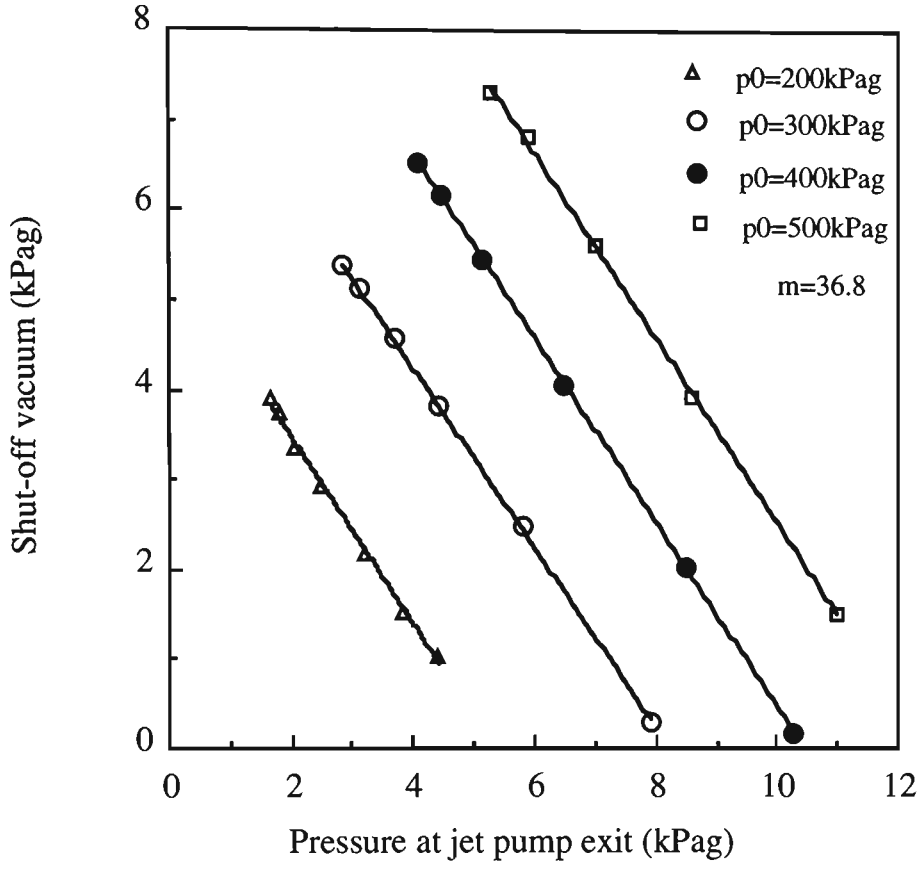

Fig. 6.8 Variation of vacuum with delivery pressure (Nozzle No. 175)

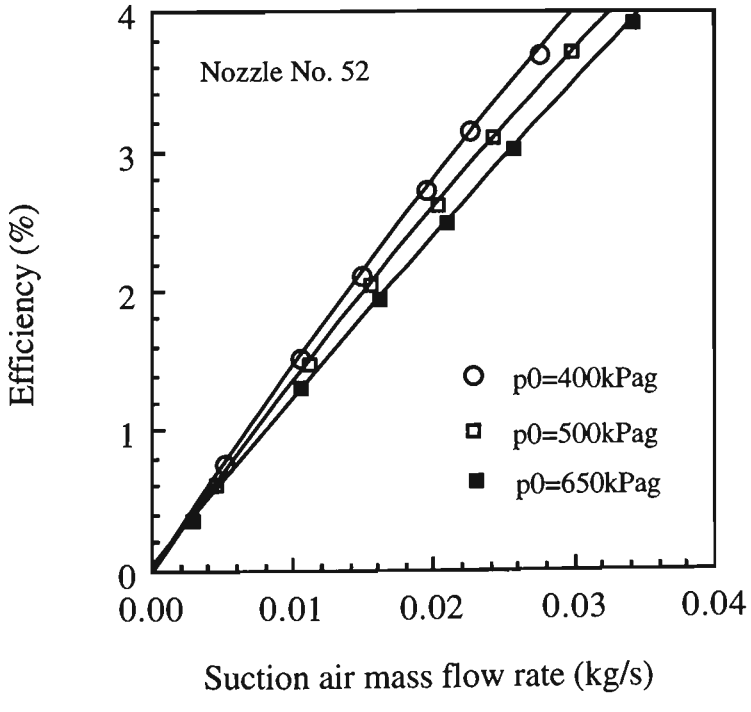

Fig. 6.9 (a) m=130

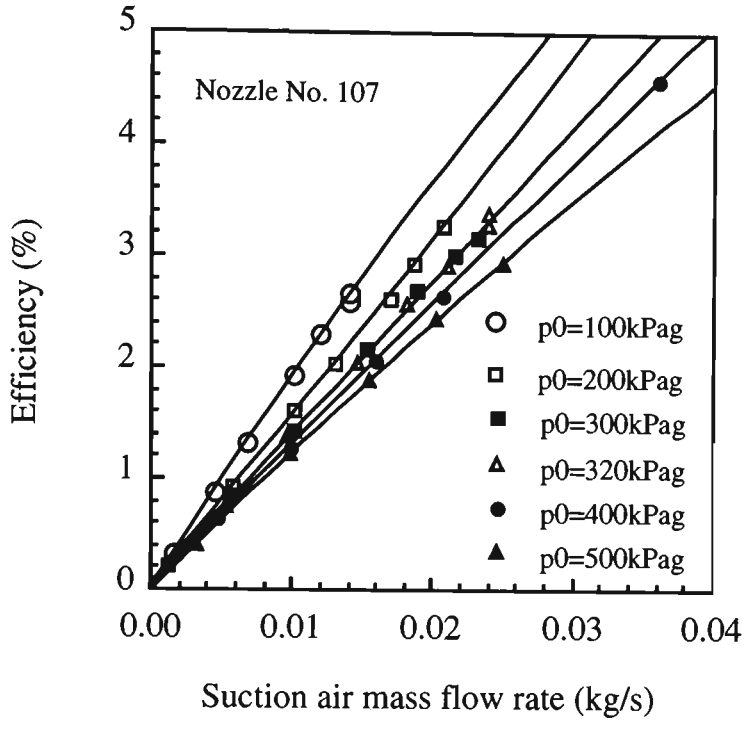

(b) m=65

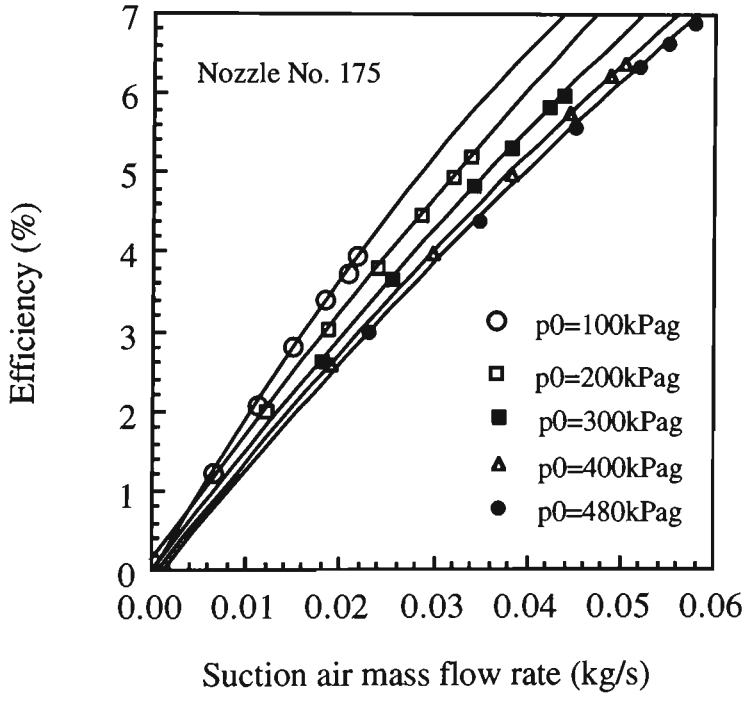

(c) m=36.8

Fig, 6.9 Influence of motive pressure on efficiency and suction air mass flow rate

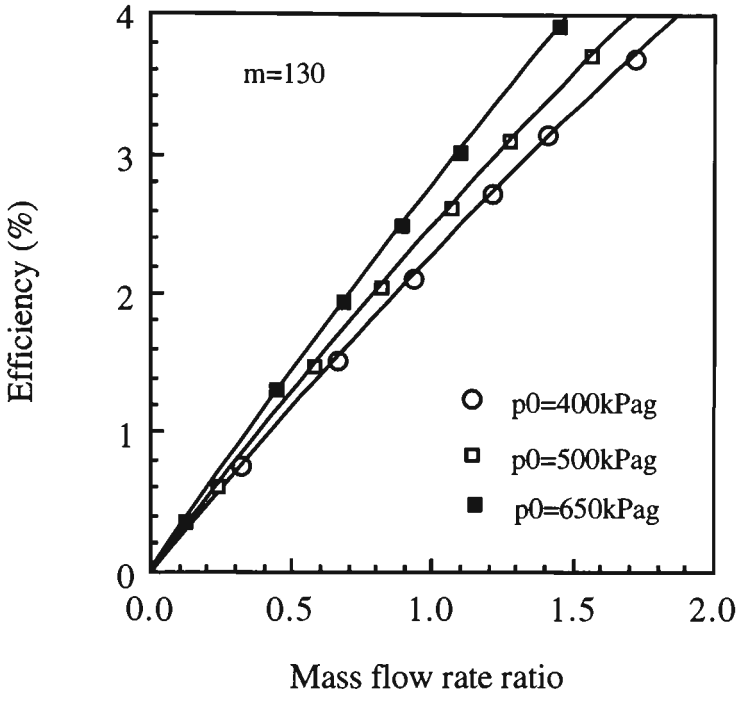

Fig. 6.10 (a) Nozzle No. 52

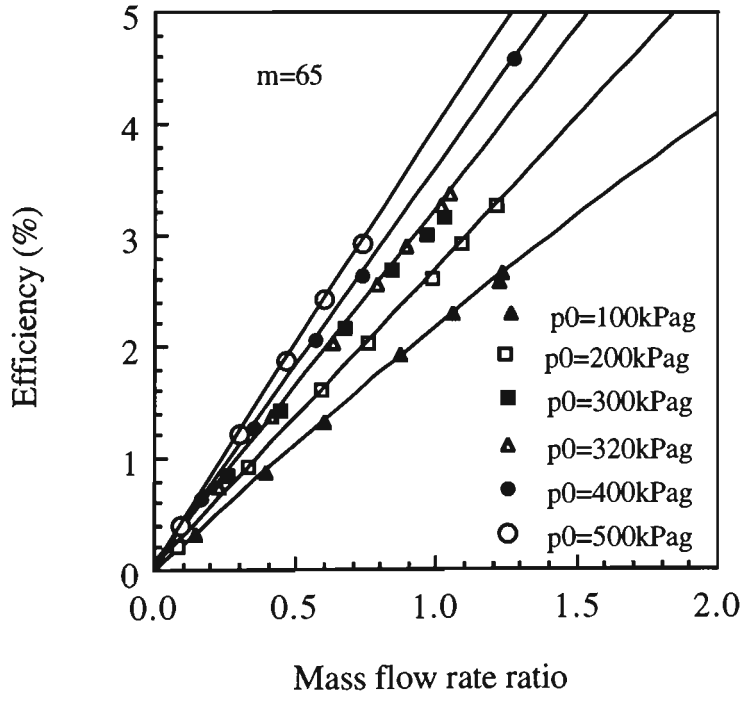

Fig. 6.10 (b) Nozzle No. 107

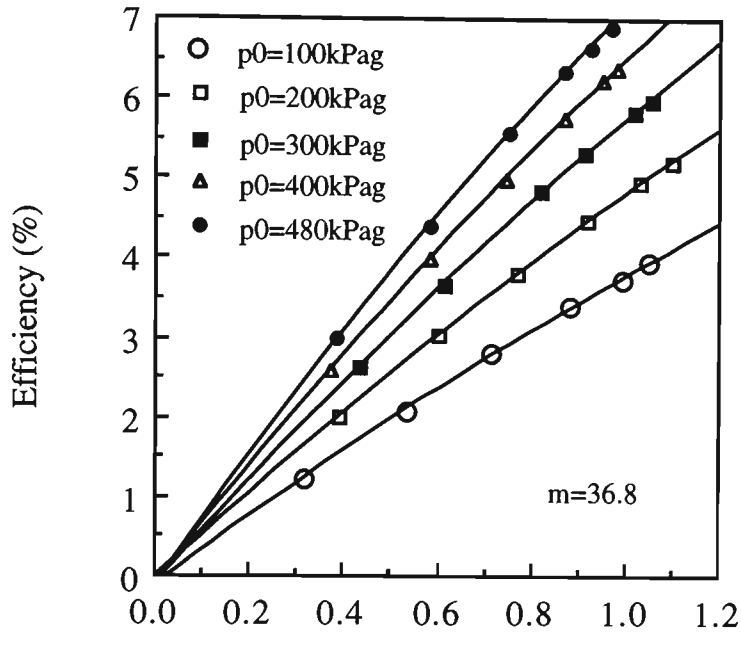

(c) Nozzle No. 175

Fig. 6.10 Influence of motive pressure on efficiency

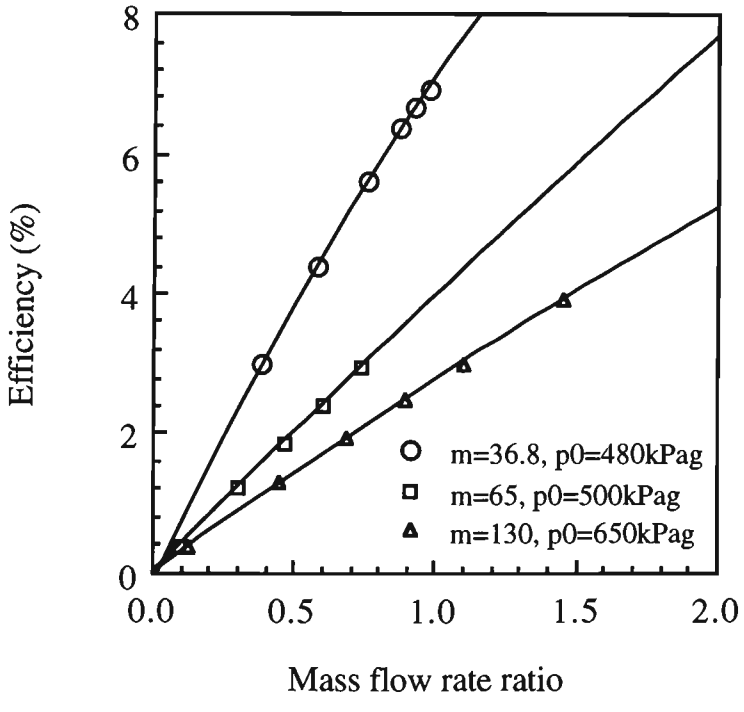

Fig. 6.11 Influence of area ratio on air-only efficiency

6.4 Air-solids Performance

The air-solids performance of an annular air-jet pump is influenced by both the operating conditions and the jet pump design. As stated in Section 5.6.1.3, the suction air mass flow rate in solid pumping is ignored in presenting the experimental data to show the influences of operating and geometrical conditions on pump performance and efficiency.

6.4.1 Influence of Operating Conditions

The operating conditions of an air-solids jet pump are expressed by the motive pressure, suction pressure and delivery pressure. The influence of motive pressure on air-solid performance is similar to that on air-only performance (see Figs. 6.1 to 6.4). A variation in motive pressure affects motive mass flow rate, pump pressure difference, delivery pressure and solids conveying rate. As shown in Figs. 6.12 to 6.14, for a given conveying rate of solids, the pump pressure difference, the delivery pressure and the pressure in the receiving hopper (generated by air-jet pump) increase with an increase in motive pressure, and vice versa; for a given pressure in the receiving hopper, the conveying rate increases as the motive pressure increases, and vice versa. It can be seen from Fig. 6.15 that the suction pressure is independent of motive pressure as long as the conveyed mass flow rate is less than the maximum discharge rate of the feed hopper (under atmospheric conditions). It has been tested that the maximum discharge capacity under atmospheric conditions is 0.4 kg/s for plastic pallets (see Table 4.4). Suction pressure decreases with an increase in solids mass flow rate because the pressure drop due to friction increases with solids mass flow rate. Figs. 6.12 to 6.14 also show that for a given motive pressure, the solids mass flow rate conveyed by the air-jet pump decreases as the pump pressure difference, the delivery pressure and/or the pressure in the receiving hopper increases, and vice versa. The reason is that an increase in receiving hopper pressure increases the delivery pressure and/or the pump pressure difference of the air-jet pump.

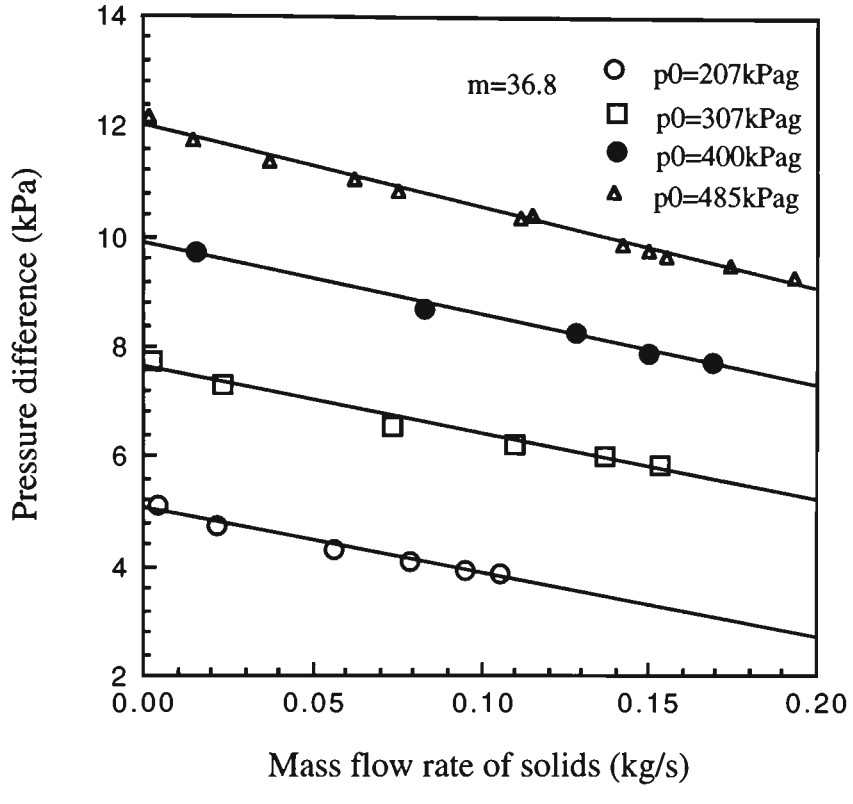

Fig. 6.12 Influence of motive pressure on dimensional performance (Nozzle No. 175)

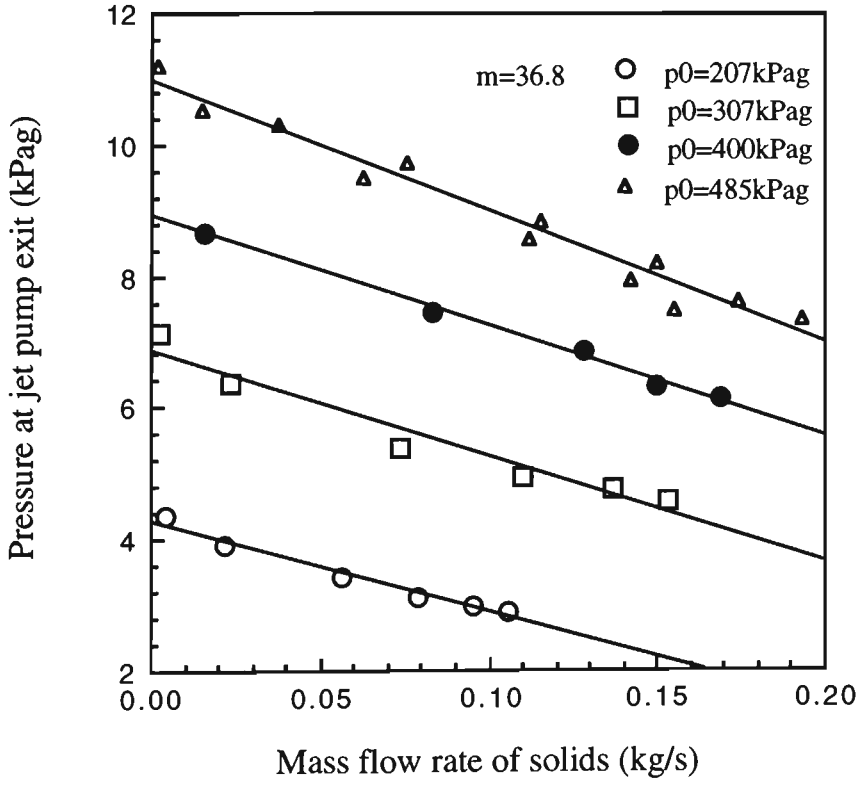

Fig. 6.13 Variation of delivery pressure with mass flow rate of solids (Nozzle No. 175)

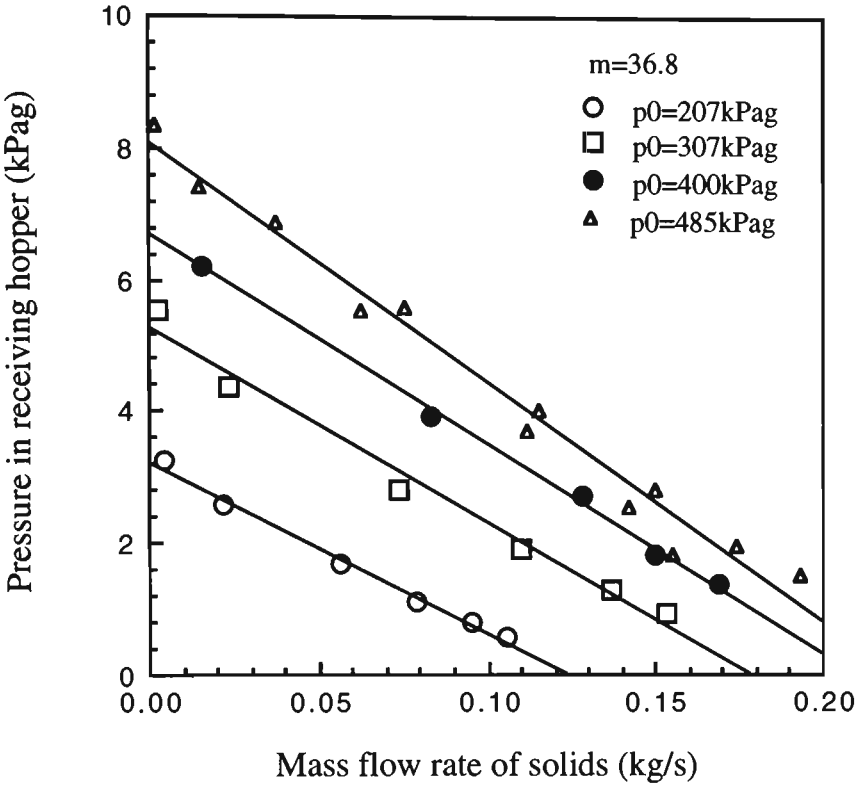

Fig. 6.14 Variation of pressure in receiving hopper with mass flow rate of solids (Nozzle No. 175)

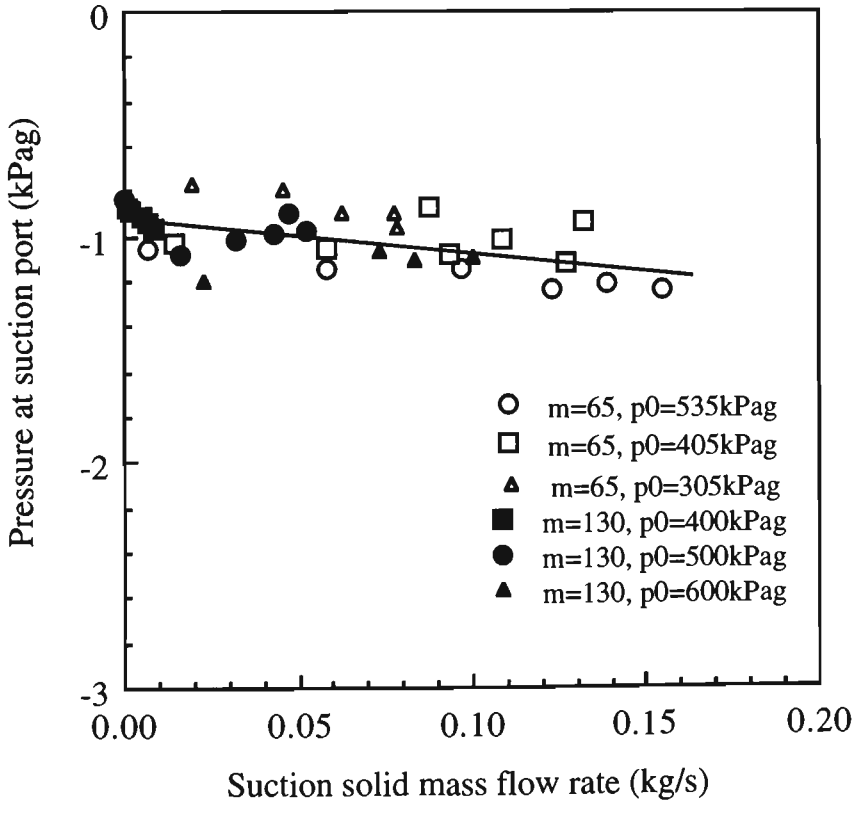

Fig. 6.15 Suction pressure of air-jet pump used for solids conveying

Fig. 6.16 shows the influence of the motive pressure on the efficiency defined by Eq. (3.11). It can be seen that for a given mass flow rate ratio the efficiency increases with increasing motive pressure. This suggests that a higher motive pressure should be employed to improve efficiency for this type of air-jet pump. It should be noted that although the increase in motive pressure will increase motive mass flow rate for a given nozzle geometry, the increase in motive pressure will decrease pressure ratio h and increase x, and also increase the suction solids mass flow rate for a given delivery pressure.

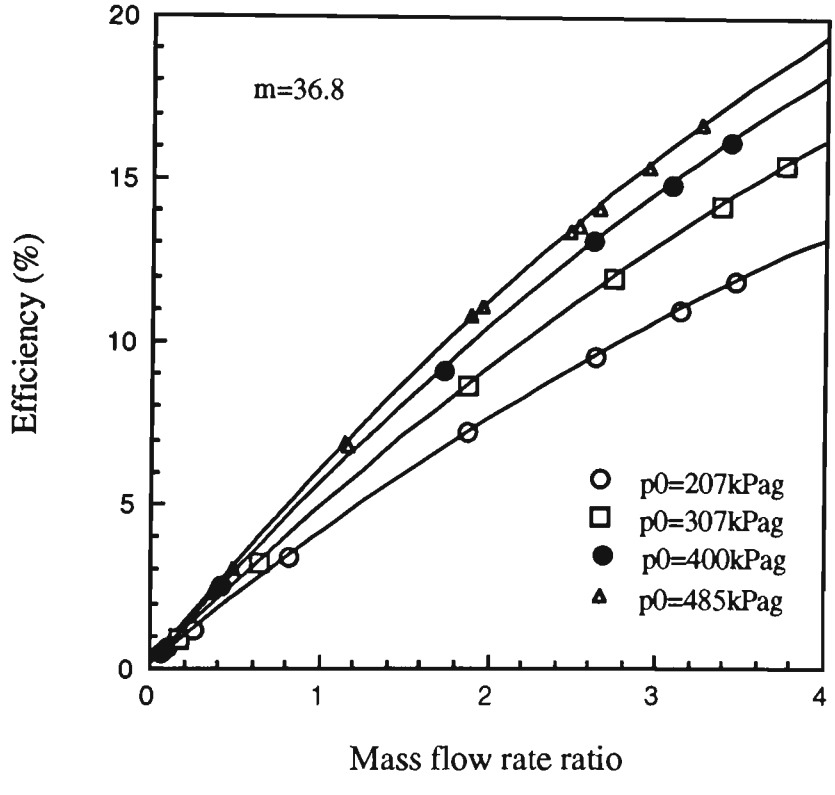

Fig. 6.16 Influence of motive pressure on efficiency (Nozzle No. 175)

6.4.2 Influence of Mixing Tube to Nozzle Area Ratio

The influence of area ratio on the air-solids jet pump performance shown in Fig. 6.17 is similar to that under the air-only conditions. For example, it can be seen from this figure that the h-x lines become flatter as m is increased and steeper as m is decreased. This means that x may increase or decrease by varying m for a given h, and for a given x, h may increase or decrease.

Fig. 6.18 shows the influence of area ratio and motive pressure on the efficiency defined by Eq. (3.11). It can be seen that for a given conveying rate, the efficiency increases with decreasing area ratio (increasing flow area of nozzle for a given mixing tube diameter). This suggests that reducing m produces a steeper h-x characteristic line, an increased pressure ratio for a given mass flow rate ratio (refer to Fig. 6.17) and a better efficiency (refer to Fig. 6.18). It can be seen form Eq. (3.6) that an increase in pressure ratio h for a given delivery pressure suggests that (for a given mass flow rate of suction solids) the motive pressure and the motive mass flow rate can be reduced to reduce the power required by the air-jet pump. However, it should be noted also that reducing m will decrease the maximum mass flow ratio and the maximum mass flow rate of solids conveyed. From Eq. (3.5), reducing x requires an increase in motive mass flow rate. For a given nozzle geometry, increasing motive mass flow rate means an increase in motive pressure. Therefore, similar to central jet pumps, there must be a compromise of motive pressure between h and x for a given area ratio. That is, there must be an optimum area ratio for a given operating condition or an optimum motive pressure for a given area ratio.

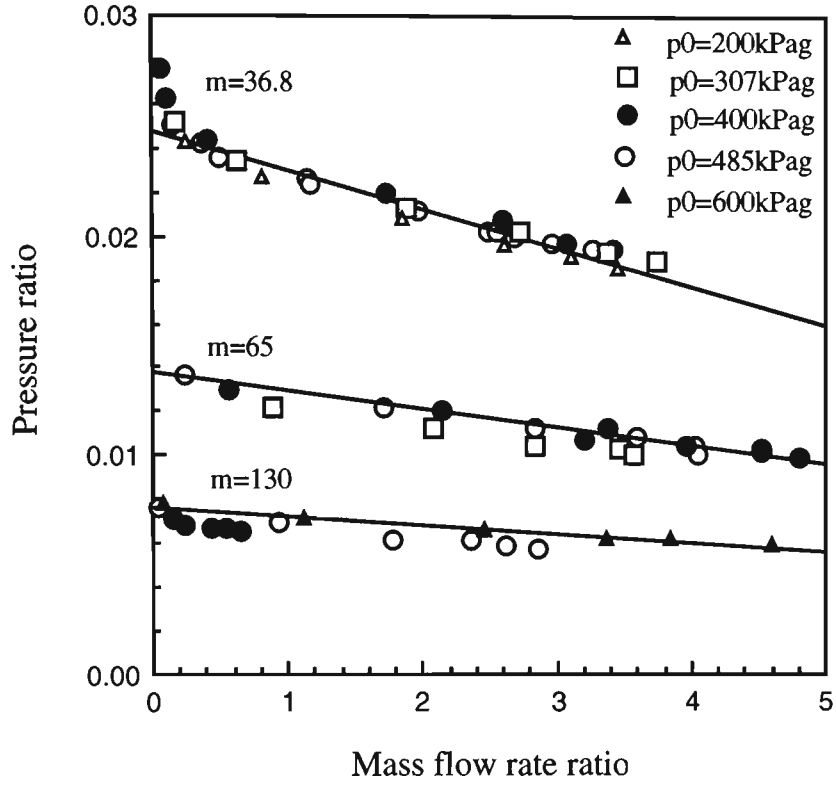

Fig. 6.17 Influence of area ratio and motive pressure on non-dimensional performance

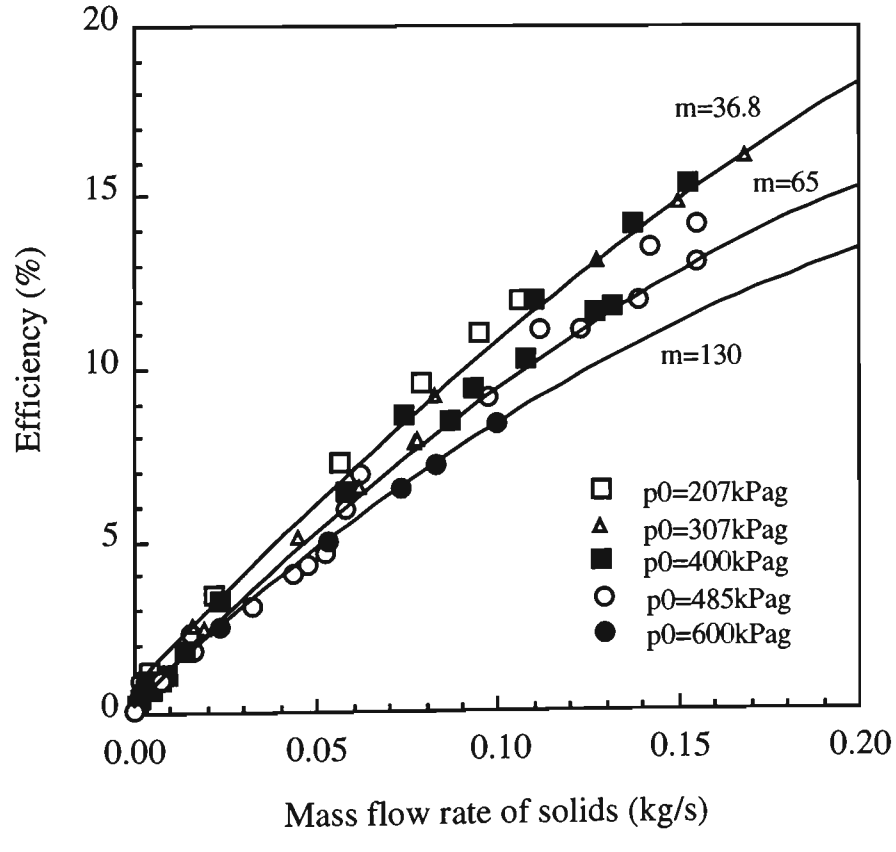

Fig. 6.18 Influence of area ratio on efficiency

6.5 Optimum Mixing Section Length

Typical static pressure distributions along the mixing section of annular air-jet pumps for air-only flow are shown in Fig. 6.19. It is seen that the static pressure increases initially due to the momentum transfer from the motive to secondary fluid and then decreases due to friction once momentum equilibrium is obtained. Therefore, there is an optimum mixing section length to obtain the maximum pressure recovery and efficiency. It can be seen from Fig. 6.19 that the location where the maximum static pressure occurs is the same for different nozzle geometries.

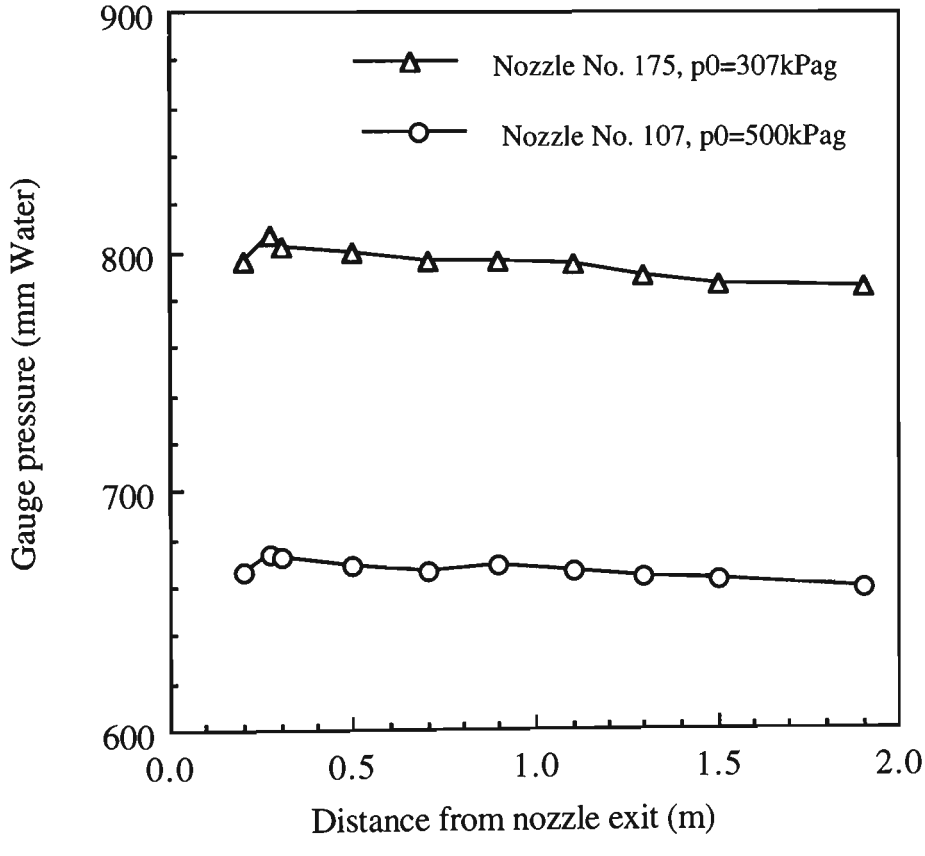

Fig. 6.19 Typical pressure distribution in mixing section of air-jet pump (air-only flow)

The pressure distribution along the mixing section of the air-solids jet pump is similar to that of air-only performance. For example, there is a substantial increase in static pressure during flow from the suction port to the mixing section. As shown in Fig. 6.20, the pressure in the mixing section initially increases due to the momentum transfer from the

motive stream to the secondary stream and then decreases once momentum equilibrium is obtained. The pressure gradient for the air-solids flow is slightly greater than that for air-only flow, which could be due to particle acceleration and wall friction. It should be noted that the location where the maximum pressure occurs for the air-solids flow is the same as that for the air-only flow. Using a mixing section length to diameter ratio L_t/d_t to represent the mixing section length for a given air-jet pump design, based on the data collected from the present test work, the optimum $L_t/d_t \approx 5.4$ for both air-only and air-solids flow (over a wide range of delivery pressures). From Fig. 6.20, it can be seen also that a further increase in pressure may be possible by using a diffuser at the location where the maximum pressure occurs. This also will improve efficiency.

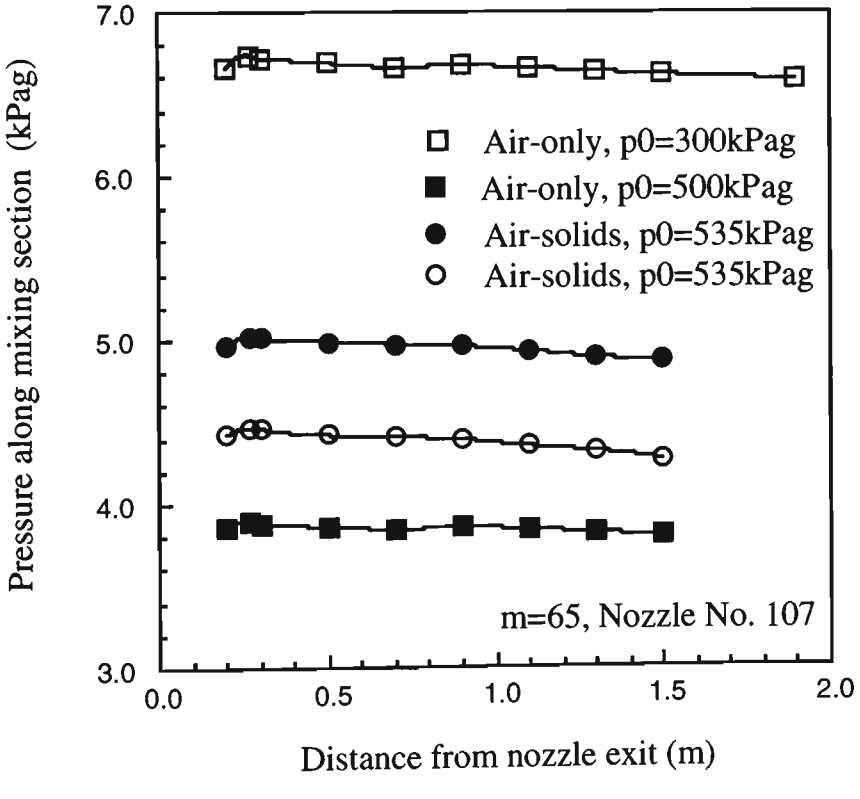

Fig. 6.20 Typical pressure distribution along mixing section

6.6 Comparison between Air-Solids and Air-Only Performance

6.6.1 Non-Dimensional Performance

The difference between non-dimensional air-only performance and air-solids performance is shown in Fig. 6.21. It can be seen that the non-dimensional performance line for air-solid flow is underneath that for air-only flow. The reason is that the solid component contributes to pressure drop in an air-solids jet pump. The pressure ratio in air-solids flow should be the same as in air-only flow when the solids mass flow rate approaches zero. The difference of ≈0.001 to 0.003 in Fig. 6.21 (*i.e.* at x=0) could be the result of measurement error. Also, the linear extrapolations shown in Fig. 6.21 (below x=1) may be inaccurate and contribute to this discrepancy.

6.6.2 Dimensional Performance

The difference between dimensional air-only performance and air-solid performance is shown in Fig. 6.22. It can be seen that the performance lines for air-solid flow is below the air-only performance line and also steeper than the air-only performance line. This is due to the influence of the solid component on friction in the air-jet pump. As the mass flow rate of solids approaches zero, both performance lines should converge to the same point. However, the difference of about 0.6 kPa shown in Fig. 6.22 may be caused by measurement error and/or inaccurate extrapolations.

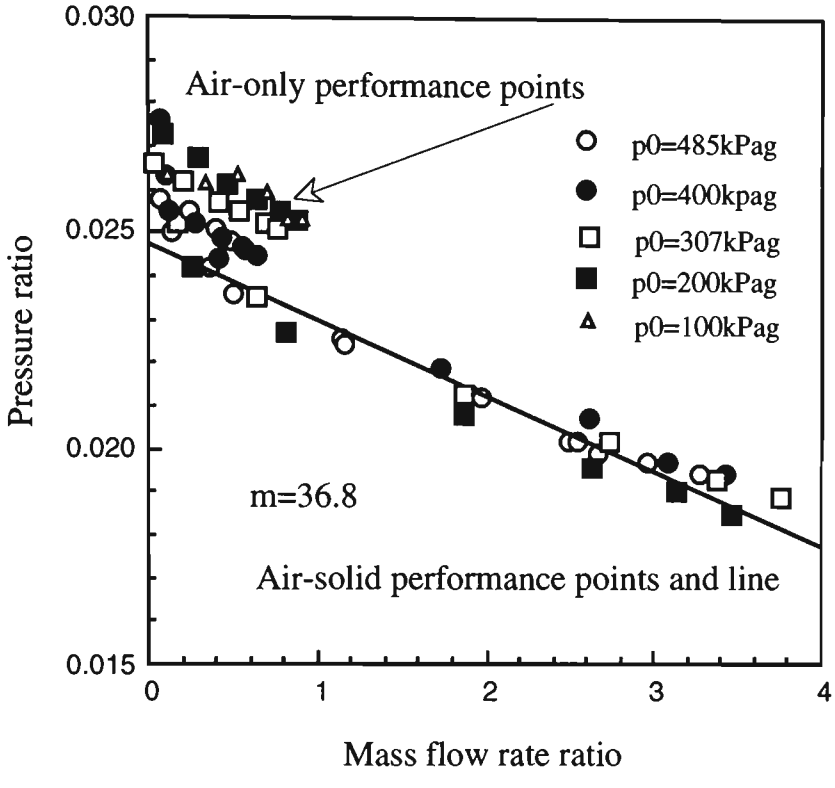

(a)

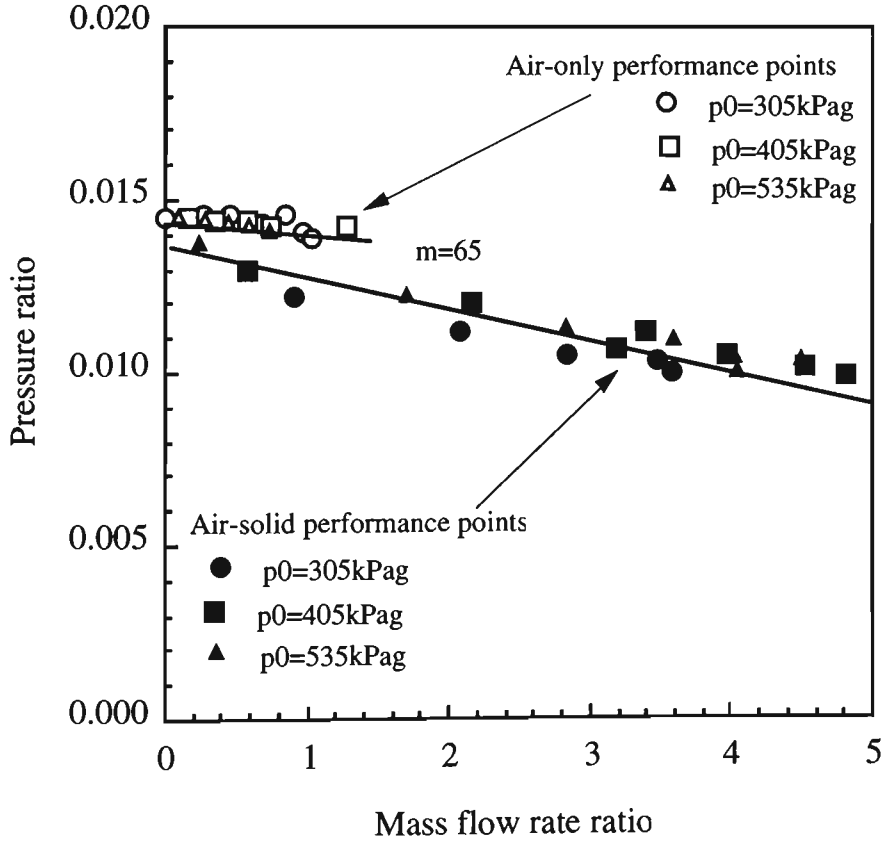

(b)

Fig. 6.21 Comparison between non-dimensional air-only and air-solid performance

(a) Nozzle No. 175, m=36.8; (b) Nozzle No. 107, m=65

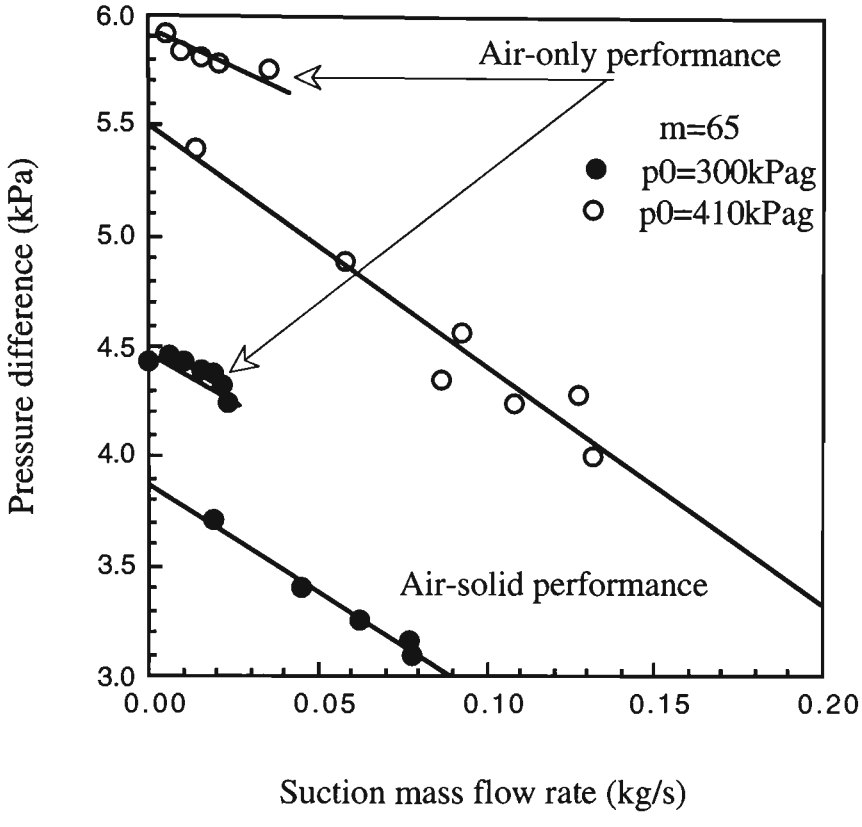

Fig. 6.22 Comparison between dimensional air-only and air-solid performance (Nozzle No. 107)

CHAPTER 7

DESIGN TECHNIQUES FOR CENTRAL JET PUMPS

7.1 Introduction

The ultimate aim of this study is to formulate a design methodology for a central air-jet pump being applied to a pneumatic conveying application. The design of an air-jet pump conveying system includes the determination of the pipeline configuration and the design of air-jet pump to produce a required solids mass flow rate and to develop the delivery pressure necessary to overcome the pressure drop across the conveying pipeline.

Analyses of air-solids pump performance have been made in Chapters 3 and 5 for central air-jet pumps. These theoretical and experimental investigations enable the formulation of a design strategy. The main distinction between analysis and design is that the analysis is concerned with the evaluation of existing jet pump and pipeline system, while the design involves determining jet pump performance for different inputs and optimising jet pump configuration and operating conditions. The evaluation of jet pump and pipeline system involves the calculation of its response under specified inputs. Therefore, the size of the various components and their configurations are given for the analysis problem, i.e. the design of the system is known. On the other hand, the design problem is to calculate sizes and shapes of various parts of the system to meet performance requirements.

Experimental results have shown that a particular mass flow rate and delivery pressure can be produced by different jet pump configurations (different area ratio and motive pressure). Among these pump configurations, there is a set of parameters that produce maximum efficiency (Chapter 5). Therefore, the jet pump must be designed by matching the pump performance to the requirements of the conveying pipeline system to achieve best efficiency and reliability. However, as stated in Chapter 2, the current design procedures are based on empiricism and only consider whether the required conveying

rate and delivery pressure are produced. This design method might ensure the reliability (as per a given specification) but not necessarily the best efficiency, as this usually is not introduced nor considered in the design. Actually, the design of a jet pump for a pneumatic conveying application involves the determination of pump dimensions and some dimensionless parameters. In this Chapter, the design methodology is formulated starting from the determination of optimum parameters (Section 7.2) followed by sizing the pump (Section 7.3). An air-jet pump feed system includes a prime mover to provide the motive air for the pump. The motive air requirement for the jet pump should match the performance of the prime mover. This topic also is considered in the presented design procedure and discussed in some related sections.

As for any other type of pump, its performance should also match the pipeline characteristics. This topic is discussed and followed by a trial and error design technique presented on the basis of determining the operating point of an air-jet pump (Section 7.4). To illustrate and demonstrate the design techniques developed in this chapter, a design example of conveying plastic pellets by using the same pipeline configuration as that in the test rig has been presented in Section 7.5.

The jet pump design procedure presented in Sections 7.2 and 7.3 can also be carried out by using optimum program techniques. A mathematical model for the optimum design of an air-jet pump is formulated and discussed in Section 7.6.

7.2 Optimum Parameters

The design of an air-jet pump includes the determination of some non-dimensional parameters so that the maximum efficiency can be obtained. The expression of efficiency defined in Section 3.2.6 can be rearranged as

$$\eta = \frac{xh}{\left[h + p_4/(p_0 - p_4)\right]\ln\left(\dfrac{1 + p_4/(p_0 - p_4)}{h + p_4/(p_0 - p_4)}\right)} \tag{7.1}$$

It can be seen from this equation that the factors affecting efficiency are h, x and both motive and suction pressure for a given m. It should be noted that the dependence of h on x is influenced by m. Hence, mass flow rate x, pressure ratio h, area ratio m and motive pressure p_0 need to be optimised for maximum efficiency (p_4 is given by the pneumatic conveying system specification). Efficiency can be generally expressed by

$$\eta = \phi(h, x, y) \tag{7.2}$$

where $y = p_4/(p_0 + p_4)$, $h = u_1(m)$, $x = u_2(m)$, $y = u_3(m)$.

Differentiating Eq. (7.2) leads to the optimisation of the geometrical and operating parameters of air-jet pumps. The optimum area ratio m_{opt} can be obtained from

$$\frac{\mathrm{d}\eta}{\mathrm{d}m} = \frac{\partial\phi}{\partial x}\frac{\mathrm{d}x}{\mathrm{d}m} + \frac{\partial\phi}{\partial h}\frac{\mathrm{d}h}{\mathrm{d}m} + \frac{\partial\phi}{\partial y}\frac{\mathrm{d}y}{\mathrm{d}m} = 0 \tag{7.3}$$

The optimum mass flow rate ratio x_{opt} and pressure ratio h_{opt} are determined by

$$\frac{\mathrm{d}\eta}{\mathrm{d}x} = \frac{\partial\phi}{\partial x} + \frac{\partial\phi}{\partial h}\frac{\mathrm{d}h}{\mathrm{d}x} + \frac{\partial\phi}{\partial y}\frac{\mathrm{d}y}{\mathrm{d}x} = 0 \tag{7.4}$$

$$\frac{\mathrm{d}\eta}{\mathrm{d}h} = \frac{\partial\phi}{\partial h} + \frac{\partial\phi}{\partial x}\frac{\mathrm{d}x}{\mathrm{d}h} + \frac{\partial\phi}{\partial y}\frac{\mathrm{d}y}{\mathrm{d}h} = 0 \tag{7.5}$$

$$\frac{\mathrm{d}\eta}{\mathrm{d}y} = \frac{\partial\phi}{\partial y} + \frac{\partial\phi}{\partial x}\frac{\mathrm{d}x}{\mathrm{d}y} + \frac{\partial\phi}{\partial h}\frac{\mathrm{d}h}{\mathrm{d}y} = 0 \tag{7.6}$$

Eqs. (7.4), (7.5) and (7.5) can become Eq. (7.3) due to

$$\frac{\mathrm{d}h}{\mathrm{d}x} = \frac{\mathrm{d}h}{\mathrm{d}m}\Big/\frac{\mathrm{d}x}{\mathrm{d}m},\quad \frac{\mathrm{d}x}{\mathrm{d}h} = \frac{\mathrm{d}x}{\mathrm{d}m}\Big/\frac{\mathrm{d}h}{\mathrm{d}m},\quad \frac{\mathrm{d}x}{\mathrm{d}y} = \frac{\mathrm{d}x}{\mathrm{d}m}\Big/\frac{\mathrm{d}y}{\mathrm{d}m} \text{ and } \frac{\mathrm{d}h}{\mathrm{d}y} = \frac{\mathrm{d}h}{\mathrm{d}m}\Big/\frac{\mathrm{d}y}{\mathrm{d}m}.$$

That is

$$\frac{\mathrm{d}\eta}{\mathrm{d}m} = \frac{\mathrm{d}\eta}{\mathrm{d}h} \tag{7.7}$$

$$\frac{\mathrm{d}\eta}{\mathrm{d}m} = \frac{\mathrm{d}\eta}{\mathrm{d}x} \tag{7.8}$$

$$\frac{d\eta}{dm} = \frac{d\eta}{dy} \tag{7.9}$$

Therefore, m_{opt} is dependent on p_{0opt}, h_{opt} and x_{opt}, or h_{opt} and x_{opt} are dependent on m *for* a given motive pressure. It can be inferred that m_{opt} can be determined by the equation showing the dependence of h_{opt}, p_{0opt}, and/or x_{opt} on m. That is, the solution of Eq. (7.4) for m is m_{opt}, and that for x is x_{opt} for a given y; the solution of Eq (7.5) for h is h_{opt} and that for m is m_{opt} for a given y.

For a given motive pressure, the jet pump performance prediction model presented in Chapter 3 can be generally expressed by

$$\psi(h, x, m) = 0 \tag{7.10}$$

The envelop curve of the family of h - x curves expressed by Eq. (7.10) using m as a parametric variable can be determined by

$$\partial\psi/\partial m = 0 \tag{7.11}$$

Differentiating Eq. (7.10) results in

$$\frac{d\psi}{dm} = \frac{\partial\psi}{\partial x}\frac{dx}{dm} + \frac{\partial\psi}{\partial h}\frac{dh}{dm} + \frac{\partial\psi}{\partial m} = 0 \tag{7.12}$$

If x is given in Eq. (7.10), $dx/dm = 0$. Eq. (7.12) can be rearranged to

$$\frac{\partial\psi}{\partial m} = -\frac{\partial\psi}{\partial h}\frac{dh}{dm} = 0 \tag{7.13}$$

It can be seen that because $\partial\psi/\partial h \neq 0$, dh/dm must be equal to 0. That is

$$\frac{\partial\psi}{\partial m} = \frac{dh}{dm} \tag{7.14}$$

By similar treatment of Eq. (7.3) to that of Eq. (7.12), it can be obtained that

$$\frac{d\eta}{dm} = -\frac{\partial\phi}{\partial h}\frac{dh}{dm} = 0 \tag{7.15}$$

It can also be seen that $\mathrm{d}h/\mathrm{d}m = 0$ due to $\partial\phi/\partial h \neq 0$. That is

$$\frac{\mathrm{d}\eta}{\mathrm{d}m} = \frac{\mathrm{d}h}{\mathrm{d}m} \tag{7.16}$$

Comparing Eqs. (7.14) and (7.16) leads to

$$\frac{\partial\psi}{\partial m} = \frac{\mathrm{d}\eta}{\mathrm{d}m} \tag{7.17}$$

Eq. (7.17) can also be derived for a given pressure ratio in Eqs. (7.10) and (7.12). Therefore, for a given mass flow rate ratio or pressure ratio, the area ratio corresponding to an envelope curve that is tangent to the family of h via x curves is the optimum area ratio.

Based on the analysis above, the optimum parameters can be determined if Eq. (7.10) is given. However, due to the complexity of $\psi(h,x,m)$, it is not practicable to determine these optimum parameters by solving directly the above equations. An alternative method is to determine correlations based on the experimental data available, as illustrated below.

1 Plot $\eta - x$ curves corresponding to different motive pressures tested for a given area ratio, as shown in Fig. 7.1 (a);

2 The optimum motive pressure and mass flow rate ratio values that correspond to the maximum efficiency can be determined from Fig. 7.1 (a);

3 Plot the h - x curve for the optimum motive pressure, as shown in Fig. 7.1 (b), and obtain the optimum pressure ratio.

It should be noted that the optimum parameters are influenced by pipeline performance. For example, trials using motive pressures 60 kPag and 70 kPag for the pump with m= 8.14, indicated that product deposition happened in pipeline. These data are not plotted in Fig. 7.1 (a). Hence, to ensure proper dilute mixture flow in pipeline, the superficial air velocity should be greater than the minimum velocity for a given bulk solid conveyed.

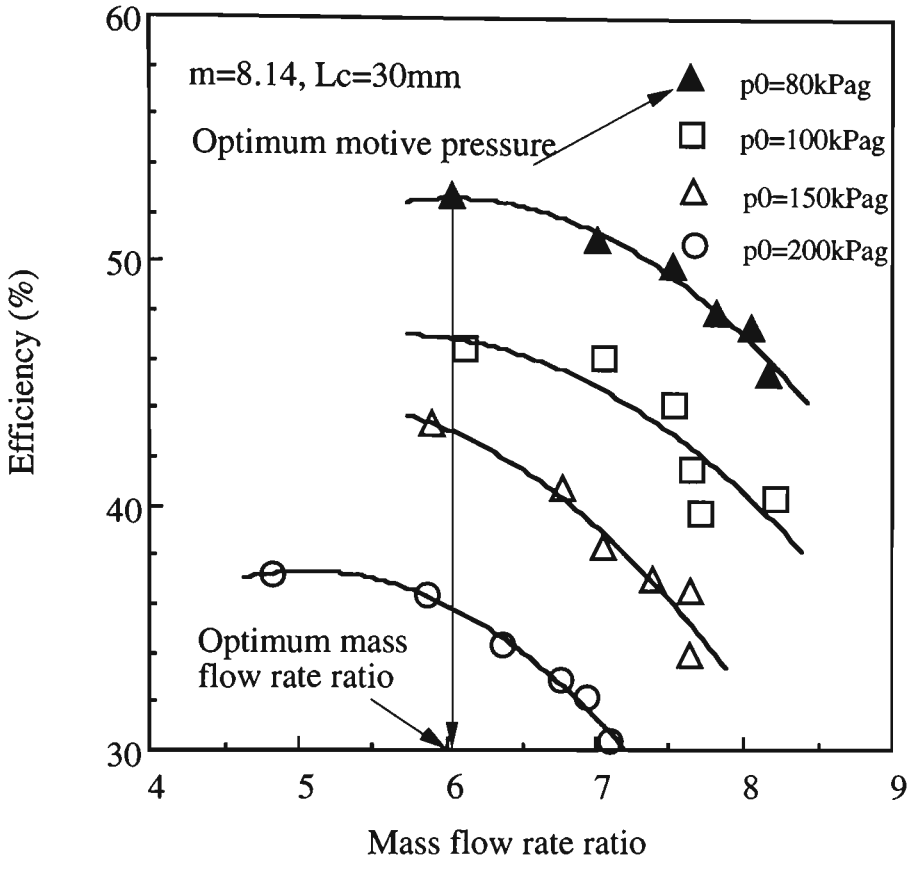

(a) Determine optimal motive pressure and mass flow rate ratio

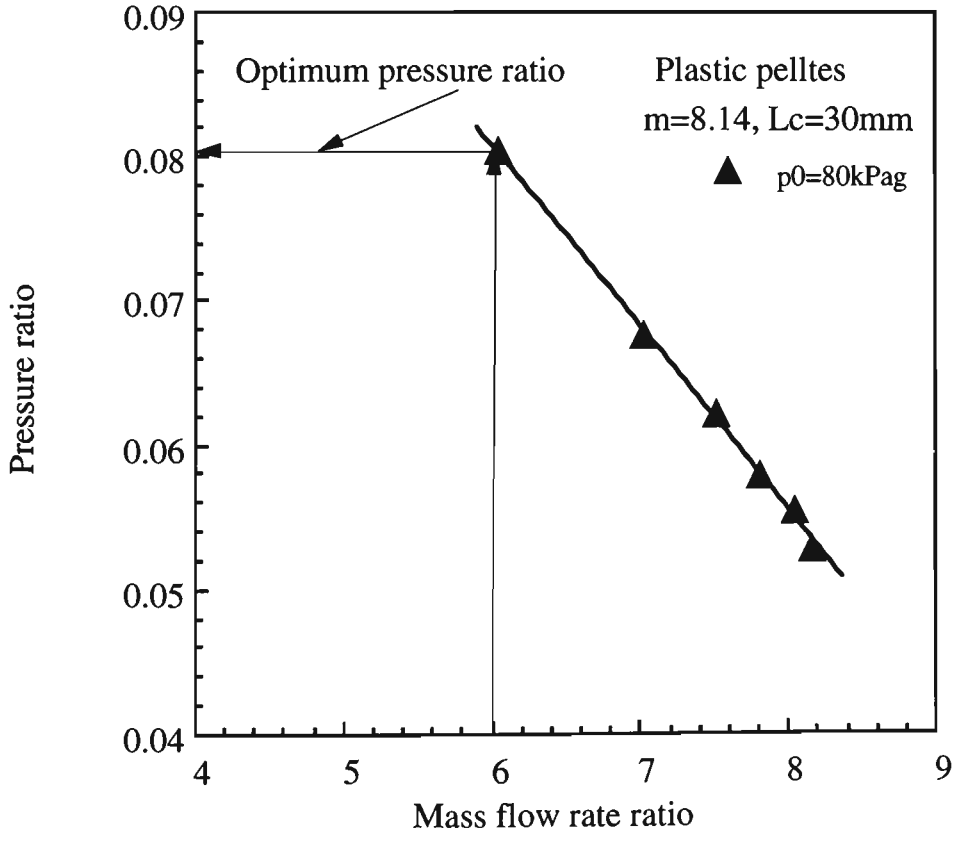

(b) Determine optimum pressure ratio

Fig. 7.1 Graphical method to determine optimum parameters from experimental data

The optimum motive pressure, pressure ratio and mass flow rate ratio values obtained by using the method described above for 5 area ratios and three types of material are plotted in Figs. 7.2 to 7.4. Based on these data, the correlations to determine optimum parameters for the central air-jet pump tested are obtained as follows:

The optimum pressure ratio depends on area ratio, and is expressed by

$$h_{opt} = 0.328(0.845^{m}) \qquad (2.5< m <25) \qquad (7.18)$$

The optimum value of motive pressure is related to area ratio and also is correlated as:

$$\frac{p_{0opt}}{p_4} = 1 + 0.081m^{1.303} \qquad (2.5< m <25) \qquad (7.19)$$

The optimum mass flow rate ratio is dependent on the material to be conveyed. Once the optimum pressure ratio h_{opt} is determined, the optimum mass flow rate ratio can be obtained either by substituting Eq. (7.18) for h in the performance prediction model or using the following correlation for x_{opt} (based on the experiments on plastic pellets for preliminary design purposes).

$$x_{opt} = 2.842\ln(1.004m) \qquad (2.5< m <25) \qquad (7.20)$$

Experimental results from conveying wheat and sorghum show that the influence of material properties on the optimum pressure ratio and the optimum motive pressure is not significant (Fig. 7.2 and Fig. 7.3). Therefore, Eqs. (7.18) and (7.19) should be able to be extended to different "similar" materials (e.g. rice, barley, urea, etc.).

The comparison of the correlations with experimental data is depicted in Figs. 7.2, 7.3 and 7.4. As pointed out above, optimum area ratio can be determined for a given h or x by using these two correlations. If no particular h or x is specified, the optimum area ratio should be between 2 and 4 (see Fig. 5.28). However, it should be kept in mind that the mass flow rate ratio is closely related to area ratio. As stated in Section 5.6.2.2, the smaller the value of m, the smaller the mass flow rate ratio. This means that for a given

conveying rate, using a small value of m may result in more motive air mass flow rate, which in turn will require an increase in pipeline diameter and capital cost. Therefore, the final determination of area ratio relies on the conveying system configuration.

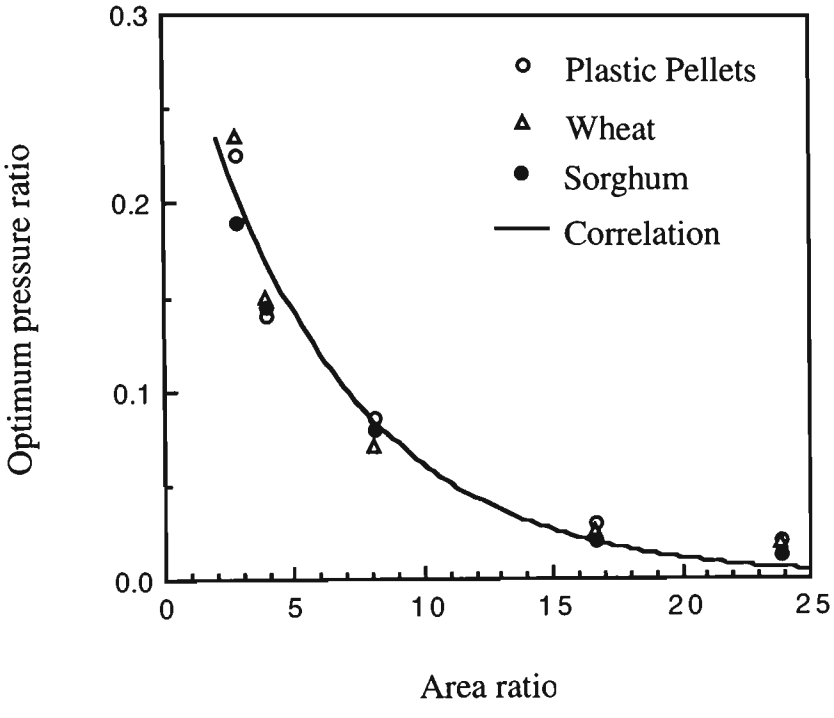

Fig. 7.2 Optimum pressure ratio correlation

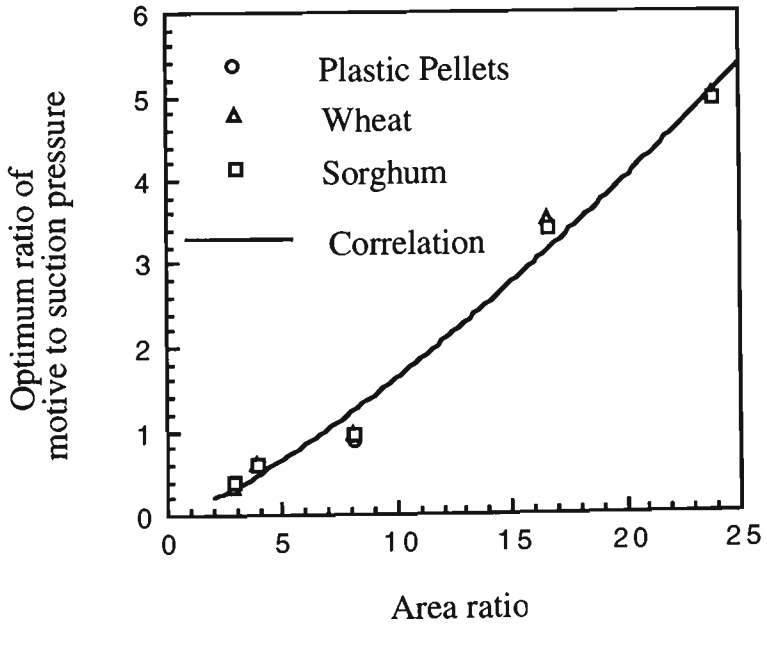

Fig. 7.3 Optimum motive pressure correlation

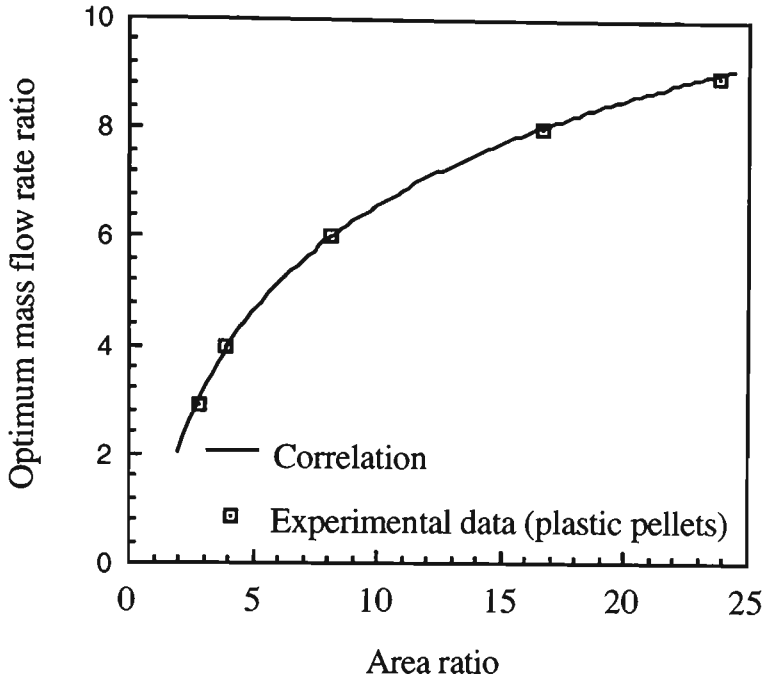

Fig. 7.4 Optimum mass flow rate ratio for plastic pellets

7.3 Design of Central Air-Jet Pumps

7.3.1 Design Procedure Outline

Generally, there are three cases involved in the design of an air-jet pump for conveying bulk solids through a pipeline. They are:

1. Suction pressure p_4, delivery pressure p_{dr} and M_{sd} are given, the parameters to be determined are p_0, M_{oa} and m;

2. Suction pressure p_4, delivery pressure p_{dr} and prime mover are given, m and M_s to be determined;

3. Suction pressure p_4, conveying rate M_{sd} and prime mover are specified, m and p_d to be determined;

Eqs. (7.18) and (7.19) combined with the performance prediction model developed in Chapter 3 provide the fundamentals to design an air-jet pump system to convey bulk solids efficiently and reliably. Based on the performance prediction model and the strategy to determine optimum parameters, the general design procedures for the three application cases listed above are given as follows.

Case 1 is a general case. The design procedure for this case is outlined below:

1. Choose area ratio $m=m_{opt}$;

2. Calculate optimum pressure ratio by using Eq. (7.18);

3. Calculate required motive pressure for the area ratio chosen by using Eq. (7.19);

4. Calculate delivery pressure p_5 by using Eq.(7.21) and check if $p_5 \geq p_{dr}$;

$$p_5 = p_4 + h(p_0 - p_4) \tag{7.21}$$

If $1.2p_{dr} > p_5 \geq p_{dr}$, calculate the dimensional pump performance and the operating point;

5. If $p_5 < p_{dr}$, increase the pressure ratio or motive pressure, calculate the optimum area ratio corresponding to the chosen pressure ratio by using Eq. (7.18) and repeat steps 3 to 6;

6. If $p_5 \geq 1.2p_{dr}$, reduce the pressure ratio or motive pressure, calculate the optimum area ratio corresponding to the chosen pressure ratio by using Eq. (7.18) and repeat steps 3 to 6;

7. Using the performance prediction model presented in Chapter 3 to calculate the mass flow rate ratio corresponding to the area ratio, pressure ratio and motive pressure determined above, calculate the motive air mass flow rate M_{oa} required;

8. Also calculate the nozzle diameter and determine other pump dimensions (Section 7.3.2);

9. Select the prime mover to match the motive pressure and air mass flow rate requirement by the designed air-jet pump.

Usually either the required solids mass flow rate or delivery pressure to be developed is of primary importance and the other of secondary significance. In the case where both are important it may need many times iteration precisely to satisfy all.

It should be noted that for energy-effective design, the operating point of the selected prime mover should be as close as possible to its best efficiency point. The discussion on the selection of prime mover is beyond the scope of this thesis and can be found in the literature [35].

Sometimes a limited motive supply may be available and it may be acceptable to modify the initial stipulation to avoid the cost of a new motive installation. This application results in the design case 2 and 3. The design procedure for case 2 is:

1. Calculate the pressure ratio h by assuming $p_5 = p_{dr}$ and p_0 = the best efficiency point of pressure of the prime mover;

2. Find the optimum area ratio corresponding to the pressure ratio determined in step 1 by using Eq. (7.19);

3. Assuming M_{oa}= the best efficiency point of mass flow rate of the prime mover, determine the nozzle diameter;

4. Calculate and determine pump dimensions (Section 7.3.2);

5. Calculate the mass flow rate ratio x by using the performance prediction model;

6. Find the conveying rate $M_s = xM_{oa}$.

The design procedure for case 3 is similar to case 2. By choosing the best efficiency point of pressure and mass flow rate of the prime mover as the motive pressure and motive mass flow rate of the jet pump to be designed, the design procedure is as follows:

1. Determine mass flow rate ratio as $x = M_s/M_{oa}$;

2. Assuming p_{0opt} = the best efficiency point of pressure, find optimum area ratio m_{opt} by using Eq. (7.19);

3. Assuming motive air mass flow rate M_{oa} = the best efficiency point air mass flow rate of the prime mover, determine the nozzle diameter and other jet pump dimensions (Section 7.3.2);

4. Calculate the pressure ratio h corresponding to the value of x, m and p_0 determined above;

5. Calculate the delivery pressure $p_d = p_5$ by using Eq. (7.21).

6. Find the conveying rate.

7.3.2 Dimensions of Air-Jet Pump

It can be seen from Fig. 3.1 that the central air-jet pump consists of some contractions and a diffuser. The pressure loss analyses of the flow elements (such as contractions, nozzle and diffuser) in jet pumps have been pursued by many investigators by applying the continuity, momentum and energy principles, which ultimately lead to an optimum design of individual elements in the jet pump. In addition, the experimental results also have shown certain useful ranges of jet pump design. These data are of great importance in the design of jet pump components. The methodology to determine the dimensions of a jet pump is suggested as follows.

7.3.2.1 Nozzle

The nozzle with gradual or abrupt contraction converts the pressure energy to kinetic energy. As stated in Chapter 2, there are different types of nozzle which can be used for air-jet pumps, for example, central convergent nozzle, annular slot and multi-hole orifice. The design of a central convergent nozzle involves the determination of diameter d_n, semicone angle ω and the contracting area ratio m_n. For a central convergent nozzle subject to subsonic flow, from Eqs. (3.20) and (3.21), the diameter can be determined by:

$$d_n = \sqrt{\frac{4M_{oa}}{c\pi Y\sqrt{2\rho_0 \dfrac{(p_0 - p_n)}{1-(A_n / A_0)^2}}}} \tag{7.22}$$

where the expansion factor Y is determined by

$$Y = \sqrt{\frac{[\kappa/(\kappa-1)](p_n/p_0)^{2/\kappa}\left[1-(p_n/p_0)^{(\kappa-1)/\kappa}\right]}{1-(p_0/p_n)}}\sqrt{\frac{1-m_n^{-2}}{1-m_n^{-2}(p_n/p_0)^{2/\kappa}}}$$

For a central convergent nozzle subject to sonic flow, the diameter can be determined by:

$$d_n = \sqrt{\frac{4M_{oa}\sqrt{T_0}}{c\pi p_0\sqrt{\dfrac{\kappa}{R}\left(\dfrac{2}{1+\kappa}\right)^{(\kappa+1)/(\kappa-1)}}}} \tag{7-23}$$

The value of the nozzle discharge coefficient c in Eqs. (7.22) and (7.23) has been discussed in Section 3.3.2, for conical convergent nozzle, c=0.95~0.985, which is similar to that for liquid flow [25].

The range of contracting ratio value is from 4 to 6, and the semicone angle can be taken as [77]

$$\omega = \arcsin\left(3\sqrt{\frac{\lambda_a}{8}\left(1+\frac{1}{m_n}\right)}\right) \tag{7.24}$$

7.3.2.2 Throat Tube

Throat tube is the most important design element of the whole jet pump, in which the mixing of motive fluid via the nozzle and suction fluid via the suction chamber takes place. The mixing of two streams is accompanied by a rise in static pressure. It has been shown [57] that a better energy transformation efficiency occurs with momentum transfer at constant area rather than at constant pressure. That is, the throat tube has parallel walls. This is fortunate since the throat tube can be a simple tube, which is easy to construct. The design of this type of throat tube involves the determination of length and diameter. From Eq. (3.4), the diameter of throat tube is be determined by area ratio and nozzle diameter as

$$d_t = \sqrt{m} d_n \tag{7.25}$$

It should be noted that the diameter of the throat tube must also accommodate the biggest particle. To date, no investigation into the influence of particle size on the determination of minimum throat tube diameter has been carried out for jet pumps subjected to gas-solid two-phase flow. However, the result of a similar investigation into liquid-solid two-phase flow has been obtained, which can be a reference for the determination of throat tube diameter [95]. If the incidence of large particles is only occasional, the throat tube diameter needs only to be a little larger, say 10% of the diameter of the largest particle. If the solids being handled are all of one size, the throat tube diameter must be at least three-times the particle size or flow may effectively cease and at least six-times the particle size if efficiency is to be unimpaired. A particle size close to or exceeding the nozzle diameter will reduce output by interference with the jet to 10% [95].

It should noted that if the diameter of throat tube determined by particle size is greater than that determined by Eq. (7.25), it is necessary to check whether the design requirement is met. Otherwise, the design procedure outlined in Section 7.3.1 needs to be repeated for the chosen throat tube diameter.

If abrasive solids are being conveyed, the throat tube will wear. It may be assumed for such applications that the bore of the throat tube is 1.025-times the nominal size. When the maximum bore exceeds the designed diameter by 10% or more, the throat tube may be regarded as notionally worn-out [95]. Maximum wear occurs about half-way along the throat tube [95]. For a jet pump, the wear of throat tube will cause an increase in area ratio, a decrease in pressure ratio and delivery pressure for a given mass flow rate and conveying rate.

Specifying a throat tube length is a difficult choice for the jet pump designer, because the performance of a jet pump having a long throat tube will be penalised by friction loses in the tube, but a short throat tube will result in a continuation of mixing into the diffuser with associated pressure loss. Usually the length of throat tube is expressed by the ratio of throat tube length L_t to throat tube diameter d_t. The optimum length of mixing tube in an actual case is that in which the static pressure rise is compensated by the pressure drop due to fiction losses. For a central jet pump, a ratio value between 5 and 7 has been recommended by previous researchers [14, 20, 46, 48, 69, 83] and discussed in Section 5.6.1.5. That is

$$L_t = 5\,d_t \text{ to } 7\,d_t \tag{7.26}$$

7.3.2.3 Throat Entry

Throat entry is an element covering the motive nozzle and gradual contraction to the diameter of throat tube. The friction losses in the throat entry are the sum of the loss at the inner wall of throat entry and the loss at the outer surface of motive nozzle. The design of this element involves the determination of the semicone angle β and the contracting ratio of inlet to outlet area. The investigation into the influence of β on the performance of a jet pump subjected to air-solids flow conducted by Chellappan and Ramaiyan [20] shows that the mass flow rate of solids increases with β. It is interesting that the optimum value

of β=15° recommended by Chellappan and Ramaiyan [20] is comparable with some results available on liquid flow that the semicone angle can be in the range between 15° and 60° [110, 114], which is comparable with that summarised by kroll [113] and suggested by other researchers for liquid and/or air-only jet pump [43, 48, 50, 65, 69]. Generally, the value of contracting semicone angle can be in the range from 15° to 45° without much influence on liquid jet pump performance [96, 97,99].

The value of contracting ratio (ratio of inlet to outlet area) can be taken between 4 and 6. The throat entry length can be determined from the contracting semicone angle and the contracting ratio determined above.

7.3.2.4 Nozzle-Throat Gap

Nozzle-throat gap is defined as the distance between the exit of the nozzle and the entry of the parallel mixing tube. For a particular throat tube configuration, efficiency increases with nozzle-throat gap and reaches an optimum value, and decreases with further increase in nozzle-throat gap. Based on the experimental results and discussion presented in Sections 5.6.1.5 and 5.6.3.3, the optimum value of the nozzle-throat gap is 50 mm, which corresponds to 1.8 d_t. Hence, from Eq. (7.25), the nozzle-throat gap for a central air-jet pump to handle solids can be determined by

$$L_c = 1.8\sqrt{m}d_n \tag{7.27}$$

It should be noted that the nozzle-throat gap must not be smaller than the throat tube diameter so that large particles can pass through the pump without obstruction.

7.3.2.5 Diffuser

A diffuser is a gradually diverging passage in which the kinetic energy of the mixed stream is converted to potential energy. It is normally found useful for jet pumps subjected to single phase [118, 119] and even liquid-gas flow [115-117]. The

designation of this component covers the determination of the diverging semicone angle and the diverging ratio of the diffuser exit to the entrance area m_d ($m_d = A_5/A_3$), which is determined by the throat tube. For a given diverging area ratio m_d, the losses due to separation increase as the diverging semicone angle θ increases, but the friction loss also increases with the decrease of diverging semicone angle due to a corresponding increase in the diffuser length. Therefore, there is a theoretical optimum semicone angle for a given diverging area ratio. In design practice, as a compromise between separation loss and friction loss, the diverging semicone angle of $\theta = 2°$ has been suggested for air-jet pumps subjected to air-solids flow [20], which is comparable with $\theta = 2°$ to $4°$ recommended for jet pumps under liquid flow condition [1]. To keep the length of diffuser reasonable, m_d =2 to 6.

The diffuser exit diameter can be determined based on throat tube diameter and m_d, and adjusted slightly to match available pipe standards.

7.4 Design of Air-Jet Pump Conveying System

7.4.1 Design Procedure

Air-jet pumps are used for feeding bulk solids into pipelines. As for any other pumping system, the air-jet pump designed for this particular pneumatic conveying duty must be matched to the characteristics of the pipeline in which it is required to work, e.g. an air-jet pump should operate as close as possible to its best efficiency point. However, in pneumatic transport applications, there are more constraints which must be take into account compared with a clean fluid system. Firstly, both pump performance and pipeline characteristics are likely to be affected by the presence of solids; in general, the system resistance (pressure drop due to friction) increases with increasing concentration. The pipeline velocity and hence motive air mass flow rate must always be kept above a certain critical value to ensure dilute flow in pipeline. Otherwise, solid deposition will occur,

with the risk of eventual pipeline blockage. These effects, depend on the design of air jet pump conveying system and the properties of the conveyed solids. The design of the air-jet pump conveying system involves the determination of pipe diameter for a particular pipeline layout and the pressure drop across the piping system and would be proceed as follows:

1. Assume the total pressure drop across over the pipeline Δp_T = 10% p_{dr} to 20% p_{dr} and the pipeline diameter $D = d_5$;

2. The pump delivery pressure required p_{dr} is the sum of the total pressure drop over the pipeline and the receiving bin pressure p_b. That is,

$$p_{dr} = (p_b + \Delta p_T) = p_b / \text{ (0.8 to 0.9)} \qquad (7.28)$$

3. Design the air-jet pump for the required M_{sd} and p_{dr};

4. Plot the jet pump characteristic curve;

5. Plot the pipeline system characteristic curve;

6. Determine the operating point and find the resulting solids mass flow rate M_{sp};

7. The design process may be finalised by comparing and checking if the solid conveying rate achieved is greater than the solids conveying rate required. If $M_{sp} \geq M_{sd}$ and $25 \leq v_{mp} \leq 40$, the design is completed; otherwise, the above procedures have to be repeated by varying Δp_T and/or D.

7.4.2 Determination of Operating Point

The mode of operation of an air-jet pump depends on the system in which it is operating. The dimensional *pump characteristic curve* shows the relation between the delivery pressure developed by the pump and the solids mass flow rate when the pump is operating at a given motive condition. If an air-jet pump is handling solids through a piping system with a receiving bin pressure p_b, the delivery pressure that the air-jet pump must develop is equal to the receiving bin pressure p_b plus the total pressure drop across the piping system. The *pipeline characteristic curve* shows the relation between the required delivery pressure and the solids mass flow rate in the pipeline. The actual operating point is the interaction of the two curves. Therefore, the determination of operating point involves the calculation of pipeline characteristic curve and the dimensional pump characteristic curve as detailed below.

7.4.2.1 Pipeline/System Characteristic Curve

The pipeline characteristic curve shows the relationship between the required pressure and the solids mass flow rate to be handled through the piping system. As mentioned above, the required pressure is the sum of the receiving bin pressure and the total pressure drop across the piping system. Generally, the receiving bin pressure is given in the design specification and is independent of solids mass flow rate. Hence, if the total pressure drop over the piping system is determined, the piping system characteristic curve can be obtained.

The total pressure drop across the piping system, Δp_T in general is comprised of

$$\Delta p_T = \Delta p_a + \Delta p_s \tag{7.29}$$

In equation (7.29), the pressure drop across the pipeline due to air flow is defined as

$$\Delta p_a = \lambda_a \frac{\rho_a v_a^2}{2D} L_p \tag{7.30}$$

where λ_a is the air-only friction factor. The value of λ_a is available in the literature [9].

Applying the continuity equation

$$v_a = 4M_a/(\pi\rho_a D^2) \tag{7.31}$$

Eq. (7.30) may be rewritten as

$$\Delta p_a = \frac{8\lambda_a L_p}{\pi^2 \rho_a D^5 \psi^2} M_s^2 \tag{7.32}$$

One popular expressions for Δp_s used in the literature is based on the definition of Barth [7] where the pressure due to solids may be expressed as

$$\Delta p_s = \lambda_s \psi \frac{\rho_a v_a^2}{2D} L_p \tag{7.33}$$

Substituting Eq. (7.31) for v_a in Eq. (7.33) leads to

$$\Delta p_s = \frac{8\lambda_s \psi L_p}{\pi^2 \rho_a D^5 \psi} M_s^2 \tag{7.34}$$

Combining Eq. (7.29) with Eqs. (7.32) and (7.34) results in

$$\Delta p_T = \frac{8(\lambda_a + \psi\lambda_s)L_p}{\rho_a \pi^2 D^5 \psi^2} M_s^2 \tag{7.35}$$

Considering that the suction air mass flow rate can be ignored comparing with the motive air mass flow rate in a properly designed air-jet pump conveying system, $\psi \approx x$. With this approximation, Eq. (7.35) becomes

$$\Delta p_T = \frac{8(\lambda_a + x\lambda_s)L_p}{\rho_a \pi^2 D^5 x^2} M_s^2 \tag{7.35 a}$$

It can be seen from Eqs. (7.35) that a reliable expression for λ_s is required before calculating the total pressure drop. Empirical expressions for λ_s were sought from the extensive review of various expressions given by Wypych and Arnold [106], and the

versatile expressions of Weber [100] were adopted for an approximate evaluation of the total pipeline pressure drop:

$$\lambda_s = 2.1\psi^{-0.3}Fr^{-1}Fr_\infty^{0.25}(d_p/D)^{-0.1} \quad (d_p \leq 0.5 \text{ mm})$$
$$\lambda_s = 0.082\psi^{-0.3}Fr^{-0.86}Fr_\infty^{0.25}(d_p/D)^{-0.1} \quad (d_p > 0.5 \text{ mm}) \tag{7.36}$$

where $Fr = v_a^2/(gD)$ and $Fr_\infty = v_\infty^2/(gd_p)$.

It can be seen from the above analysis that the total pipeline pressure drop for transporting bulk solids is based on the type of solid involved. A typical plot of the pressure drop across the pipeline shown in Fig. 4.1 versus mass flow rate of solids obtained from experiment is shown in Fig. 7.5 (a), and compared with that calculated by using Eqs. (7.36). The pressure drop over the same pipeline due to air-only flow is plotted in Fig. 7.5 (b), and compared with that calculated by using the Blasius friction factor equation ($\lambda_a = 0.3164/R_e^{0.25}$). The calculation of air-only pressure drop according to equation $\Delta p_a = 0.5\left[\left(101^2 + 0.004567M_a^{1.85}L_pD^{-5}\right)^{0.5} - 101\right]$ [6] also is plotted on this figure for comparison. It can be seen from Fig. 7.5 (a) that the predicted pressure drop is under-estimated as the mass flow rate of solids is increased. For this reason, Eq. (7.36) is modified based on the present experimental observations as:

$$\lambda_s = 0.7728Fr^{-0.86}Fr_\infty^{0.25}(d_p/D)^{-0.1} \quad (3.5 < d_p < 4, \psi \leq 16) \tag{7.37}$$

The resulting comparison is quite good as shown in Fig. 7.5 (a).

Fig. 7.6 shows the influence of motive pressure on the pressure drop across the pipeline. It can be seen that as the motive pressure increases, the pressure drop increases for the entire range of solids mass flow rate. The reason is that the air mass flow rate increases with motive pressure. As a result, the air velocity and the solids velocity increase with an increase in motive pressure.

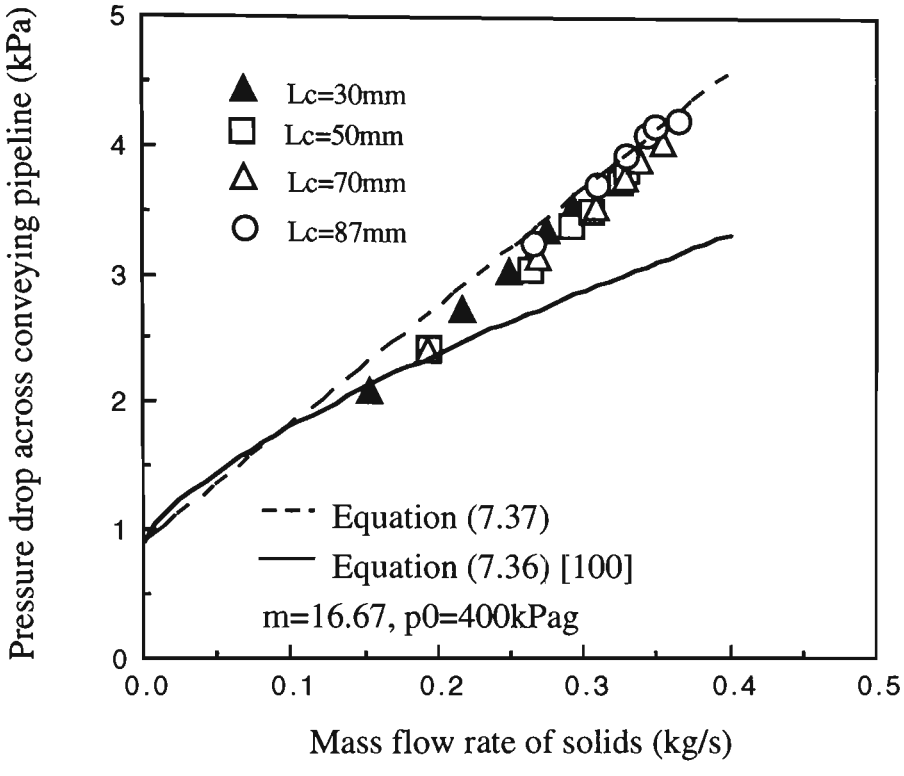

(a) Air-solids flow

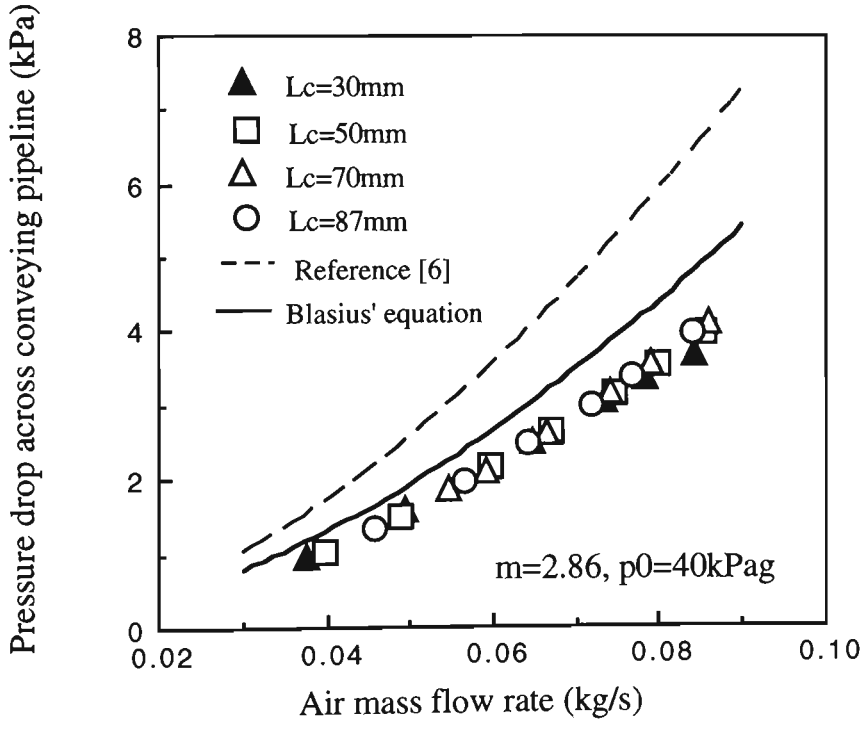

(b) Air-only flow

Fig. 7.5 Typical pressure pipeline drop

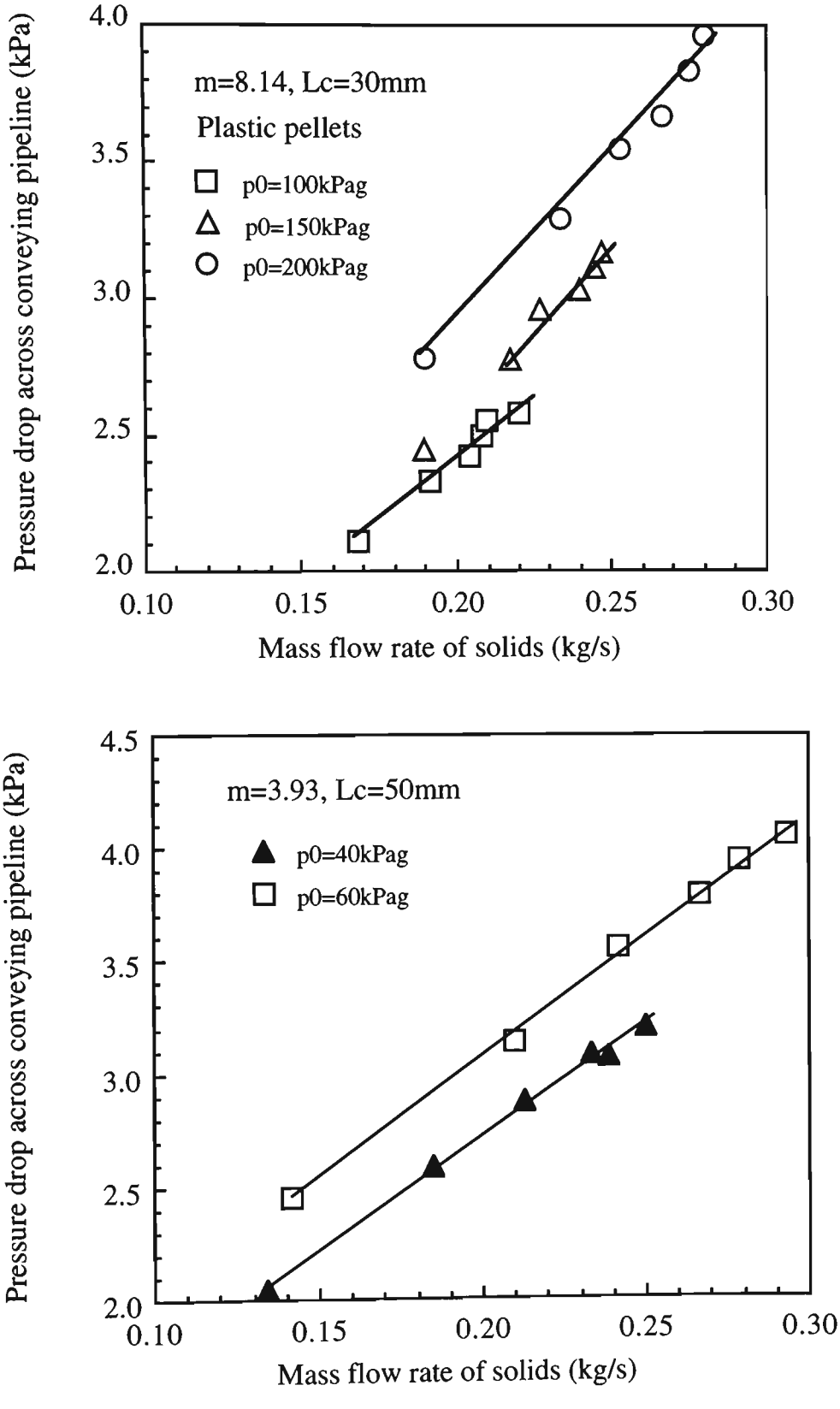

Fig. 7.6 Influence of motive pressure on pressure drop

The total pressure drop across the pipeline also can be estimated by scale-up [106] using experimental data once the pipeline is configured.

Based on the determination of the total pressure drop across the piping system, the piping system characteristic curve can be obtained by

$$p_{dr} = p_b + \Delta p_T \tag{7.38}$$

For most pneumatic transport applications, the receiving bin pressure is atmospheric pressure, that is p_b=0, and the piping system characteristic curve can be expressed by the total pressure drop with respect to the solids mass flow rate through the pipeline.

7.4.2.2 Dimensional Pump Characteristic Curve

The non-dimensional pump performance may be calculated by using the performance prediction model presented in Chapter 3 once the pump dimension is determined. This non-dimensional performance can be converted to dimensional characteristics by using the conversion relations presented in Section 3.2.5, once the area ratio m, motive pressure p_0 and motive air mass flow rate M_{oa} are defined. A typical plot of dimensional pump characteristic curve is shown in Fig. 5.5.

7.4.2.3 Operating Point

Once the pipeline and non-dimensional or dimensional pump characteristic curves are obtained, the operating point of a jet pump may be determined graphically or numerically based on the condition that the delivery pressure generated is equal to the conveying pressure required by the piping system. The corresponding intersection point defines the operating pressure and mass flow rate of solids delivered by the jet pump. This is best determined by plotting the pump and pipeline characteristic curves on the one diagram, as indicated generally in Fig 7.7 (a). The point at which the two curves intersect give an indication of what will take place. For example, based on the system characteristic curve shown in Fig 7.5 (a) and the pump characteristic curve (m = 16.67, d_n = 5.8 mm, p_o = 400 kPag), Fig 7.7 (b) provides one actual operating point for the test rig used.

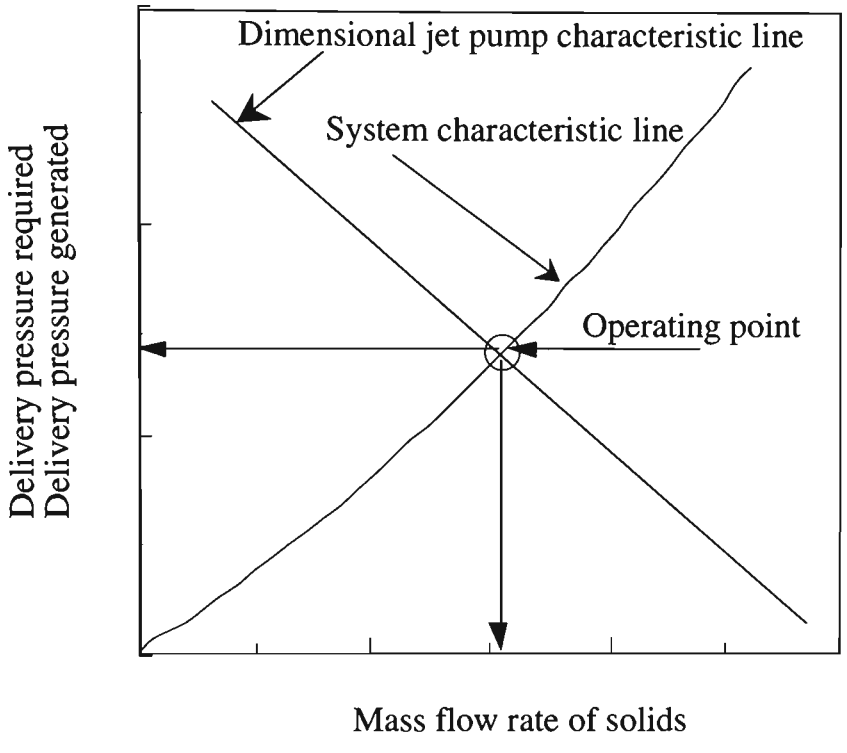

(a) Method used to determine operating point

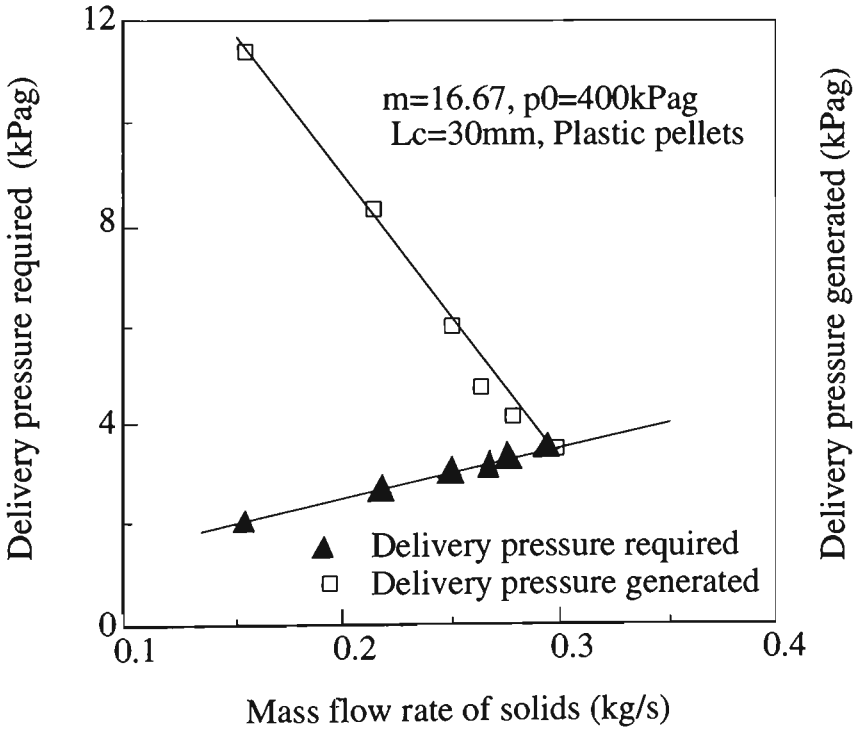

(b) Example of finding operating point

Fig. 7.7 Graphical method to determine the operating point of air-jet pump conveying system

7.4.3 Matching Jet Pump and Pipeline

The design of an air-jet pump conveying system (choice of an air-jet pump and the pipeline diameter) for a particular situation is complicated by the large number of alternatives that are possible. First of all, there are many different pump dimensions with a variety of area ratios. Also the operating characteristics can be changed by changing the motive conditions (motive pressure and motive air mass flow rate), and selecting different diameters of pipeline will provide variations in pipeline characteristics. In addition, either the motive condition of an air-jet pump or the particle properties will cause a change in pipeline characteristics.

As stated above, the operating conditions of the jet pump should be close to the best efficiency point. However, the particular values of operating condition may or may not be those for the maximum efficiency of the particular pump. If they are not, this means that the jet pump designed is not exactly suited to the specific conditions (energy will be wasted and operation will not be economical). Over-design is damaging for energy and motive air consumption. If the same solids mass flow rate is pumped with an over designed pump, then the larger motive air mass flow rate has to flow through the pipeline with a lower solid concentration. Alternatively, the jet pump has to operate at a solid mass flow rate less than the value at best efficiency point, M_{sopt}. It is also preferable to operate the jet pump at relatively lower area ratio and motive pressure in order to reduce the capital cost and energy consumption.

Hence, the procedure for designing an air-jet pump conveying system generally should be on a trial and error basis. Fortunately, for a given application case, if the required delivery pressure is evaluated properly, the application of the methodology for the design of an air-jet pump presented in Sections 7.2 and 7.3 will result in pump operation close to peak efficiency under the given delivery pressure. However, the proper evaluation of the pressure drop across the pipeline depends on the motive condition of the air-jet pump, the

scale-up model and particle properties. Therefore, a trial and error procedure to determine the pipeline diameter is unavoidable in the design of an air-jet pump conveying system so that an optimum option can be obtained.

7.5 Case Study

To illustrate the design techniques presented above, an example is given below:

The design problem is described as: design a central air-jet pump to convey plastic pellets of particle density ρ_p= 850 kg/m^3 and bulk density ρ_b=530 kg/m^3 in the pipeline shown in Fig. 4.1. The required conveying rate is 0.15 kg/s discharging to atmosphere. The material is fed under gravity to the suction port of the pump. Assuming that the total pressure drop across the pipeline system is 8 kPa and the pipe diameter is 50 mm, determine the required jet pump dimension, motive pressure and motive air mass flow rate.

This design problem belongs to Case 1 outlined in Section 7.3.1. By using the design procedure presented in Section 7.2, the optimum design parameters are determined. Based on these optimum design parameters, the required motive pressure and motive air mass flow rate are obtained. The dimensions of the air-jet pump are determined according to the formulation and consideration given in Section 7.3. The operating point of the air-jet pump is determined graphically by the intersection of the dimensional pump performance curve and the pipeline characteristic line. These calculations are summarised below.

- From the design problem considered, M_{sd}=0.15 kg/s, D=52 mm, p_b=100 kPa abs, Δp_T=8 kPa and p_4=100 kPa abs. Using Eq. (7.38), p_{dr}=108 kPa abs;

- Selecting m=2.9, the optimal pressure ratio is obtained from Eq. (7.18), where $h_{opt} = 0.328(0.845^{2.9}) = 0.201$;

- The optimum value of the motive pressure is obtained from Eq. (7.19), where

$p_{0opt} = 100\{1 + 0.081(2.9^{1.303})\} = 132.4$ kPa;

- Using Eq. (7.21), the delivery pressure generated is obtained, where
  $p_5 = 100 + 0.201(132.4 - 100) = 106.5$ kPa;
- As p_5 is close to p_{dr} and $p_5 < p_{dr}$, by adjusting p_o to 145 kPa, the delivery pressure is changed to $p_5 = 100 + 0.201(143 - 100) = 109.0$ kPa. It can be seen that $p_{dr} < p_5 < 1.2p_{dr}$;
- For conveying plastic pellets, Eq. (7.20) is used to obtain the optimum mass flow rate ratio, where $x_{opt} = 2.842\ln(1.004 \times 2.9) = 3.03$
- The motive air mass flow rate required is obtained, where
  $M_{oa} = 0.15/3.03 = 0.05$ kg/s;
- The nozzle diameter is determined by Eq. (7.22), where $d_n = 14.4$ mm;
- The throat tube diameter is determined by using Eq. (7.25), where $d_t = 25.4$ mm;
- The throat tube length is determined from Eq. (7.26), where
  $L_t = 5.6 \times 25.4 = 142.4$ mm;
- The nozzle throat gap is obtained from Eq. (7.27), where
  $L_c = 1.8\sqrt{2.9} \times 14.4 = 45$ mm;
- The dimensions of diffuser are obtained from geometrical relationship, where, θ=8°,
  $L_d = (D - d_t)/(2\tan\theta) = (50 - 25.4)/(2 \times 0.1405) = 87.5$ mm;

The pump characteristics corresponding to the pump dimensions determined above are estimated using the performance prediction model developed in Chapter 3 (Eq. 3.62 and related equations). Based on the predicted results, a relationship between solids mass flow rate and delivery pressure is plotted on Fig. 7.8 (a). The solids mass flow rate corresponding to the required delivery pressure is obtained from this plot. The relationship between predicted efficiency and solids mass flow rate is plotted on Fig. 7.8 (b). Results obtained from experiments for the pump with similar dimensions also are plotted on Fig. 7.8 (a) and (b) for comparison. It can be seen that the designed pump operates very close to its best efficiency point for the required condition.

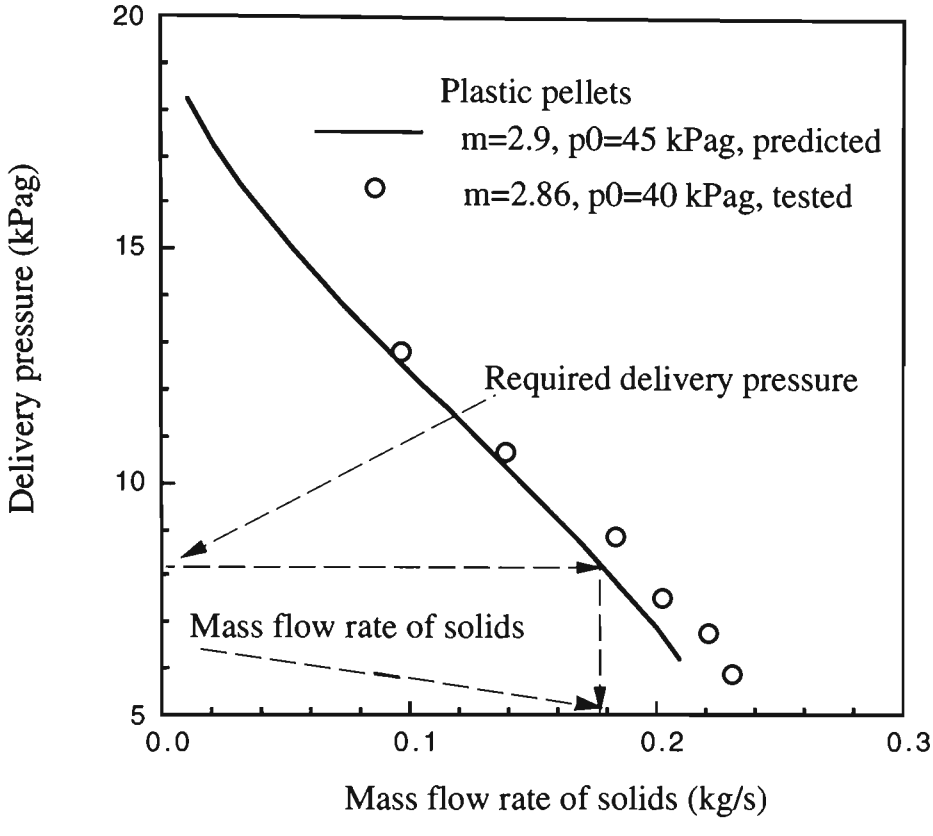

(a) Determine mass flow rate of solids

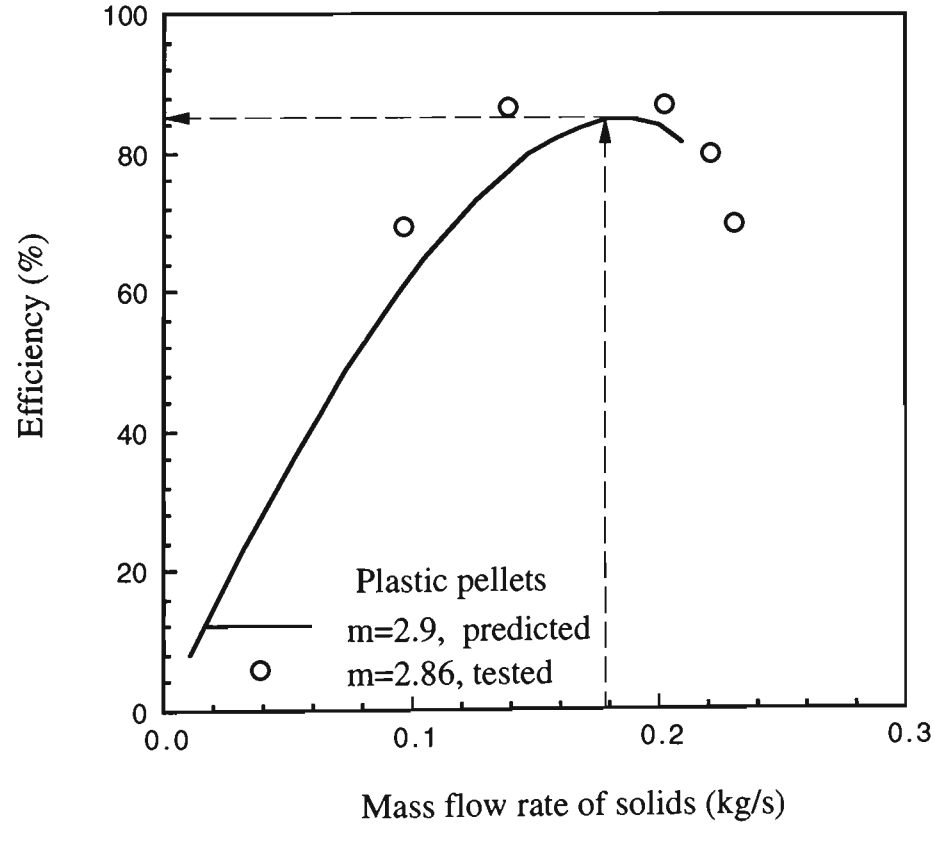

(b) Determine efficiency

Fig. 7.8 Graphical approach to determine solids mass flow rate and efficiency

All the design results are listed in Table 7.1. A comparison between the expected design and experimental demonstration is also made in this table. It can be seen that the design agrees well with the experimental results.

Table 7.1 Design results and demonstration

Parameters	Design value	Experimental observation
m	2.9	2.86
d_n (mm)	14.4	14.1
d_t (mm)	25.4	23.7
L_c (mm)	45	50
L_t (mm)	142.4	129
L_d (mm)	87.5	60
p_0 (kPag)	45	40
M_{oa} (kg/s)	0.053	0.051
M_s (kg/s)	0.176	0.181
η (%)	85	88

7.6 Optimal Design of Air-Jet Pump Conveying Systems

To automate those tedious trial-and-error aspects of the design process to some extent, optimisation techniques can be applied to virtually any engineering design situation (e.g. the design of structures, chemical process, water distribution pipeline systems, and many more). Figure 7.9 shows the optimum design process involving the application of optimisation techniques. The analysis and optimisation are essential constituents of an iterative process leading to a feasible and finally optimum design.

As stated in Section 7.4, a trial and error procedure is inevitable in the design of air-jet pump conveying system in order to obtain an optimum option. Hence, optimisation techniques also can be applied to the design process of air-jet pump conveying system to obtain economical and better designs.

The application of optimisation techniques in the design of water-jet pump was reported in 1986 [1]. However, available literature reveals that the full potential of optimisation

techniques has not been exploited in the design process of air-jet pump conveying systems. The reason is that there is no proper mathematical formulation of the design problem available. The formulation of air-jet pump performance presented in Chapter 3 provides the essential analytical tool required in the optimal design process of air-jet pump conveying system. In the following section, the application of optimisation techniques in the design of air-jet pump and associated system operating under a given application requirement will be considered to find various geometrical and operating parameters for the best efficiency.

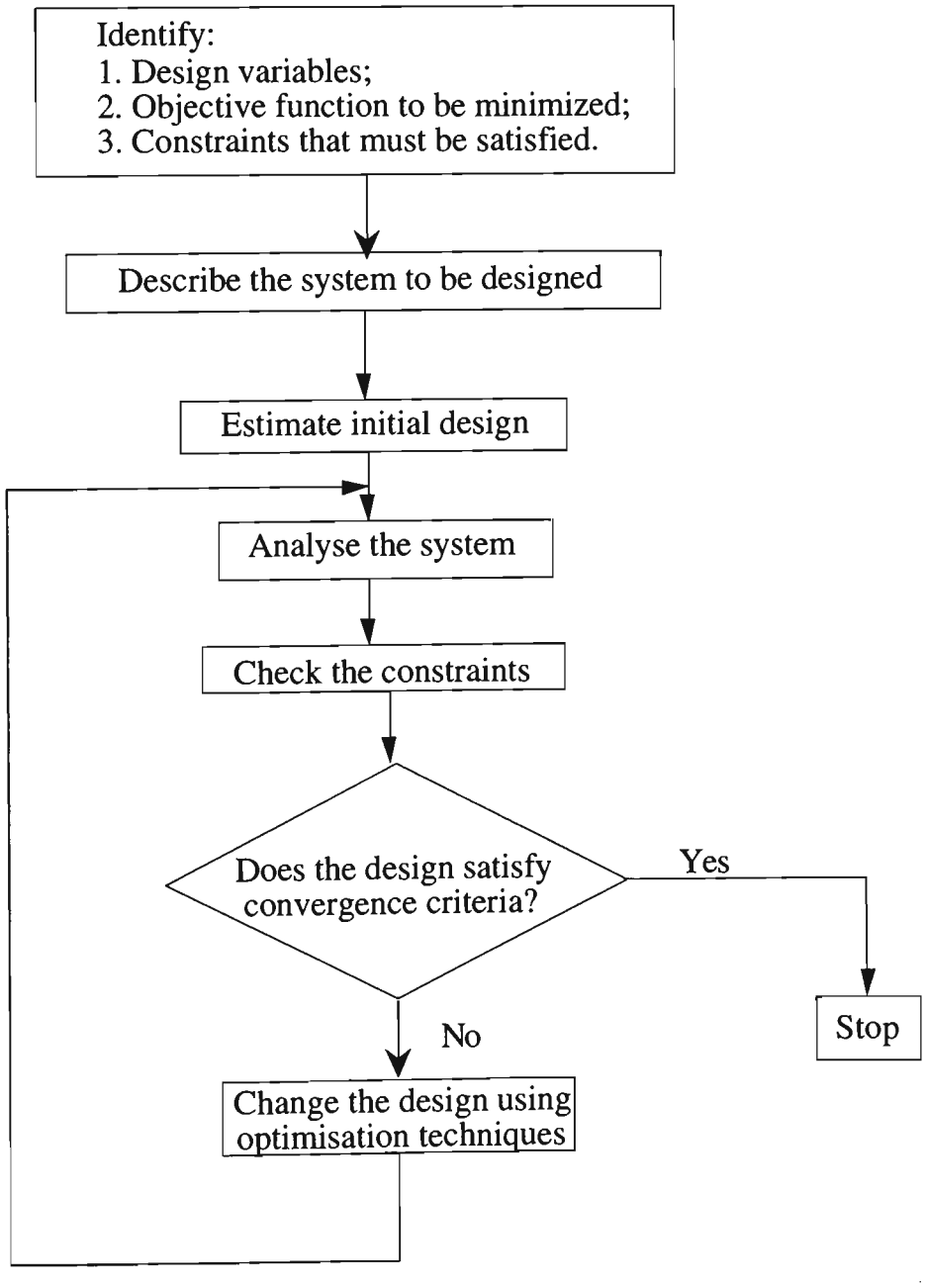

Fig. 7.9 Optimal design process

7.6.1 Optimum Design Problem Formulation

Any optimisation problem involves the identification of design variables, objective functions and constraints, and transcribing the verbal description into a mathematical statement. Proper mathematical formulation of the optimal design problem is a key to good solutions. This rigorous formulation of the design problem also is helpful to gain a better understanding of the problem. They are detailed below for the design of air-jet pumps.

7.6.1.1 Design Variables

The formulation process begins by identifying a set of variables to describe the system, called design variables. Once the variables are given numerical values, a design of the system is determined. Whether or not this design works is another question. Hence, design variables are those preselected variables which can take independent values in the design process. The other data of the problem are either given at the beginning of the design process or can be expressed in terms of the design variables. For the design of a central air-jet pump to convey bulk solids in a pipeline, the following parameters are considered as the design variables.

X_1 = area ratio, m;

X_2 = mass flow rate ratio, x;

X_3 = motive pressure, p_0;

X_4 = length of throat tube, L_t/d_t;

X_5 = diverging ratio of diffuser outlet to throat bore area, m_d;

X_6 = contracting ratio of nozzle inlet to outlet area, m_n;

X_7 = contracting semicone angle of throat entry, ;

X_8 = diverging semicone angle of diffuser, θ.

Hence, the vector of design variables X becomes

$$X \equiv \begin{Bmatrix} X_1 \\ X_2 \\ X_3 \\ X_4 \\ X_5 \\ X_6 \\ X_7 \\ X_8 \end{Bmatrix} \equiv \begin{Bmatrix} m \\ x \\ p_0 \\ L_t/d_t \\ m_d \\ m_n \\ \beta \\ \theta \end{Bmatrix} \tag{7.39}$$

All the above mentioned variables in the design vector X are the operating parameters and the physical dimensions of the jet pump component whose values can be taken independently in the specified zone.

7.6.1.2 Objective Function

A design problem usually has several solutions which may satisfy the functional requirements adequately. Therefore, a criterion is needed to judge whether or not a given design is better than another. This criterion is called the objective function. The objective function in a general optimisation problem represents a basis for the choice between alternative acceptable designs. A valid objective function must be influenced by the variables of the design problem, that is, it must be a function of the design variables. In most of the practical design problems the minimisation of cost or pressure loss, or the maximisation of profit, rigidity or efficiency is taken as the objective. In the design of air-jet pump conveying system, the maximisation of efficiency expressed in Eq. (7.1) is chosen as the objective function.

Assuming that the values of the design variables are known at the beginning of the analysis and will be modified during the design-analysis iterative process, based on the

theoretical analysis presented in Chapter 3, the main equations required for the evaluation of objective function are repeated below for convenience.

$$q_a = \frac{(1-c_{vs})S\frac{\rho_{o1}}{\rho_p}x}{c_{vs}+(1-c_{vs})S\frac{\rho_{4a}}{\rho_p}} \tag{3.40}$$

$$\frac{\overline{p_4}-p_1}{z} = (1+k_{41})\frac{C^2(q_a\frac{p_4}{p_1}+q_p)^2}{(m-1)^2}\frac{\rho_{s1}}{\rho_{o1}} \tag{3.43}$$

$$C = \frac{m-a_n^{\ 2}}{(\frac{2L_c}{d_n}\tan\beta+\sqrt{m}-a_n)\cos\beta[2a_n+(\frac{2L_c}{d_n}\tan\beta+\sqrt{m}-a_n)\cos^2\beta]} \tag{3.44}$$

$$\frac{p_2-p_1}{z} = \frac{(m-1)^2+x^2(q_a\frac{p_4}{p_1}+q_p)C^2-(1+k_{12})\{\zeta_{o2}(m-1)^2+x^2(q_a\frac{p_4}{p_2}+q_p)\zeta_{s2}\}}{(1+x)(m-1)^2} \tag{3.46}$$

$$\frac{p_3-p_2}{z} = \frac{2x(q_p+q_a\frac{p_4}{p_2})\zeta_{s2}}{m(m-1)}+\frac{2\zeta_{o2}}{m}-\frac{(1+x)(\frac{p_1}{p_3}+q_a\frac{p_4}{p_3}+q_p)(2\mu_3+k_{23})}{m^2} \tag{3.48}$$

$$\frac{\overline{p_5}-p_3}{z} = \frac{(1-k_{35})(1+x)}{m^2}(\frac{p_1}{p_3}+q_a\frac{p_4}{p_3}+q_p) \tag{3.50}$$

$$k_{12} = \frac{(\lambda_a+\psi\lambda_p)\frac{L_c}{d_n}(1+q_a\frac{p_4}{p_1})^2(1+x)}{\zeta_{o2}(m-1)^2+\zeta_{s2}x^2(q_p+q_a\frac{p_4}{p_2})} \tag{3.56}$$

$$k_{23} = \frac{(\lambda_a+\psi\lambda_p)L_t/d_t}{(1+\frac{\rho_p q_p/\rho_{o1}}{1+\rho_{a4}q_a/\rho_{o1}})(1+\frac{q_p}{q_a p_4/p_3+p_1/p_3})} \tag{3.57}$$

$$k_{35} = \frac{\xi_d}{(1+\frac{\rho_p q_p/\rho_{o1}}{1+\rho_{a4} q_a/\rho_{o1}})(1+\frac{q_p}{q_a p_4/p_3 + p_1/p_3})} \tag{3.58}$$

$$\alpha = \frac{\frac{\overline{p_4}}{p_0 - p_4} \ln(\frac{p_0}{p_1})}{1+\ln(\frac{p_0}{p_1})\frac{C^2(q_a p_4/p_1 + q_p)^2(1+k_{41})\rho_{s1}/\rho_{o1}}{(m-1)^2(1+k_{01})}} \tag{3.60}$$

$$h = \frac{\alpha}{(1+k_{01})}(\frac{\overline{p_5} - p_3}{z} + \frac{p_3 - p_2}{z} + \frac{p_2 - p_1}{z} + \frac{p_1 - \overline{p_4}}{z}) \tag{3.62}$$

Usually, the values of the coefficients involved in the above equations are known, and the quantities of M_{sd} and p_{dr} are the pre-assigned parameters. The sequence to calculate the objective function is shown in Fig. 7.10.

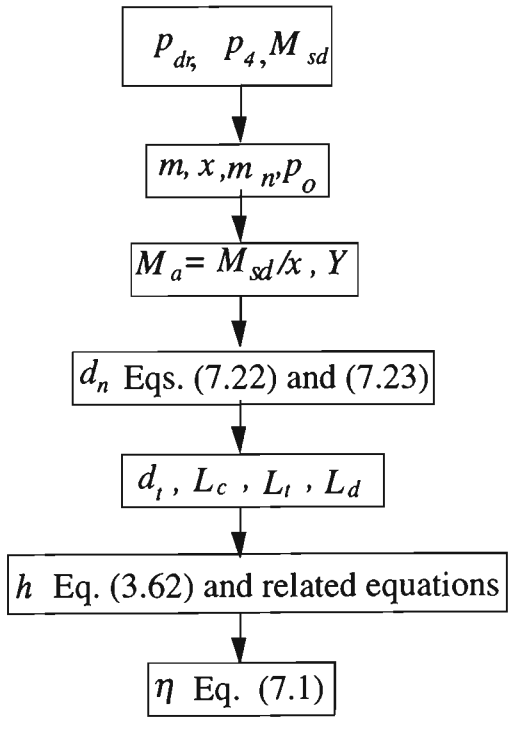

Fig. 7.10 Objective function calculation procedure

7.6.1.3 Design Constraints

Proper formulation of an optimal design problem is of paramount importance because the optimum solution will only be as good as the formulation. For example, if a critical constraint is ignored in the formulation, the optimum solution will most likely violate it because optimisation methods tend to exploit errors or uncertainties in the design models. This is due to the fact that if the constrains are not properly formulated, the optimisation techniques will take designs in the portion of the design space where either the design is absurd or dangerous. Note also that if too many constraints are included on the system or if these constraints are inconsistent, there may not be any solution to the optimal design problem. Therefore, proper care must be exercised in defining and developing expressions for the constraints.

The air-jet pump conveying system is designed to perform within a given set of constrains. These constrains must be influenced by the design variables. Generally, in the design of air-jet pumps, the following requirements are to be met from physical and operational considerations.

1. All the physical dimensions should have positive real values;

2. From the physical design limitations, the following inequalities exist:

   $d_5 > d_t$; $d_t > d_n$; $d_0 > d_n$; $d_4 > d_t$;

3. The diameters of the diffuser at the outlet and that of the throat entry are not to exceed a certain maximum value;

4. The pressure ratio h should be within a specified range 0 to 0.7;

5. The throat tube length should be within the specified range of $3d_t$ to $10d_t$;

6. The mass flow rate at the jet pump exit should be more than M_{oa};

7. The variation range of area ratio is from 1.5 to 25 as discussed in Section 3.9, and that of mass flow rate ratio is from 0.1 to 15 based on the experimental data shown in Fig. 5.24;

8. The semi-cone angle of diffuser should be within the specified lower and upper bounds of 2° to 4°, and the semi-cone angle of throat entry should be within the range 10° to 60°;

9. The length of diffuser should be kept reasonable, that is, the area ratio of diffuser should be within some lower bound, ≤ 4.

10. The delivery pressure at the jet pump exit should be greater than the pressure required by the pipeline system;

11. The superficial air velocity at the jet pump exit should between 20 and 40 m/s.

These constraints have been incorporated in the statement of the standard optimisation problem.

7.6.1.4 Mathematical Statement of the Optimal Design Problem

The formulation of an optimum design problem involves transcribing a verbal description of the problem into a well-known mathematical statement. The optimal design of an air-jet pump conveying system is to maximise the efficiency by optimising the jet pump geometry and operating parameters, but the general optimal design model treats only with minimisation problems. This is not a restriction as the maximisation of say function $f(x)$ is equivalent to the minimisation of a transformed function $-f(x)$. Hence, the optimisation problem described above can be stated in the format of a non-linear programming problem as follows:

Find X which minimises

$$f(X) = -\eta = -\frac{xh}{[h + p_4/(p_0 - p_4)]\ln\left(\frac{1 + p_4/(p_0 - p_4)}{h + p_4/(p_0 - p_4)}\right)} \tag{7.40}$$

subject to the constraints

$$g_1 \quad (X) = 0 - h \le 0 \tag{7.41}$$

$$g_2 \quad (X) = h - 0.7 \le 0 \tag{7.42}$$

$$g_3 \quad (X) = M_{oa} - M_d \le 0 \tag{7.43}$$

$$g_4 \quad (X) = 100 - \overline{p_4} \le 0 \tag{7.44}$$

$$g_5 \quad (X) = \overline{p_4} - 101.3 \le 0 \tag{7.45}$$

$$g_6 \quad (X) = 0.1 - x \le 0 \tag{7.46}$$

$$g_7 \quad (X) = x - 15 \le 0 \tag{7.47}$$

$$g_8 \quad (X) = 0.0 - d_n \le 0 \tag{7.48}$$

$$g_9 \quad (X) = d_n - d_0 \le 0 \tag{7.49}$$

$$g_{10} \quad (X) = 3d_t - L_t \le 0 \tag{7.50}$$

$$g_{11} \quad (X) = L_t - 10d_t \le 0 \tag{7.51}$$

$$g_{12} \quad (X) = d_n - d_t \le 0 \tag{7.52}$$

$$g_{13} \quad (X) = d_t - d_5 \le 0 \tag{7.53}$$

$$g_{14} \quad (X) = d_5 - d_{\max} \le 0 \tag{7.54}$$

$$g_{15} \quad (X) = 2 - m_n \le 0 \tag{7.55}$$

$$g_{16} \quad (X) = m_n - 6 \le 0 \tag{7.56}$$

$$g_{17}(X) = 1.5 - m \leq 0 \tag{7.57}$$

$$g_{18}(X) = m - 25 \leq 0 \tag{7.58}$$

$$g_{19}(X) = 2 - \theta \leq 0 \tag{7.59}$$

$$g_{20}(X) = \theta - 4 \leq 0 \tag{7.60}$$

$$g_{21}(X) = 10 - \beta \leq 0 \tag{7.61}$$

$$g_{22}(X) = \beta - 60 \leq 0 \tag{7.62}$$

$$g_{23}(X) = p_{5R} - p_5 \leq 0 \tag{7.63}$$

$$g_{24}(X) = 2 - m_d \leq 0 \tag{7.64}$$

$$g_{25}(X) = m_d - 4 \leq 0 \tag{7.65}$$

Eqs. (7.41) - (7.47) represent the behaviour constraints, whereas Eqs. (7.48) - (7.65) represent the geometrical or side constraints which impose limits on the size of the design variables. It can be seen that the objective function of Eq. (7.40) is a non-linear function of the design variables. Therefore, the mathematical programming problem formulated above is a non-linear programming problem.

7.6.2 Brief Description of Solution Methods

Numerical methods for optimal design are conceptually different to the analytical methods described in Section 7.2 and 7.3. Using numerical methods, an initial design estimated for the optimum point is pre-selected and changed iteratively until optimal conditions are satisfied. The process may require several iterations. Thus, with numerical methods, an iterative process has to be used to satisfy the optimal conditions.

It turns out that constrained optimisation problems can be transformed to a sequence of unconstrained problems [4]. The basic idea is to construct a composite function, as shown in Eq. (7.66), using the objective and constraint functions. It also contains certain parameters, referred to as penalty parameters that penalise the composite function for violation of constraints. The larger the violation, the larger is the penalty. Once the composite function is defined for a set of penalty parameters, it is minimised using any of the unconstrained optimisation techniques. The basic procedure is to choose an initial design estimate $X^{(0)}$, and define the function Φ of Eq. (7.66). The controlling parameter r also is selected initially. The function Φ is minimised for X while keeping r fixed. The controlling (penalty) parameter r are then adjusted based on certain conditions and the composite function is redefined and minimised. The process is continued until there is no significant improvement in the estimate for the optimum point.

$$\Phi(X,r) = f(X) + P(\mathrm{h}_k(X), \mathrm{g}_i(X), r) \tag{7.66}$$

where r is a vector of controlling (penalty) parameters and P is a real valued function whose action of imposing the penalty is controlled by r. The form of penalty function P depends on the method used. Therefore, unconstrained optimisation methods can be used to solve constrained problems.

In summary, the fundamental idea of numerical methods for solving non-linear optimisation problems is to start with a reasonable estimate for the optimal design. Objective and constraint functions and their derivatives are evaluated at this point. Based on these functions, the design is moved to a new point. The process is continued until either optimal conditions or some other terminating criteria are satisfied. The iterative process represents an organised search through the design space for points that represents local minima. Thus, the procedures are often called the search techniques or direct methods of optimisation. The preceding iterative process can be summarised as follows:

Step 1 Estimate a reasonable starting design $X^{(0)}$. Set the iteration count k = 0.

Step 2 Computerise a search direction in the design space. This calculation generally requires an objective function value as well as a constraint function and their gradients.

Step 3 Check for convergence of the algorithm. If it converges, terminate the iterative process. Otherwise, continue.

Step 4 Calculate a positive step size.

Step 5 Calculate the new design based on the step size obtained in step 4.

Set k=k+1 and go to step 2.

It is a generally accepted fact that the correct formulation of a problem takes roughly 50% of the total effort needed to solve it. Many numerical methods for solving non-linear optimisation problem have been developed over the last several decades. Some are better than others and research in this area continues to develop still better techniques [4].

For the solution of the problem described above, the penalty function Davidon-Fletcher-Powell method [4] of unconstrained optimisation and two-point interpolation technique of one-dimensional minimisation has been employed. This method also is referred to as the Sequential Unconstrained Minimisation Technique or SUMT [4] in the literature. The basic idea of the penalty function approach is to define the composite function P in Eq. (7.66) in such a way that if there are constraint violations, a larger penalty gets added to the objective function. Based on the definition of penalty function provided in [4], Eq. (7.66) becomes:

$$\Phi(X, r^{(k)}) = f(X) + r^{(k)} \sum_{j=1}^{p} \frac{1}{g_i(X)} + \frac{1}{\sqrt{r^{(k)}}} \sum_{k=1}^{n} [h_k(X)]^2 \qquad (7.67)$$

It can be shown that as $r \to 0$, $X(r) \to X^{(*)}$ where $X(r)$ is the minimum of the transformed function and $X^{(*)}$ is a solution of the original constrained optimisation problem. The

convergence of the iterative method for the calculation of jet pump efficiency has been found to be satisfied.

7.6.3 Numerical Results and Discussion

To demonstrate the optimisation model developed in this section and illustrate the application of optimisation techniques to the jet pump design process, the example described in Section 7.5 has been solved by using the optimum design methodology presented above (Eqs. (7.40) to (7.65)) and Fortran coding. A flow-chart for this calculation is shown in Fig. 7.11. A program for optimising $\Phi(X,r)$ also is included in Appendix C. Two different sets of starting value of each design variables and the optimisation results are given in Table 7.2. The variation of controlling (penalty) parameter r and function $\Phi(X,r)$ with design variables in the optimisation process is provided in Tables 7.3 and C-1. It can be seen clearly that $\Phi(X,r)$ approaches $f(X)$ as $r \rightarrow 0$.

Table 7.2 Starting values and optimisation results

Design variable	Lower bound	Upper bound	First starting value	Optimum value (1)	Second starting value	Optimum value (2)
m	2	25	2.8	3.03	2.9	3.2
x	1	15	3.0	3.1	3.1	2.91
p_0 (kPag)	10	500	57	39.04	68	35.01
L_t/d_t	3	10	5.6	5.1	7.4	5.1
m_n	2	6	3	5.48	5	5.86
β (°)	10	60	30	10.00	49	10.1
θ (°)	1	4	3	3.91	5	4.22
m_d	2	6	3	2.09	3.3	2.0

As stated in Section 7.6.2, the fundamental ideal of using numerical methods to solve non-linear optimisation problems is to start with a reasonable estimate for the optimisation problem concerned. Objective and constraint functions and their derivatives are evaluated at this starting point. Based on these functions, the design is moved to a new point. This

process is continued until either optimal conditions or some other terminating criteria are satisfied. Hence, the final solution does not depend on starting values. Even using the values that are very close to the optimum solution as starting values, different possible solutions to the design problem will be searched and compared to find the optimal solution when implementing the computer program. However, different starting points may require different computing times to reach the optimal point. In reality, it is difficult to determine a reasonable estimate for a optimisation problem from a mathematical point of view. The example included in this section is used to illustrate and demonstrate the optimisation approach developed. It is reasonable to determine starting values based on the calculations presented in Section 7.5 for the same design problem.

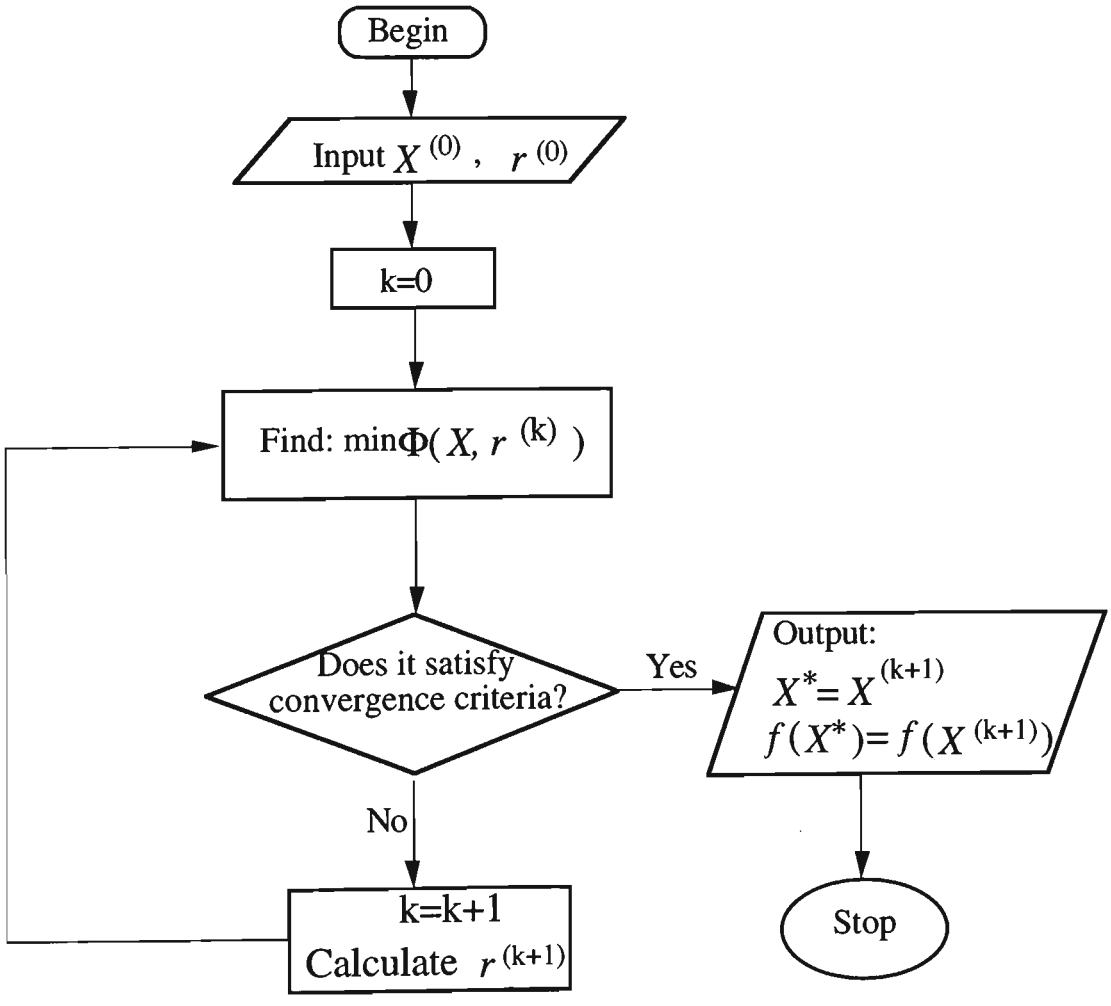

Fig. 7.11 Flow-chart to demonstrate the optimisation process

Table 7.3 provides the variation of objective function value, design variables and controlling (penalty) parameter in the optimisation process of using the first set of starting

values. For example, area ratio m starts from 2.8, changes into 2.98 after first iteration, and approaches 3.03 by a series iterations; the objective function value after first iteration is -0.846, reaches its minimum -0.917 after iteration process etc. It should be noted that for each iteration, all these design variables vary between their low and upper bounds given in Table 7.2 to find a combination of these variable that satisfy all constraints. A similar presentation for the second set of starting values in the optimisation process is included in Table C-1.

Table 7.3 Variation of objective function values with controlling parameter and design variables for first set of starting values

k	$-f(X)$	$\Phi(X,r)$	r	x	m	L_t/d_t	m_d	p_0	m_n	β	θ
1	-0.846	23.37	0.1	3.033	2.98	6.11	2.52	40.84	5.59	21.57	3.21
2	-0.856	3.99	0.02	3.035	2.99	6.11	2.44	40.40	5.59	19.31	3.32
3	-0.890	0.952	0.004	3.075	3.014	5.49	2.22	39.51	5.56	13.41	3.44
4	-0.909	-0.703	0.0008	3.096	3.025	5.18	2.11	39.19	5.50	11.26	3.65
5	-0.914	-0.871	0.00016	3.101	3.028	5.08	2.092	39.10	5.50	10.35	3.78
6	-0.916	-0.906	0.000032	3.103	3.030	5.04	2.088	39.07	5.49	10.22	3.89
7	-0.917	-0.914	0.0000064	3.104	3.031	5.01	2.086	39.05	5.48	10.04	3.91
8	-0.917	-0.916	0.0000012	3.104	3.031	5.01	2.086	39.04	5.48	10.02	3.91
9	-0.917	-0.917	0.00000003	3.104	3.031	5.01	2.086	39.04	5.48	10.01	3.91

Numerous experiments were undertaken by varying the motive pressure, area ratio, and mass flow rate ratio to demonstrate the optimisation results. It can be seen from Fig. 5.28 that the optimum area ratio is 2.86 for the five area ratios investigated. For this area ratio, the dependence of efficiency on the motive pressure and mass flow rate ratio is illustrated by Fig. 7.12. The optimum motive pressure and mass flow rate ratio are obtained from this figure. Based on the optimum motive pressure and mass flow rate ratio, an optimum pressure ratio is obtained from Fig. 5.23. The optimum parameters obtained from the optimisation techniques are compared in Table 7.4 with those obtained experimentally. It can be seen from Table 7.4 that the values of the determined optimum parameters are in good agreement with those investigated experimentally for optimum performance. As

shown in this table, further improvement on efficiency may be possible by varying the area ratio and the motive pressure. In this optimisation procedure, the theoretical model developed in Chapter 3 is used to determine the relationship between motive pressure, area ratio, solid to air mass flow rate ratio and pressure ratio. The good agreement between optimisation results and experimental data also support the validity of the performance prediction model developed in Chapter 3.

Table 7.4 Comparison between optimisation results and experimental data (plastic pellets)

Parameters	Optimisation results	Experimentally obtained optimum parameters
m_{opt}	3.03	2.86
h_{opt}	0.208	0.225
x_{opt}	3.1	2.9
p_{0opt}(kPag)	39.04	40
η (%)	92	90

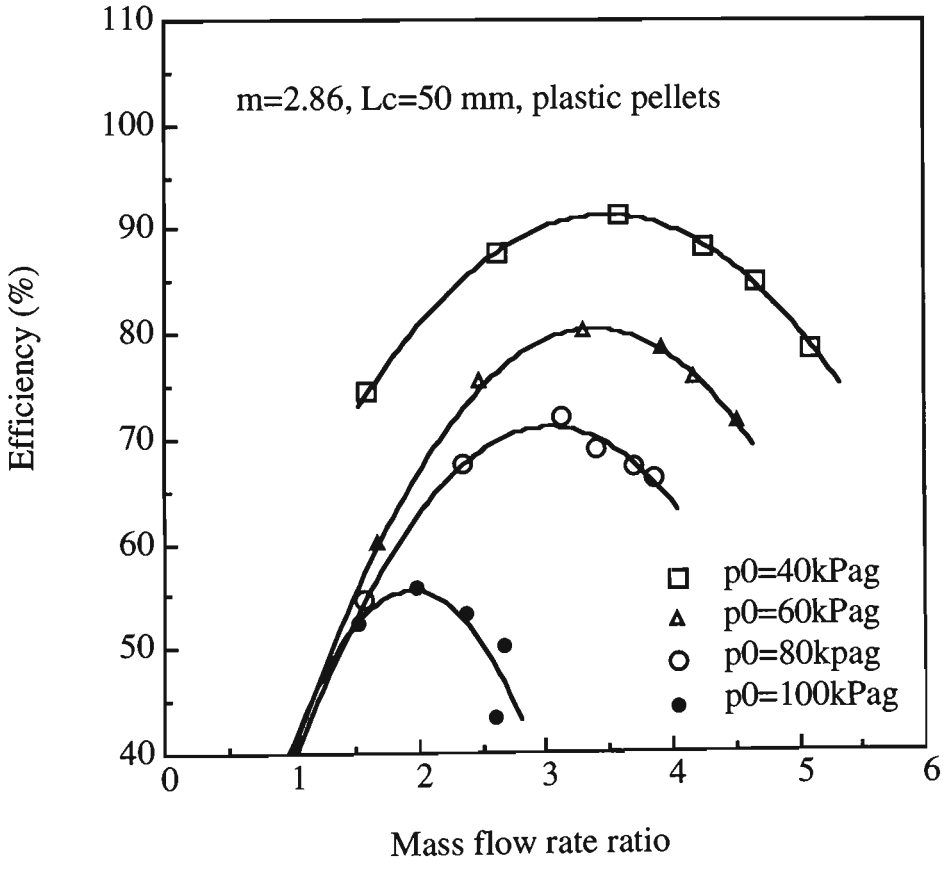

Fig. 7.12 Variation of efficiency with motive pressure and mass flow rate ratio

CHAPTER 8

CONCLUSIONS AND SUGGESTIONS FOR FURTHER WORK

8.1 Conclusions

This study was performed in order to develop a mathematical model for predicting the performance of air-jet pumps subjected to air-solids flow. For this purpose, a theoretical analysis was carried out. The modelling approach offers a meaningful and relatively inexpensive complementary alternative for examining air-jet pump performance. Numerous experiments on various central air-jet pump designs were undertaken to demonstrate the theoretical analysis and to investigate the influence of geometrical parameters and operating conditions on performance so that the optimum parameters can be obtained. Experimental data were compared with the results obtained from the performance prediction model. The performance prediction model developed in this work was found to provide results which agreed very well with experimental data.

The design procedure of central air-jet pumps based on the performance prediction model also was formulated for the convenience of practical design purpose. For the requirement of energy-effective design, optimal design parameters for a given application requirement have been introduced and correlated with experimental data. Optimisation techniques also have been used to obtain optimal design parameters. The optimisation results also agree well with the empirically determined optimal design parameters.

Considerable experiments also were carried out on a jet pump with an annular multi-hole ring nozzle to investigate the factors that influence jet pump characteristics, and to find the difference between this type of pump and central air-jet pump, so that the options to improve efficiency can be determined.

The theoretical analysis, experimental investigations, findings and numerical calculations of this research also lead to the following principal conclusions:

1. Performance Representation and Research Approach

- Air-jet pump performance, whether air-only or air-solids, can be represented by using the parameters defined in Section 3.2. Either dimensional or non-dimensional characteristic curves can be used to present performance graphically. Conversion between non-dimensional and dimensional characteristics can be made by using Eqs. (3.7) and (3.8).

- To evaluate the energy-effectiveness of a jet pump, efficiency defined by Eq. (3.9) for air-only condition and Eq. (3.11) for air-solids flow conditions was introduced. These definitions enable a comparison of air-jet pumps operating in different systems.

- As a result of the performance representation developed in this thesis, the influence of the conveying pipeline system on jet pump performance can be eliminated while investigating air-jet pump characteristics. However, in an air-jet pump conveying system, the complex influence of conveying pipeline must be considered by pipeline characteristics. The actual conveying rate is given by the intersection of the jet pump characteristic and pipeline characteristic curves. In this way, numerous research results available in the literature on air-solids flow through pipelines may be utilised.

2. Factors Influencing Central Air-Jet Pump Performance

Both air-only and air-solids central air-jet pump performance and efficiency depend on area ratio, nozzle-throat gap, motive pressure, suction mass flow rate, delivery pressure and hence, conveying distance. The clearly defined trends are:

- Nozzle geometry has a significant influence on the efficiency and performance of the jet pump for a given diameter of mixing section. This influence can be represented by area ratio. Employing small values of area ratio may obtain higher efficiency while using greater values of area ratio may achieve higher mass flow rate ratios. Decreasing area ratio may generate higher pressure ratios for a given mass flow rate ratio, while increasing area ratio may increase mass flow rate ratio for a given pressure ratio. Therefore, an optimum area ratio exists for a given operating condition.

- There is an optimum value of motive pressure for a given air-jet pump design. As motive pressure increases, pump pressure difference for a given suction mass flow rate increases, so do the shut-off vacuum and the suction mass flow rate for a given jet pump pressure difference. However, reducing the motive pressure may result in an increase in efficiency for a given jet pump geometry.

- The optimum value of the motive pressure increases with area ratio, and may be determined by using Eq. (7.19).

- The maximum mass flow rate ratio of a central air-jet pump for conveying bulk solids depends strongly on material properties (such as bulk density and particle density, et al.). For the materials listed in Table 4.3, the value of the maximum mass flow rate ratio reaches around 16 with m=23.84.

- A thorough investigation has been conducted to identify the optimum nozzle-throat gap for central air-jet pumps. Based on the results obtained in the present research, the optimum value of nozzle-throat gap for the air-jet pump subjected to both air-only and air-solids flow conditions is in the range $L_c = 1.5d_t$ to $2.1d_t$.

- There exists an optimum pressure ratio or mass flow rate ratio to maximise the efficiency for a given jet pump configuration (or an optimum motive pressure and jet

pump configuration for a given suction mass flow rate). The optimum pressure ratio may be determined by using Eq. (7.18).

- Employing small values of area ratio may obtain a higher shut-off vacuum while using greater values of area ratio may achieve higher mass flow rate ratios.

3. Factors Influencing Annular Multi-hole Air-Jet Pump Performance

- The area ratio of throat tube to nozzle exit area also has a significant influence in both air-only and air-solid pump performance for a given operating condition. Employing small values of area ratio may obtain higher efficiency while using greater values of area ratio may achieve higher mass flow rate ratios. An optimum area ratio exists for a given mass flow rate ratio;

- The optimum mixing section length represented by L_t/d_t is around 5.4 for the different nozzle configurations tested, based on the measurement of pressure distribution along the mixing section. It is possible to improve efficiency by using a diffuser at the end of mixing section;

- The maximum efficiency under air-only conditions obtained during the present tests is about 7% for an annular air-jet pump with m=36.8 (Nozzle No. 175). The maximum efficiency obtained during the tests on plastic pellets, is 16.5% for an air-jet pump with m=36.8 (Nozzle No. 175). The maximum mass flow rate of solid conveyed is 0.17 kg/s with an air consumption of 0.055 kg/s and motive pressure of 400 kPag. An improvement in efficiency is possible by modifying the geometry of the air-jet pump (reducing area ratio) and optimising the characteristic performance for specified designs and given operating conditions (choosing motive pressure).

- The shut-off vacuum is dependent on jet pump design, motive and delivery pressure. Reducing the area ratio may result in an increase in shut-off vacuum for given motive and delivery pressures.

- Both air-only and air-solid performance and efficiency depend mainly on motive pressure for a given air-jet pump configuration. Hence, there is an optimum design of air-jet pump for a given operating condition, and an optimum value of motive pressure for a given air-jet pump design. In contrast with central air-jet pumps, for annular jet pump, increasing motive pressure may increase conveying rate and improve efficiency, and vice versa;

4. Performance Prediction and Design Strategy Formulation

- A mathematical model to predict air-solid jet pump performance has been formulated based on fundamental principles of fluid dynamics and solved numerically. Analytical and computational results obtained using the proposed model for five different central jet pump geometries under various operating conditions to convey a particular product show good agreement with experimental data, as shown in Figs. 3.8 to 3.13.

- Theoretical predictions also agree well with the experimental results of Dawson et al. [28], as shown in Fig. 3.14.

- Whether under subsonic or sonic flow conditions, the motive mass flow rate through both convergent nozzle and annular multi-hole ring nozzle can be well predicted by using Eqs. (3.20) and (3.21). In these equations, the discharge coefficient may take the same value as that for incompressible flow under the same value of Reynolds number. The discharge coefficient for incompressible flow is widely available in engineering literature.

- A design procedure based on the proposed analytical model has been formulated for designing effective and reliable air-jet pump conveying systems (Section 7.3) by establishing optimum parameters for a given application situation.

5. Comparison between Air-only and Air-Solids Performance

- Air-solid performance trends appear to be similar to air-only performance for both central and annular jet pumps (e.g. maximum exit pressure, the influence of area ratio, motive pressure, delivery pressure and pressure distribution along the mixing section etc.).

6. Comparison between Central and Annular Air-Jet Pumps

- Based on the assessment of either efficiency over the range of back pressures considered or conveying mass flow rate discharged under atmospheric condition for the same pipeline system, the central air-jet pump is much more energy-efficient than the annular air-jet pump.

- Annular air-jet pumps have advantages over central air-jet pumps in the aspects of reducing wear and diminishing particle damage due to non-intersection helix flow pattern in the mixing tube. Also, annular air-jet pumps are preferable in some special applications, such as feeding abrasive materials and/or the feed stock containing lumps.

7. Optimum Design of Air-Jet Pump Conveying System

- Proper sizing of the jet pump geometry and selection of operating parameters play a vital role in the design of effective air-jet pump and associated conveying system.

- A mathematical model (Eqs. (7.40) to (7.65))for optimal design of air-jet pump conveying system has been formulated by using optimisation techniques, based on the performance prediction model developed in Chapter 3. A computer program has been developed for solving this model. This approach unifies the jet pump design methodology. The optimisation results show good agreement with those optimum parameters obtained from experiments. Hence, it is preferred to apply this approach in the design of an air-jet pump conveying system.

- Based on the research progress presented in this thesis, it is possible to develop a commercial software for designing air-jet pumps to convey bulk solids pneumatically in pipeline.

8.2 Suggestions for Further Work

To understand completely air-solids flow behaviour in a jet pump and the interaction between air-solids flow and jet pump geometry, for the purpose of designing and operating jet pump systems more efficiently and reliably, further investigations are suggested below:

1. Velocity field measurements by using say LDA techniques for both central and annular jet pumps operating under air-solids flow conditions are necessary in order to understand the behaviour of particles, especially for annular air-jet pump with multi-hole ring nozzle.

2. Numerical simulation of velocity and pressure fields in the jet pump operating under air-solids flow conditions may provide alternatives for improving jet pump design and performance. Also, this approach may be helpful for better understanding of the interaction between air and particles in air-solids two phase flow. Some commercial computer codes may be modified for the two-dimensional modelling work involved.

3. The analysis approach applied to central air-jet pumps in this study may be extended to annular air-jet pumps with multi-hole ring nozzle.

4. The design procedure developed for central air-jet pumps may be extended to annular air jet pumps. Furthermore, the optimisation model and the solution procedure presented for central air-jet pumps may be applied to the design of annular air-jet pumps with a few modifications such as constraints, the relationship between h and x etc.

5. More products with different physical characteristics (especially powders) need to be tested to increase the data base of experimental data and to demonstrate further the various analysis and design procedures.

The air-solids jet pump has never achieved the acceptance of other feeding devices in pneumatic conveying applications. For this to occur, application design must be simplified and stereo-typed to an extent which has not been possible in an atmosphere of inadequate understanding. It is hoped and expected that the present research and development will provide the remedy.

REFERENCES

1. Aggarwal, D.K., Gupta, R.S. and Vasandani, V.P., Optimum design of jet pump, Journal of the Institution of Engineers (India), Vol. 66, Pt. Me6, 1986, pp. 139-134.

2. Antonovich, S.A., Design of jet pumps (ejectors), Energomashinostroenie, No. 9, 1958, pp. 8-13.

3. Arbel, S. and Manheimer-Timnat, Y., The performance of multi-nozzle ejectors, Israel J. Tech., Vol. 12, No. 3-4, 1974, pp. 212-220.

4. Arora, J.S., Introduction to optimum design, McGraw-Hill, Inc., U.S.A, 1989, pp. 337-340.

5. Arkadov, Y.K., A gas ejector with a helical nozzle, Fluid Mechanics - Soviet Research, Vol. 4, No. 2, 1975, pp 154-63.

6. Atlas Copco Air Compendium, Atlas Copco AB, Stockholm, Sweden, 1975.

7. Barth, W., Chemie-Ing.-Techn., Vol. 30, 1958, p.171.

8. Bauer, B., Theoretical and experimental investigations on jet apparatus for compressible fluids (jet compressors), V.D.I. Forsch., 514, 1966.

9. Blevins, R.D., Applied fluid mechanics handbook, Von Nostrand, New York, 1986, pp. 89-94, 257-262.

10. Bohnet, M. and Wagenknecht, U., Investigations on flow conditions in gas/solid injectors, Ger. Chem. Eng., No. 1, 1978, pp. 298-304.

11. Bohnet, M., Aerodynamic calculation of gas/solid injectors, Pneumatech 1, International Conference on Pneumatic Conveying Technology, 3-5 May, 1982.

12. Bohnet, M., Design of gas-solids injectors, Chapter 30 of Handbook of Fluids in Motion, Edited by Nichocas, P. et al., Ann Arbor Science, 1983, pp. 785-805.

13. Bohnet, M., and Teifke, J., New results on the efficiency of energy transformation in gas/solid injectors, Reliable Flow of Particulate Solids Proceedings, Bergen, Norway, CHR Michelsen Institute, Dept. of Science & Technology, 20-22 August, 1985.

14. Bonnington, S.T., King, A.L. and Hemmings, J.A.G., Jet pumps and ejectors: a state of art, review and bibliography, 2nd edition, Cranfield, U. K., BHRA Fluid Engineering, 1976.

15. Bonnington, S.T., Jet pumps and ejectors: a state of art, review and bibliography, 1st edition, Cranfield, U. K., BHRA Fluid Engineering, 1972.

16. Bonnington, S.T. and Watts, D., The state of the art of jet pump design, BHRA Report TN830, November, 1964.

17. Bruno, A.I., Pump units for cyclone elevator, U. S. Patent 3857651, 1974.

18. Cairns, J.R. and Na, T.Y., Optimum design of water jet pumps, Transactions of ASME, Vol. 92, Series D, No. 1, March 1970, pp. 11-20.

19. Cement jet pumps, Type TsSND-40, Gidrotekh. Stroit., No. 6, 1974, pp. 60-61 (In Russian).

20. Chellappan, S. and Ramaiyan, G., Experimental study of design parameters of gas/solid injector feeder, Powder Technology, Vol. 48, 1986, pp. 141-144.

21. Cheers, F., Development of an air ejector, National Research Council of Canada, Report No. NF-31. 1956, pp. 1-11.

22. Croft, D.R. and Lilley, D.G., Jet pump design and performance analysis, A.I.A.A. Paper, pp. 176-183, 1976.

23. Cunningham, R.G., Hansen, A.G. and Na, T.Y., Jet pump cavitation, Transaction of ASME, Vol. 92, Series D, No. 3, September 1970, pp. 483-494.

24. Cunningham, R.G., Liquid jet pump modelling: effects of axial dimensions on theory-experiment agreement, Proc. 2nd Symposium on jet pumps & ejectors and gas lift techniques, BHRA, March 24-26, 1975, Paper F1, pp. F-1 to F-15.

25. Daugherty, R. L., Franzini, J. B. and Finnemore, E. J., Fluid Mechanics with Engineering Applications, Metric Edition, McGraw-Hill Co., 1989, pp. 410-413.

26. Davies, C. E., Dawson, S. G. B and Hartley, M., Venturi feeders for pneumatic conveying: Characteristics of different feeder types, CHEMECA '90, Australian Chemical Engineering Conference, 27-30 August, 1990, Auckland, New Zealand.

27. Davis, G.S., Mitra, A.K. and Roy, A.M., Momentum transfer studies in ejectors, Correlation for three-phase (air-liquid-solid) systems, Ind. Engng. Chem. Vol. 6, No. 3, July, 1967, pp. 299-302.

28. Dawson, S. G. B, Harris B. J. and Davies, C. E., Characteristics of venturi feeders for powders, CHEMECA '89, Australian Chemical Engineering Conference, 23-25 August, 1989, Broadbeach, QLD.

29. Debreczeni, E. *et al.* , Hydraulic transport systems in the mining industry using jet slurry pumps, Hydrotransport 6, Vol. 1, paper G-3, 1979, pp. 315-328.

30. Dixon, G. Plastic pneumatic conveying and bulk storage, Edited by Butters, G., Applied Science Publishers, London, 1981, pp. 20-129.

31. Elrod, H.G., The theory of ejectors, J. Appl. Mech., Vol. 12, No. 3, 1945, pp. 170 - 174.

32. Fabris, G. and Fejer, A.A., Confined mixing of multiple jets, Transaction of ASME, Vol. 96, Series I, No. 2, 1974, pp. 92-6.

33. Fish, G.F, The Solid-handling jet pump, Brit. Chem. Engng. & Process Technology, Vol. 17, No. 5, May, 1972, pp. 423-427.

34. Flugel, G., The design of jet pumps, V.D.I. Forsch, Vol. 395, 1939, pp. 1-21 (In German).

35. Fluid mover: pumps, compressors, fans and blowers, Edited by Jay Matley, McGraw-Hill, New York, 1979.

36. Fox, L. S., Venturi eductors in pneumatic conveying systems - Particularly for reducing rotary valve wear, Powder and Bulk Solids Handling and Processing, Rosemount, Illinois, 1984, Proc. Tech. Prog., pp. 544 -556.

37. Fox, L. S., Campbell, K. and Irwin, K., Fox venturi eductors replace airlocks in highly abrasive furnace slag application, Powder Handling and Processing, Vol. 4, No. 3, September 1992, pp. 326-327.

38. Fox Solids Conveying Eductors, Bulletin 301A, Nu-Con A4.

39. Fuji, S., Gomi, M. and Sugahara, N., A study on the large scale air-ejector, National Aerospace Lab. (Japan) Report No. NAL TR-109, 1966.

40. Gibbons, E.J., Design a venturi feeder for dry bulk storage, Chemical Engineering, 1961, pp. 158-160.

41. Gilbert, G.B. and Hill, P.G., Analysis and testing of two dimensional slot nozzle ejectors with variable area mixing sections, Proc. 2nd Symp. on Jet Pumps & Ejectors and Gas Lift Techniques BHRA Fluid Engineering, Cambridge, U.K., 1975, Paper D3, pp. D3-45 to D3-64.

42. Gudzenko, N.V., Zaichenka, M.E. and Lartin, L., Jet pump, U. S. Patent 4028009, 1977.

43. Hansen, A.G. and Kinnnavy, R., The design of water-jet pumps, Part 1- Experimental determination of optimum design parameters, ASME Paper 65-WA/FE-31, November 1965, pp. 1-8.

44. Hedges, K.R. and Hill, P.G., Compressible flow ejectors, Part 2 - flow field measurements and analysis, ASME Vol. 96, Series I, J. Fluids Engineering, No. 3, 1974, pp. 282-88.

45. Helmbold, H.B., Comparison of mixing process in subsonic jet pumps, J. Aeron. Sci., Vol. 22, No. 6, 1955, pp. 435-437.

46. Hill, B. J., Two dimensional analysis of flow in jet pumps, ASCE, J. Hydraulics Div., Vol. 99, 1973, pp. 1009-1026.

47. Howell, R.R., Experimental operating performance of a single-stage annular air-ejector, NASA Tech. Note D-23, 1959, pp. 1-35.

48. Ichiro, W., Experimental investigations concerning pneumatic ejectors, with special reference to the effect of dimensional parameters on performance characteristics, Proc. of Symposium on Jet Pumps and Ejectors, London, BHRA, November 1972, pp. 97-120.

49. Jumpeter, A.M., Jet pumps, Section 4 of Pump handbook, Edited by Karassik, I.J. *et al.*, McGraw-Hill Inc., 1976, pp. 4.1 to 4.25.

50. Kalmykov, I.I. and Mosin, I.I., Effect of certain geometrical parameters on the operation of an ejector with a conical mixing chamber, Aviats. Tekhn., vol 14, No. 1, 1971, pp. 104-12.

51. Kalyanraman, R. and Miltra, A.K., Performance studies in a multi-hole nozzle ejector, Proc. 5th Nat. Conf. on Fluid Mechanics & Fluid Power (Nat. Soc. of Fluid Mechanics & Fluid Power, India), Bombay, 1974, pp. B83-87.

52. Karassik, I.J. and Carter, R., Centrifugal pumps, McGraw-Hill Inc., 1960, pp 318-323.

53. Kastner, L.J. and McGarry, J.B., Mass flow and the mixing process in low velocity air ejectors, Engineer, Vol. 210, No. 5453, 1960, pp. 190-192.

54. Kastner, L.J. and Spooner, J.R., An investigation of the performance and design of the air ejector employing low-pressure air as the driving fluid, Proc. I. Mech. E., Vol. 162, No. 2, 1950, pp. 149-66.

55. Keenan, J.H. and Neuman, E.P., A simple air ejector, J. Appl. Mech., Vol. 9, No. 2, 1942, pp. A-75-81.

56. Keenan, J.H., Neuman, E.P. and Lustwerk, F., An investigation of ejector design by analysis and experiment, J. Appl. Mech., Vol. 17, No. 3, 1950, pp. 299-309.

57. Kentfield, J.A.C. and Barnes, R.W. The prediction of the optimum performance of ejectors, Heat & Fluid flow, Vol. 2, No. 2, 1972, pp. 115-125.

58. Keys S. and Chambers, A. J., Pneumatic conveying of copper strip, Bulk Solids Handling, Vol. 10, No. 2, May 1990, pp. 155-158.

59. Khuntia, S. and Murty, J.S., Integrated slurry mixing and feeding system using jet pump for hydraulic transportation of solid, The 3rd International symposium on liquid-solid flows, FED-Vol. 75, 1988, pp. 211-216.

60. Kmiec, A., An analytical study of flows in gas/solid injectors, Pneumatech 3, International Conference on Pneumatic Conveying Technology, 24-26 March, 1987, pp. 169-197.

61. Kotwal, D.C., Reddy, Y.R. and Kar, S., Mixing of two concentric jets, Journal of the Hydraulic Division, ASCE, Vol. 94, No. HY2, March, 1968, pp. 505-514.

62. Kudirka, A.A. and Gluntz, D.M., Convention on pumps for nuclear power plants, I. Mech. E., Paper C96/74, April 22-25, 1974, pp. 75-82.

63. Lewis, R.A., An experimental analysis of a jet inducer with multiple nozzles calibrated in liquid mercury and in water, Symposium on Cavitation in Fluid Machinery, ASME, November, 1965, pp. 109-19.

64. Lorenz, H., Technische hydromechanik, R. Oldenburg, Berlin and Munich, Germany, 1910.

65. Lu, H. Theory and application of jet pumps technology, Water Resources and Electrical Power Pres, Beijing, P. R. China (in Chinese), 1987, pp. 206-214.

66. Mason, J.S., Mills, D., Reed, A.R. and Woodcock, C.R., Pneumatic handling of Bulk Materials, Short Course Notes, Thames Polytechnic, London, U.K., 1983, Session A7.

67. Michell, J.W., Design parameters for subsonic air-air ejectors, Stanford Univ., Teach. Report, AD 212 391, 1958, pp. 1-63.

68. Mitra, A.K. and Roy, A.N., Studies on the performance of ejectors: correlation for air-air systems, Indian J. of Technol., Vol. 2, No. 9, 1964, pp. 315-316.

69. Mueller, N.H.G., Water jet pumps, Proc. of ASCE, Vol. 90, No. HY3, May 1964, pp. 83-111.

70. Nazarov, V. D., Mamontov, V. I., Snitivker, G. A., Chasnyk S. M. and Panin, O. K., System for pneumatic transport of dust, Translated from Metallurgy, No. 11, November, 1989, Plenum Publishing Corporation, 1990, pp. 25-26.

71. Neve, R.S., Computational fluid dynamics analysis of diffuser performance in gas-powered jet pumps, Int. J. Heat and Fluid Flow, Vol. 14, No. 4, 1993, pp. 401-407.

72. Paulson, C.J. and Philipp, D.H., Feeding solids into gas streams, Chemical Engineering, 1972, pp 94-96.

73. Pittman, A. N. and Mason, J. S., Pneumatic conveying of bulk solids using a vacuum aerated feed nozzle, Powder & Bulk Solids Conference, Rosemont, Illinois, May 13-15, 1986, Proceedings, pp. 188-202.

74. Pneumatic conveying equipment, Renmin Jiaotong Press, Beijing, P. R. China, 1974.

75. Pogorelov, V. I., Theory of ejectors designed for transporting tows, Machines and Apparatus, Translated from Khimicheskie Volokna, No. 1, 1990, pp. 39-42.

76. Rankine, J.M., On the mathematical theory of combined streams, Royal Soc., London, England, Vol. 19, 1870, p. 90.

77. Reddy, Y.R. and Kar, S., Theory and performance of water jet pumps, Journal of Hydraulic Division, ASCE, Vol. 94, No. HY5, 1968, pp. 1261-1281.

78. Anon, Removing flyash with air eductors, Power, Vol. 119, No. 8, 1975, p. 49.

79. Salam, T. F. and Gibbs, B. M., Solid circulation between fluidised beds using jet pumps, Powder Technology, Vol. 52, 1987, pp. 107-116.

80. Salam, T.F. and Glbbs, B.M., Gas and solid discharge from a fluidised bed using jet pump, Powder Technology, Vol. 50, 1987, pp. 111-120.

81. Sanger, N. L, Non-cavitation and cavitation performance of two low-area-ratio water jet pumps with throat lengths of 5.66 diameters, N. A. S. A. Tech. Note TN-D-4759, August, 1969, pp. 1-34.

82. Sanger, N. L, Non-cavitation and cavitation performance of two low-area-ratio water jet pumps having throat lengths of 7.25 diameters, N. A. S. A. Tech. Note TN-D-4445, March, 1968, pp. 1-60.

83. Sanger, N. L., An experimental investigation of several low-area ratio water jet pumps, ASME, J. Basic Eng., Vol. 92, 1970, pp. 11-20.

84. Schmitt, H., Diversity of jet pumps and ejectors techniques, Proc. of the 2nd Symposium on jet pumps & ejectors and gas lift techniques, Organised by BHRA, 1975, Paper A4.

85. Schulz, F., Abhandlungen des Dokumentationszentrums fur Technik und Wirtschaft, No. 3, 2nd ed. Vienna, 1952 (in German).

86. Segler, G., Pneumatic grain handling, Braunschweig, Germany, 1951, pp. 75-150.

87. Shimizu, Y., Nakamura, S., Kuzuhara, S and Kurata, S., Studies of the configuration and performance of annular type jet pumps, Journal of Fluids

Engineering, Transactions of the ASME, Vol. 109, No. 3, September 1987, pp. 205-212.

88. Shook, C.A. and Roco, M.C., Slurry flow: principles and practice, Butterworth-Heinemann, Reed publishing Inc. USA, 1991, pp. 9-10.

89. Soo, S.L., A venturi injector for large mass flow ratios of solids to air, Powder & Bulk Solids Conference, Rosemont, USA, May 7-9, 1985, Proceedings, pp. 669-670.

90. Stepanoff, A.J., Centrifugal and axial flow pumps, John Wiley & Sons, Inc., 1967, pp 402-424.

91. Takashima, Y., The maximum performance and design of ejectors for handling various gases, Chem. Engng. (Tokyo), Vol. 19, No. 9, 1955, pp. 446-456.

92. Third, A.D., The air ejector, J. Royal Tech. Coll., Vol. 1, No. 4, 1927, pp. 84-103.

93. Thomson, J., On a jet pump or apparatus for drawing up water by the power of a jet, Report, British Assoc., London, England, 1852, p. 130.

94. Wakefield, A.W., Practical solids-handling jet pumps, Proc. of the first symposium on jet pumps and ejectors, BHRA, London, 1972, pp. 183-202.

95. Wakefield, A.W., Jet Pumps, Chapter 18 of Slurry handling: design of solid-liquid systems, Edited by Brown, N.P. and Heywood, N.I., Elsevier Applied Science, London, 1991, pp. 353-376.

96. Wang, D., An experimental study of the influence of structural factors on the performance of liquid jet pumps, Proceedings of the 3rd National Conference on Jet pumps & Ejectors and Jetting Technology, December 1989, Organized by the

Fluid Engineering Institution of Chinese Mechanical Engineering Society (In Chinese).

97. Wang, D., An experimental investigation of the performance of adjustable liquid jet pumps, Proceedings of 3rd National Conference on Jet pumps & Ejectors and Jetting Technology, December 1989, Organized by the Fluid Engineering Institution of Chinese Mechanical Engineering Society (In Chinese)

98. Wang, D., The characteristics prediction and design method of proportioning jet pumps, Journal of Irrigation, Drainage and Hydro-power, Vol. 15, No. 9, 1989 (In Chinese).

99. Wang, D. and Wypych, P.W., Water-only performance of proportioning jet pump for hydraulic transportation of solids, Powder Technology, Vol. 84, No. 1 1995, pp. 56-64.

100. Weber, M., Correlation analysis in the design of pneumatic transport plant, Bulk Solids Handling, Vol. 2, 1982, pp. 231-233.

101. Westway, S.F., An investigation into the performance of venturi eductors for the transport of solids particles in pipelines, ME Thesis, Thames Polytechnic, 1987.

102. Westaway, S. F., Woodcock, C. R., Malso, J.S. and Fox, L., Pneumatech 3, Channel Island, U. K., 1987, pp. 183-197.

103. Whitaker, R., An experimental study into cold air ejector mixing duct losses for computerised design purposes, Proc. 2nd Symp. on Jet Pumps & Ejectors and Gas Lift Techniques (BHRA Fluid Engineering), Cambridge, U.K., 1975, Paper D2, pp. D2-25 to D2-44.

104. Wood, S.A. and Bailey, A., Horizontal carriage of granular material by a injector-driven air stream, Proc. I. Mech. E., 142, 1939, p149.

105. Wypych, P.W. and Arnold, P.C., A standardised-test procedure for pneumatic conveying design, Bulk Solids Handling, Vol. 5, No. 4, 1985, pp. 755-763

106. Wypych, P.W. and Arnold, P.C., On improving scale-up procedures for pneumatic conveying design, Powder Technology, Vol. 50, 1987, pp. 281-294

107. Ushimaru, K., Bernstein, S. and Crowe, C.T., Design and application of an advanced slurry jet pump, Presented at the winter annular meeting of the ASME, Fluids Engineering Division, FED Vol. 31, November 17-22, 1985, pp. 75-83.

108. van den Hooff, J.J., A new conveying ejector for dry solids, Bulk Solids Handling, Vol. 8, No. 1, 1988, p. 85.

109. van der Lingen, T.W., A jet pump design theory, Tans. ASME, Vol. 82, Series D, No. 4, 1960, pp. 947-960.

110. Vyas, B.D. and Kar, S., Standardisation of water jet pumps, Symposium on Jet Pumps and Ejectors (BHRA Fluid Engineering), Proceedings, 1972, pp. 155-170.

111. Grupping, A.W., Coppes, J.L.R. and Groot, J.G., Fundamentals of oil-well jet pumping, SPE Production Engineering, Feb. 1988, pp. 9-14.

112. Hatzlavramldls, D.T., Modelling and design of jet pumps, SPE Production Engineering, Nov. 1991, pp. 413-419.

113. Kroll, A.E., The design of jet pumps, Chem. Engng. Progr., Vol. 1, No. 2, 1947, pp. 21-24.

114. Watson, F.R.B., The production of a vacuum in an air tank by means of a steam jet, Proceedings of the Institution of Mechanical Engineers, 124, 1933, pp. 231-264.

115. Neve. R.S., The performance and modelling of liquid jet gas jet pumps, Int. J. Heat Fluid Flow, Vol. 9, No. 2, 1988, pp. 156-164.

116. Neve. R.S., Diffuser performance in two-phase jet pumps, Int. J. Heat Fluid Flow, Vol. 12, No. 2, 1991, pp. 267-272.

117. Owen, I., Abdul-Ghani, A. and Amini, A.M., Diffusing a homogenised two-phase flow, Int. J. Multiphase flow, Vol. 18, No. 4, 1992, pp. 531-540.

118. Engineering Sciences Data Unit, Ejectors and jet pumps: design and performance for compressible air flow (Data Item No. 84029), ESDU, International Ltd., London, 1988.

119. Engineering Sciences Data Unit, Ejectors and jet pumps: design and performance for compressible air flow (Data Item No. 88002), ESDU, International Ltd., London, 1988.

120. Vyas, B.D. and Kar, S., Study of entrainment and mixing process for an air to air jet ejector, Proc. 2nd Symp. on Jet Pumps & Ejectors and Gas Lift Techniques (BHRA Fluid Engineering), Cambridge, U.K., 1975, Paper C2, pp. C2-15 to C2-25.

121. Weber., M., StrÖmungs-FÖrdertechnik, Otto Krausskopf-Verlag, Gmbh, Mainz, 1974.

A Derivation of Some Equations in Chapter 3

Equation (3.41)

For one dimensional compressible flow of real fluid, Euler Equation can be written as

$$dp/\rho + vdv + dE = 0 \tag{A-1}$$

where E stands for energy loss.

Integrating Eq. (A-1) for nozzle flow as shown in Fig. A-1 leads to

$$\int_0^n \frac{dp}{\rho} + \int_0^n v_o dv_o + \int_0^n dE = 0 \tag{A-2}$$

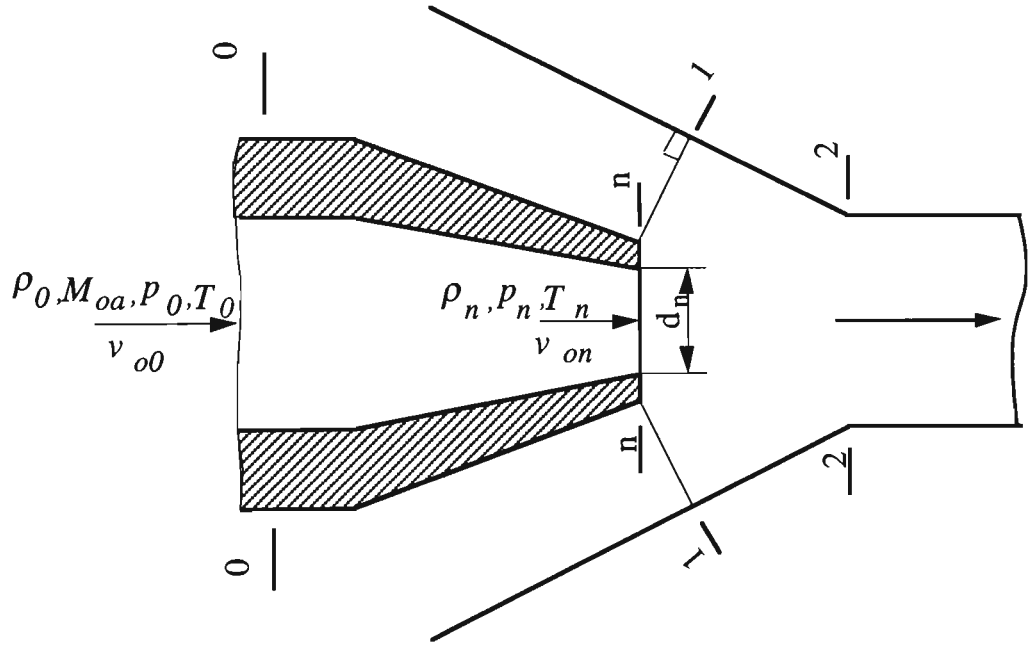

Fig. A-1 Nozzle section details

The equation of state for an ideal gas is:

$$\rho = \frac{p}{RT} \tag{A-3}$$

For isotheral compressible flow, $T_0 = T_n$. Substituting Eq. (A-3) for ρ in Eq. (A-2) and integrating Eq. (A-2) give

$$RT_n \ln(p_0/p_n) = \frac{v_{on}^2 - v_{o0}^2}{2} + \int_0^n dE \tag{A-4}$$

Considering $RT_n = p_n/\rho_n$, Eq. (A-4) can be rearranged as:

$$p_n \ln(p_0/p_n) = \rho_n \frac{v_{on}^2 - v_{o0}^2}{2} + \rho_n \int_0^n dE \tag{A-5}$$

Note that $v_{on} = v_{o1}$, $\rho_n = \rho_{o1}$ and for subsonic flow, $p_n = p_1$.

Letting $\rho_n \int_0^n dE_{on} = \frac{k_{01}\rho_{o1}v_{o1}^2}{2}$, Eq. (3.41) can be obtained by considering $v_{o0} = 0$.

Equations (3.42) and (3.43)

During air-jet pump operation, solid particles flow into the suction chamber of the pump through sections 4-4 and 1-1 under a pressure difference between these two sections (see Fig. A-2). For a properly designed pump, solids move very slowly into the suction chamber which is full of solids. Also the pressure variation is not obvious. Hence, the secondary flow stream through the suction port is considered as incompressible. The energy equation for the secondary flow stream between sections 4-4 and 1-1 shown in Fig. A-2 can be written as:

$$p_4 + \frac{\rho_{s4}v_{s4}^2}{2} = p_1 + \frac{\rho_{s1}v_{s1}^2}{2} + k_{41}\frac{\rho_{s1}v_{s1}^2}{2} \tag{A-6}$$

Considering the definition of $\overline{p_4} = p_4 + \frac{\rho_{s4}v_{s4}^2}{2}$, Eq. (A-6) can be rearranged as:

$$\overline{p_4} - p_1 = (1 + k_{41})\frac{\rho_{s1}v_{s1}^2}{2} \tag{A-7}$$

Which is Eq. (3.42).

Dividing both sides of Eq. (3.42) by z leads to

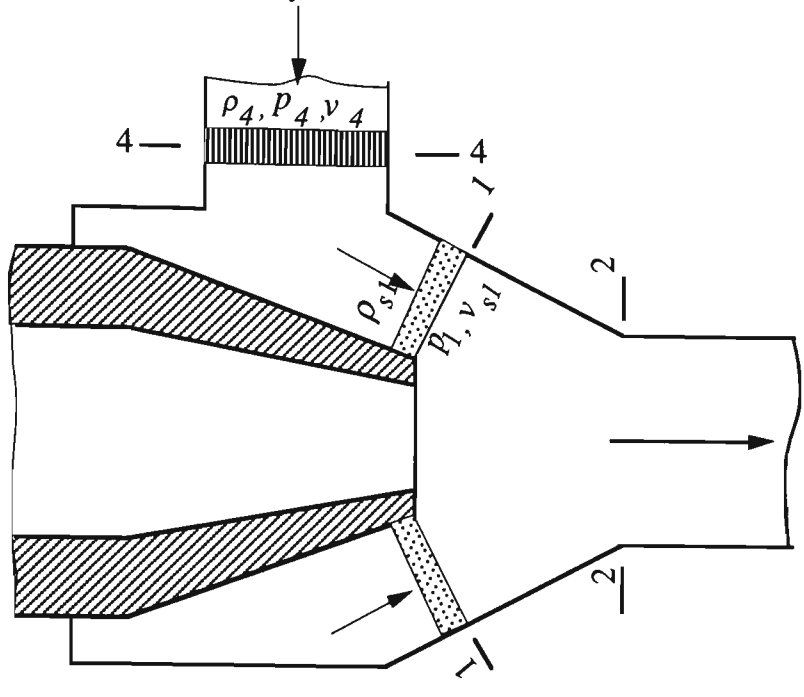

Fig. A-2 Suction or secondary flow details

$$\frac{\overline{p_4} - p_1}{z} = (1 + k_{41}) \frac{\rho_{s1} v_{s1}^2}{\rho_{o1} v_{o1}^2} \tag{A-8}$$

However:

$$v_{s1} = Q_{s1}/A_{s1};\ v_{o1} = Q_{o1}/A_n;\ A_{s1} = \frac{A_3 - A_n}{C};\ Q_{s1} = Q_{sa}\frac{p_4}{p_1} + Q_{sp}$$

Hence, $$\frac{v_{s1}}{v_{o1}} = \left(q_p + q_a \frac{p_4}{p_1}\right)\frac{C}{m-1} \tag{A-9}$$

Eq. (3-43) is obtained by substituting Eq. (A-9) for v_{s1}/v_{o1} into Eq. (A-8).

Equation (3.44)

Suction area ratio is defined as the ratio of area occupied by secondary flow at section 1 - 1 to the area of secondary flow at section 2 -2. That is:

$$C = \frac{A_2 - A_n}{A_{s1}} \tag{A-10}$$

From Fig. A-3, the cross-sectional area of secondary flow at section 1-1 can be expressed by:

$$A_{s1} = 2\pi\left(\frac{d_w}{2} + \frac{d_1' - d_w}{4}\cos^2\beta\right)\frac{d_1' - d_w}{2}\cos\beta \tag{A-11}$$

From Fig. A-3, it can be seen that

$$d_1' = d_3 + 2L_c\tan\beta \tag{A-12}$$

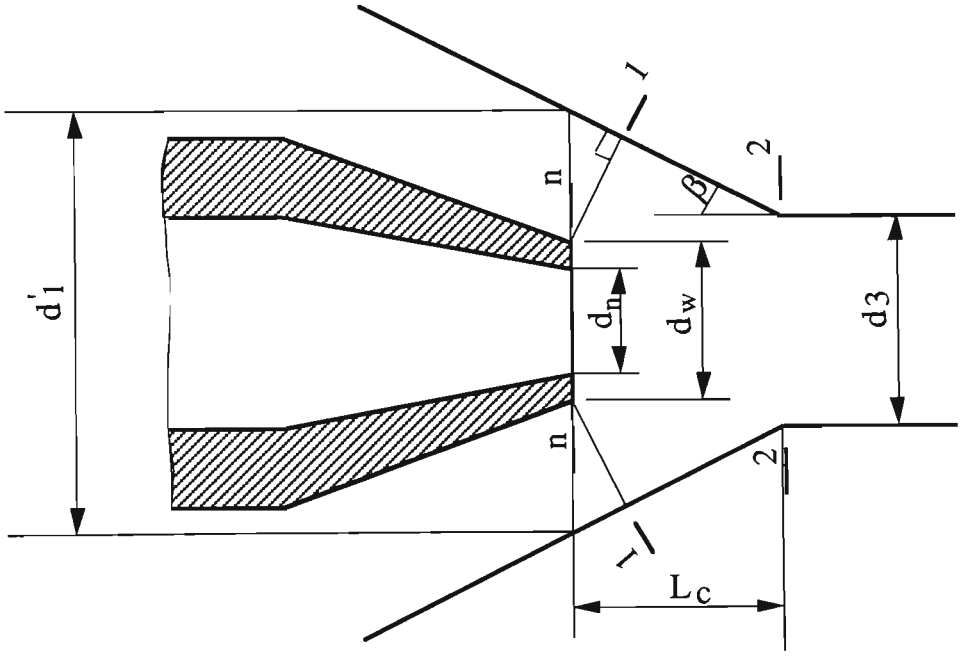

Fig. A-3 Schematic diagram for calculating suction area ratio

Substituting Eq. (A-12) into Eq. (A-11) leads to

$$A_{s1} = \frac{\pi}{4}d_n^2\left(\sqrt{m} + L_c\tan\beta - \frac{d_w}{d_n}\right)\cos\beta\left[2\frac{d_w}{d_n} + \left(\sqrt{m} + \frac{2L_c}{d_n}\tan\beta - \frac{d_w}{d_n}\right)\cos^2\beta\right] \tag{A-13}$$

$$A_3 = \pi d_3^2/4 \tag{A-14}$$

$$A_n = \pi d_n^2/4 \tag{A-15}$$

Eq. (3-44) is obtained by combining Eqs. (A-10), (A-13) - (A-15).

Equations (3.45) and (3.46)

As shown in Fig. A-4, considering the motive and secondary flow stream at sections 1-1 and 2-2 as a non-mixed two-component flow, the energy equation can be applied to each component flow between sections 1-1 and 2-2. That is,

For the motive flow stream,

$$\rho_{o1}Q_{o1}\left(p_1+\frac{\rho_{o1}v_{o1}^2}{2}\right)=\rho_{o1}Q_{o1}\left(p_2+\frac{\zeta_{o2}\rho_{o2}v_{o2}^2}{2}\right)+k_{12}\rho_{o1}Q_{o1}\frac{\zeta_{o2}\rho_{o2}v_{o2}^2}{2} \tag{A-16}$$

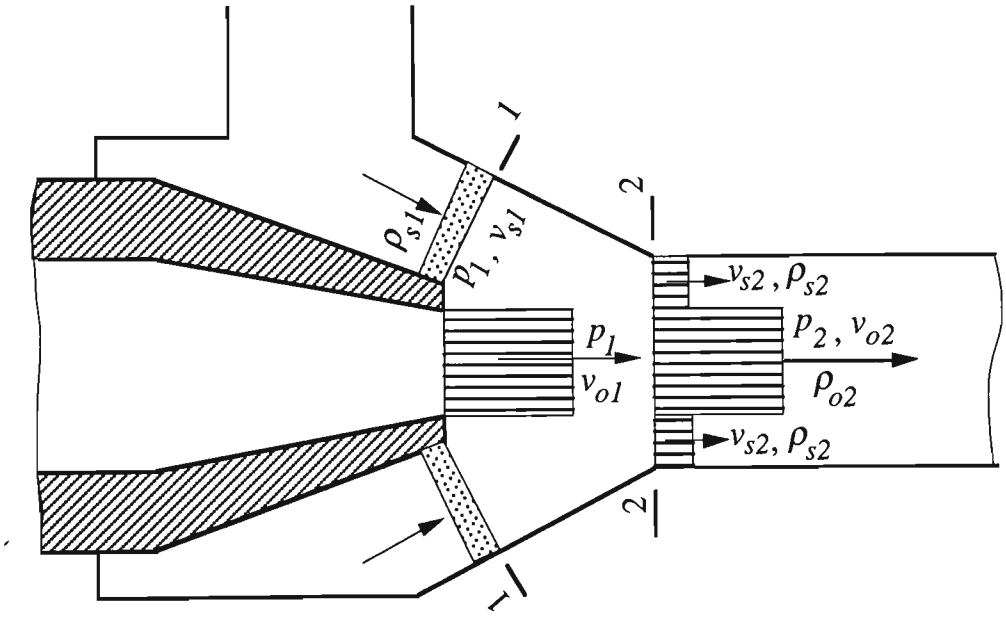

Fig. A-4

Similarly, for the stream of secondary flow,

$$\rho_{s1}Q_{s1}\left(p_1+\frac{\rho_{s1}v_{s1}^2}{2}\right)=\rho_{s1}Q_{s1}\left(p_2+\frac{\zeta_{s2}\rho_{s2}v_{s2}^2}{2}\right)+k_{12}\rho_{s1}Q_{s1}\frac{\zeta_{s2}\rho_{s2}v_{s2}^2}{2} \tag{A-17}$$

By adding Eq. (A-16) to Eq. (A-17), Eq. (3.45) is obtained.

Dividing both sides of Eq. (3.45) by $z=\rho_{o1}v_{o1}^2/2$ leads to

$$\frac{p_2-p_1}{z}=\frac{\left(\rho_{o1}Q_{o1}+\rho_{s1}Q_{s1}\frac{\rho_{s1}v_{s1}^2}{\rho_{o1}v_{o1}^2}\right)+(1+k_{12})\left(\rho_{o2}Q_{o2}\zeta_{o2}\frac{\rho_{o2}v_{o2}^2}{\rho_{o1}v_{o1}^2}+\rho_{s2}Q_{s2}\zeta_{s2}\frac{\rho_{s2}v_{s2}^2}{\rho_{o1}v_{o1}^2}\right)}{\rho_{o1}Q_{o1}+\rho_{s1}Q_{s1}} \tag{A-18}$$

By combining

$$x=\frac{\rho_{s1}Q_{s1}}{\rho_{o1}Q_{o1}},\ \rho_{o1}Q_{o1}=\rho_{o2}Q_{o2},\ \rho_{s1}Q_{s1}=\rho_{s2}Q_{s2},\ v_{s2}=Cv_{s1}\ \text{and}\ \frac{v_{s1}}{v_{o1}}=\left(q_a\frac{p_4}{p_1}+q_p\right)\frac{C}{m-1}$$

with Eq. (A-18) and introducing $\rho_{o2}v_{o2}^2=k_{o2}\rho_{o1}v_{o1}^2$ (assuming that the average motive jet velocity is maintained between sections 1-1 and 2-2, $k_{o2}=1$), Eq. (A-18) is rearranged as Eq. (3-46).

Equations (3.47) and (3.48)

As shown in Fig. (A-5), the momentum at section 2-2 is the sum of that of the motive and secondary flow stream, that is, $\rho_{s2}Q_{s2}v_{s2}\varsigma_{s2}+\rho_{o2}Q_{o2}v_{o2}\varsigma_{o2}$; the momentum at section 3-3 is expressed by $\rho_{m3}Q_3v_3\mu_3$, where ς_{s2} and μ_3 are coefficients introduced to take into account the effects of non-uniform velocity distribution across the section and velocity slip between air and solid particles on momentum. The momentum loss between sections 2-2 and 3-3 due to wall friction and mixing between two flow steams is considered as

$k_{23}\rho_{m3}Q_3v_3/2$. Hence, the momentum equation between sections 2-2 and 3-3 is written as

$$(p_3-p_2)A_2=\rho_{s2}Q_{s2}v_{s2}\varsigma_{s2}+\rho_{o2}Q_{o2}v_{o2}\varsigma_{o2}-\rho_{m3}Q_3v_3\left(\mu_3+\frac{k_{23}}{2}\right) \tag{3.47}$$

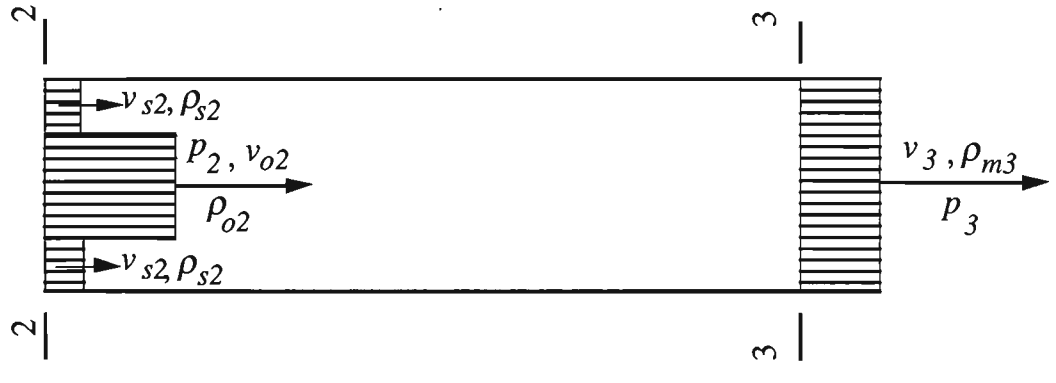

Fig. A-5 Throat tube details

Dividing both sides of Eq. (3.47) by $z=\rho_{o1}v_{o1}^2/2$ and inserting the following relations from mass conservation and the assumption of isothermal flow condition,

$$\frac{v_{s2}}{v_{o1}} = \frac{q_p + q_a \dfrac{p_4}{p_2}}{m-1} \qquad \frac{v_3}{v_{o1}} = \frac{q_a \dfrac{p_4}{p_3} + q_p + \dfrac{p_1}{p_3}}{m}$$

$$\frac{\rho_3}{\rho_{o1}} = \frac{1+x}{q_a \dfrac{p_4}{p_3} + \dfrac{p_1}{p_3} + q_p} \qquad \frac{\rho_{s2}}{\rho_{o1}} = \frac{x}{q_a \dfrac{p_4}{p_2} + q_p}$$

result in Eq. (3.48).

Equations (3.49) and (3.50)

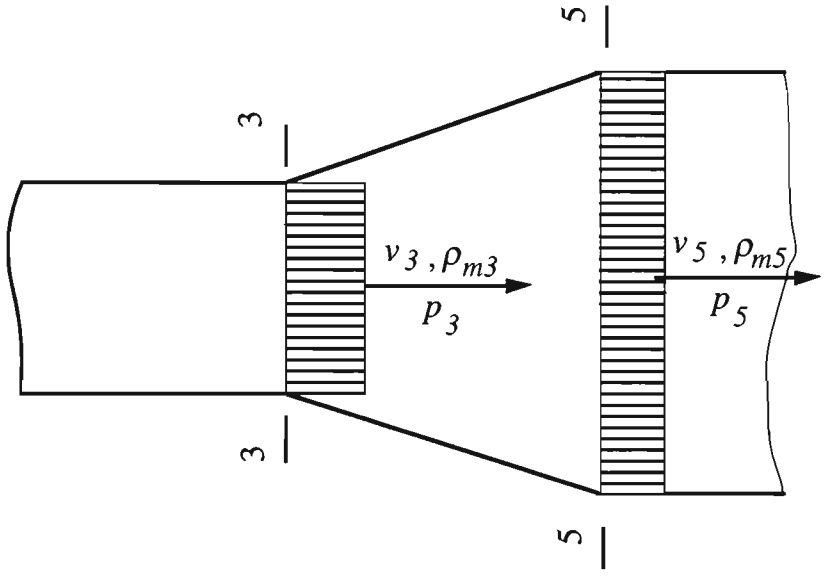

Fig. A-6 Diffuser details

Assuming that air and solid particles are well mixed before entering the diffuser, using the energy equation to such a flow condition as shown in Fig. A-6 results in

$$p_3 + \frac{\rho_{m3} v_3^2}{2} = p_5 + \frac{\rho_{m5} v_5^2}{2} + k_{35} \frac{\rho_{m3} v_3^2}{2} \qquad \text{(A-19)}$$

where $k_{35} \dfrac{\rho_{m3} v_3^2}{2}$ represents the energy loss in the diffuser due to wall friction, dispersion and separation. Noting that $\overline{p_5} = p_5 + \dfrac{\rho_{m5} v_5^2}{2}$, Eq. (A-19) is transformed into

$$\overline{p_5} - p_3 = (1 - k_{35}) \frac{\rho_{m3} v_3^2}{2} \qquad \text{(3.49)}$$

Dividing both sides of Eq. (3.47) by $z = \rho_{o1} v_{o1}^2 / 2$ and combining with $\frac{v_3}{v_{o1}} = \frac{q_a \frac{p_4}{p_3} + q_p + \frac{p_1}{p_3}}{m}$, Eq. (3.49) becomes Eq. (3.50).

Equation (3.51)

ψ is defined as the ratio of solid mass flow rate to air mass flow rate. Noting that

$M_p = \rho_p Q_p$ and $M_a = \rho_{o1} Q_{o1} + \rho_{a4} Q_{sa4}$, ψ is expressed as

$$\psi = \frac{\rho_p Q_p}{\rho_{o1} Q_{o1} + \rho_{a4} Q_{sa4}} \tag{A-20}$$

Dividing both numerator and denominator by $\rho_{o1} Q_{o1}$, Eq. (A-20) becomes

$$\psi = \left(\frac{\rho_p}{\rho_{o1}} \frac{Q_p}{Q_{o1}} \right) \Big/ \left(1 + \frac{\rho_a}{\rho_{o1}} \frac{Q_{sa}}{Q_{o1}} \right) \tag{A-21}$$

By noting $q_p = \frac{Q_p}{Q_{o1}}$, $q_a = \frac{Q_{sa4}}{Q_{o1}}$ and $\rho_{a4} = \rho_{o1} \frac{p_4}{p_1}$, Eq. (A-21) is rearranged as Eq. (3.51).

Equations (3.53) - (3.55)

Using the Darcy-Weisbach equation to represent the energy loss and introducing $\psi \lambda_p \frac{L_c}{d_n} \frac{\rho_{a2} v_{a2}^2}{2}$ [7] to account for the extra energy loss due to the air-solid mixture flow, the energy equations for the motive flow and the secondary streams between sections 1-1 and 2-2 can be expressed by

$$\rho_{o1} Q_{o1} \left(p_1 + \frac{\rho_{o1} v_{o1}^2}{2} \right) = \rho_{o1} Q_{o1} \left(p_2 + \frac{\varsigma_{o2} \rho_{o2} v_{o2}^2}{2} \right) + \left(\lambda_a + \psi \lambda_p \right) \frac{L_c}{d_n} \rho_{o1} Q_{o1} \frac{\rho_{a2} v_{a2}^2}{2} \tag{A-22}$$

and

$$\rho_{s1} Q_{s1} \left(p_1 + \frac{\rho_{s1} v_{s1}^2}{2} \right) = \rho_{s1} Q_{s1} \left(p_2 + \frac{\varsigma_{s2} \rho_{s2} v_{s2}^2}{2} \right) + \left(\lambda_a + \psi \lambda_p \right) \frac{L_c}{d_n} \rho_{s1} Q_{s1} \frac{\rho_{a2} v_{a2}^2}{2} \tag{A-23}$$

Comparing Eqs. (A-22) and (A-23) with Eqs. (A-16) and (A-17) results in

$$k_{12}\left(\rho_{o2}Q_{o2}\frac{\varsigma_{o2}\rho_{o2}v_{o2}^2}{2}+\rho_{s2}Q_{s2}\frac{\varsigma_{s2}\rho_{s2}v_{s2}^2}{2}\right)=\left(\lambda_a+\psi\lambda_p\right)\frac{L_c}{d_n}\rho_2Q_2\frac{\rho_{a2}v_{a2}^2}{2} \tag{3.53}$$

The momentum equation for the flow stream between sections 2-2 and 3-3 can also written as

$$\left(p_3-p_2\right)A_2+\tau_f\pi d_3L_t=\rho_{s2}Q_{s2}v_{s2}\varsigma_{s2}+\rho_{o2}Q_{o2}v_{o2}\varsigma_{o2}-\mu_3\rho_{m3}Q_3v_3 \tag{A-24}$$

where τ_f is the shear stress between the flow stream and the wall of the throat tube.

It is obtained by comparing Eqs. (A-24) and (3.47), so that

$$k_{23}\rho_{m3}Q_3v_3/2=\tau_f\pi d_3L_t \tag{A-25}$$

For air-only flow $\tau_f=\frac{\lambda_a}{8}\rho_{a3}v_{a3}^2$. In similarity, it is assumed that for an air-solid mixture flow, $\tau_f=\frac{\lambda_a+\psi\lambda_p}{8}\rho_{a3}v_{a3}^2$. Substituting this expression for τ_f in Eq. (A-25) leads to

$$k_{23}\rho_{m3}Q_3v_3/2=\frac{\lambda_a+\psi\lambda_p}{8}\rho_{a3}v_{a3}^2\pi d_3L_t \tag{A-26}$$

By noting that $Q_3=\frac{\pi d_3^2}{4}v_3$, Eq. (A-26) is transformed into Eq. (3.54).

Using the energy loss coefficient ξ_d to account for the energy losses in the diffuser, the energy equation for the flow stream sections 3-3 and 5-5 is expressed by

$$p_3+\frac{\rho_{m3}v_3^2}{2}=p_5+\frac{\rho_5v_5^2}{2}+\xi_d\frac{\rho_{a3}v_{a3}^2}{2} \tag{A-27}$$

Comparing Eqs. (A-19) and (A-27) leads to Eq. (3.55), that is

$$k_{35}\frac{\rho_{m3}v_3^2}{2}=\xi_d\frac{\rho_{a3}v_{a3}^2}{2} \tag{3.55}$$

Equations (3.56) - (3.58)

Solving Eq. (3.53) for k_{12} leads to

$$k_{23} = \left(\lambda_a + \psi\lambda_p\right)\frac{L_c}{d_n}\frac{\rho_{a2}v_{a2}^2}{\rho_{o1}v_{o1}^2}\frac{1+x}{\left(\varsigma_{o2} + x\dfrac{\varsigma_{s2}\rho_{s2}v_{s2}^2}{\rho_{o1}v_{o1}^2}\right)} \tag{A-28}$$

From mass conservation and by the assumption of isothermal flow, it is derived that

$$\frac{\rho_{a2}}{\rho_{o1}} \approx 1 \qquad \frac{v_{a2}}{v_{o1}} = \left(1 + q_a\frac{p_4}{p_1}\right)\Big/(m-1) \qquad \frac{v_{s2}}{v_{o1}} = \frac{q_p + q_a\dfrac{p_4}{p_2}}{m-1} \qquad \frac{\rho_{a2}}{\rho_{o1}} = \frac{x}{q_a\dfrac{p_4}{p_2} + q_p}$$

The substitution of these equations into Eq. (A-28) results in Eq. (3.56).

Solving k_{23} from Eq. (A-26) leads to

$$k_{23} = \left(\lambda_a + \psi\lambda_p\right)\frac{L_t}{d_3}\frac{\rho_{a3}v_{a3}^2}{\rho_{m3}v_3^2} \tag{A-29}$$

Based on the assumption of isothermal flow and from mass conservation, the following relations are obtained.

$$\frac{\rho_{a3}}{\rho_{m3}} = \left(1 + \frac{q_p}{\dfrac{p_1}{p_3} + q_a\dfrac{p_4}{p_3}}\right)\Bigg/\left(1 + \frac{\dfrac{\rho_p}{\rho_{o1}}q_p}{1 + q_a\dfrac{\rho_{a4}}{\rho_{o1}}}\right), \qquad \frac{v_{a3}}{v_3} = \left(1 + \frac{q_p}{\dfrac{p_1}{p_3} + q_a\dfrac{p_4}{p_3}}\right)^{-1}$$

By combining these equations with Eq. (A-29), Eq. (3.57) is obtained.

Eq. (3.55) can be rearranged as

$$k_{35} = \xi_d\frac{\rho_{a3}}{\rho_{m3}}\frac{v_{a3}^2}{v_3^2} \tag{A-30}$$

By inserting the expression of density ratio ρ_{a3}/ρ_{m3} and velocity ratio v_{a3}/v_3, Eq. (A-30) is rearranged as Eq. (3.58).

B Computer Program to Predict Central Air-Jet Pump Performance

```
      PROGRAM MAIN

C-------------------------------------------------------------------------------------------C
C THIS PROGRAM CALCULATES THE DIMENSIONLESS PERFORMANCE OF  C
C GAS-SOLID JET PUMP WITH CONIC NOZZLE LOCATED IN CENTRAL LINE.C
C-------------------------------------------------------------------------------------------C

      DOUBLE PRECISION LAMDAG,K01,KS,K1,K2,K3,KX
      PARAMETER (PI=3.14159,LAMDAG=0.025,G=9.81,PA=101300,K01=0.12,
     * KS=0.4,S=1.)
      INTEGER I,J
      DIMENSION HR(15),QR(15),K1(15),K2(15),K3(15),PX1(15),PX2(15),
     * PX3(15),PX5(15),KX(15)
      DOUBLE PRECISION P1,P2,P3,PC,RUG,RUB,RUP,LAMDAP,KSAI,Z
1,K12,K23,K3C,HR,QR,QM,ALFA,QG,QP,BETA,RUR,C,RUGS,RU01,P0,PS,KO
      DOUBLE PRECISION PSS,M
      COMMON
1,P2,P3,PC,LAMDAP,KSAI,Z,K12,K23,KO2,K3C,QG,QM,QP,BETA
      COMMON/COM1/P0,PS,M,RUB,RUP,RUG
      PSS=PS
      BETA=(RUB-RUG)/(RUP-RUG)
      DO 200 I=1,12
      QM=0.5*I
      CALL INIT(C)
       CALL SUBP1(PSS,C,ALFA,RUR,RU01,RUS1,RUGS)
      CALL SUBP2(C,RU01,RUGS)
      CALL SUBP3(RU01,RUGS)
      CALL SUBPC
      K1(I)=K12
      K2(I)=K23
      K3(I)=K3C
      PX1(I)=P1-PA
      PX2(I)=P2-PA
      PX3(I)=P3-PA
      PX5(I)=PC-PA
      KX(I)=KSAI
      HR(I)=(PC-PSS)/Z
      HR(I)=ALFA*HR(I)/(1+K01)
      QR(I)=QM
      IF (HR(I).LE.0) GOTO 300
200   CONTINUE
      J=I+1
300   J=I-1
       OPEN(6,STATUS='old',FILE='c:\wang\fox\p2a.dat')
      WRITE(6,90) M,C
90     FORMAT ('M=',F5.2,5X,2HC=,F10.3)
      DO 50 I=1,J
       WRITE(6,100) QR(I),HR(I),K1(I),K2(I),K3(I),PX1(I),PX2(I),PX3(I),
     * PX5(I),KX(I)
50    CONTINUE
100   FORMAT (10F12.4)
```

```
      END

      BLOCK DATA
       DOUBLE PRECISION P0,PS,RUB,RUP,RUG,M
       COMMON/COM1/P0,PS,M,RUB,RUP,RUG
        DATA P0,PS,M,RUB,RUP,RUG/141300,101300,2.86,793,
      # 1424,1.2/
      END

      SUBROUTINE INIT(C)
      DOUBLE PRECISION C1,LN2DN,A,C
       DOUBLE PRECISION P0,PS,M,RUB,RUP,RUG
       COMMON/COM1/P0,PS,M,RUB,RUP,RUG
       LN2DN=3.6
      BETAG=15
      BETAG=3.14/180*BETAG
       A=1.2
      C1=2*LN2DN*TAN(BETAG)+DSQRT(M)-A
      C=(M-1)/(C1*COS(BETAG)*(2*A+C1*COS(BETAG)**2))
      RETURN
      END

       SUBROUTINE SUBP1(PSS,C,ALFA,RUR,RU01,RUS1,RUGS)
      DOUBLE PRECISION LAMDAG,K01,KS,S,MU1
      PARAMETER
       1(LAMDAG=0.025,G=9.81,PA=101300,K01=0.12,KS=0.4,S=1.,MU1=1.0)
       DOUBLE PRECISION PSS,C,ALFA,RUR,RUS1,RUGS,M
       DOUBLE PRECISION PR01,Z1,Z2,RUG1,RU01,DELTA,P11
      DOUBLE PRECISION
      P1,P2,P3,PC,LAMDAP,KSAI,Z,K12,K23,KO2,K3C,QG,QM,
       1QP,BETA,P0,PS,RUB,RUP,RUG

COMMON//P1,P2,P3,PC,LAMDAP,KSAI,Z,K12,K23,KO2,K3C,QG,QM,QP,BETA
       1/COM1/P0,PS,M,RUB,RUP,RUG
       P1=PSS
5      IF (P1.GT.(0.528*P0)) THEN
          Pn=P1
        ELSE
          Pn=0.528*P0
       ENDIF
       PR01=P0/Pn
       RUG1=RUG*P1/PA
       RUGS=RUG*PS/PA
       RU01=RUG1
       RUS1=RUG1*(1-BETA)+RUP*BETA
       RUR=RUS1/RU01
      QG=S*(1-BETA)*QM*(RU01/RUP)/(BETA+(1-BETA)*RUG/RU01)
      QP=BETA*QG/(1-BETA)
       Z1=(PSS-P1)*(1+K01)/(Pn*DLOG(PR01))
       Z2=(1+KS)*(C**2*(QG*PS/P1+QP)**2)/((M-1)**2)*RUS1/RU01
       DELTA=ABS(Z2-Z1)
       IF (DELTA.LE.0.0000001)  GOTO 10
       P11=P1-DELTA
       IF (P11.LE.0)  P11=P1+2*DELTA
       P1=P11
```

```
    GOTO 5
10   Z=P1*DLOG(PR01)/(1+K01)
     ALFA=(PSS/(P0-
PSS)*DLOG(PR01))/(1+DLOG(PR01)*C**2*(QG*PS/P1+QP)**2
    1*(1+KS)*MU1*RUR/((1+K01)*(M-1)**2))
     RETURN
     END

      SUBROUTINE SUBP2(C,RU01,RUGS)
     DOUBLE PRECISION LN2DN,LAMDAG
     PARAMETER(LN2DN=3.6,LAMDAG=0.025)!Lc=50mm
      DOUBLE PRECISION P21,DELTA,PRS1,C,Z1,Z2,RU01,RUGS,QGM,COEF,M
     DOUBLE PRECISION
P1,P2,P3,PC,LAMDAP,KSAI,Z,K12,K23,KO2,K3C,QG,QM,
     1QP,BETA,P0,PS,RUB,RUP,RUG

COMMON//P1,P2,P3,PC,LAMDAP,KSAI,Z,K12,K23,KO2,K3C,QG,QM,QP,BETA
     1/COM1/P0,PS,M,RUB,RUP,RUG
     LAMDAP=0.00175
      P21=P1
      PRS1=PS/P1
      KO2=1.
      KS2=1.
     QGM=RUGS/RU01*QG
5    Z1=(P21-P1)*(1+QM)/Z
     KSAI=(QM-QGM)/(1+QGM)
      K12=(LAMDAG+KSAI*LAMDAP)*LN2DN
      K12=K12*(1+QG*PRS1)**2*(1+QM)*RUGS/RU01/PRS1/
     1(KO2*(M-1)**2+KS2*(QM**2)*(QP+QG*PS/P21))
      Z2=(M-1)**2+(C**2)*QM**2*(QG*PRS1+QP)-(1+k12)*
     1(KO2*(M-1)**2+QM**2*(QG*PS/P21+QP)**2)
      Z2=Z2/((M-1)**2)
      WRITE(*,100) Z1,Z2
100   FORMAT (2F12.8)
     DELTA=ABS(Z1-Z2)
      IF (DELTA.LE.0.000001) GOTO 10
      IF (DELTA.LE.1) COEF=1500.0
      IF (DELTA.GT.1) COEF=100
      IF (Z2) 20,30,30
20    P21=P21-COEF*DELTA
     IF (ABS(Z1).GT.ABS(Z2)) GOTO 30
     GOTO 5
30    P21=P21+COEF*DELTA
     GOTO 5
10    P2=P21
     RETURN
     END

      SUBROUTINE SUBP3(RUO1,RUSG)
     DOUBLE PRECISION L23D3,MU3,LAMDAG
     PARAMETER(L23D3=5.6,MU3=1,LAMDAG=0.025)
     DOUBLE PRECISION
P31,DELTA,RUO1,RUSG,Z1,Z2,RURP,RURG,COEF,ZP,M
     DOUBLE PRECISION
P1,P2,P3,PC,LAMDAP,KSAI,Z,K12,K23,KO2,K3C,QG,QM,
```

```
     1QP,BETA,P0,PS,RUB,RUP,RUG

COMMON//P1,P2,P3,PC,LAMDAP,KSAI,Z,K12,K23,KO2,K3C,QG,QM,QP,BETA
     1/COM1/P0,PS,M,RUB,RUP,RUG

     P31=P2
     RURP=RUP/RUO1
     RURG=RUSG/RUO1
5    K23=(LAMDAG+KSAI*LAMDAP)*L23D3/((1+RURP*QP/(1+RURG*QG))*
    1(1+QP/(QG*PS/P31+P1/P31)))
     ZP=(1+QG*RURG+QP*RURP)*(P1/P31+QG*PS/P31+QP)*(2*MU3+K23)/M
     Z1=(P31-P2)*M/Z
     Z2=2*(QG*RURG+QP*RURP)*(QP+QG*PS/P2)/(M-1)+2*KO2-ZP
     WRITE(*,100) Z1,Z2
100  FORMAT (2F12.8)
     DELTA=ABS(Z2-Z1)
     IF (DELTA.LE.0.000001) GOTO 10
     IF (DELTA.LE.1) COEF=2000.0
     IF (DELTA.GT.1) COEF=1000.0
     IF (Z2) 30,40,40
30   P31=P31-0.7*COEF*DELTA
     IF (ABS(Z1).GT.ABS(Z2)) GOTO 40
     GOTO 5
40   P31=P31+COEF*DELTA
     GOTO 5
10   P3=P31
     RETURN
     END

     SUBROUTINE SUBPC
     DOUBLE PRECISION
P1,P2,P3,PC,LAMDAP,KSAI,Z,K12,K23,KO2,K3C,QG,QM,
     1QP,BETA,P0,PS,RUB,RUP,RUG,AD,SITA,SITAD,LAMDAG,M
     PARAMETER(LAMDAG=0.025,AD=2,SITA=7.23)
COMMON//P1,P2,P3,PC,LAMDAP,KSAI,Z,K12,K23,KO2,K3C,QG,QM,QP,BETA
     1/COM1/P0,PS,M,RUB,RUP,RUG
     SITAD=3.14159/180*SITA
     K3C=(LAMDAG+KSAI*LAMDAP)/(8*DTAN(SITAD))*(1-1/(AD*AD))+
    1(AD-1)/(AD+1)*DSIN(2*SITAD)*(1-1/(AD*AD))
      K3C=K3C/((1+RURP*QP/(1+RURG*QG))*
    1(1+QP/(QG*PS/P31+P1/P31)))
     PC=(1-K3C)*(1+QM)*(P1/P3+QG*PS/P3+QP)/M**2
     PC=Z*PC+P3
     RETURN
     END
```

C Computer Program for Optimum Design of Central Air-Jet Pumps

```
      PROGRAM MAIN
C-----------------------------------------------------------------------------------------C
C  THIS PROGRAM OPTMISES THE DIMENSIN AND PERFORMANCE OF GAS-
C  SOLID JET PUMP WITH CONIC NOZZLE LOCATED IN CENTRAL LINE.
C-----------------------------------------------------------------------------------------C
      IMPLICIT REAL *8(A-H,O-Z)
       INTEGER CYCLE,FUN,HK,GK,FK,N
       PARAMETER (N=8,FK=1,GK=25,HK=1)
      DIMENSION
       X(N),X0(N),XX(N),X3(N),FX(FK),GX(GK),HX(HK),S(N+1,N),
     *BL(N),BU(N)
       COMMON/COM1/KK,NF/COM3/FUN/COM2/MINN,ITER,CYCLE
     */COM6/R,FX1
       NF=0
        write(*,*)'input R'
       READ(*,*)R
        X(1)=3.
        X(2)=2.8
        X(3)=5.6
        X(4)=3.
        X(5)=57.
        X(6)=3
        X(7)=30.
        X(8)=3.
        BL(1)=2.5
        BL(2)=2.85
        BL(3)=3.
        BL(4)=0.5
        BL(5)=30.
        BL(6)=2.
        BL(7)=10.
        BL(8)=1.
        BU(1)=10.
        BU(2)=25.
        BU(3)=10.
        BU(4)=10.
        BU(5)=200.
        BU(6)=6.
        BU(7)=60.
        BU(8)=3.9
        N1=N+1
         OPEN(8,STATUS='NEW',FILE='outp.dat')
         WRITE(8,3)N,N1,FK,GK,HK,X,BL,BU
3        FORMAT(5X,2HN=,I3,3X,3HN1=,I3,3X,3HFK=,I3,3X,3HGK=,I3,3X,
       *3HHK=,I3/5X,5HX(I)=,2F9.4,3X,6HBL(I)=,2F9.4,3X,6HBU(I)=,2F9.4/)
          CALL FMIN(X,X0,X3,N,N1,FX,GX,HX,S,FK,GK,HK,BL,BU,F,XX)
10      WRITE(8,2)KK,CYCLE,FUN,NF,ITER,MINN,FX,X
2
FORMAT(5X,3HKK=,I3,5X,6HCYCLE=,I5,5X,4HFUN=,I5,5X,3HNF=,I5,5X,
         *5HITER=,I5,5X,5HMINI=,I5/10X,2HF=,F15.9,8X,2HX=,3F15.9/)
```

```
      CLOSE(6)
      STOP
      END
C     FUNCT
        SUBROUTINE FUNCT(X,Y,N,FX,FK,GX,GK,HX,HK)
      IMPLICIT REAL *8(A-H,O-Z)
       INTEGER FK,GK,HK,FUN
       DIMENSION X(N),FX(FK),GX(GK),HX(HK)
      COMMON/COM3/FUN/COM6/R,FX1
       CALL F(FX,FK,X,N)
       CALL G(GX,GK,X,N)
       CALL H(HX,HK,X,N)
       FUN=FUN+1
C      WRITE(*,1)X,FX,GX,HX
C      FORMAT(5X,5HX(I)=,2F15.9/5X,6HFX(1)=,F15.9/5X,6HGX(I)=,5F15.9/
C     *5X,6HHX(I)=,F15.9//)
       IF(FUN.NE.1)GOTO 2
       FX1=FX(1)
2      SF=0.0
       SG=0.0
       SH=0.0
       DO 10 K=1,FK
10     SF=SF+FX(K)
       DO 11 K=1,GK
11     SG=SG+1.0/GX(K)
       DO 12 K=1,HK
12     SH=SH+HX(K)*HX(K)
       IF(R.NE.0)GOTO 20
       IF(FUN.NE.1)GOTO 20
       R=ABS(SF/SG)
        IF(SH.NE.0)R=ABS(SF/SG/SH)
20     Y=SF+R*SG+SH/SQRT(R)
C       WRITE(*,4)FUN,X,FX,GX,HX,Y,SF,SG,SH,R
C  4   FORMAT(3X,4HFUN=,I5,3X,16F9.4//)
       RETURN
       END

         SUBROUTINE PENA(T,Y,XX,N,S,FX,FK,GX,GK,HX,HK,N1)
      IMPLICIT REAL *8(A-H,O-Z)
       INTEGER FK,GK,HK
        DIMENSION XX(N),S(N1,N),FX(FK),GX(GK),HX(HK)
      COMMON/COM8/I/COM11/T0
      T0=T-T0
      DO 10 K=1,N
10     XX(K)=XX(K)+T0*S(I,K)
      T0=T
        CALL FUNCT(XX,Y,N,FX,FK,GX,GK,HX,HK)
      RETURN
      END

      SUBROUTINE RANDOM
      IMPLICIT REAL *8(A-H,O-Z)
      REAL M,M35,M36,M37
      COMMON/COM4/M,M35,M36,M37,Q
      M=M*5.0
```

```
      IF(M.GE.M37)M=M-M37
      IF(M.GE.M36)M=M-M36
      IF(M.GE.M35)M=M-M35
      Q=M/M35
      RETURN
      END

      SUBROUTINE RE(A,B,C,D)
      IMPLICIT REAL *8(A-H,O-Z)
      B=A
      D=C
      RETURN
      END

        SUBROUTINE LINE(H0,T,Y,XX,N,X,S,FX,FK,GX,GK,HX,HK,N1)
      IMPLICIT REAL *8(A-H,O-Z)
       INTEGER FK,GK,HK
        DIMENSION XX(N),X(N),S(N1,N),FX(FK),GX(GK),HX(HK)
      COMMON/COM11/T0/COM9/Y0/COM10/LIN/COM5/EPS
      DO 11 K=1,N
11    XX(K)=X(K)
      HT=H0
      T2=H0
      T0=0.0
      T1=0.0
      Y1=Y0
700   CALL PENA(T2,Y2,XX,N,S,FX,FK,GX,GK,HX,HK,N1)
      DO 10 K=1,GK
      IF(GX(K).GE.1.E-15)GO TO 10
      T2=T2*.5
      GOTO 700
10    CONTINUE
      IF (Y2.LT.Y1)GO TO 200
      HT=-HT
      CALL RE(T1,T3,Y1,Y3)
100   CALL RE(T2,T1,Y2,Y1)
      CALL RE(T3,T2,Y3,Y2)
200   T3=T2+HT
        CALL PENA(T3,Y3,XX,N,S,FX,FK,GX,GK,HX,HK,N1)
      DO 20 K=1,GK
      IF (GX(K).GE.1.E-15)GO TO 20
      HT=HT*.5
      GO TO 200
20    CONTINUE
      IF (Y2.LE.Y3)GO TO 300
      HT=HT+HT
      GO TO 100
300   C1=(Y3-Y1)/(T3-T1)
      C2=((Y2-Y1)/(T2-T1)-C1)/(T2-T3)
      IF(ABS(C2).LT.1.E-10)GO TO 400
      T4=0.5*(T1+T3-C1/C2)
      IF((T4-T1)*(T3-T4).LE.0.)GO TO 400
        CALL PENA(T4,Y4,XX,N,S,FX,FK,GX,GK,HX,HK,N1)
      A=1.
      IF(ABS(Y2).GE.1.)A=Y2
```

```
      IF(ABS((Y2-Y4)/A).LT.EPS) GOTO 30
      IF(ABS(T2-T1).LT.1.E-15) GOTO 30
      IF(ABS(T2-T3).LT.1.E-15) GOTO 30
      GO TO 40
30    IF(Y2.GT.Y4)GO TO 500
      GO TO 400
40    IF((T4-T2)*HT)70,70,50
50    IF(Y2-Y4)60,60,55
55    CALL RE(T2,T1,Y2,Y1)
      CALL RE(T4,T2,Y4,Y2)
      GO TO 300
60    CALL RE(T4,T3,Y4,Y3)
      GO TO 300
70    IF(Y2-Y4)80,80,75
75    CALL RE(T2,T3,Y2,Y3)
      CALL RE(T4,T2,Y4,Y2)
      GO TO 300
80    CALL RE(T4,T1,Y4,Y1)
      GO TO 300
400   CALL RE(T2,T,Y2,Y)
      GO TO 600
500   CALL RE(T4,T,Y4,Y)
600   LIN=LIN+1
      RETURN
      END

        SUBROUTINE MINI(X3,N,XX,X,FX,GX,HX,FK,GK,HK,S,N1,X0)
      IMPLICIT REAL *8(A-H,O-Z)
       INTEGER FK, GK,HK,DFI,CYCLE
        DIMENSION X3(N),XX(N),X(N),FX(FK),GX(GK),HX(HK),S(N1,N),X0(N)
      COMMON /COM2/MINN,ITER,CYCLE/COM5/EPS/COM7/H0,F0/COM8/I
      COMMON/COM12/SDX/COM9/Y0
       MINN=MINN+1
       SDX=1.E10
100   ITER=ITER+1
        WRITE(*,*)'SDX,EPS',SDX,EPS
      IF(SDX.LE.EPS)GO TO 1000
      Y0=F0
      F1=F0
      DFM=0.0
      DFI=1
      DO 30 I=1,N
        CALL LINE(H0,T,F2,XX,N,X,S,FX,FK,GX,GK,HX,HK,N1)
      DO 10 K=1,N
10     X(K)=X(K)+T*S(I,K)
        CALL FUNCT(X,F2,N,FX,FK,GX,GK,HX,HK)
      DF=F1-F2
      Y0=F2
      F1=F2
      IF(DF.LE.DFM)GO TO 30
      DFM=DF
      DFI=I
30    CONTINUE
      DO 40 K=1,N
       X3(K)=2*X(K)-X0(K)
```

```
40    S(N+1,K)=X(K)-X0(K)
        CALL FUNCT(X3,F3,N,FX,FK,GX,GK,HX,HK)
      SDX=0.
      DO 45 K=1,N
45    SDX=SDX+(X(K)-X0(K))**2
      SDX=DSQRT(SDX)
      IF(F3.GT.F0) GO TO 65
      IF((F0-2*F2+F3)*(F0-F2-DFM)**2.GT.0.5*DFM*(F0-F3)**2)GO TO 65
      DO 55 I=DFI,N
      DO 55 K=1,N
55    S(I,K)=S(I+1,K)
      Y0=F2
      I=N
        CALL LINE(H0,T,F0,XX,N,X,S,FX,FK,GX,GK,HX,HK,N1)
      DO 60 K=1,N
       X0(K)=X(K)+T*S(N,K)
60    X(K)=X(K)+T*S(N,K)
        CALL FUNCT(X,F0,N,FX,FK,GX,GK,HX,HK)
      GO TO 100
65    IF(F3-F2) 70,80,80
70    F0=F3
      DO 75 K=1,N
      X0(K)=X3(K)
75    X(K)=X3(K)
      GO TO 100
80    DO 85 K=1,N
85    X0(K)=X(K)
      F0=F2
      GO TO 100
1000   ITER=ITER-1
      RETURN
      END

      SUBROUTINE
FMIN(X,X0,X3,N,N1,FX,GX,HX,S,FK,GK,HK,BL,BU,Y,XX)
      IMPLICIT REAL *8(A-H,O-Z)
       INTEGER FK,GK,HK,FUN,CYCLE
      REAL M,M35,M36,M37
        DIMENSION X(N),X0(N),X3(N),XX(N),FX(FK),GX(GK),HX(HK),S(N1,N)
     *,BL(N),BU(N)
      COMMON /COM4/M,M35,M36,M37,Q/COM6/R,FX1/COM10/LIN
      COMMON /COM7/H0,F0/COM5/EPS/COM2/MINN,ITER,CYCLE/COM3/FUN
      M=2657863
      M35=2.**35
      M36=2.*M35
      M37=2.*M36
      FOM=1.E10
       H0=0.01
      EP=1.E-4
      EPS=1.E-4
      C=0.2
      R=R/C
      ITER=0
      CYCLE=0
       FUN=0
```

```
      LIN=0
      MINN=0
      DO 5 K=1,N
5      X0(K)=X(K)
      DO 10 I=1,N
      DO 8 K=1,N
8      S(I,K)=0.
10     S(I,I)=1.
100    R=R*C
      CYCLE=CYCLE+1
      WRITE(*,1)CYCLE,R
1      FORMAT(10X,6HCYCLE=,I5,3X,2HR=,F12.5/)
200       CALL FUNCT(X,F0,N,FX,FK,GX,GK,HX,HK)
      IF(MINN.NE.0)GO TO 60
      DO 25 I=1,GK
      IF(GX(I).GE.0) GO TO 25
      DO 20 K=1,N
      CALL RANDOM
      WRITE(*,19)Q
19       FORMAT(5X,'Q=',F10.6)
20     X(K)=BL(K)+Q*(BU(K)-BL(K))
      GO TO 200
25     CONTINUE
60        CALL MINI(X3,N,XX,X,FX,GX,HX,FK,GK,HK,S,N1,X0)
      WRITE(*,2)ITER,F0,FX(1)
      DO 61 K=1,N
61     WRITE(*,3)K,X(K)
2      FORMAT(8X,5HITER=,I5,3X,3HF0,E19.9,3X,6HFX(1)=,E19.9/)
3      FORMAT(15X,2HX(,I2,2H)=,F15.9/)
62     DO 65 I=1,GK
      IF(GX(I).LT.1.E-15)GO TO 300
65     CONTINUE
      IF(ABS((FOM-F0)/F0).LT.EP) GO TO 300
      IF(ABS(FOM).LT.F0) GO TO 300
      FOM=F0
      GO TO 100
300     M=ABS((FX1-FX(1))/FX1)
      WRITE(*,1)CYCLE,R
      WRITE(*,2)ITER,F0,FX(1)
      DO 77 K=1,N
77     WRITE(*,3)K,X(K)
      WRITE(*,4)M,FX1,FX(1),GX(1),HX(1)
4      FORMAT(5X,21HAGS((FX1-FX(1))/FX1)=,E19.9,5X,
     * 22HHOLDVALUE OF FUNCTION=,E19.9,5X,
     *  20HMINIMIZE FUNCTION IS,E19.9/5X,6HGX(1)=,5F15.9,5X,6HHX(1)=,
     * F15.9/)
      RETURN
      END

      SUBROUTINE F(FX,K,X,N)
      IMPLICIT REAL*8(A-H, O-Z)
       REAL *8 P0,M,L23D3,LN2DN,QM,H,Ms,PY,PP,D0,P5D,DN,MA,X,PS,FX
      DIMENSION FX(K),X(N)
      COMMON/COM1/KK,NF
      COMMON/one/PS,MS
```

```
COMMON/COMT/DN,H,MA,P5D,D0
PS=101300
MS=0.16
P5D=109300.
P0=X(5)*1000.+100000.!CONVERT to ABSOLUTE PRESSURE
M=X(2)
L23D3=X(3)
LN2DN=X(4)
QM=X(1)
Ma=Ms/X(1)
AnA0=1/X(6)
BTAG=X(7)
SITA=X(8)
CALL FINDdn(dn,AnA0,p0,ps,Ma)
D0=SQRT(x(6))*DN
 CALL H2X(H,p0,m,l23d3,ln2dn,qm,btag,sita,ps)
PY=Ps/(P0-PS)
 PP=P0/(P0-PS)
FX(1)=-H*X(1)/((H+PY)*DLOG(PP/(H+PY)))
 NF=NF+1
RETURN
END
```

Table C-1 Variation of objective function values with controlling parameter and design variables for second set of starting values

k	$f(X)$	$\Phi(X,r)$	r	x	m	L_t/d_t	m_d	p_0	m_n	β	θ
1	-0.916	42.500	0.2	2.93	3.18	6.12	2.53	36.7	5.68	29.7	4.11
2	-0.917	7.768	0.04	2.93	3.18	6.11	2.52	36.8	5.68	26.4	4.13
3	-0.938	0.808	0.008	2.92	3.19	5.73	2.31	36.2	5.73	21.0	4.23
4	-0.956	-0.598	0.0016	2.91	3.20	5.37	2.15	35.6	5.80	17.5	4.11
5	-0.967	-0.890	0.00032	2.91	3.21	5.17	2.07	35.2	5.84	12.8	4.20
6	-0.971	-0.953	0.000064	2.91	3.21	5.10	2.04	35.1	5.86	11.7	4.25
7	-0.973	-0.968	0.0000128	2.91	3.21	5.09	2.01	35.0	5.86	10.5	4.24
8	-0.974	-0.972	0.00000256	2.91	3.21	5.09	2.01	35.0	5.87	10.4	4.23
9	-0.974	-0.973	0.00000051	2.91	3.21	5.09	2.00	35.0	5.87	10.2	4.23
10	-0.974	-0.973	0.00000011	2.91	3.21	5.09	2.00	35.0	5.87	10.1	4.23
11	-0.974	-0.974	0.00000002	2.91	3.21	5.08	2.00	35.0	5.87	10.1	4.22

D Publications List as PhD Candidate

1. Wang, D. and Wypych, P.W., Water-only performance of proportioning jet pumps for hydraulic transportation of solids, ***Powder Technology,*** Vol. 84, No. 1, 1995, pp. 56-64.

2. Wang, D. and Wypych, P.W., Air-only performance of central air-jet pumps for the transport of bulk solids in pipelines, ***International Journal of Powder Handling & Processing***, Vol. 7, No. 2, 1995, pp. 111-118.

3. Wang, D. and Wypych, P.W., Central air-jet pump performance for the pneumatic transport of bulk solids, ***International Journal of Powder Handling & Processing***, Vol. 7, No. 3, 1995, pp. 213-218.

4. Davis, M R and Wang, D., Dual pressure drop metering of gas-liquid mixture flows, ***International Journal of Multi-phase Flow,*** Vol. 20, No. 5, 1994, pp. 865-884.

5. Wang, D. and Wypych, P.W., Investigation into central air-jet pump performance for the transport of bulk solids in pipelines, ***5th International Conference on Bulk Materials Handling,*** 10-12 July, 1995, Newcastle, Australia.

6. Wang, D. and Wypych, P.W., Operation performance of air-jet pump for the transport of bulk solids in pipelines, ***Bulk Handling Exhibition & Conference, Asia***, 19-21, September 1995, Singapore.